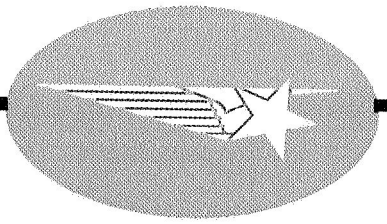

Lockheed

MISSILES & SPACE COMPANY

A GROUP DIVISION OF LOCKHEED AIRCRAFT CORPORATION

SUNNYVALE, CALIFORNIA

HREC-0374-1
LMSC/HREC A791239

LOCKHEED MISSILES & SPACE COMPANY

HUNTSVILLE RESEARCH & ENGINEERING CENTER

HUNTSVILLE RESEARCH PARK

4800 BRADFORD BLVD., HUNTSVILLE, ALABAMA

EXPERIMENTAL INVESTIGATION OF THE DYNAMIC RESPONSES OF A LAUNCH VEHICLE MODEL

FINAL REPORT

February 1968

Contract NAS8-20374

by

C.S. Chang

APPROVED BY: Donald M. McDonald

D. McDonald, Manager
Structures & Mechanics Dept.

J. S. Farrior

J. S. Farrior
Resident Manager

FOREWORD

This final report is prepared by the Lockheed Missiles & Space Company under Contract NAS8-20374 between the Huntsville Research & Engineering Center and NASA/Marshall Space Flight Center.

Analyses and experiments were performed by the Structures and Mechanics Department.

This project was conducted under the direction of Dr. George F. McDonough, Jr., Deputy Chief, Dynamic Analysis Branch, Aero-Astrodynamics Laboratory.

SUMMARY

An experimental program to investigate the elastic and damping properties of a 1/5-scale structural model of launch vehicle Saturn SA-1 had been accomplished. Dynamic responses of the model under sinusoidal and random excitations were studied.

ACKNOWLEDGMENTS

Significant contributions by the following persons of the Structures and Mechanics Department of Lockheed Missiles & Space Company, Huntsville Research & Engineering Center, are acknowledged.

J. Haukohl - Testing, Data Reduction, and Preparation of Final Report

H. Kilgore - Instrumentation Setup and Testing

G. V. Giese-Koch - Preliminary Planning.

CONTENTS

Section 1
INTRODUCTION

Analytical techniques to predict dynamic characteristics (natural frequency, mode shape, and generalized mass) of large, complex structures, such as the Saturn I launch vehicle, have been able to produce excellent results in recent years (Reference 1). Consequently, the degree of confidence which one can place on the results of dynamic response analyses is primarily a function of the accuracy of knowledge of parameters such as damping and structural nonlinearities.

For nonlinear structures, the success of a dynamic analysis depends greatly upon the ability to make accurate predictions over a wide range of excitations and responses. Experimental methods are urgently needed to determine nonlinear structural properties and, at the same time, to provide a test bed for theoretical results using the determined properties.

Previous experimental results (References 2 and 3) have shown an indication of nonlinearity for both Saturn I and Saturn V launch vehicles. This was found to be true for bending vibrations of such vehicles in pre-launch, cantilevered conditions, as well as in simulated flight conditions. Because of the large size and complexities of the full-scaled structures, extensive dynamic response tests on prototypes have not been feasible. Scaled model testing combined with analyses provide a good means of predicting the full-scale behavior.

Experimental capability was developed, and techniques to perform these tests were investigated in this program. A 1/5-scale structural model of launch vehicle Saturn SA1 (Reference 4) was used for the tests.

Elastic and damping properties of the model were measured by dynamic tests under various sinusoidal excitations. The model was then subjected to white-noise random excitation and to simulated dynamic loads expected from ground winds. Sinusoidal test data were obtained for four specimen configurations,* with the model cantilevered to ground at its thrust structures. Test results are contained in Appendix C of this report. Test methods and test instrumentation are described in Appendix B.

Three additional short tests were conducted to investigate (1) the effect of base stiffness on modal frequencies of the cantilevered structure, (2) the effect of response (deformation) in one mode on the damping in another mode, and (3) the effect of internal pressurization of the booster tanks on modal damping. Results from these tests are self-explanatory and are included in Appendix B.

*See Appendix A for definitions of the configurations.

Section 2
RESPONSE TO SINUSOIDAL EXCITATION

2.1 NONLINEAR MODAL EQUATION OF MOTION

Nonlinear modal equations of motion are merited under the assumption that "small" nonlinearities in elastic and damping properties of a structure do not rule out, qualitatively, modal description of its responses, but at the same time, introduce non-negligible errors in the magnitude of response when analyzed as a linear structure under the same excitation. A method to use experimental data to construct the nonlinear modal equation of motion for Saturn-type structures was established in Reference 5. This basic approach was modified for the purpose of this program, so that it no longer relies upon a knowledge of the specific form of the hysteretic "force-deflection" relationship as in Reference 5. The modified approach is shown below.

Let the equation of motion governing the steady-state modal response of a structure be

$$m\ddot{x} + c\dot{x} + k_o x + H(x, \dot{x}) = P_o \cos\omega t \qquad (2.1)$$

where m is the generalized mass for the mode in question, c the viscous damping, k_o the generalized stiffness for the undamped structure, and $H(x, \dot{x})$ a yet unspecified nonlinear damping force which is a function of the response, x, and the velocity, $\dot{x}$. The periodical excitation amplitude is P_o, and the excitation frequency is ω. Assuming an approximate solution of the form

$$x(t) = x_o \cos(\omega t - \phi) \qquad (2.2)$$

to Equation (2.1), the response amplitude, x_o, and the phase difference between response and excitation, ϕ, can be obtained. Assume also

$$H(x, \dot{x}) = a \cos(\omega t - \phi) + b \sin(\omega t - \phi) \tag{2.3}$$

with

$$a = \frac{1}{\pi} \int_0^{2\pi/\omega} H \cos(\omega t - \phi)\, \omega dt \tag{2.4}$$

and

$$b = \frac{1}{\pi} \int_0^{2\pi/\omega} H \sin(\omega t - \phi)\, \omega dt \tag{2.5}$$

For hysteresis type of force-deflection relationship, a and b are functions of frequency only indirectly through the response amplitude. Furthermore, b can be identified with the energy dissipated per cycle of vibration, D_h, due to dissipation caused by H:

$$b = -\frac{D_h}{\pi x_o} \tag{2.6}$$

Combining Equation (2.1) through (2.6), the following simultaneous equations may be obtained

$$\left(1 - \frac{\omega^2}{\omega_o^2}\right) \frac{x_o k_o}{P_o} + \frac{a}{P_o} = \cos\phi \tag{2.7}$$

$$\frac{(D_o + D_h)}{\pi P_o x_o} = \sin\phi \tag{2.8}$$

with $\omega_o = (k_o/m)^{\frac{1}{2}}$ being the limit of natural frequency of the structure as the amplitude tends to zero, and D_c the energy dissipated per cycle due to viscous damping.

The coefficient a is a function of x_o, whose form may be easily determined when $\phi = \pi/2$. Denoting the excitation frequency which yields this condition by ω_ϕ, Equation (2.7) becomes

$$a_\phi = \left(\frac{\omega_\phi^2}{\omega_o^2} - 1 \right) k_o x_{o\phi} \tag{2.9}$$

where the subscript ϕ indicates that values at $\phi = \pi/2$ are being considered. More specifically, the frequency ω_ϕ is a function of the response amplitude x_o, and can be determined experimentally by varying P_o and measuring ω_ϕ and $x_{o\phi}$. Once the form of ω_ϕ as a function of $x_{o\phi}$ is established, so is the form of Equation (2.9), which also holds for all other frequencies for a hysteretically damped structure, i.e.,

$$a = \left[\frac{\omega_\phi^2(x_o)}{\omega_o^2} - 1 \right] k_o x_o \tag{2.10}$$

where the quantity $\omega_\phi(x_o)$ is the resonant frequency (at which $\phi = \pi/2$) under an excitation amplitude which induces a resonant response amplitude numerically equal to x_o. Equation (2.7) can now be written as:

$$\left[\omega^2(x_o) - \omega^2 \right] \frac{m x_o}{P_o} = \cos\phi \tag{2.11}$$

The total energy dissipated per cycle of steady-state vibration,

$$D = D_c + D_h,$$

can again be most easily measured at $\phi = \pi/2$. According to Equation (2.8),

$$D_\phi = \pi P_o x_{o\phi} \tag{2.12}$$

Again, D_ϕ is the value of D at $\phi = \pi/2$. If both viscous damping and structural damping are present, and neither is known quantitatively, the measurement task to determine them is very difficult. For structures whose damping is primarily due to hysteresis effects, D is relatively independent of frequency and its form can be determined by the measured relationship between P_o and x_o. Let

$$P_o = P_\phi(x_{o\phi}) \quad \text{at} \quad \phi = \pi/2$$

then

$$D_\phi = \pi P_\phi(x_{o\phi})\, x_{o\phi}$$

and by previously used arguments,

$$D = \pi P_\phi(x_o)\, x_o$$

and substituting into Equation (2.8) yields

$$\frac{P_\phi(x_o)}{P_o} = \sin\phi \tag{2.13}$$

where $P_\phi(x_o)$ is the value of the excitation amplitude which will induce a resonant response amplitude (at $\phi = \pi/2$) which is numerically equal to x_o.

Eliminating the phase angle between Equations (2.11) and (2.13), the following frequency response equation is obtained:

$$m\left[\omega_\phi^2(x_o) - \omega^2\right] x_o = \pm\left[P_o^2 - P_\phi^2(x_o)\right]^{1/2} \tag{2.14}$$

with $\omega_\phi(x_o)$ and $P_\phi(x_o)$ being experimentally determined functions.

A special case of interest is that of "linear structural damping," whose frequency response may be derived from the general form of Equation (2.14) by assuming

$$\omega_{\phi}(x_o) = \omega_o = \text{a constant} \tag{2.15}$$

and

$$P(x_o) = g k_o x_o \tag{2.16}$$

so that, upon substitution into Equation (2.14) and re-arranging terms, the following is obtained:

$$\frac{x_o}{P_o/k_o} = \frac{1}{\sqrt{\left(1 - \frac{\omega^2}{\omega_o^2}\right)^2 + g^2}} \tag{2.17}$$

The solution Equation (2.17) is identical to that obtained using the "complex restoring force" $k_o(1+ig)$ in the equation of motion. (See, for example, Reference 6.) The present derivation has the advantage that, in addition to being able to handle nonlinearity, the system under consideration is not forced to assume a physically unrealizable, complex spring by the mathematics. Of course, Equation (2.17) may still describe a nonrealizable structure because of the questionable validity of Equations (2.15) and (2.16).*

2.2 TEST DESCRIPTION

The 1/5-scale model of Saturn SA-1 described in Reference 1 was set up at Lockheed/Huntsville in a vertical, cantilevered condition and tested by sinusoidal excitation. Tests include frequency sweep, mode shape survey, resonant response, generalized mass measurement, and free vibration decay.

*Indeed, if damping follows the specific form considered in Reference 5, Equation (2.16) would lead to the conclusion that ω_o has an infinite value, contradicting Equation (2.15).

Four specimen conditions (see Appendix A for definitions) were tested over extended dynamic ranges. The first two cantilevered bending modes were studied for each specimen configuration according to the procedures outlined in Appendix B. Sinusoidal test data are shown in Sections C-A through C-D, Appendix C.

2.3 SUMMARY OF SINUSOIDAL TEST DATA

Table 2-1 is a summary of test data obtained with sinusoidal excitations. Listed in the column under "Natural Frequency" are extrapolated limiting values of resonant frequencies as the amplitudes of excitation and responses were decreased. Resonant frequency shift data were obtained during resonant response amplitude tests and are plotted and shown as functions at resonant nose response amplitudes in Appendix C. The lowest usable data from the experiments were usually governed by the signal-to-noise ratio of the instrumentation.

The generalized mass test results are shown in the next column to the right. The method of measurement, as well as the principle involved, are described in Appendix B. Accuracies of test data for generalized mass are questionable for test Configurations A, B, and C, for different reasons which are discussed later. For test Configuration D, a significant improvement of data consistancy was observed due to the combination of the use of new and better test equipment and better test methods.

For Configurations A and B, weights were added to the "spider beam" structure of the model to induce change in resonant frequencies which were not sufficiently high to warrant accurate measurements. For Configuration A, the first mode resonant frequency is approximately 2.6 cps, and it was difficult to determine the 90° phase difference frequency between force and accelerations on the screen at a CRT oscilloscope with desired accuracy for generalized mass tests. Fortunately, for Configuration A, damping for the first mode was found to be linear and it was possible to extract

Table 2-1

Summary to Sinusoidal Test Data

Configuration	Mode No.	Natural Frequency ω_o (rad/sec)	Generalized Mass, m, (at Station 185) (lb-sec^2/in.)	Generalized Stiffness, K_o, (lb/in.)	Damping: $D = J(T_o - T_1)^n$ J	n	T_1 (in.-lb)	Equivalent Percent Critical Damping: At Low Response Amplitude	At High Response Amplitude
A	1	16.43	5.02	1.435×10^3	0.139	1.0	<0.02	1.02 - 1.22	
	2	123.0	0.93	0.141×10^6	0.256	0.952	.0009	0.97 - 2.44	
	3	467.8	*	*	*	*	*	*	
B	1	26.8	4.50	3.91×10^3	0.60	0.87	0.1	3.96 - 1.95	
	2	123.5	0.60	0.091×10^6	0.73	0.855	<0.08	8.77 - 6.62	
	3	514.7	0.605	0.16×10^6	*	*	*	*	
B_1	1	26.8	4.50	3.15×10^3	0.33	0.94	<0.08	3.27 - 2.65	
		*	*	*	*	*	*	*	
		*	*	*	*	*	*	*	
C	1	12.32	22.8	3.47×10^3	0.195	1.06	0.084	0.69 - 1.64	
	2	86.55	1.85	0.0142×10^6	0.400	1.205	<0.015	1.14 - 2.65	
	3	277.6	7.15	0.548×10^6	*	*	*	*	
D	1	11.49	26.7	3.47×10^3	0.156	1.255	<0.08	0.74 - 1.43	
	2	40.09	12.7	0.0212×10^6	0.175	1.0	0.009	0.1 - 1.43	

*Information not obtained.

information for the generalized mass from free vibration and steady-state damping data. For Configuration B, the major difficulty was due to the extremely nonlinear response of the structure (Figure C-B-33, Appendix C) and to the high degree of dependency of the nonlinearity upon preloads in the outer LOX tanks. Generalized mass data for the second mode in Configuration B was, at best, questionable. For Configuration C, the first resonant frequency was again very low and 90^{o} phase frequency was not accurately measureable with the equipment available at the time of test. For Configuration D, an oscilloscope with a long trace retention time was obtained and used to determine accurately the 90^{o} phase relationship between force and response. The resulting generalized mass measurement was self consistent, and showed good agreement with free vibration data. The generalized stiffness values listed in Table 2-1 are calculated from data in the first two columns.

The relationship between energy dissipation per cycle of steady-state vibration and the total vibratory energy for each mode is calculated from data obtained from resonant dwell tests:

$$D = \pi P_o x_o \qquad \text{at} \quad \phi = \pi/2$$

and

$$T_o = \frac{1}{2} m \omega^2 x_o^2 \qquad \text{at} \quad \phi = \pi/2$$

T_o being the peak total kinetic energy. Results on the relationship between D and T_o are plotted in Figures 2-1 through 2-4. An empirical relationship of the general form

$$D = J(T_o - T_1)^n$$

is noted for all results except those for Configuration B. Values of J, n, and T_1 are tabulated in Table 2-1 also. Figures 2-1 through 2-4 use the same format of data presentation of Reference 2 for full-scaled Saturn I prototype dynamic test data, which obeys the damping law

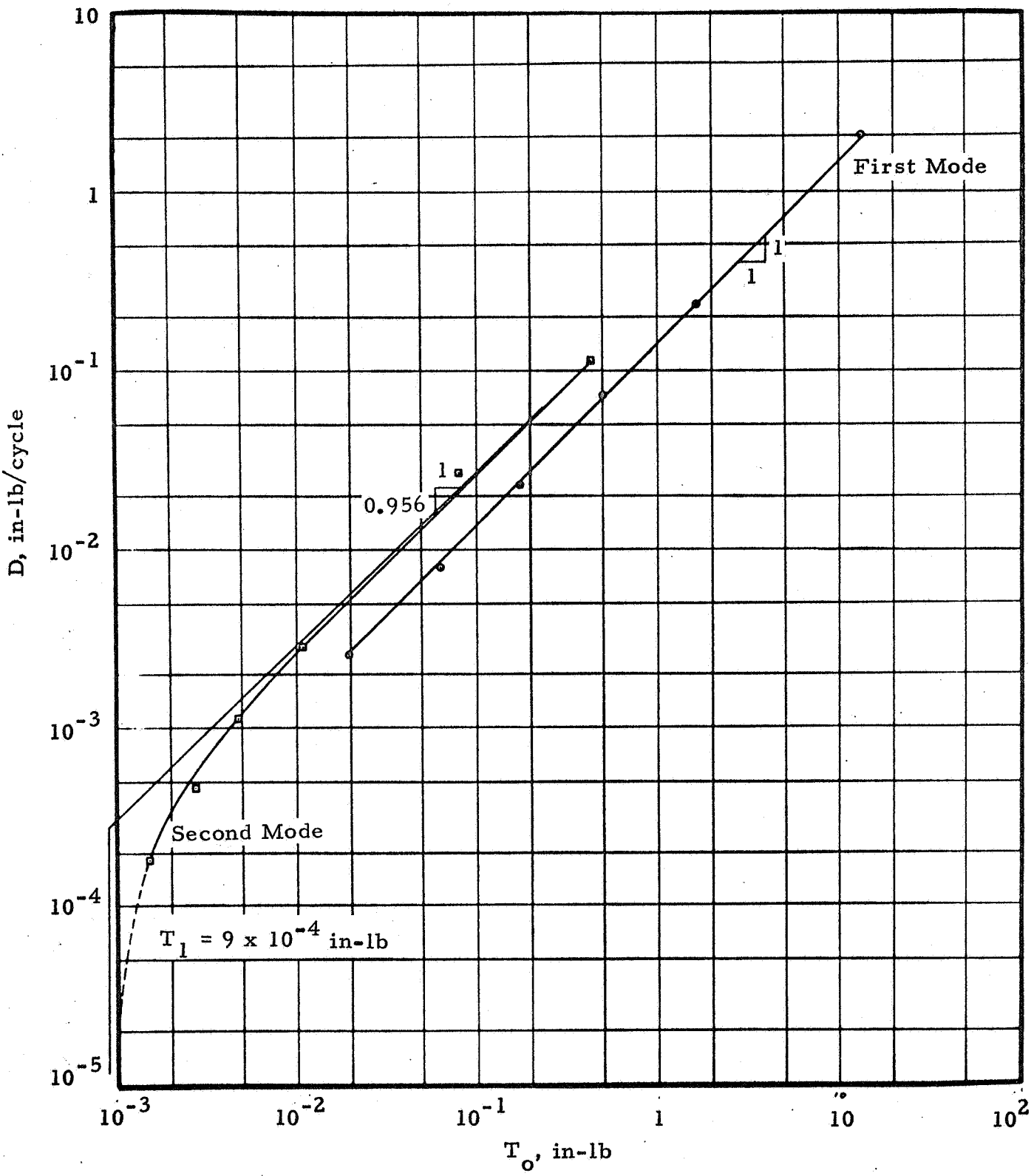

Figure 2-1 - Dissipated Energy vs Peak Kinetic Energy, Configuration A

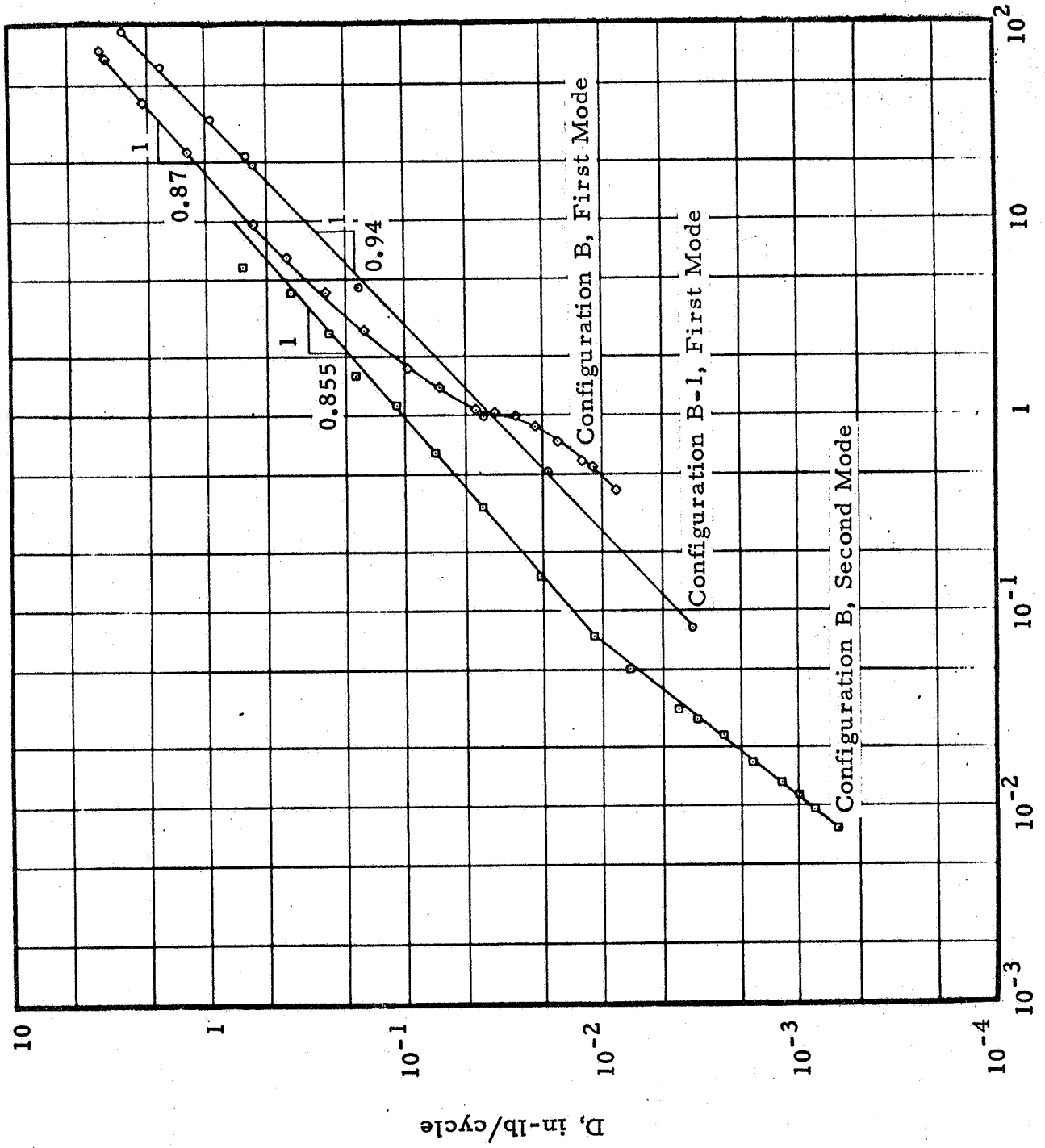

Figure 2-2 - Dissipated Energy vs Peak Kinetic Energy, Configurations B, B-1

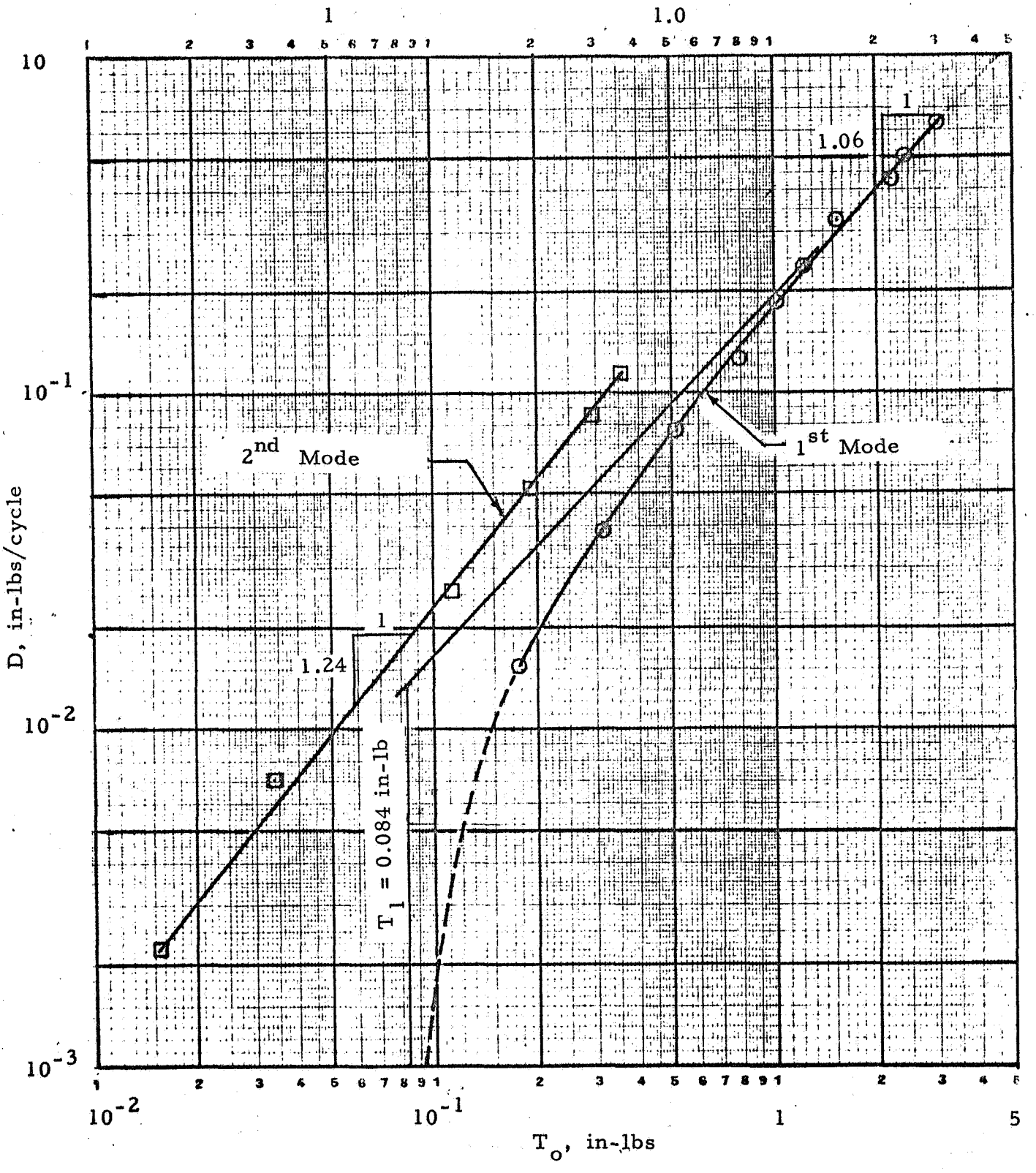

Figure 2-3 - Dissipated Energy vs Peak Kinetic Energy, (Configuration C)

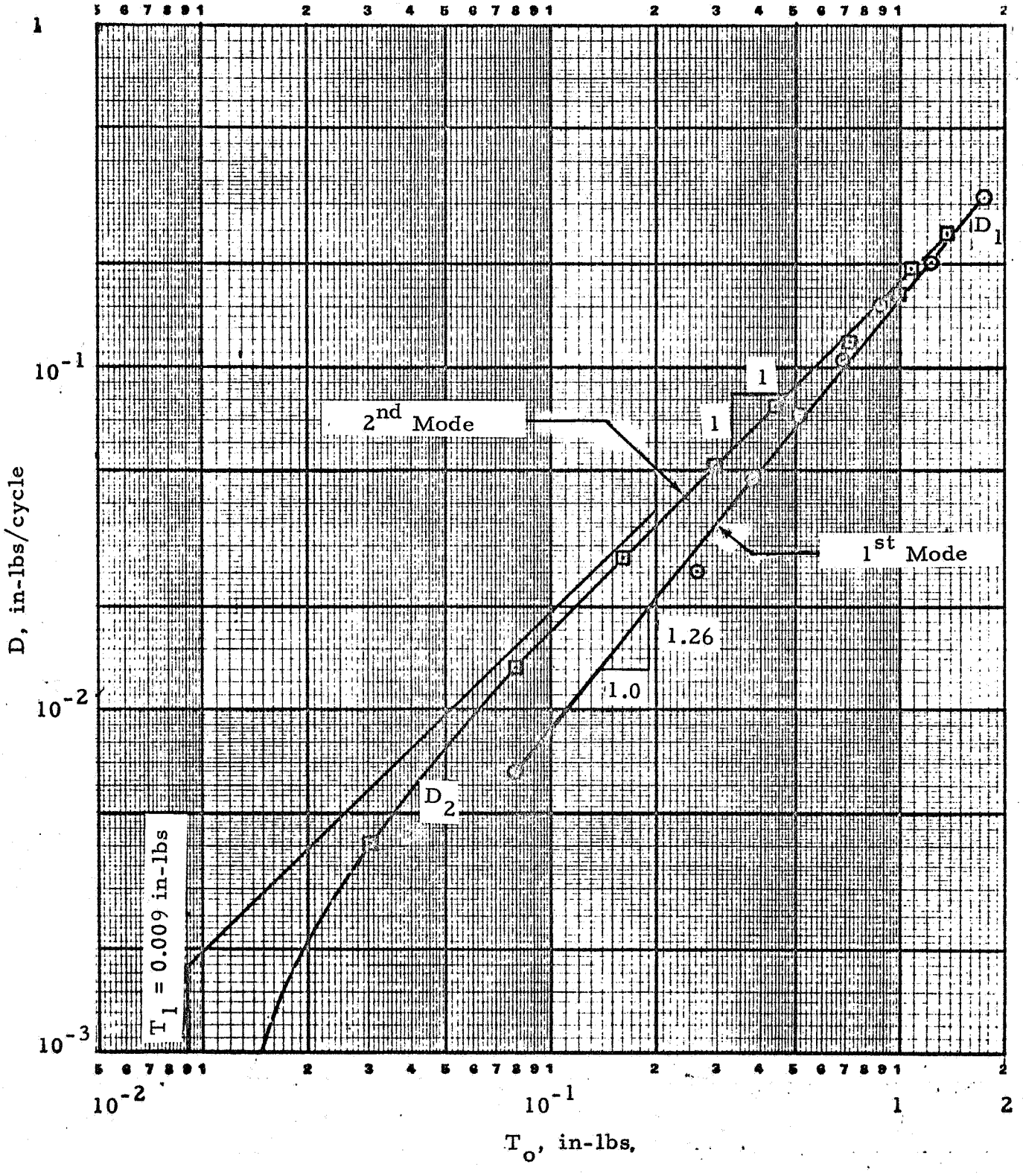

Figure 2-4 - Dissipated Energy vs Peak Kinetic Energy, (Configuration D)

$$D = 1.98\ T_o^{0.8} \qquad (2.18)$$

This relationship was also found to be valid for a full-scale Saturn V prototype in free-free bending vibration modes (Reference 3).

Present test data for the model in cantilevered modes show similar behavior although the coefficient J is quite different. The exponent n is found to be no lower than 0.855.

The last column in Table 2-1 shows equivalent viscous modal damping (shown as percent of critical damping) computed from resonant dwell data according to the formula:

$$\text{percent critical damping} = \frac{D}{4\pi T_o} \times 100$$

Free vibration decay data were also obtained. However, for all modes in all test configurations decay data were difficult to use because of "beating" with response in another bending mode in a plane perpendicular to the plane of excitation. This problem is, of course, common to most structures with radial symmetry and, with mutually perpendicular modes of near identical modal frequencies, are almost always present. This difficulty is exemplified by the two decay records shown in Figure 2-5. The lower trace represents a time history of the nose acceleration component in the plane of excitation before and after its removal at time t_o; the upper trace is a simultaneous time history of the other (perpendicular) acceleration component. Damping measurement was, of course, not possible from such data. Measurement of damping in the steady-state, on the other hand, is more reliable.

For the first two modes of the model in Configuration B, both the x_o vs P_o curve of Figure C-B-33 and the D vs T_o curve of Figure 2-2 show unusual nonlinearities. For force amplitudes above 1.0 pound, the first mode P_o vs x_o relationship fits the equation

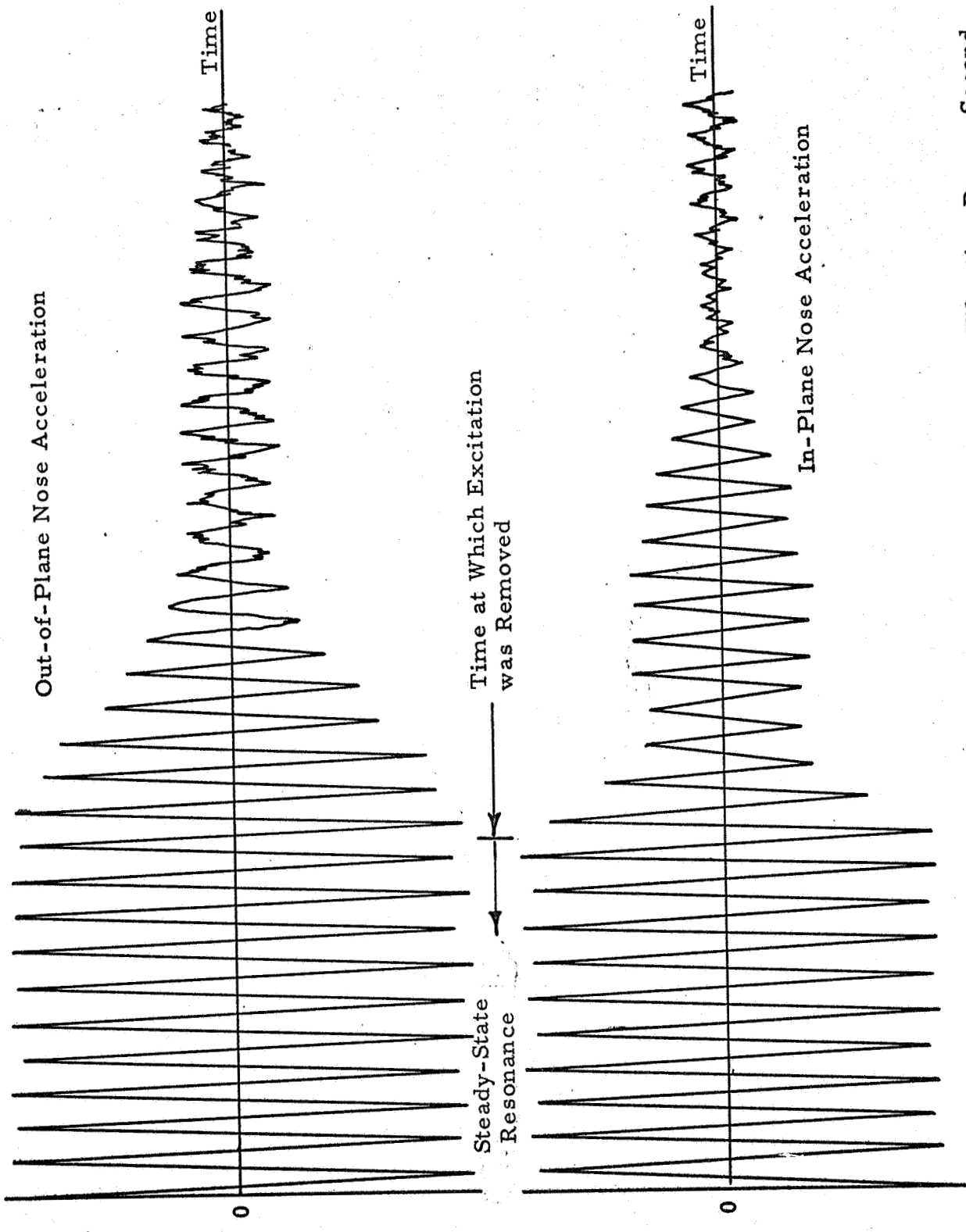

Figure 2-5 - Simultaneous Recordings of In-Plane and Out-of-Plane Free Vibration Decay, Second Mode, Configuration B-1

$$P_o = 40(x_o - 0.004)^{0.74}$$

with P_o in pounds and x_o in inches.

The corresponding D vs T_o fits the equation

$$D = 0.60(T_o - T_1)^{0.87} \tag{2.19}$$

For force amplitudes less than 1.0 pound, the relationship appears to be linear:

$$P_o = 38 x_o$$

Postulating that the nonlinearity was due to "loose" outer LOX tank attachments, a portion of the tests for Configuration B was re-run after the preloads in the outer tanks were increased by an arbitrary amount.* The resulting D vs T_o curve is also shown in Figure 2-2 and is seen to be closer to a linear relationship. The corresponding P_o vs $x_{o\phi}$ is shown in Figure 2.6 which is the same as Figure C-B-33a.

For large values of T_o, i.e., for $T_o \gg T_1$, Equation (2.19) becomes

$$D_\phi = 0.60\, T_o^{0.87}$$

which is quite similar to Equation (2.18) for full-scale structures. It may be postulated that loosely connected structural components, such as the outer LOX tank of the full-scale Saturn I, are the primary source of the observed nonlinearity.

*The tightened structure, without internal pressurization, is designated as the Configuration B-1.

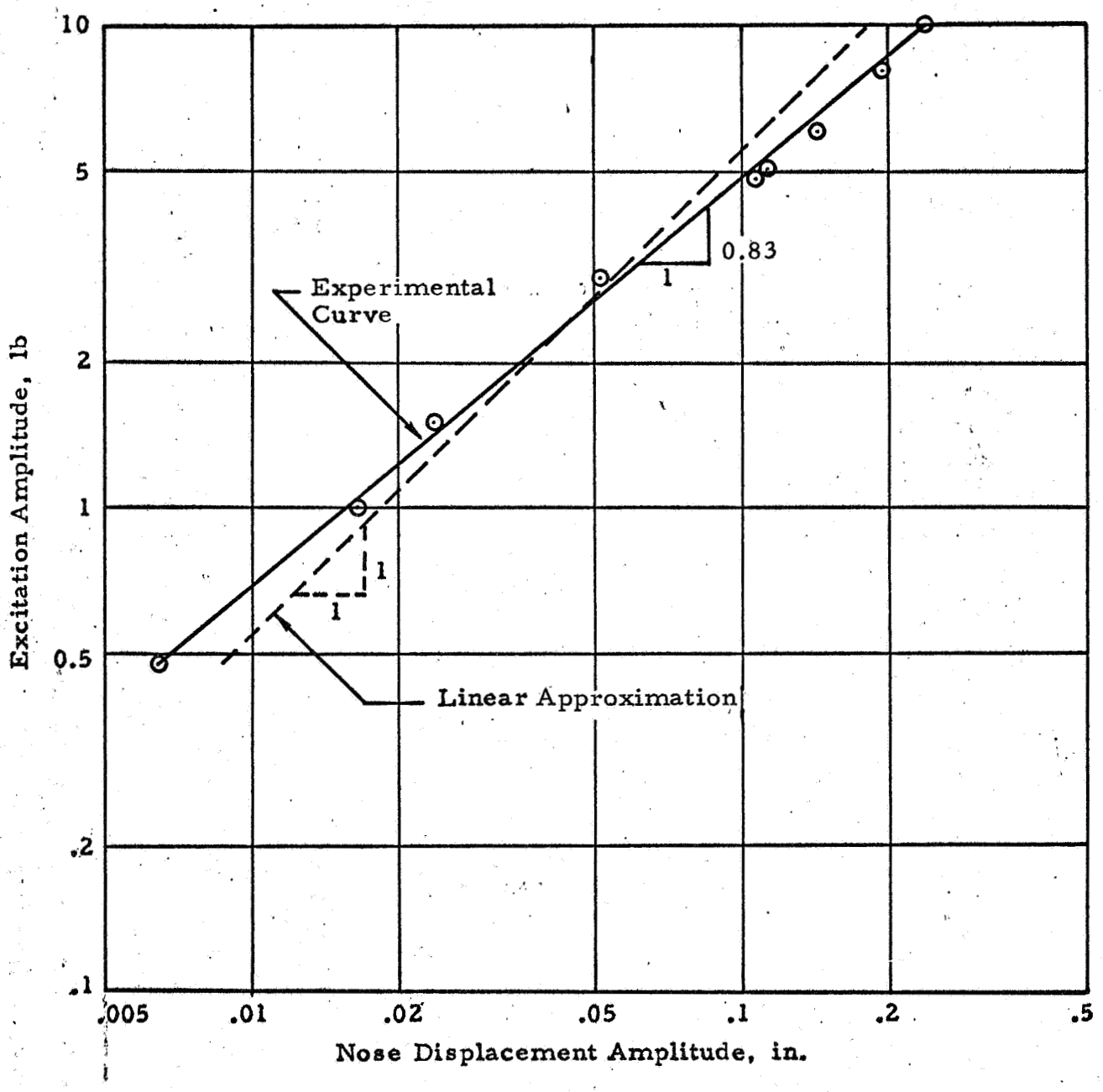

Figure 2-6 - First Mode Resonant Response, Configuration B-1

2.4 COMPARISON OF MEASURED FREQUENCY RESPONSE WITH ANALYTICAL RESULTS

Measured frequency shift and resonant response data for the first mode of Configuration B-1 were used to compute the frequency response of both analytical and experimental results are shown in Figure 2-7 for comparison. It is observed that for frequencies below resonance, analytical results agree with experimental data extremely well. For higher frequencies, however, measured data are greater than analytical predictions. These discrepancies are probably due to the presence of the second bending mode. The presence of out-of-plane modes close to the in-plane modal frequencies tend to make the apparent band width wider and is a second contributing factor to the discrepancies. In general, it may be concluded that good agreement was found between analytical and test results. This indicates that, among other things, the assumption of low viscous damping is justified for the model.

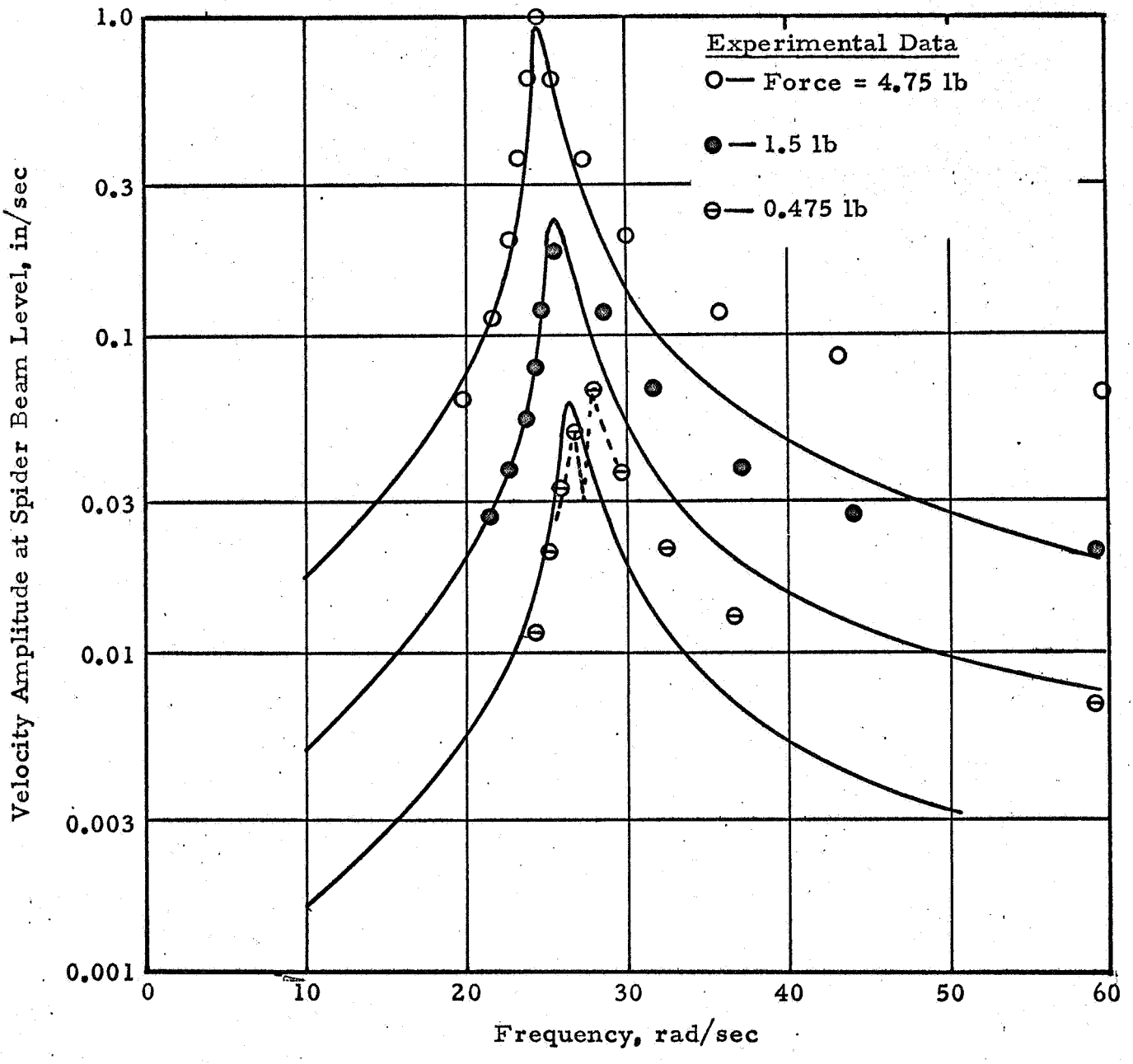

Figure 2-7 - Calculated and Measured First Mode Frequency Response (Configuration B-1)

Section 3
RESPONSE TO RANDOM EXCITATIONS

Experimental random vibration studies were restricted to studies of the first two bending modes of the model in Configuration B-1 (all outer booster tanks on, all tanks empty, no internal pressurization, and "tightened" outer LOX tanks). As discussed in Section 2, the structure behavior was found to be nearly linear. Random responses for the first bending mode are compared with analytical results in this section.

3.1 MEAN-SQUARE MODAL RESPONSE

With a "white noise" excitation spectrum, the mean square modal response of a system with linear structural damping was analyzed by Crandall (Reference 7). The complex restoring force approach mentioned in Section 2 was used. Crandall's result may be summarized as follows:

The equation of motion is

$$m\ddot{x} + k_o(1 + ig)x = N(t) \tag{3.1}$$

where x is the deflection of the point of force application, $i = \sqrt{-1}$, and $N(t)$ a white noise excitation with a constant mean square spectral density S_o.

The complex frequency response for the system is

$$H(\omega) = \frac{1}{m(\omega_o^2 - \omega^2 + i g \omega_o^2)} \tag{3.2}$$

The mean square spectral density $S_x(\omega)$ of the response $x(t)$ is

$$S_x(\omega) = H(\omega)\, H(-\omega) S_o$$

$$= \frac{S_o/m^2}{\left(\omega_o^2 - \omega^2\right)^2 + g^2\, \omega_o^4} \qquad (3.3)$$

For small values of g, the response is narrow band, and the expected mean square of the response is

$$E[x^2] = \int_{-\infty}^{\infty} S_x(\omega)\, d\omega = \frac{\pi S_o}{g m^2 \omega_o^3} \left[\frac{1 + (1 + g^2)^{\frac{1}{2}}}{2(1 + g^2)}\right]^{\frac{1}{2}} \qquad (3.4)$$

The expected mean square of the response velocity is

$$E[\dot{x}^2] = \frac{\pi}{g m^2 \omega_o} \left[\frac{1 + \sqrt{1 + g^2}}{2(1 + g^2)}\right]^{\frac{1}{2}} S_o \qquad (3.5)$$

A linear approximation is selected for the first mode, Configuration B-1, according to Figure 2-6. The 90^o phase frequency of the approximate linear system is assumed to be constant

$$\omega_\phi = \omega_o = 26.8 \text{ rad/sec}$$

Other parameters for the linear system are

$$m = 4.50 \text{ lb-sec}^2/\text{in.}$$

$$k_o = m\omega_o^2 = 3250 \text{ lb/in.}$$

$$g = 0.048$$

$$x_{SB}/x_{nose} = 0.353$$

The coefficient on the right-hand side of Equation (3.5) is

$$\frac{\pi}{g m^2 \omega_o}\left[\frac{1 + (1 + g^2)^{\frac{1}{2}}}{2(1 + g^2)}\right]^{\frac{1}{2}} = 6.20 \times 10^{-3}$$

so that

$$E\left[\dot{x}^2\right] = 6.20 \times 10^{-3} S_o \tag{3.6}$$

The measured mean square velocity response at the nose is shown in Figure 3-1 along with the theoretical response for the linearized system.

The discrepancy between experimental and theoretical results were found to be exactly due to linearization. In other words, given the random experimental data of Figure 3-1, and asked to choose a linear system to approximate the original system, one would end up with an approximation identical to that chosen from sinusoidal data.

3.2 PEAK-RESPONSE UNDER SINE-PLUS-RANDOM EXCITATION

In the investigation of ground-wind induced oscillatory loads on the Saturn V launch vehicle in the prelaunch condition, extensive tests were conducted in the NASA/Langley Research Center's 16-ft transonic wind tunnel on a 3% aeroelastic model. First bending mode damping in a series of tests was simulated by an electromagnetic damper developed by Lockheed/Huntsville (Reference 8). In a particular test, the maximum bending response over a two-minute q-dwell test for various values of damping was obtained. The slope of the line representing test data is steeper than the slope of the line representing the response of a linear system to a sinusoidal excitation.

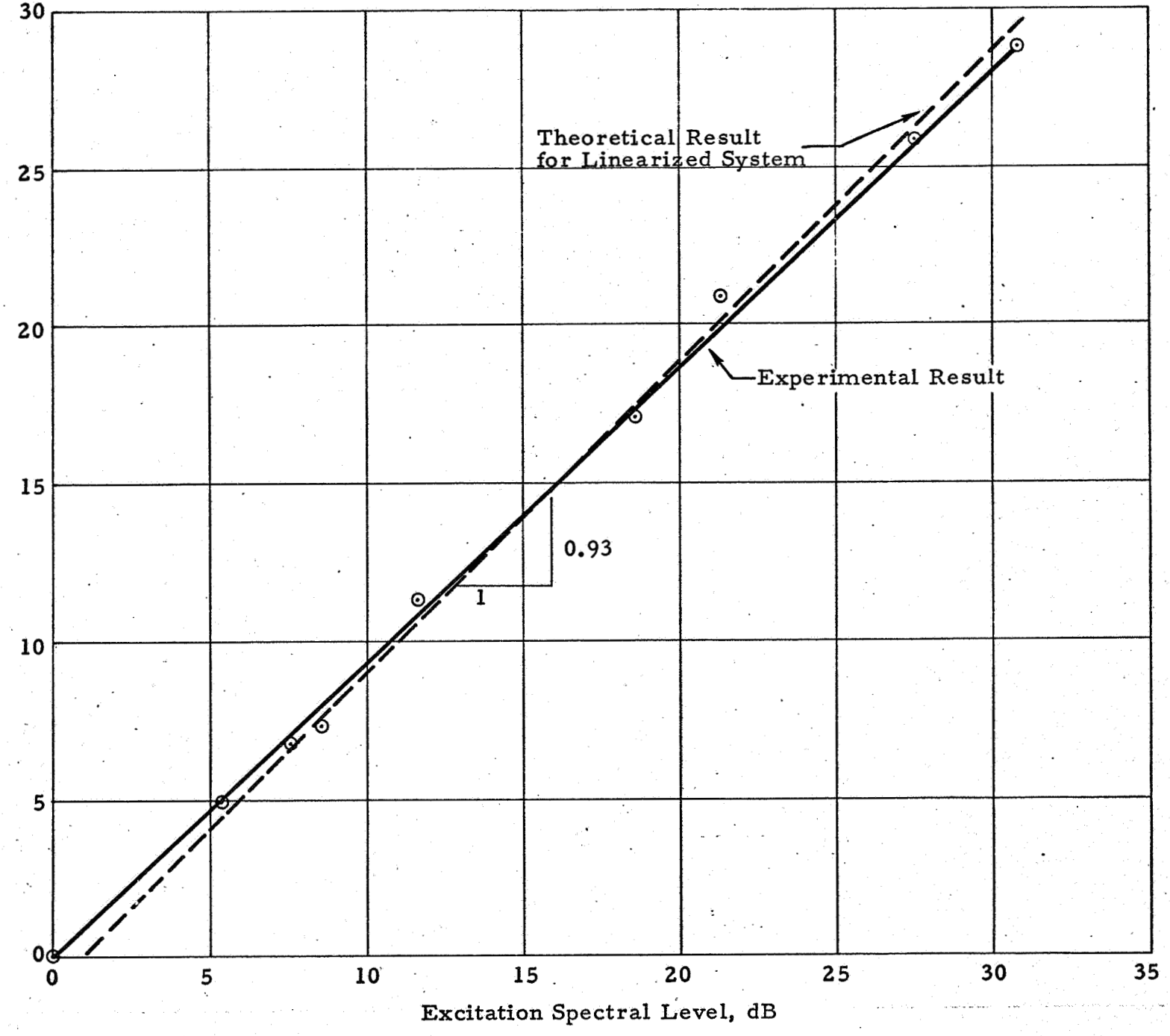

Figure 3-1 - First Mode Mean Square Response, Configuration B-1

There were speculations that the unsteady aerodynamic loading on an oscillatory cylinder could be characterized by a wide band noise, with a sinusoidal component at the natural frequency of the cylinder superimposed. An analysis by Pope (Reference 9) had been made to investigate the possibility that the steeper-than-unity slope of the data curve was due to a sine-plus-random type of excitation. Pope, in Reference 9, concluded that this type of excitation could not produce response peaks of the observed type. In Reference 9, the system is characterized by the linear, modal equation of motion of the form

$$\ddot{x} + 2\zeta \omega_o \dot{x} + \omega_o^2 x = \frac{P_o}{m} \cos \omega_o t + N(t) \qquad (3.7)$$

where ζ = fractional critical damping and all other symbols have previously defined meaning. Further, N(t) is a band limited white noise with zero mean, unity variance ψ_o, spectral level S_o, and bandwidth from zero to ω_c. The mean square response of the system to N(t) only is

$$\psi = E[x^2] = \frac{\pi S_o}{4\zeta \omega_o^3}$$

the mean square response to the sinusoidal excitation is

$$\frac{x^2}{2} = \frac{P_o^2}{8\zeta^2 k_o^2}$$

the input signal-to-noise ratio is defined to be

$$N_o = \frac{P_o/m}{\sqrt{\psi_o}} = \frac{P_o}{m}$$

The output signal-to-noise ratio is

$$N = \frac{x}{\sqrt{\psi}} = \frac{P_o/2\zeta k_o}{\sqrt{\pi S_o/4\zeta\omega_o^3}}$$

The probability density function of the output signal has the form (Reference 10)

$$f(R) = \frac{R}{\psi} \exp\left[-\frac{1}{2}\left(\frac{R^2}{\psi} + N\right)\right] I_o\left(\frac{NR}{\psi^{\frac{1}{2}}}\right)$$

where R is the standardized envelope and I_o is the modified Bessel function of order zero. The probability distribution function is

$$F(R) = \int_o^R f(R)\, dr \qquad (3.8)$$

the 99.99% envelope responses were obtained for various values of ζ and N_o by numerically integrating Equation (3.8). The results are shown in Figure 3-2 along with wind tunnel test data. It is evident from these results that for high damping, the slopes of all curves tend to the value of 0.5, because random responses predominate for high damping. For small damping values, the slope of the peak response curves are different for different values of the input signal-to-noise ratio. At one extreme, N = 0 and the slope of the curve is -0.5 for all values of ζ. At the other extreme, $N^{-1} = 0$ and the slope tends to -1.0. For all other values of N, the limiting slope is between -0.5 and -1.0. In no case was the slope found to be steeper than -1.0.

In the present study, the 1/5-scale model of Saturn was tested with a concentrated sine-plus-random force at various signal-to-noise ratios. Since the damping added to the model was always proportional to the instaneous modal velocity and was truly viscous in nature, assumption of

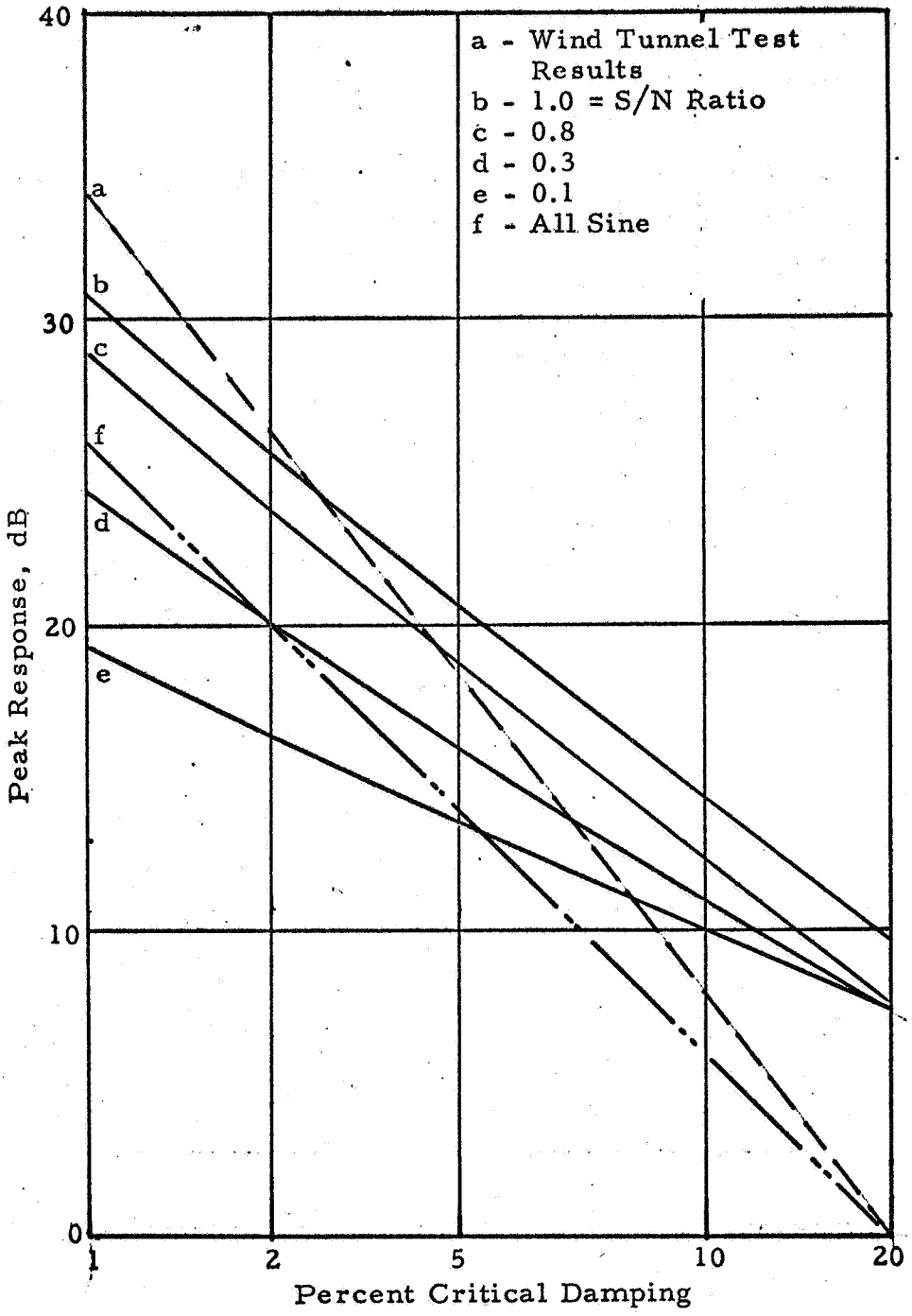

Figure 3-2 - Theoretical Peak Response vs Damping Relationships

viscous damping is justified for the above analyses. (See Appendix B for detailed test procedures.) The resulting peak response vs damping curves are shown in Figure 3-3.

For pure random excitations, the slope of curves A and B (Figure 3-3) are indeed -0.5. The slope for curves for intermediate values of signal-to-noise ratio becomes steeper than -1 for small damping.

Experimental and analytical results, therefore, are different in the present investigation. Furthermore, the disagreement is similar in nature to that found between analyses and wind tunnel test data. Attempts to resolve this situation have not been successful, and the problem provides a challenging task for future studies.

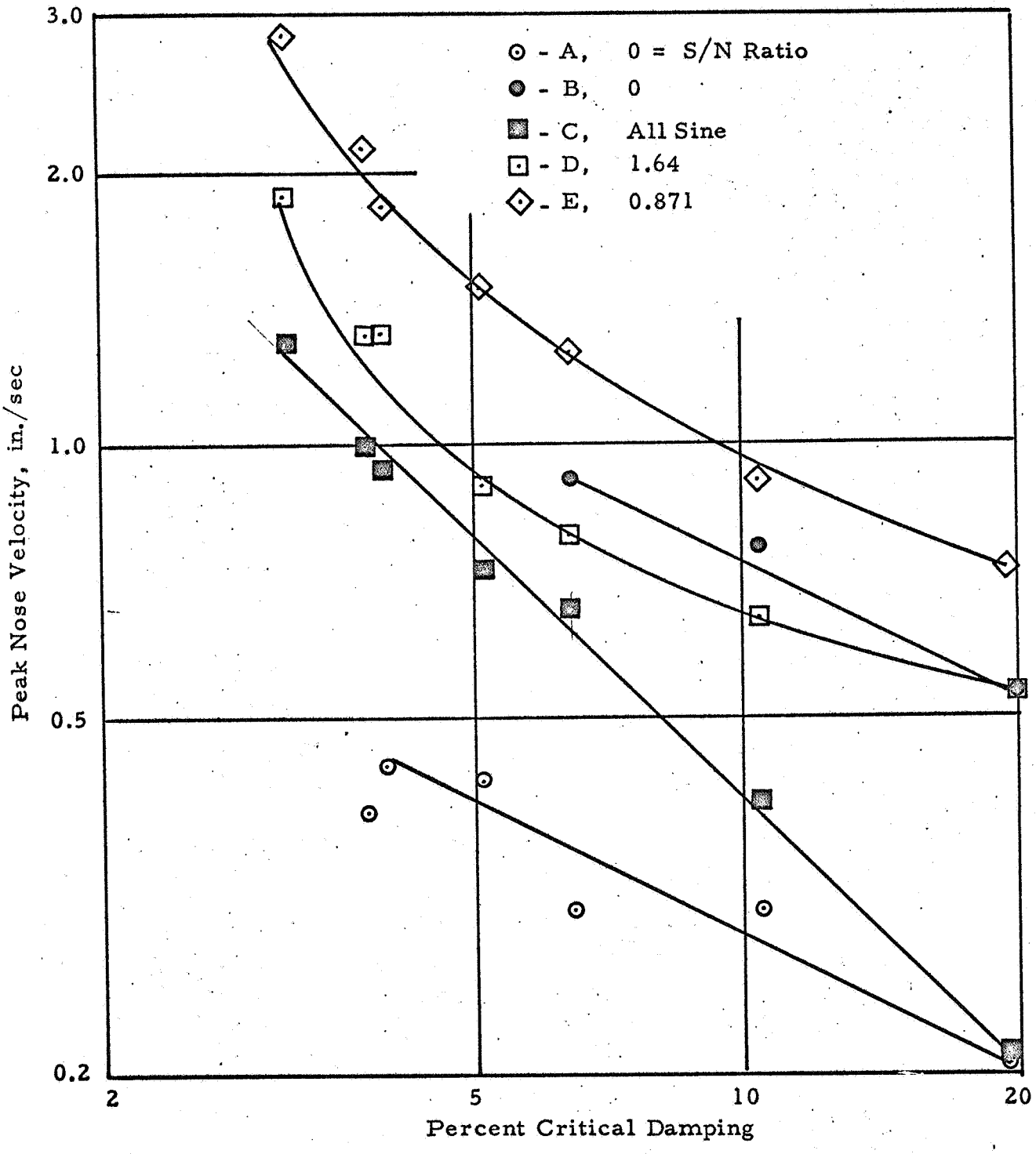

Figure 3-3 - Peak Response vs Damping

Section 4
CONCLUSIONS AND RECOMMENDATIONS

This report described an experimental program to investigate modal responses of the Saturn vehicle type of structures under sinusoidal and random excitations.

Theoretical predictions based on resonant response data are shown to be accurate for both the sinusoidal case and the random case. From the success of these predictions, it is concluded that the necessary and sufficient parameters required to define a bending mode are the generalized mass, the relationship between resonant response and excitation amplitudes, and the relationship between the resonant frequency and the response amplitude. In a particular example used in Section 3, the resonant frequency was assumed constant and equal to the limit of the actual frequency as the amplitude of resonant response approaches zero. Resulting theoretical prediction was shown to agree with experimental data. It may, therefore, be postulated that in general the small-amplitude resonant frequency (a constant) can be used to analyze the responses of the structure in place of the variable resonant frequency without introducing appreciable errors. Since both generalized masses and the natural frequencies of a structure are predictable with good accuracy by presently available analytical techniques, resonant response vs excitation relationships are the only additional information required to specify the modes of vibrations.

According to Equation (2.12), the required information may be directly obtained from the relationship between the energy dissipated per cycle and the deformation amplitude, which for structural damping can be obtained by integration of energy dissipation due to material and joint damping over the volume of the structure, by static testing, by a combination of both, or by dynamic testing.

As a continuation to the present investigation, a study program is recommended to obtain, analytically, the energy dissipation per cycle of vibration from material damping and structural joint damping data for a complicated structure and to use the resulting relationship for modal analyses. An experimental effort should be sustained concurrently with the analytical study to confirm results at all levels of analyses, including a final evaluation of the predicted dynamic responses under various types of excitations.

In the present study, experimental results on response peaks due to sine-plus-random excitations did not agree with analytical predictions. Several explanations, analytical and experimental, are plausible. Further investigations into this area should also be fruitful.

Section 5

REFERENCES

1. Whetstone, D. and M. L. Pearson, "Vibrational Characteristics of Large Complex Space Vehicles," Final Report, Contract NAS8-20161, LMSC/HREC A783589, Lockheed Missiles & Space Company, Huntsville Research & Engineering Center, Huntsville, Ala., 20 December 1966.

2. Chang, C. S., "Damping in Multi-Beam Vibration Analyses," LMSC/HREC A710116, Lockheed Missiles & Space Company, Huntsville Research & Engineering Center, Huntsville, Ala., November 1964.

3. Kiefling, L., "Official Dynamics Data, Tolerances, Damping and Local Effects Estimated for Saturn V Vehicles," NASA/MSFC Memorandum R-AERO-DD-22-67, 19 April 1967.

4. Mixon, Catherine, and Arman, "Investigation of the Lateral Vibration Characteristics of a 1/5-Scale Model of Saturn SA-1," NASA TN D1593, 1963.

5. Chang, C. S. and R. E. Bieber, "Synthesis of Structural Damping," Final Report, Contract NAS8-20387, LMSC/HREC A783875, Lockheed Missiles & Space Company, Huntsville Research & Engineering Center, March 1967.

6. Handbook of Engineering Mechanics, Chapter 61-16, Vibrations, W. Flugge, Editor, p. 61-14, McGraw-Hill Book Co., New York, 1962.

7. Crandal, S. H., "Dynamic Response of Systems with Structural Damping," Contract No. 49(638)-564, AFOSR1561, October 1961.

8. Chang, C. S., "Operations Manual for the Lockheed Electromagnetic Model Damper System," LMSC/HREC A791011, Lockheed Missiles & Space Company, Huntsville Research & Engineering Center, Huntsville, Ala., December 1967.

9. Pope, J. E., "Comparison of Maximum Bending Response of A Saturn V Wind Tunnel Test Model as A Function of Damping with Some Theoretical Results," LMSC/HREC A783443, Lockheed Missiles & Space Company, Huntsville Research & Engineering Center, Huntsville, Ala., 3 November 1965.

10. "Selected Papers on Noise and Stochastic Processes," N. Wax, Editor, Dover Publications, New York, N. Y., 1954.

Appendix A

DESCRIPTION OF TEST SPECIMEN

Appendix A
DESCRIPTION OF TEST SPECIMEN

A.1 SPECIMEN DESCRIPTION

The 1/5-scale structural model of Saturn Launch Vehicle SA-1 was constructed by NASA/Langley Research Center. It was constructed by direct scaling and represents the full scale structure in detail. A thorough discussion of model design, construction, and scaling is contained in Reference 4. This model was tested in the simulated pre-launch configuration in this program. Figure A-1 shows the model in the test towers. A brief description of the model is given in the following:

First Stage: The first stage, or booster, consists of a 21-inch diameter center tank (the Center LOX Tank), surrounded by eight 14-inch diameter outer tanks. Eight outrigger beams at the base and a spider beam network at the top is the supporting structure of all tanks. On the full-scale vehicle, four alternating outer tanks and center tank contain liquid oxygen and the four remaining outer tanks contain fuel. The Outer LOX Tanks and Center LOX Tank support the upper-stage weight in a ratio determined by the preload applied to the Outer LOX Tanks. This preload is a function of torque on the outer tank upper mounting bolts and, for this test, was adjusted such that approximately 40% of the upper-stage weight was supported by the Outer LOX Tanks. The four Outer Fuel Tanks have sliding pin joints at their tops and thus carry no axial loads. Details of outer tank attachments are shown in Figure A-2. All outer tanks and the center tank were pressurized to 4.5 - 5.0 psi and 9.5 - 10 psi, respectively, for this test, except when specifically noted to the contrary.

Second Stage: The main structural member is an outer shell which is supported by the spider beam-adapter assembly at its base, and supports the

third stage at the top. An inner ballast tank is connected to the outer shell by eight radial trusses.

Third Stage: The third stage is a ballast tank which supports the nose cone and simulated payload.

Holddown: To simulate the prelaunch condition of the vehicle, the model was held down at the extremities of the eight outriggers of the simulated thrust structure, see Figure A-3 for some of the holddown details.

Bending stiffness of the model center structure (upper stages, spider beam, center LOX tank and thrust structure) is shown in Figure A-4*, and mass distribution is shown in Figure A-5. Model station reflects the height in inches above the bottom of the simulated engines.

Figures A-6 and A-7 show corresponding properties for the outer booster tanks.

A.2 SPECIMEN TEST CONFIGURATIONS

A.2.1 Test Configuration A

Test configuration A is the model without the outer booster tanks. Water was not added to simulate fuel in this configuration, and there is no air pressure.

A.2.2 Test Configuration B

Test configuration B is the basic test specimen plus the eight outer booster tanks. In this case loading of the LOX tanks was necessary to distribute the weight evenly.

*Obtained from Reference 5.

A.2.3 Test Configuration B-1

Test configuration B-1 is the same as configuration B with the exception that the booster tanks were not pressurized.

A.2.4 Test Configuration C

Test configuration C is the same as test configuration B with the top two tanks (second and third stages) ballasted with water.

A.2.5 Test Configuration D

Test configuration D is the same as test configuration B with all tanks ballasted with water. Water is used as ballast to simulate LOX and fuel. This configuration is comparable to the ground winds problem associated with the 100% fueled condition before liftoff.

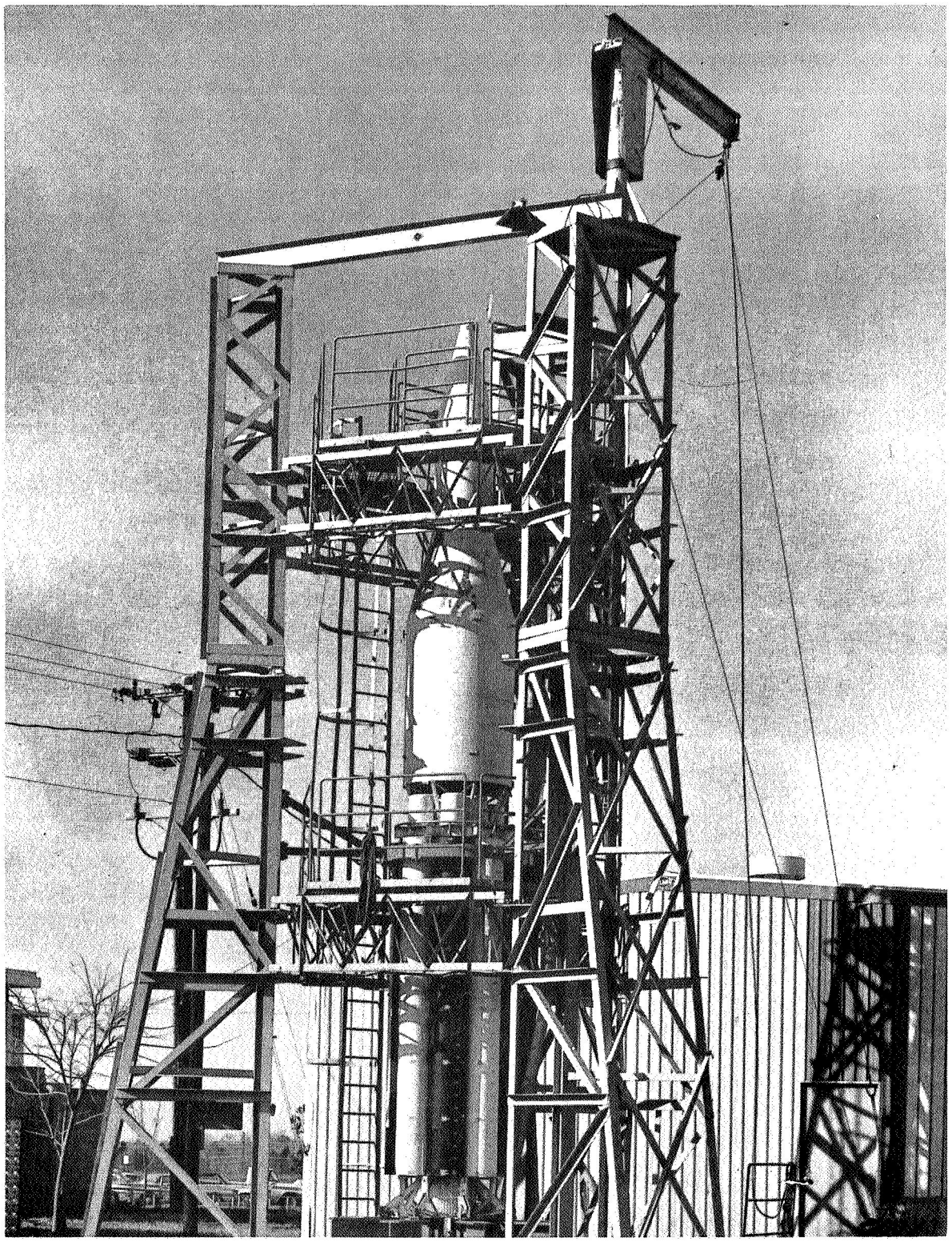

Figure A-1

1/5-Scale Structural Model of Saturn I in Dynamic Test Stand at Lockheed/Huntsville

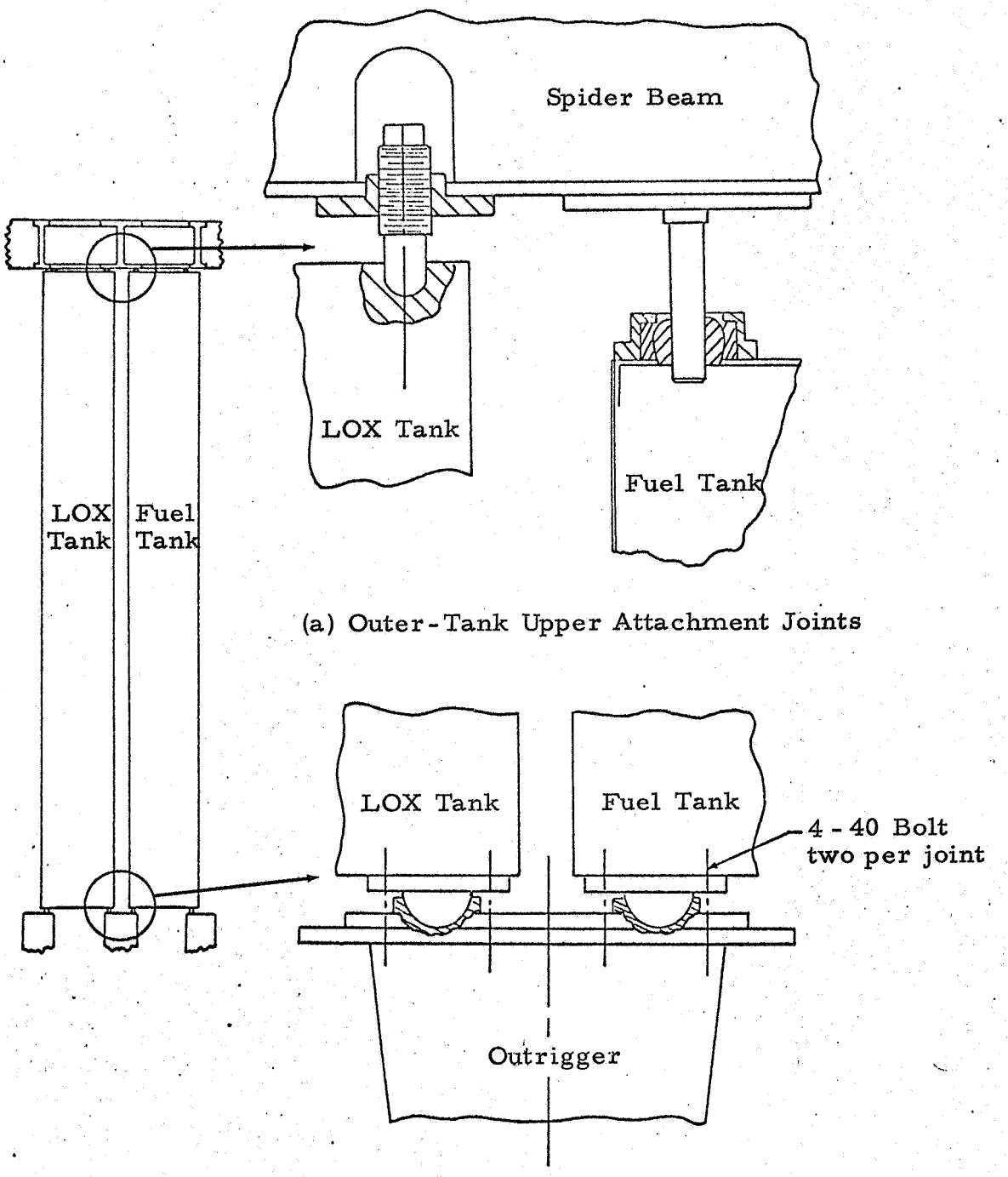

(a) Outer-Tank Upper Attachment Joints

(b) Outer-Tank Lower Attachment Joints

Figure A-2 - Sketch of Outer-Tank Attachment Joints

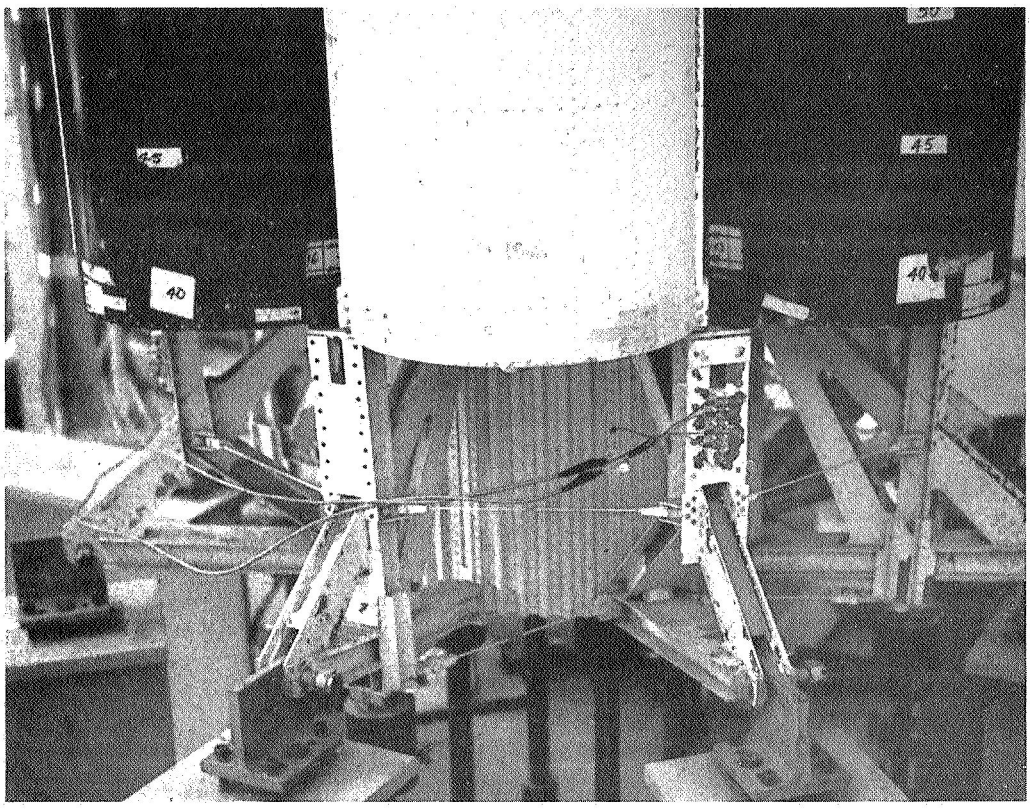

Figure A-3
Base Support

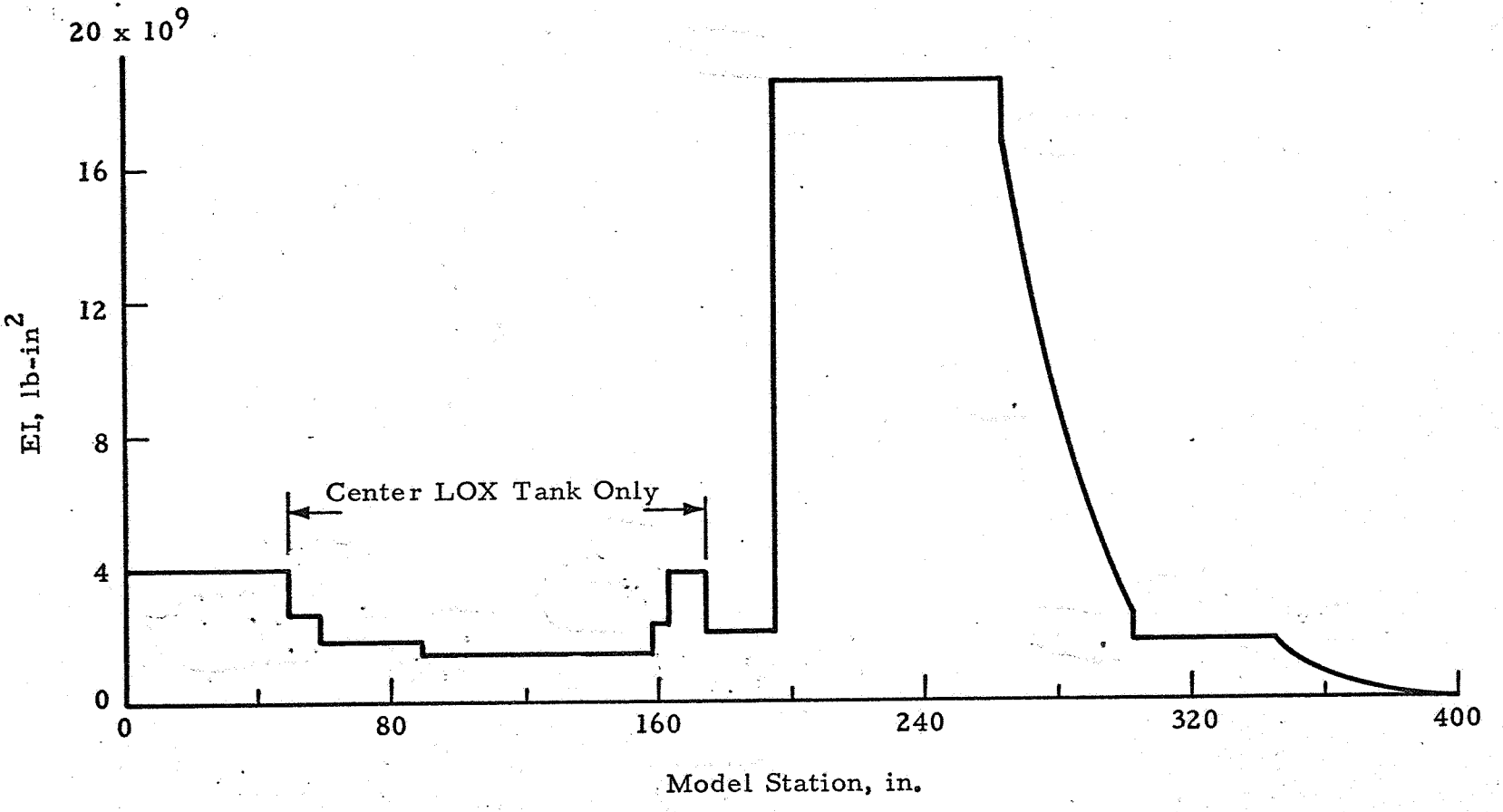

Figure A-4 - Bending Stiffness Distribution of 1/5-Scale Saturn Model

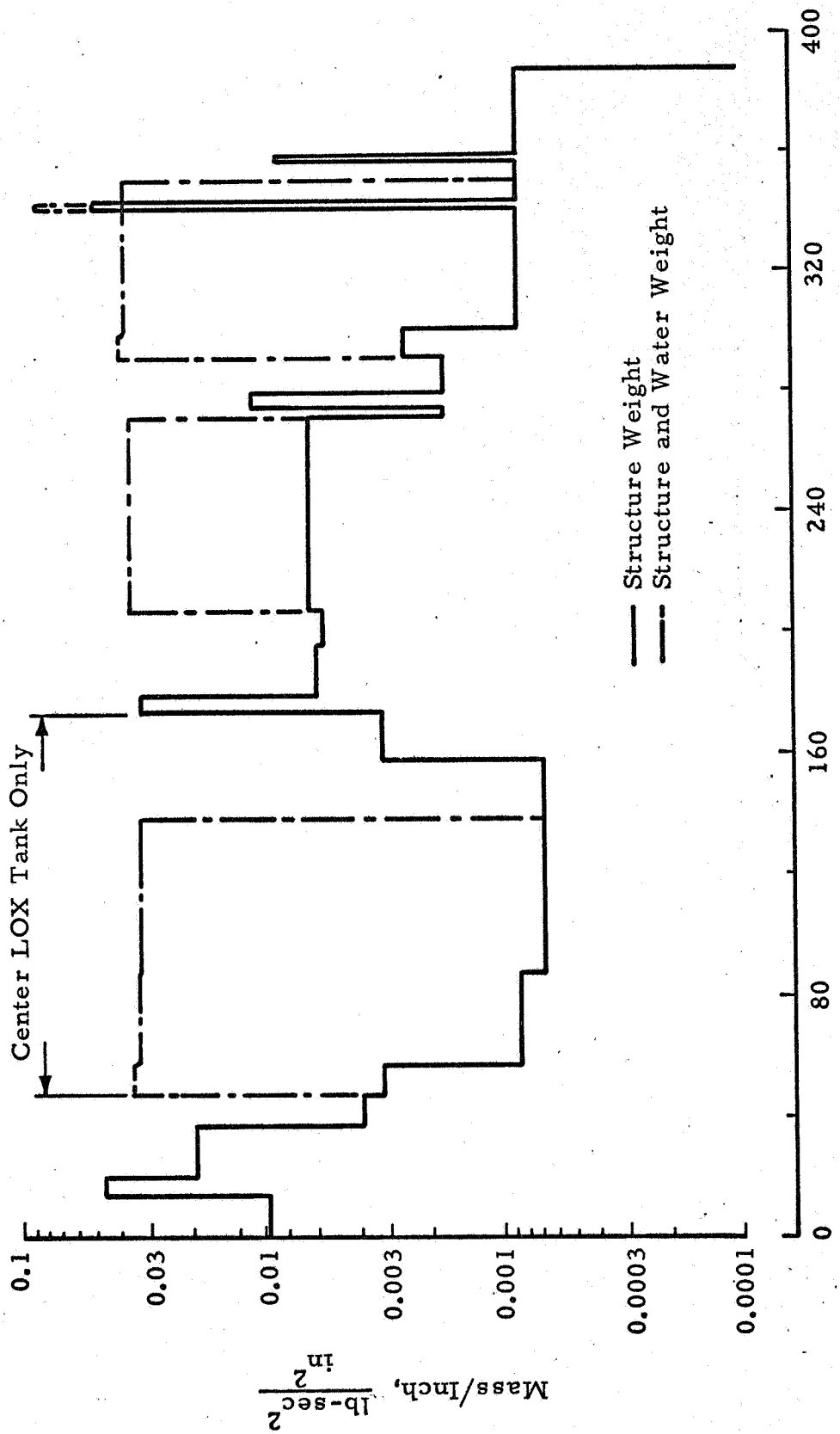

Figure A-5 - Distribution of Mass of 1/5-Scale Saturn Model

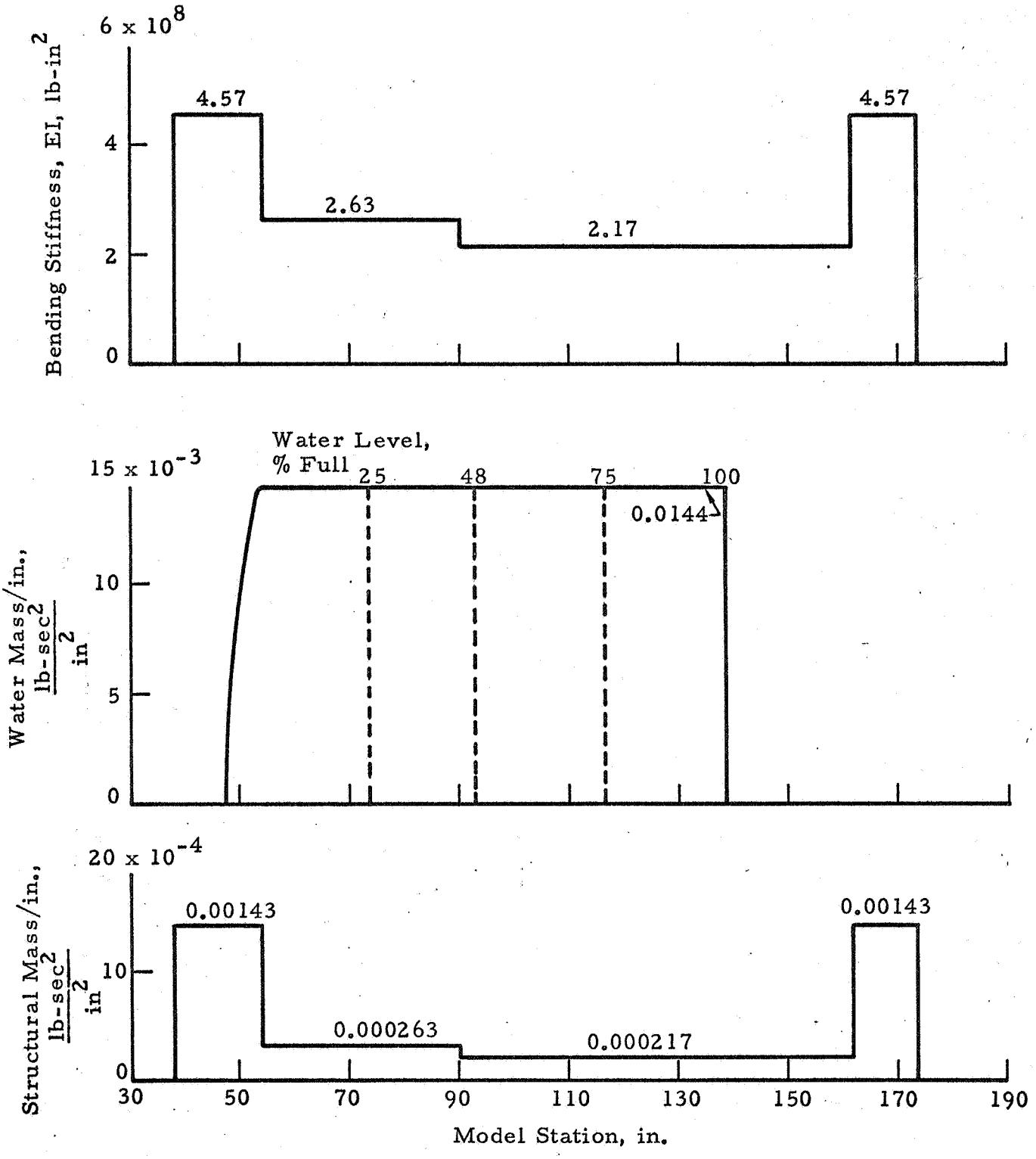

Figure A-6 - Distribution of Mass and Bending Stiffness of Outer LOX Tank: 1/5-Scale Saturn Model; Total Length, 135.5 inches

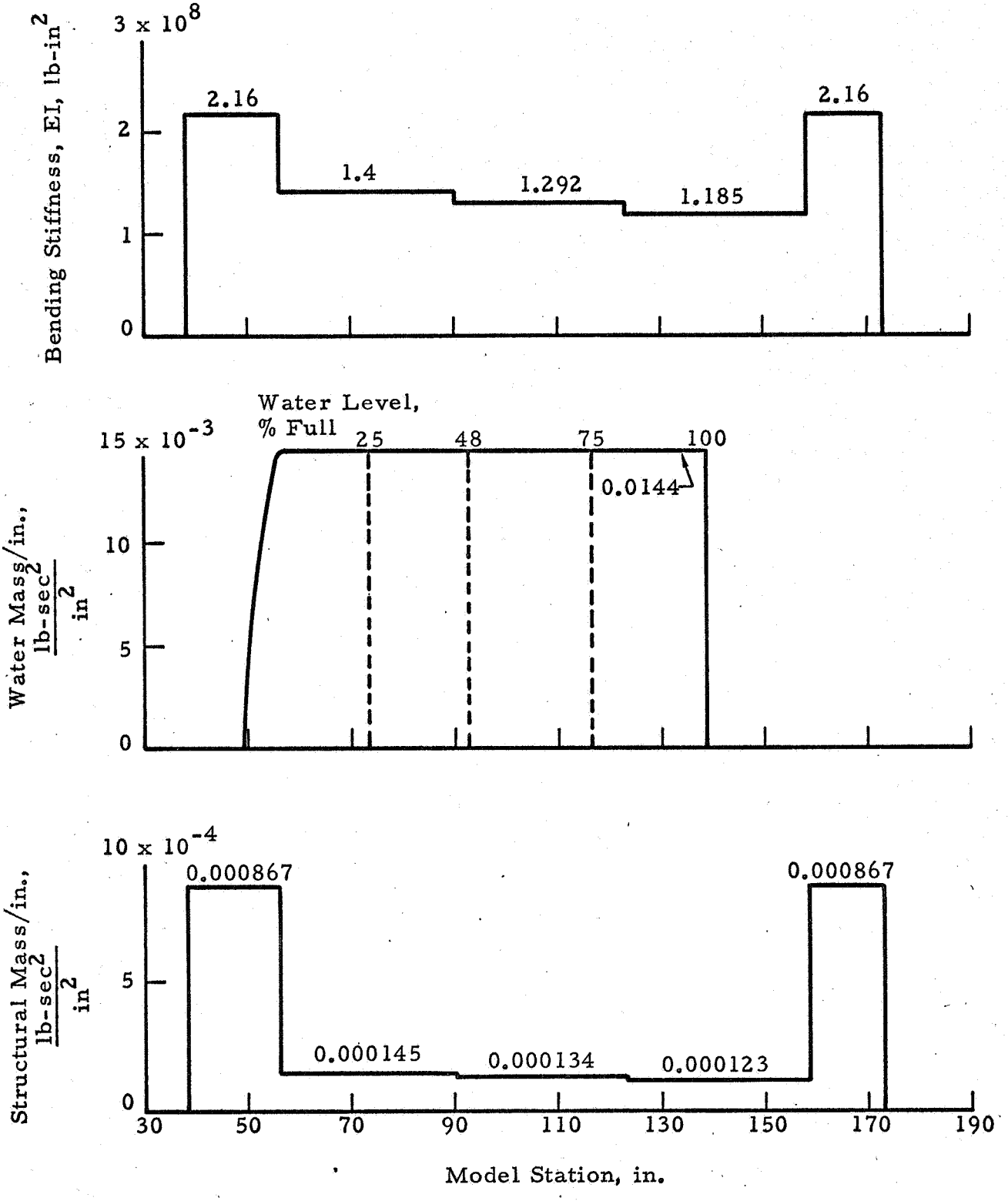

Figure A-7 - Distribution of Mass and Bending Stiffness of Fuel Tank: 1/5-Scale Saturn Model; Total Length, 134.78 Inches

APPENDIX B

TEST SETUP, INSTRUMENTATION AND TEST PROCEDURES

Appendix B
TEST SETUP, INSTRUMENTATION AND TEST PROCEDURES

B.1 EXCITATION

Periodic and random excitations (concentrated forces) were applied to the vertically cantilevered model specimen by electrodynamic force generators (shakers). A single permanent magnet shaker was used to generate the desired horizontal forces in all tests except one, where a second identical shaker was used to provide additive linear viscous damping to the specimen. The shaker has a force capability of 50 pounds (o-pk) and an allowable stroke of 0.35 in. The frequency response of this shaker extends from 0c to some 5,000 cps. Its armature weighs 0.18 lb and it is suspended by two springs with a combined stiffness of approximately 30 lb/in. The shaker armature, therefore, does not materially add mass or spring stiffness to the model.

The shaker was mounted rigidly on a massive steel ring connecting the three test towers. The shaker armature is attached to the "spider beam" of the model between the first and second stages, and is so oriented that the line of action of the applied force is horizontal, and passes through the centerlines of two outer fuel tanks and of the center LOX tank (see Figure B-1).

A strain-gaged force transducer* is located on the spider beam to provide measurements of the applied force. In addition to this force gage and a flexible "shaker rod," a displacement transducer is mounted between the shaker armature and the model to measure displacement responses at the

*All transducers are described in a subsequent section in this appendix.

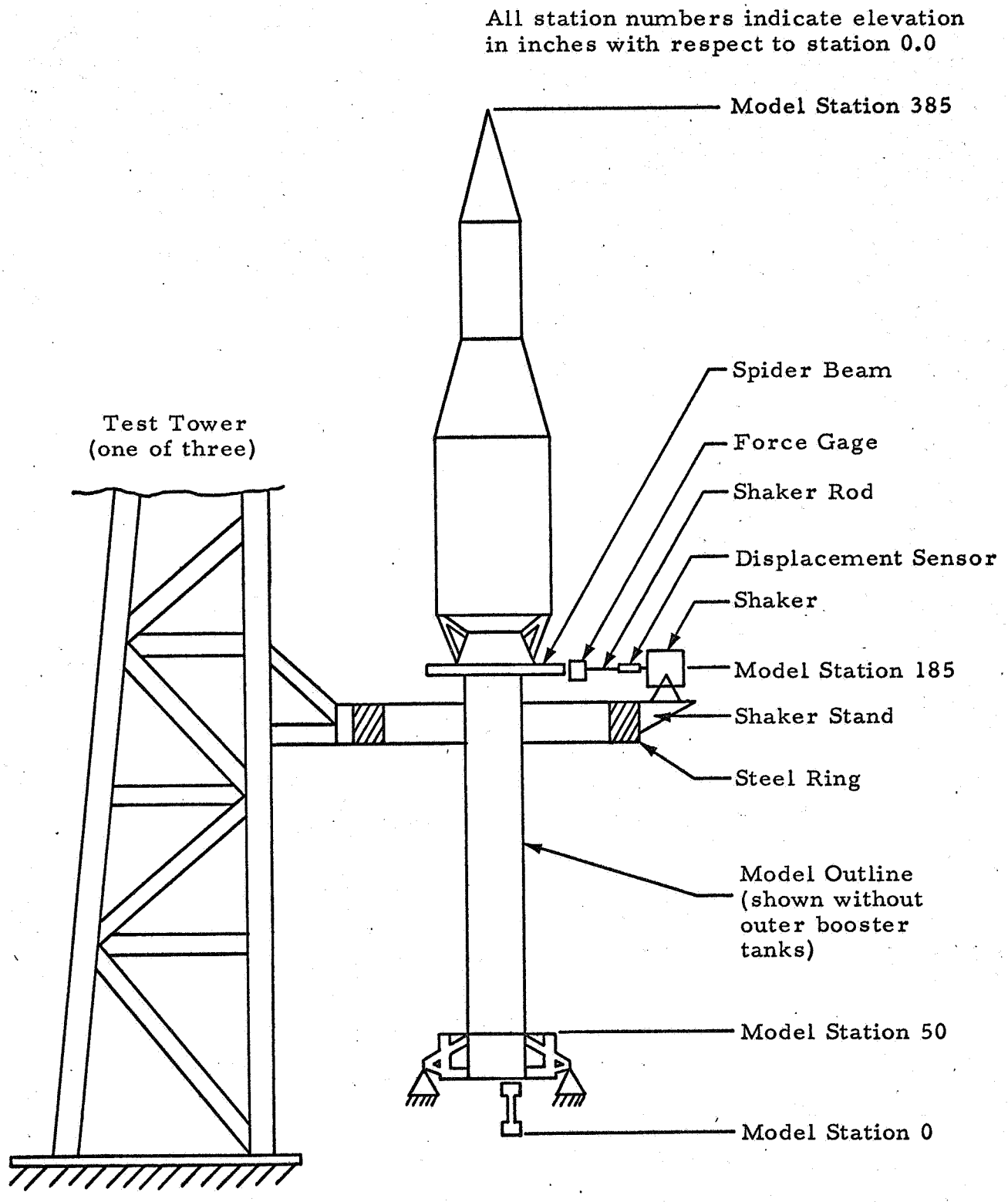

Figure B-1 - Model Outline and Shaker Mounting Schematic

point of excitation. Figure B-2 is a photograph showing details of the mechical connection between the shaker armature and model.

Electrical current needed to generate the force with this shaker is supplied by a 300 volt-ampere power amplifier which has a usable frequency range from 0 to 30 kc. This power amplifier, like most others, delivers a voltage output according to the input voltage signal it receives. Since a resonating mechanical system attached to the shaker armature represents a variable impedance to the power amplifier, the armature current vs input voltage is usually a function of the frequency. Automatic gain control is usually required to compensate for the impedance variations if a constant force level is required and the driving signal for the power amplifier is a constant level voltage source. Figure B-3a shows a typical application where such an amplitude servo is used.

In order to generate a random force with a specified spectrum, elaborate equipment is usually required to solve the problem of sharply varying impedance due to load resonance. Without such equipment (which usually includes a wide band spectrum analyzer and a "Random Vibration Equalizer"), a white noise voltage applied to the power amplifier produces sharp notches and peaks in the resulting force spectrum at each resonant frequency of the test specimen.

A simple but effective method was used in conducting the random vibration experiments in this program. The method is simply to increase the total load impedance of the shaker by a large constant value with a series resistor to decrease the percent change of the load impedance. A very flat force spectrum can be obtained with this arrangement.

Figure B-3b shows a schematic for the basic random excitation system.

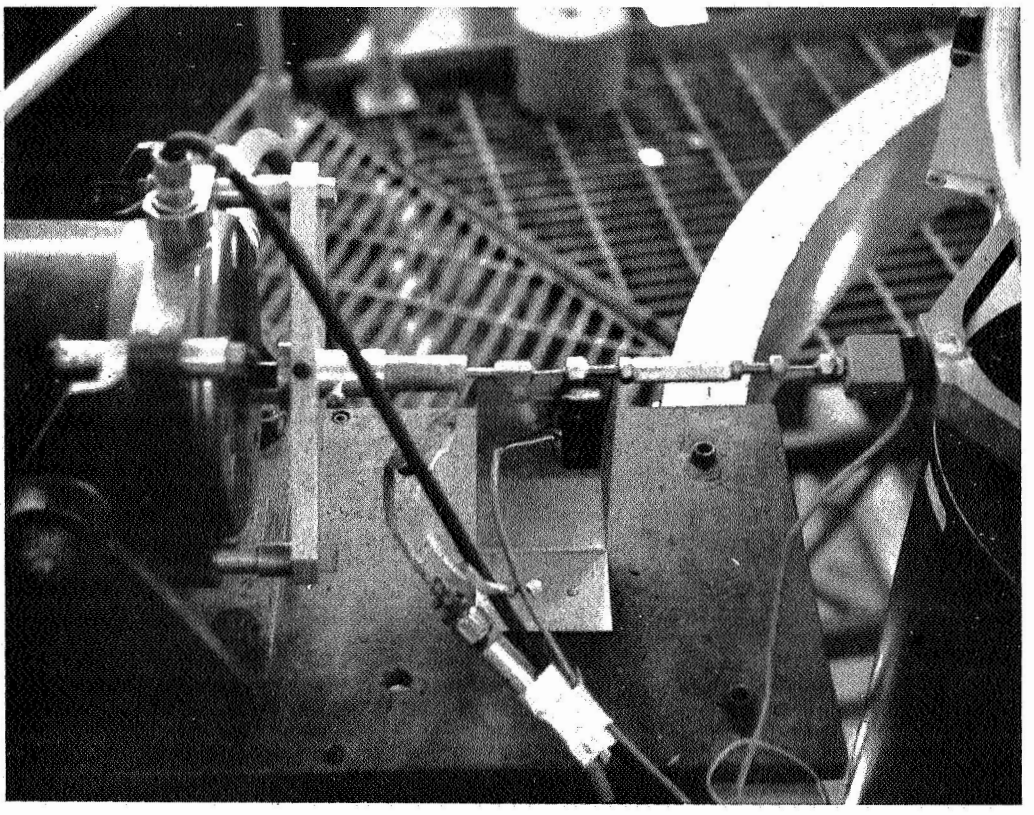

Figure B-2

Shaker Rod Assembly

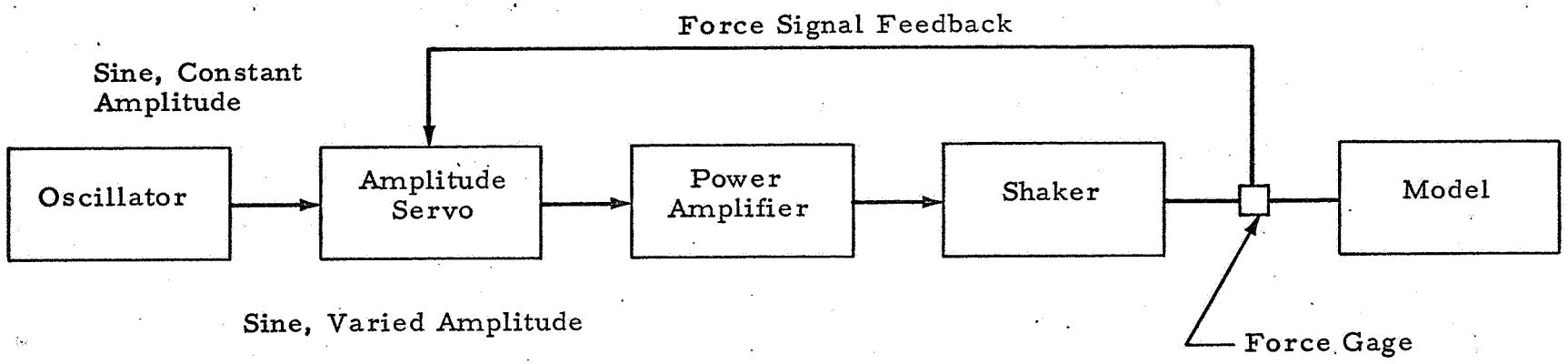

(a) Sine Excitation

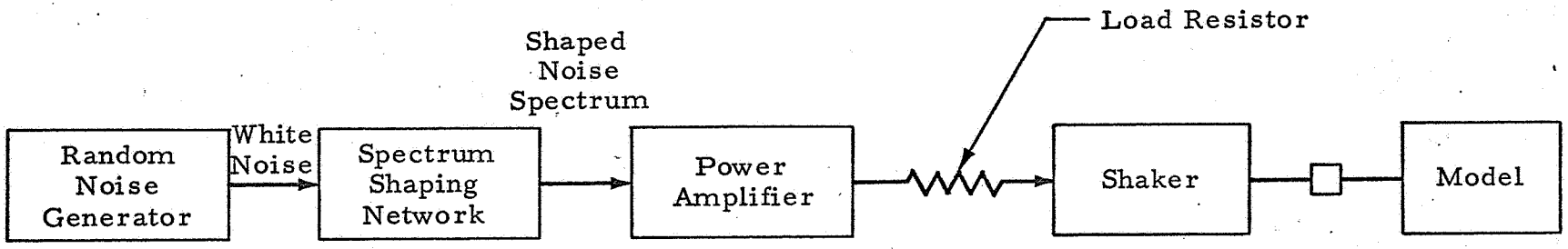

(b) Random Excitation

Figure B-3 - Functional Block Diagrams for Force Generation

B.2 TRANSDUCERS AND INSTRUMENTATION

B.2.1 Accelerometers and Their Locations

A total of 120 piezoelectric accelerometers were manufactured and calibrated under a Lockheed Independent Development Program.* This accelerometer has a fundamental resonant frequency of 5,000 cps and can be used to measure low-level accelerations to frequencies near 1.5 cps while maintaining a true-phase response.

A charge amplifier is used to convert the output charge of the piezoelectric accelerometer to a voltage signal proportional to the instantaneous acceleration experienced by the transducer. The particular charge amplifier used for this purpose has a lower limit on frequency response of 2.0 cps. The charge amplifier gain can be set to produce an overall sensitivity of 5 volts/g for all accelerometers used.

Since more than 100 accelerometers were used for mode shape tests, and only four charge amplifiers were available for conditioning their outputs, (manual) switching was required to share the charge amplifiers. Figure B-4 shows locations of the accelerometers at different stations on the test specimen. There were altogether 78 accelerometers mounted on the model excluding the outer booster tanks. Three accelerometers were used at each station on the model to measure model responses in the direction of excitation and perpendicular to it. Each transducer was attached to the model with its sensitive axis tangential to the model outer wall so that local wall deformations (which is radial) do not introduce an error to the output signal.

A total of 26 additional accelerometers were used to instrument two of the eight outer booster tanks. Using the designation indicated in Figure B-5,

*Chang, C. S., "Development of a Piezoelectric Vibration Transducer," TM 54/50-66, LMSC/HREC A784202, April 1967.

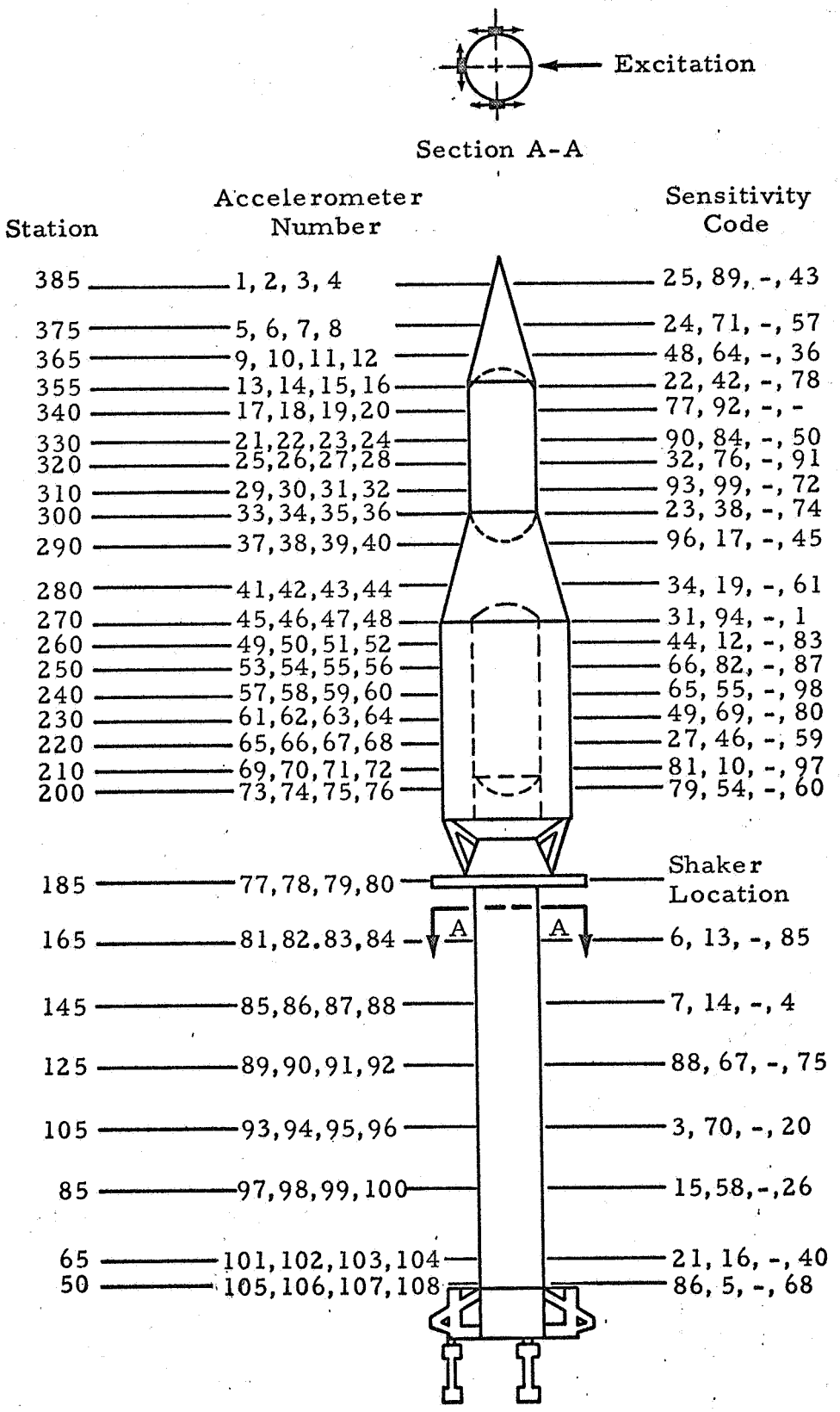

Figure B-4 - Accelerometer Locations in Model Center Structure

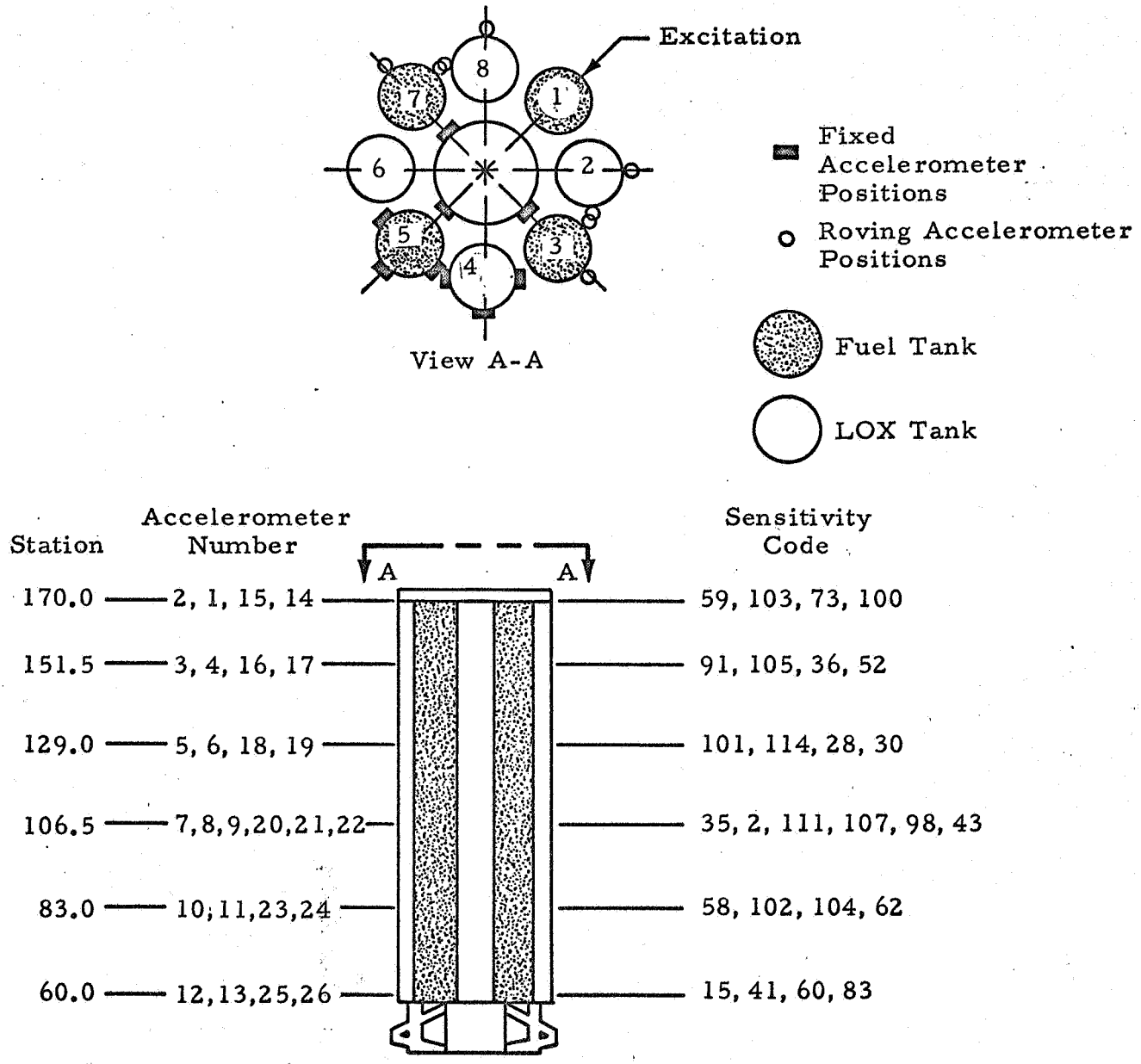

Figure B-5 - Accelerometer Locations on Outer Booster Tanks

LOX Tank 4 and Fuel Tank 5 were the instrumented tanks. Figure B-5 also shows locations of accelerometers on the outer booster tanks. Section A-A in Figure B-5 shows the accelerometer positions on Tanks 4 and 5 as dark rectangles. The circles denote the positions of a roving accelerometer used to measure responses of all other outer tanks at Station 105. Figure B-6 is a photograph of a typical accelerometer mounted on the model. An insulating cement was used for mounting so that accelerometer cases are not electrically grounded to the model.

After all tests were performed for Configuration A, several accelerometers were removed from the model to be used on Tanks 4 and 5. Removal of the accelerometers from the upper stage of the model did not severely affect mode shape measurements there since very little bending or twisting took place near the nose of the cantilevered model.

Individual sensitivity of each transducer is tabulated in Table B-1. The sensitivities are given in terms of output charge (picocoulombs) per unit acceleration (g's).

B.2.2 Velocity Sensor

A velocity sensor was used to provide a convenient signal for determining 90 degree phase conditions between excitation and response. The output of this transducer was also used in many instances for free-vibration damping measurements. The velocity sensor was located on the spider beam diametrically opposite to the shaker rod assembly. It has a calibrated sensitivity of 584 mV/(in/sec). Since the output impedance of this transducer is low (13 kΩ at dc) and since no power supply is required, its sensitivity is least affected by day-to-day environmental changes. This velocity transducer is ideally suited for providing test control signals.

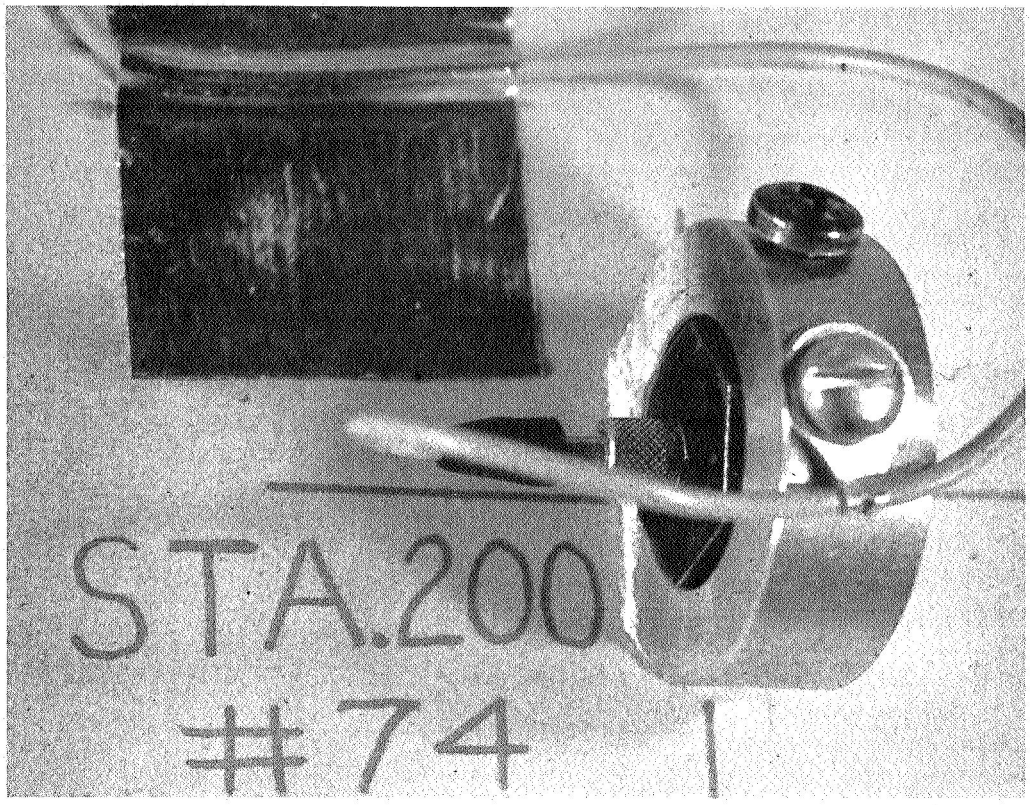

Figure B-6
Typical Accelerometer Mounting

Table B-1

Accelerometer Sensitivity Code and Corresponding Sensitivity

Sens. Code - Sens. pc/g	Sens. Code - Sens. pc/g	Sens. Code - Sens. pc/g	Sens. Code - Sens. pc/g	Sens. Code - Sens. pc/g
1 - 35.5	26 - 29.5	51 - ~	76 - 35	101 - 27.5
2 - 31.4	27 - 29	52 - 32.5	77 - 25	102 - 28.5
3 - 27.7	28 - 28	53 - 31	78 - 26.5	103 - 31
4 - 28.5	29 - ~	54 - 30	79 - 31	104 - 31
5 - 31	30 - 29	55 - 26.5	80 - 33.5	105 - 31
6 - 34.5	31 - 29	56 - 31	81 - 27	106 - 26.5
7 - 25	32 - 31	57 - 28.5	82 - 31	107 - 32
8 - ~	33 - ~	58 - 27	83 - 26.5	108 - 27
9 - 32	34 - 31	59 - 26	84 - 33	109 - ~
10 - 35.5	35 - 25.5	60 - 30	85 - 27	110 - ~
11 - ~	36 - 30.5	61 - 25.5	86 - 33	111 - 27.5
12 - 30	37 - 31	62 - 25.5	87 - 30	112 - ~
13 - 25.5	38 - 31	63 - ~	88 - 26.5	113 - ~
14 - 31	39 - 35	64 - 29	89 - 28	114 - 32
15 - 32	40 - 27	65 - 25	90 - 28	115 - ~
16 - 31	41 - 28	66 - 27	91 - 30	116 - ~
17 - 28	42 - 29	67 - 29	92 - ~	117 - 27
18 - ~	43 - 30.5	68 - 28	93 - 28	118 - ~
19 - 32	44 - 29	69 - 33	94 - 30	119 - ~
20 - 26.5	45 - 29	70 - 29.5	95 - ~	120 - ~
21 - 30	46 - 33	71 - 28	96 - 29	121 - ~
22 - 28	47 - ~	72 - 26	97 - 27.5	122 - ~
23 - 30	48 - 31	73 - 31	98 - 28.5	123 - ~
24 - 31	49 - 29	74 - 29	99 - 31	124 - ~
25 - 35	50 - 29	75 - 30	100 - 28	125 - ~

B.2.3 Displacement Sensor

As indicated in Section B.1, a displacement sensor was also used at the spider beam level to monitor the displacement response. This is of the linear variable differential transformer (LVDT) type. An ac power supply is required, and the output signal of the transducer must be demodulated to provide a displacement proportionate voltage signal. Since the LVDT is a displacement sensor, it is not suited for response measurements at high frequencies where model displacement responses are very small. The primary function of the LVDT is to monitor the stroke of the shaker armature which is largest at low frequencies. The overall LVDT-demodulator sensitivity is fixed and is 4.90 volts/inch.

B.2.4 Force Transducer

Also mentioned in Section B.1 is a force transducer which was used to measure the excitation applied to the model and in case of sine tests, to provide a feedback signal for automatic force amplitude control.

The force transducer uses semi-conductor strain gages as transducing elements. Typical strain gage instrumentation is required to excite and balance this force gage and to condition its output signal. Throughout the tests, an overall sensitivity of 0.2 volts/pound force was used. When used with a carrier preamplifier, forces from 0 to 480 cps can be measured accurately by this system.

B.2.5 Strain Gages

Metal foil type strain gages were used to measure bending moment responses of the model center LOX tank, and to measure outer LOX tank preloads.

The strain gage resistances are nominally 120 ohms and the gage factor, 2.04. Standard strain gage instrumentation was used.

B.2.6 Shaker Armature Current Measurement

A resistor was placed in series with the shaker armature to measure the current in the output circuit of its power amplifier. This current is directly proportional to the force applied to the specimen. In many instances when the instrumentation normally used for the force transducer was needed for other purposes, the armature current signal was used to provide force measurements.

Resistance values from one to 30 ohms have been alternately used depending on specific requirements of tests.

B.3 DATA RECORDING METHODS

Frequency sweep, damping and random vibration tests required continuous recording. The methods are outlined below. For all other tests, direct meter readings were obtained during tests and recorded.

B.3.1 Frequency Sweep Test Data

An x-y recorder was used to record response (or forcing) amplitude versus frequency. A narrow bandpass, tracking filter* was used to filter out practically all but signals of the fundamental frequency which is determined by the excitation frequency. This same equipment also provides a dc output signal proportional to the amplitude of the filtered signal for recording purposes.

The audio oscillator** used to provide the excitation signal also provides dc output voltages which are proportional to the frequency and its logarithm for recording purposes. Using an x-y plotter for the amplitude and

*Spectral Dynamics Corporation's Model SD101A "Dynamic Analyzer."
**Spectral Dynamics Corporation's Model SD 104-5 Sweep Oscillator.

frequency signals, automatic recording of a frequency response test could be obtained by placing the oscillator in the "sweep" mode, i.e., the output frequency of the oscillator being made to continuously vary over a preselected range.

Approximately 80% of frequency sweep data was recorded in the above described manner. For the other 20% of the data, the amplitude of the response was converted into a dB scale (with respect to + 0.1895 Vdc) by a logarithmic converter before recording on the x-y plotter.

B.3.2 Damping Data

Free vibration decay data were recorded with an oscillograph. The instantaneous response signal or the logarithm of the response signal was recorded as a function of time.

An alternate method of recording free-vibration damping data was to make a photographic record of the signal as it was displayed on the screen of a CRT oscilloscope. The later method, of course, did not provide as much resolution and accuracy and was used only in cases when the oscillograph was not available.

B.3.3 Random Time History

Random response time histories were recorded on magnetic tape. FM recordings were made for random test data for later analyses. Because of the low frequency nature of the data, they were recorded at the slowest tape speed possible (1-7/8 ips) so that a maximum ratio of playback to recording speeds may be realized (32 to 1) during analysis.

B.4 TEST PROCEDURES

B.4.1 Frequency Response

For each specimen configuration, frequency response curves were obtained at several excitation levels. The frequency range covered in most of the frequency response tests was from 2.0 cps to 120 cps. During the last part of the program, additional frequency responses were obtained with the frequency scale greatly expanded on the x-y plotter to produce velocity frequency response curves from 2.0 cps to 30 cps in detail.

In all frequency sweep tests, the force level was kept reasonably constant by using an automatic amplitude control equipment.* The normal operating frequency range of this unit is from 5 cps to 10 kc. When used below 5 cps, it does not hold the force completely constant. Rather, a gradual force increase from 5 cps downward was always observed. However, this automatic level control can still even out any sharp peak and notch even at frequencies well below the specified limit of 5 cps. For each set of frequency sweep tests (i.e., for each test configuration) a record of force amplitude vs frequency was made to: (1) check that the force amplitude was, indeed, kept reasonably constant through the test frequency range; and (2) to obtain force ratios for correcting frequency response data at low frequencies where the amplitude control unit does not perform ideally.

Following each force sweep, acceleration response curves of several points on the specimen under one force level, and at the nose of the model under several force levels were obtained in sequence.

Figure B-7 is a functional block diagram showing frequency response test setup.

*Spectral Dynamics Corporation's Model SD 105, Amplitude Servo/Monitor

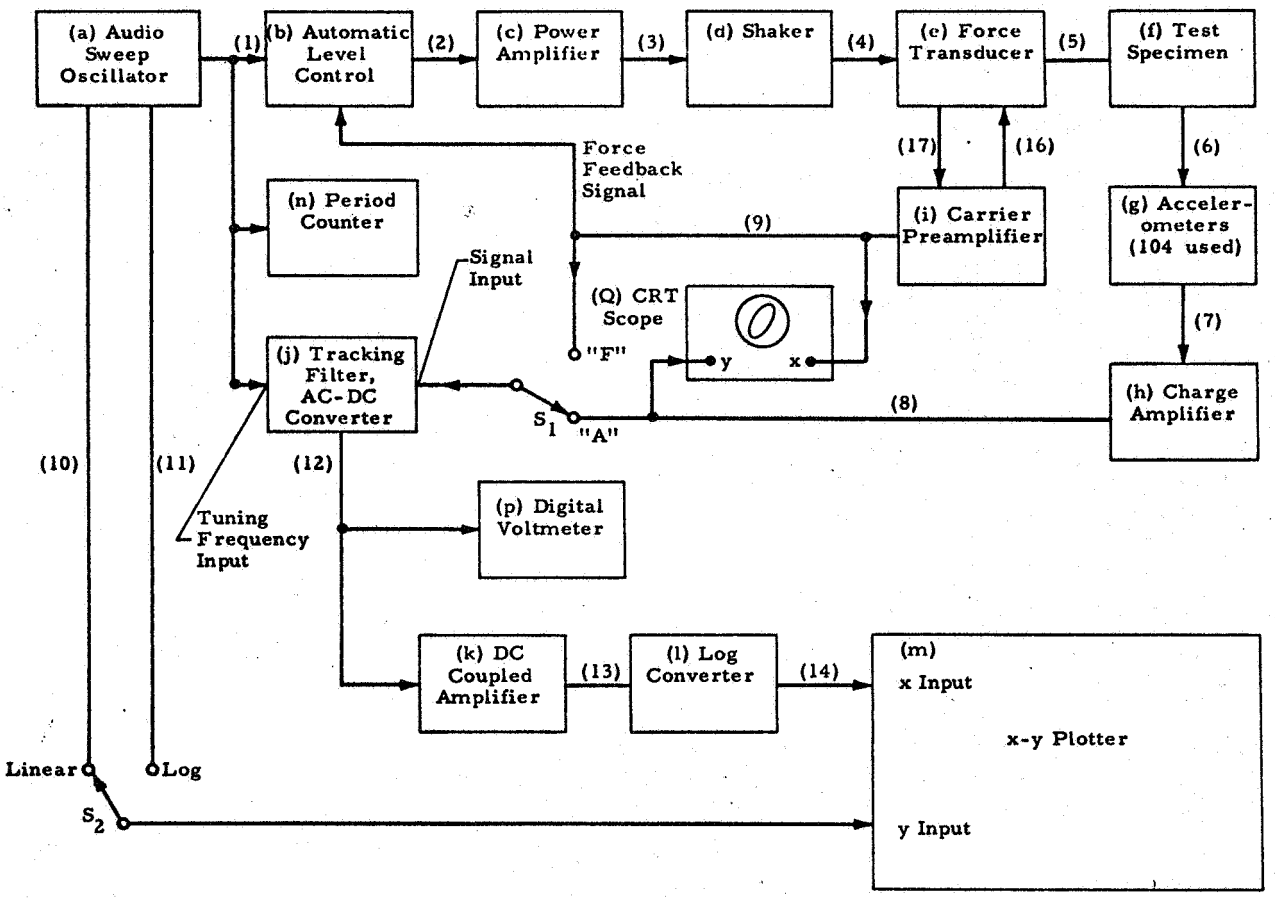

Signal Identification

1. Sine signal (voltage) constant amplitude, 2 - 120 cps
2. Sine signal (voltage) compensated amplitude, 2 - 120 cps
3. Sine signal (current), 2 - 120 cps
4. Force
5. Force
6. Acceleration
7. Acceleration signal (charge)
8. Acceleration signal (voltage)
9. Force signal (voltage)
10. dc voltage proportional to frequency
11. dc voltage proportional to log (frequency)
12. dc voltage proportional to amplitude of input signal
13. Signal (12) amplified
14. Log signal (14), 0 dB = 0.1895 Vdc

Equipment List

a. Spectral Dynamics SD104A-5 (sweep oscillator)
b. Spectral Dynamics SD105 (amplitude servo/monitor)
c. Ling TP300 power amplifier (300 VA)
d. Ling-Goodman VG 50 vibration generator (J_o lb force)
e. Schaevitz-Bytrex JP 50 (force transducer)
f. 1/5-scale Saturn I model
g. Piezoelectric accelerometers (LMSC/HREC)
h. Endevco 2713A (charge amplifier)
i. Hewlett-Packard/Sanborn 350-1100B (carrier preamplifier)
j. Spectral Dynamics SD101A (dynamic analyzer)
k. Philbric USA-3 (operational amplifier)
l. Hewlett-Packard/Sanborn 350-1400 (log preamplifier)
m. Hewlett-Packard 7000A (x - y plotter)
n. Beckman 7350 (universal EPUT and timer)
p. Nonlinear Systems 481 (digital voltmeter)
q. Hewlett-Packard 141A (MEM Scope)

Figure B-7 - Frequency Response Instrumentation Block Diagram

Frequency response data curves are shown in Appendix C according to test configuration.

B.4.2 Mode Shape

Bending vibration mode shapes under steady-state resonance were measured for each specimen configuration. Resonance for each mode was first determined by tuning the excitation frequency until either the acceleration response signal was 90 degrees out of phase with respect to the force or the velocity response signal was in phase with force (an x-y oscilloscope was used for this purpose). Once resonance at a force amplitude was established, the output amplitude of each piezoelectric accelerometer was read in rapid succession by manually switching transducer leads to the input of the charge amplifiers. The excitation and monitor equipment used for mode shape survey was essentially the same as that used for the frequency sweep test shown in Figure B-7. The log preamplifier and the x-y plotter were not used. Acceleration amplitudes were measured by the Dynamic Analyzer and read with the aid of a digital voltmeter. The frequency was measured by a digital period counter.

Mode shape data were recorded, and IBM input cards punched directly from this record. A digital computer program had been used to compute the normalized (with respect to the nose amplitude) deflection at each measured modal station. Both in-plane and out-of-plane components of response amplitudes were computed from the readings of the three tangentially mounted accelerometers at each station. Mode shapes were plotted using the NASA/MSFC SC-4020 plotter.

For resonant frequencies below 3.0 cps, the time constant of the smoothing filter of the output stage of the ac-to-dc converter in the SD 101A Dynamic Analyzer was not sufficiently long and the amplitude representing signal fluctuated to make it difficult to take data. In such cases, the RC time constant was increased by a 1 megohm series resistor and a 60μf shunting capacitor to improve the reading capability.

Mode shape data are collected in Appendix C according to test configurations.

B.4.3 Resonant Response

Relationship between excitation and response amplitudes at steady-state resonance was measured for each configuration for the first two or three bending modes. The same instrumentation used for mode shape survey was used for this test. For each mode, the steady-state nose acceleration was measured at 90-degree phase frequency (between force and acceleration) at many force amplitudes. The range of force amplitudes covered was usually the same as that used for the frequency sweep tests for each specimen configuration and was usually 30 dB or more.

The 90-degree phase frequency for each measured point was always recorded so that: (1) displacement amplitudes may be calculated from data; and (2) a relationship between 90-degree phase frequency and resonant response displacement amplitude can be defined for each mode.

Curves showing results of this resonance dwell test are summarized in Appendix C.

B.4.4 Generalized Mass

Generalized mass for each of the first two or three bending modes was measured for each specimen configuration. The method of measurement is based on the following principle:

For the n^{th} mode of vibration of a beam-like structure in bending the generalized mass

$$m_n = \int_0^{\ell} \left[m(x)\, \phi_n^2(x) + J(x)\, \psi_n^2(x) \right] dx$$

where x is the axial coordinate, m(x) the mass per unit length of the beam at x, J(x) the mass moment of inertia at x, $\phi_n(x)$ the bending deflection mode shape, and $\psi_n(x)$ the bending slope mode shape. The peak kinetic energy for the structure responding entirely in the n^{th} mode is

$$T = \frac{1}{2} m_n \omega_n^2 q_n^2 \tag{B.1}$$

where ω_n is the model frequency and q_n the model response amplitude.

If a small mass, δ_m, is added to the beam at $x = x_o$, and if the addition of δ_m does not introduce a corresponding change in J(x), and furthermore, if δ_m is sufficiently small such that it has negligible effect on $\phi_n(x)$ and $\psi_n(x)$, then the new generalized mass is

$$m'_n = m_n + \phi_n^2(x_o)\, \delta_m$$

The new peak kinetic energy is

$$T = \frac{1}{2} m'_n \omega'^2_n q'^2_n \tag{B.2}$$

where ω'_n is the new model frequency, and q'_n the new model response amplitude. Since $\phi_n(x)$ and $\psi_n(x)_V$ are assumed unchanged by the addition of δ_m, the peak potential energy, for response in the n^{th} mode of the structure would also remain unchanged if

$$q'_n = q_n \tag{B.3}$$

since

$$T = V \tag{B.4}$$

and

$$T' = V \tag{B.5}$$

The following relationship is obtained from Equations (B.1) through (B.5)

$$m_n \omega_n^2 = \left[m_n + \phi_n^2(x_o)\, \delta_m\right] \omega_n'^2$$

or

$$m_n = \frac{\phi_n^2(x_o)\, \delta_m}{2\, \delta_\omega / \omega_n} \qquad \text{(B.6)}$$

where $\delta_\omega = \omega_n - \omega_n'$. The generalized mass can, therefore, be measured by adding a known, small mass δ_m at $x = x_o$, and measuring the resulting change of the model frequency, while keeping the model response amplitude constant.

In practice a series of small weights can be successively added to and subtracted from the structure and a curve plotted between $\phi_n^2(x_o)\, \delta_m$ and δ_ω / ω_n. According to Equation (B.6), the slope of this curve at $\delta_m = \delta_\omega = 0$ is a measure of the generalized mass. During the test program, the frequency at which the phase difference between response acceleration and the forcing function was 90 degrees, was used as ω_n, the model frequency for the generalized mass test.

For test configurations A and B, weights were added to the model at the spider beam (shaker) level for generalized mass tests. For specimen configurations C and D weights were added to a higher station to obtain measurable frequency changes (up to 5% variations).

Test setup for generalized mass measurement is similar to that shown in Figure B-7. In addition, the modal response was kept constant by monitoring the output at the displacement transducer (LVDT) mounted on the spider beam level, and by making necessary changes of the excitation level. For the second and third bending modes, it was found that adjustment of the excitation level was not necessary.

Results of generalized mass measurements are presented in Appendix C according to test configurations.

B.4.5 Damping

The energy dissipated per cycle of vibrations of the model in each of the modes studied was measured by the decay of free vibration after the model has been brought up to steady-state resonance in the mode of interest by suitable sinusoidal excitation. Energy dissipation per cycle at resonance can also be calculated by the amount of work done by the excitation force over a cycle of response at resonance.

The test setup for damping measurements was essentially the same as that used for resonant response measurements. Excitation was removed after steady-state resonance had been reached by opening the power amplifier-to-shaker armature circuit.

Open circuiting the armature ceases the current flow and hence, removes the exciting force immediately.

Instrumentation employed to record damping data are shown in the functional block diagram of Figure B-8. A log converter* was used so that equal measurement resolution is obtained for a range of response amplitude of 50 dB. A low pass filter was usually employed to eliminate most of the unavoidable high frequency mechanical and electrical noises in the signals being recorded. Use of low pass filters was found to be necessary to measurement accuracy. Care was exercised to make sure that filters (or any other equipment in the signal path) did not introduce errors into the damping data. Signals from accelerometers, the velocity sensor, the displacement sensor and strain gages were alternately used for damping measurements.

*Only signal levels above + 0.1895V are converted to a dB scale by this electronic device. For damping tests, only positive peaks need to be measured and this converter performed satisfactorily.

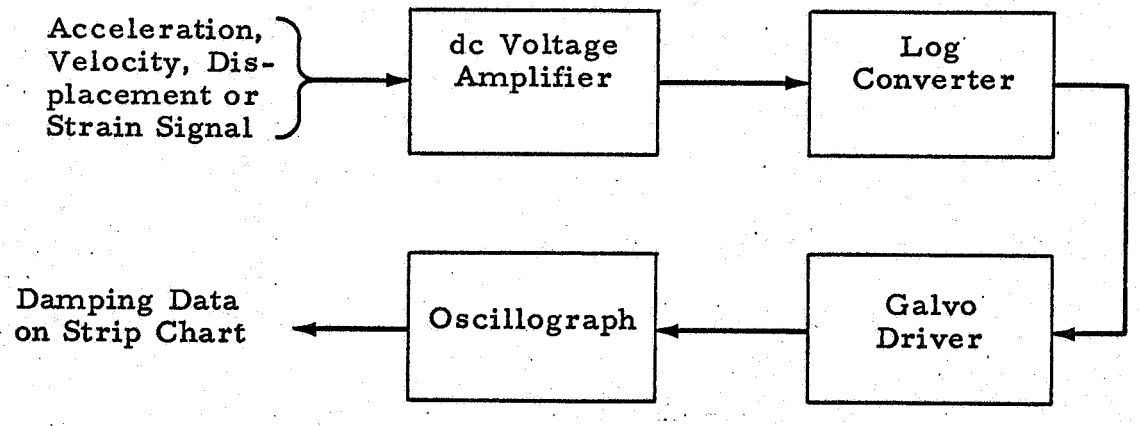

Figure B-8 - Equipment for Recording Damping Data

Figure B-9 shows an exceptionally "good" damping trace obtained with positive signals above + 0.1895 volts converted to a dB scale. The relatively constant slope of the response peaks of the illustration in Figure B-9 indicated that damping is constant over the response range recorded. Damping data were read from oscillograph recordings.

B.4.6 Random Vibration Tests

Three types of random vibration tests were conducted for the model with all outer booster tanks on, empty, and without internal pressurization. They are: (1) spectrum response; (2) peak response vs damping; and (3) mean square response vs excitation spectral level. Procedures for each test are discussed individually in the following.

B.4.6.1 Spectrum Response

Time histories of velocity responses of the model under Gaussian white noise excitation were recorded on FM magnetic tape for spectrum analysis purposes. Figure B-10 is a functional block diagram showing test setup for this purpose.

The random noise generator provided a Gaussian signal source that had a band-limited white noise spectrum (0 - 120 cps). A low-pass filter (0 - 27 cps) was used to further reduce the spectrum width so that only the first two bending modes of the specimen could be excited. The 20-ohm series resistor in the power amplifier-shaker circuit served two purposes: it minimized the peaks and notches in the force spectrum due to specimen resonance,* and it provided a voltage signal which was a direct measure of the force being applied to the specimen.

*The peak-to-notch force ratio for the first specimen resonance was improved from 1.20 to 1.04 by this series resistor, as determined by a sine sweep test.

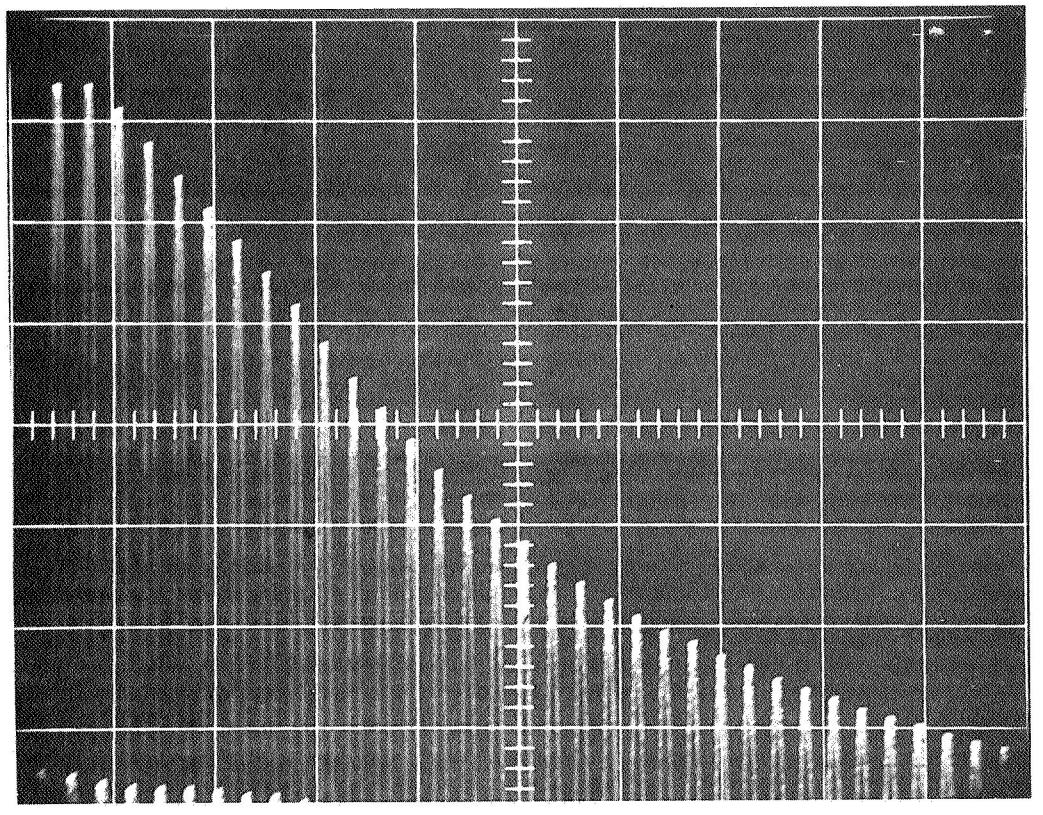

Figure B-9

Typical Free Vibration Decay

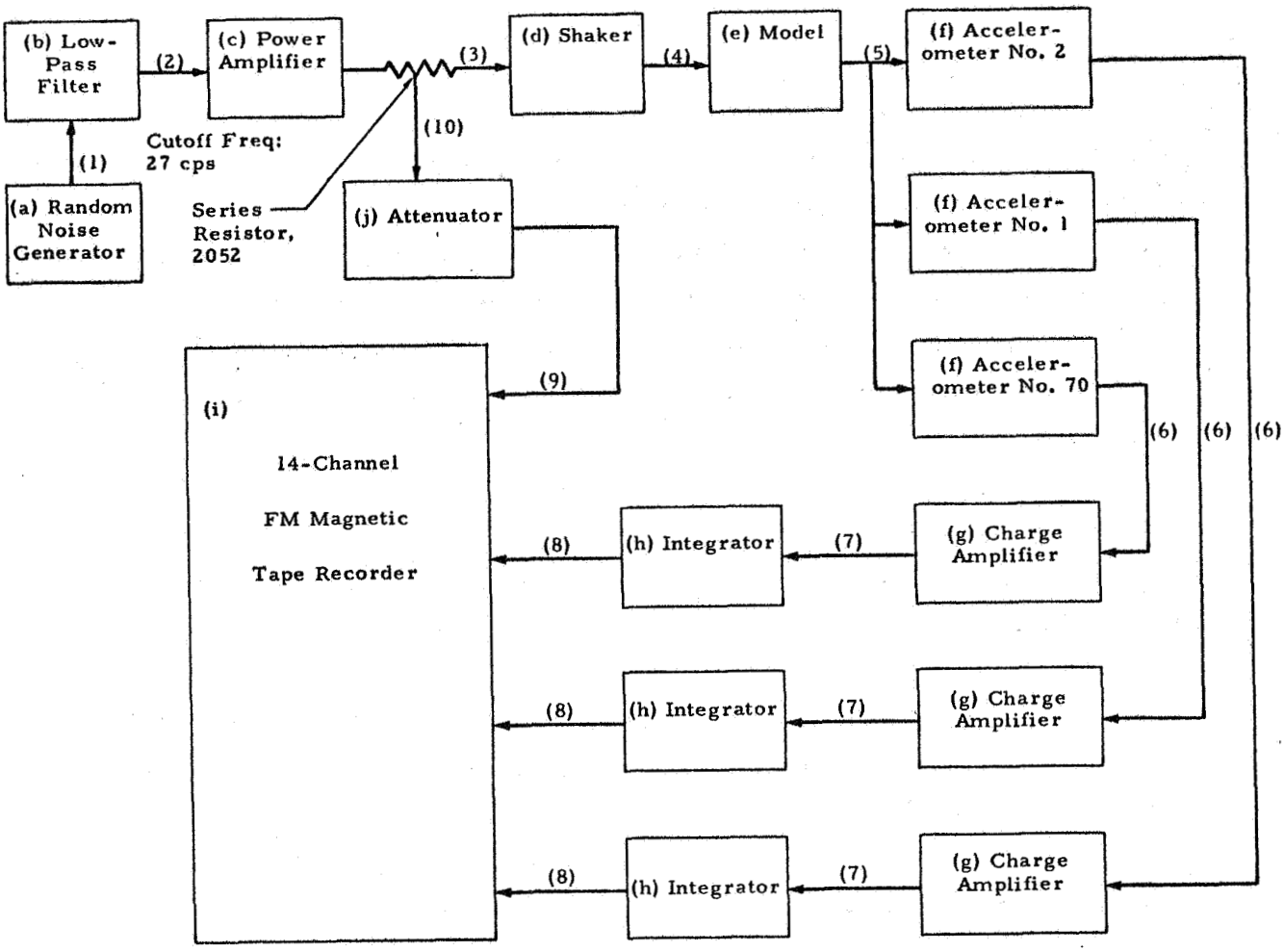

Equipment

a. Elgenco 312A (Gaussian Noise Generator)
b. SKL 302 (electronic filter)
c. Ling Tp-300 power amplifier
d. Ling-Goodman VG 50 vibration generator
e. 1/5-scale Saturn SAI model
f. LMSC/HREC developed accelerometers
g. Kistler 503 (charge amplifiers)
h. Tektronics operational amplifiers (type 0 scope plug-in units)
i. Precision instruments 2114 (magnetic tape recorder)
j. Philbrick USA-3 operational amplifier

Signals

1. Gaussian, band limited (0 - 120 cps) white noise
2. Gaussian, band limited (0 - 27 cps) white noise
3. Gaussian, band limited (0 - 27 cps) white noise (current)
4. Gaussian, band limited (0 - 27 cps) white noise force
5. Double (first and second modes) narrow band accelerations
6. Charges proportional to 5.
7. Voltages proportional to 5.
8. Velocity signals
9. force signal

Figure B-10 - Random Vibration Test Setup

Specimen responses were picked up by accelerometers. Three acceleration signals were time-integrated and recorded simultaneously on FM magnetic tape at 1-7/8 ips tape speed. Integration of the acceleration signals was found necessary because the tape recorder has a 43-dB dynamic range and because the second mode acceleration signal levels were so high that if it spanned this maximum usable dynamic range, the first mode acceleration response signal would be in the noise level of the system and could not be detected. Integration changed the signal ratio between first and second modes to a tolerable value for the tape recorder.

An analog spectrum analysis method was used to reduce taped data. The key equipment used to do this analysis is the tracking filter (Spectral Dynamic SD 101A) with a tunable 2.0 cps pass band.

The data on FM tape was first transferred to another tape. The playback speed used during this transfer was 60 ips. An FM tape loop was made onto which the speeded-up data was recorded, at 7-1/2 ips. The tape loop was approximately 24 feet long, and when a tape loop playback speed of 15 ips was used, data repeated approximately every 20 seconds.

Through increased playback speed the data frequency was increased by the factor of 64. The first mode response in real time is approximately 4.5 cps. On playback, this is changed to 288 cps. The tape loop, therefore, contained approximately 5,480 cycles of data at the lowest frequency, and provided a sufficient length for a reasonable confidence level of the analyzed results. Let

$$B = \text{bandwidth of analysis filter} = 2.0 \text{ cps}$$

and

$$T = \text{length of data} = 19.2 \text{ seconds}$$

then the number of statistical degrees of freedom*

$$n = 2BT$$

Therefore,

$$n = 2 \times 2.0 \times 19.2 = 76.8$$

The following confidence levels of the analysis can be obtained from the Chi-Square Distribution Chart.

$\frac{\text{(True RMS)}}{\text{(Measured RMS)}}$	Confidence Level %
1.6 to 0.71	98
1.4 to 0.8	90
1.3 to 0.83	80
1.2 to 0.88	60
1.15 to 0.94	30

Averaging of the spectrum was made by an RC circuit, with $R = 10^6$ ohms and $c = 20 \times 10^{-6}$ farads. The averaging time is, therefore, 20 seconds which is greater than the tape loop length in seconds (19.2). As a consequence, the output of this RC averaging circuit is an average of all data contained on the tape loop. The analysis filter sweep rate is determined by the averaging time constant and is 0.05. A sweep rate of 0.14 cps/second was actually used. Spectrum analysis instrumentation is shown in Figure B-11.

*According to ASD/TDR 61-123, "The Application of Statistics to the Flight Vehicle Vibration Problem," Wright-Patterson Air Force Base, Ohio, December 1961.

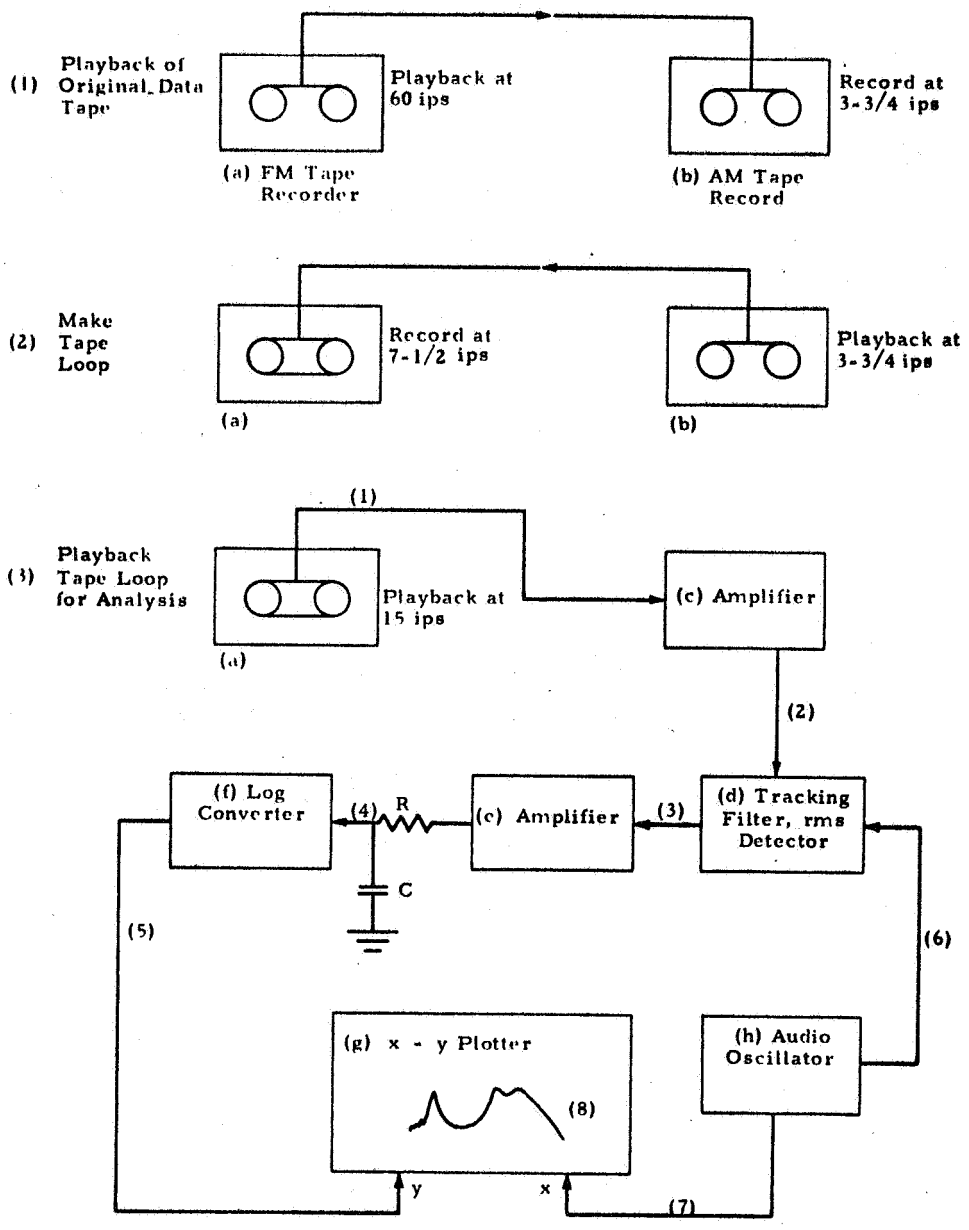

Equipment

a. Precision instrument 2114
b. Sony (AM tape recorder)
c. Philbrick USA-3 (operational amplifier)
d. Spectral Dynamics SD101A (dynamic analyzer) (filter bandwidth: 2.0 cps)
e. Philbrick USA-3 (operational amplifier)
f. Hewlett-Packard/Sanborn 350-1400 (log preamplifier)
g. Hewlett-Packard 7000A (x - y plotter)
h. Spectral Dynamics SD104A-5 (audio sweep oscillator)

Signals

1. Response (frequency shifted up 5 octaves)
2. (1) amplified
3. dc voltage proportional to RMS of (2) filtered by 2.0 cps filter at frequency set by tuning signal from (h)
4. Average RMS
5. Log of (4), ref = 0.1895 volts
6. Tuning signal
7. dc proportional to center frequency of 2 cps filter
8. Curve representing spectrum of (1) vs frequency

Figure B-11 - Power Spectrum Density Analysis Method

The sinusoidal calibration signals were played back in identical manner and using an empirical factor supplied by the manufacturer of the tracking filter, a calibration signal for the power spectral density (PSD) was obtained.

Power spectrum density curves are included at the end of Appendix C-B. The flatness of the PSD curve for the force signal proved the effectiveness of the series resistor in the power amplifier-shaker armature circuit to minimize peaking due to specimen resonances.

The probability distributions of the excitation and of response peaks were investigated. The excitation was found to be truly Gaussian, and the response peaks, Raleigh (Figures B-12 and B-13).

B.4.6.2 Peak Response Versus Damping

The relationship between peak response of a structure subjected to random-plus-sine excitation and damping was studied. The sine portion of excitation was tuned to the resonant frequency of the first mode of the model. The random portion of the excitation is band limited and centered around the first mode. No other mode was excited.

Modal damping of the structure was varied by the use of an active damper which is described below.

The damper system (Figure B-14) consists of a 50-pound shaker, a power amplifier and a velocity sensor. The shaker was located directly opposite to the one which provided excitation. From Figure B-14, it is seen that the force applied to the model specimen by the damping shaker is always proportional to the velocity and in phase with (or opposite to) the instantaneous velocity of the specimen, adding negative (or positive damping, respectively) to the model. The amount of damping is dependent on the gain between the velocity and the power amplifier, and is, therefore, adjustable.

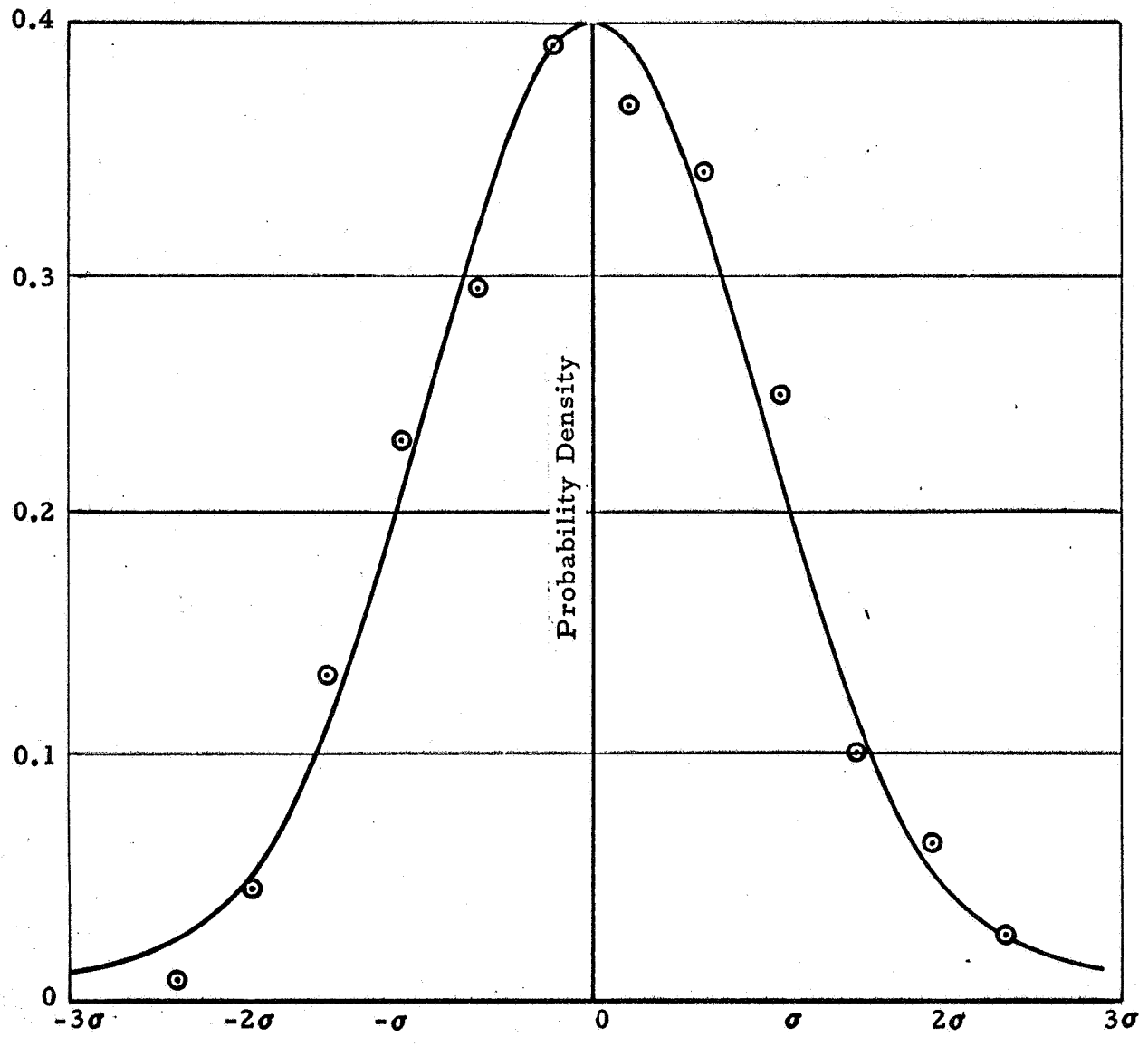

Figure B-12 - Probability Distribution of Excitation

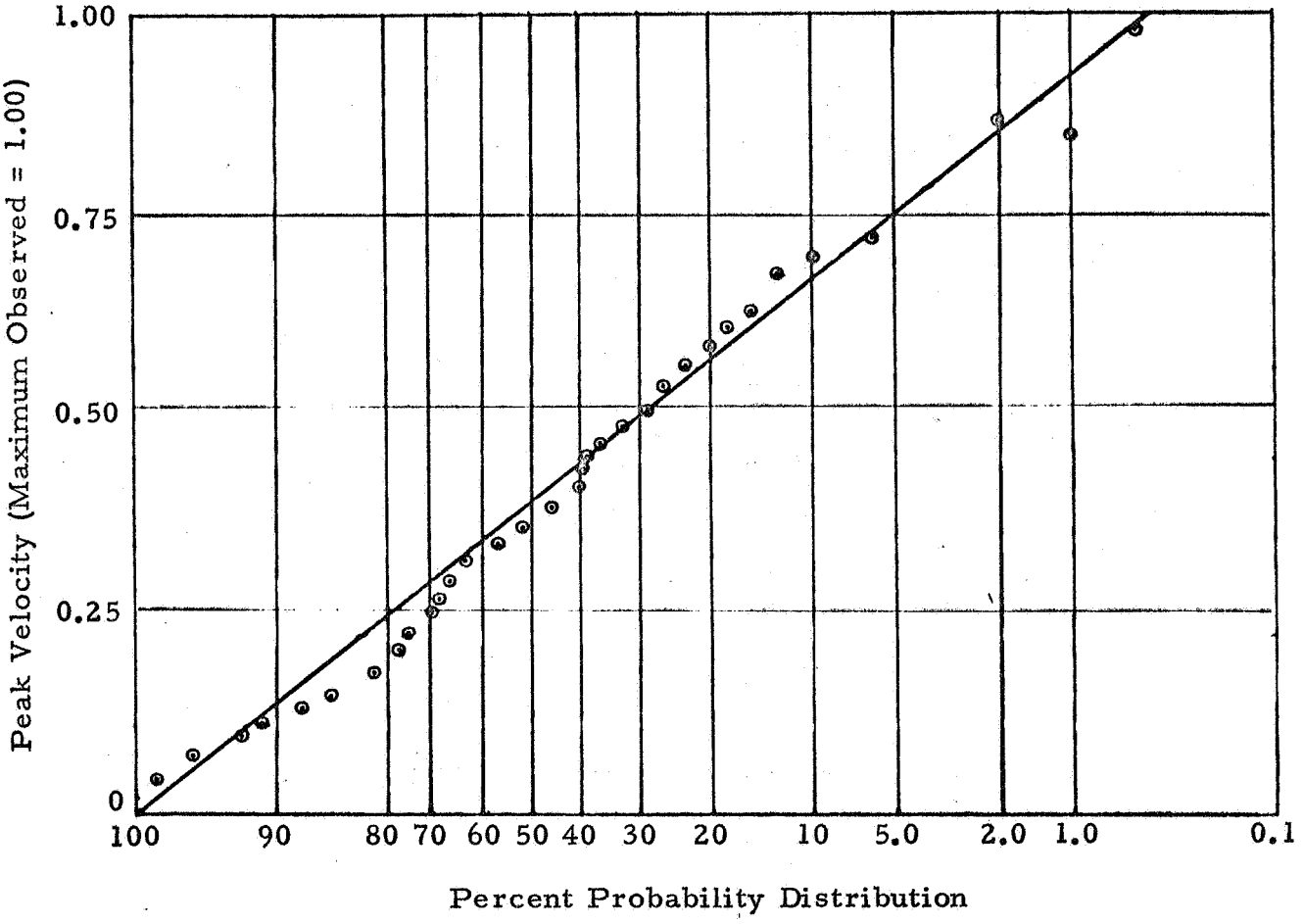

Figure B-13 - Probability Distribution of Velocity Peaks Observed at Station 210

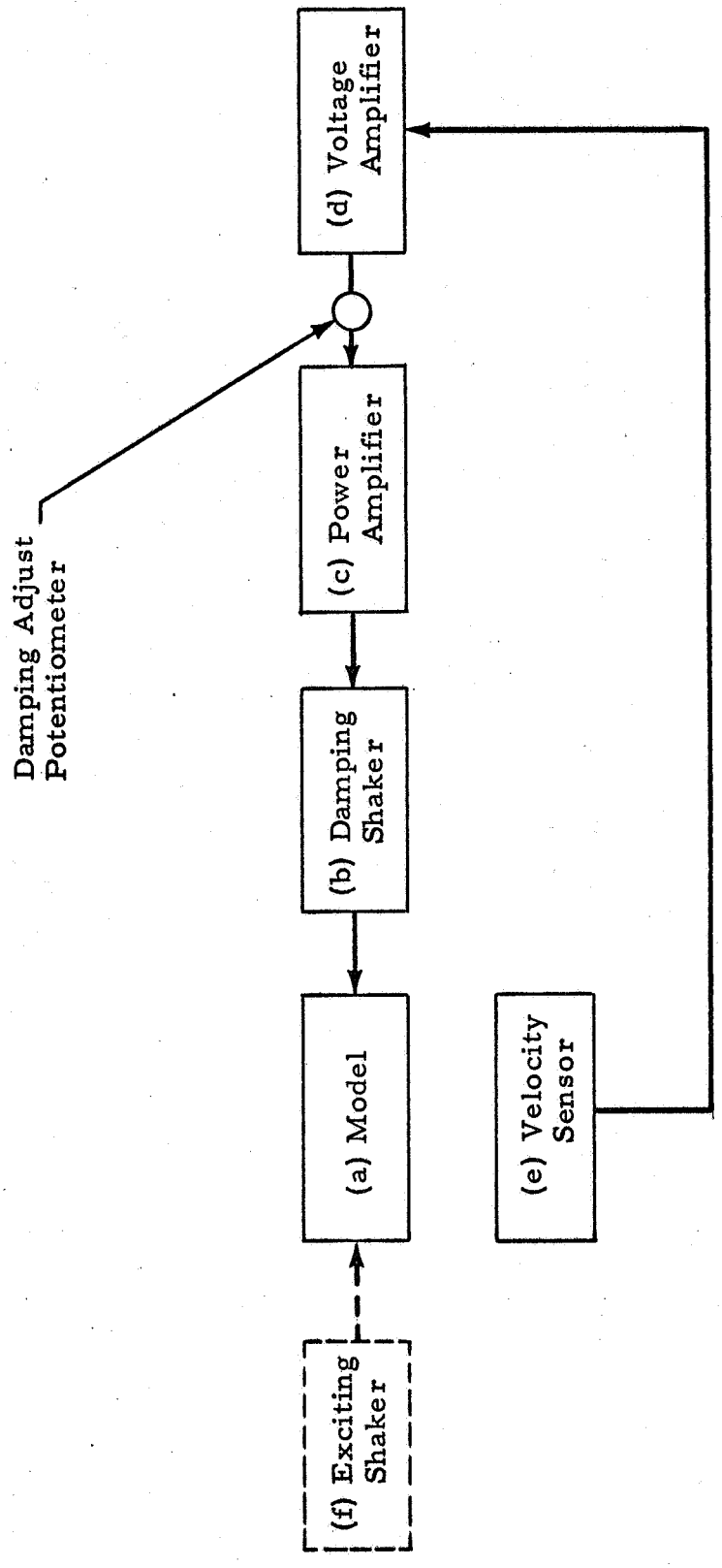

Figure B-14 - Active Damper System Schematic

Free vibration decay curves were obtained to calibrate the resultant damping of the model against gain settings of the gain adjust potentiometer. The results are tabulated in Table B-2, which shows that a maximum to minimum equivalent modal damping ratio of 19.4:1 can be realized by adjusting the control potentiometer.

Table B-2

MODAL DAMPING VS ATTENUATOR POTENTIOMETER SETTINGS

Potentiometer Setting	Modal Damping* by Percent of Critical
+ 400	19.4
+ 200	10.5
000	6.53
- 100	5.05
- 150	4.06
- 170	3.90
- 190	3.12

*All damping values measured by force level of 1.5 lb, 0 - pk.

Figure B-15 shows the system used for providing the sine-plus-random excitation to the model, for monitoring, and for recording the resulting data. Tests were conducted for seven different damping levels ranging from 3.12% to 19.4% (approximate, percent critical damping coefficients). The lower damping values were obtained by adding negative linear viscous model damping to the structure via the system described earlier, and the higher damping values, by adding positive damping.

For each damping system gain setting the model was excited to first mode resonance and then the excitation was removed. Free vibration decay records were taken to determine the equivalent model damping coefficient of the model under the prescribed conditions.

Mean square sinusoidal excitation of 0 and 1.125 lb^2, and random excitation of 0, 0.417 lb^2 were combined in the sine-plus random tests as outlined in Table B-3.

Table B-3
SINE PLUS RANDOM EXCITATIONS

		Mean Square of Sine Excitation, lb^2	
		0	1.125
Mean Square of Random Excitation lb^2	0		Test C
	0.417	Test A	Test D
	1.480	Test B	Test E

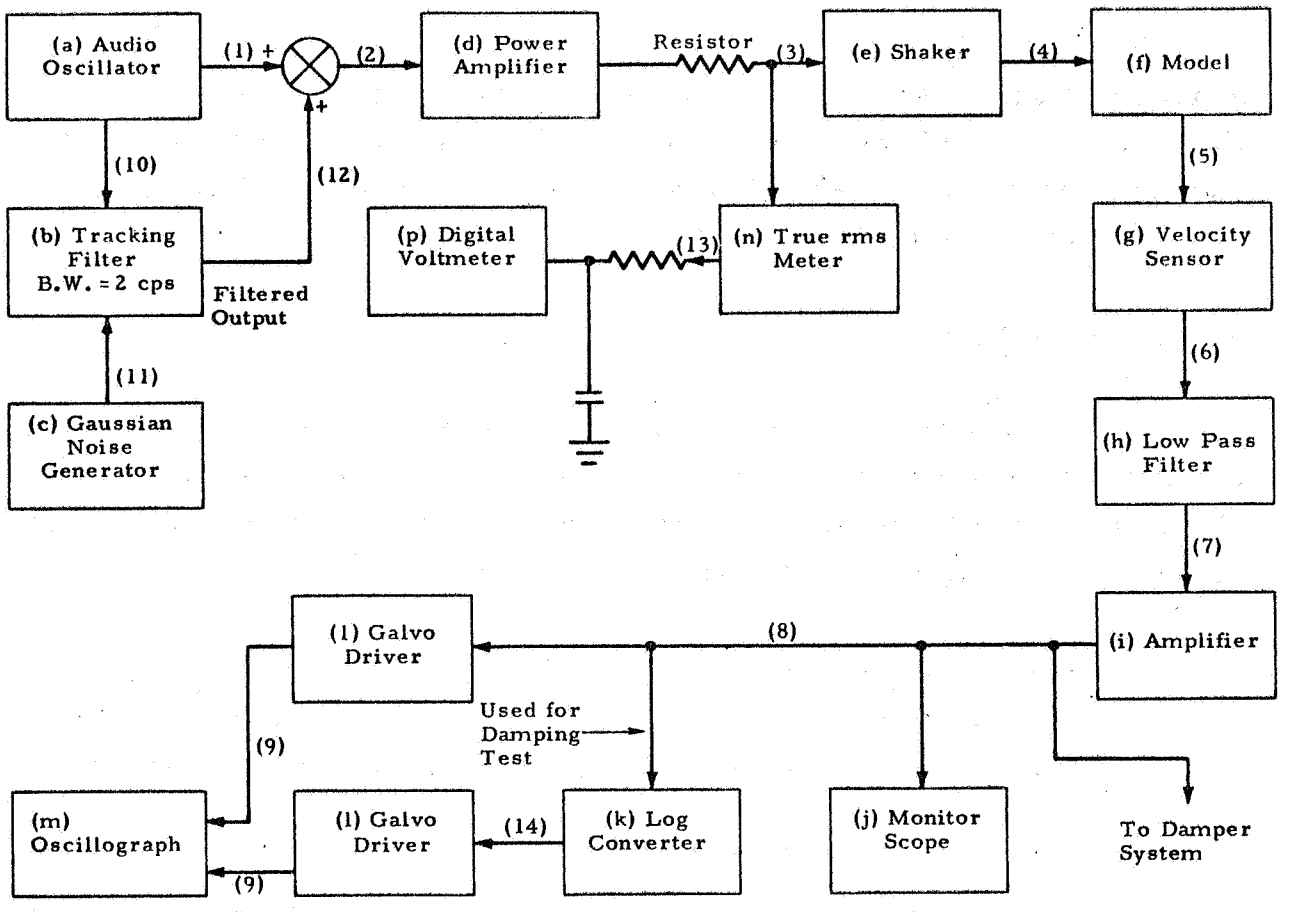

Equipment

a. Spectral Dynamics SD104A-5 (sweep oscillator)
b. Spectral Dynamics SD101A (dynamic analyzer with 2 cps tracking band pass filter)
c. Elgenco 312A (Gaussian noise generator, 0 - 120 cps)
d. McTintosh Mc-75 (audio power amplifier, 75 watts)
e. Ling-Goodman VG 50 (vibration generator)
f. 1/5-scale Saturn SAI model
g. Hewlett-Packard/Sanborn 6 LV1 (velocity sensor)
h. SKL 302 (filter)
i. Tektronics type "0" scope plug-in (operational amplifier)
j. Hewlett-Packard 141A (MEM scope)
k. Hewlett-Packard/Sanborn 350-1400 (log preamplifier)
l. CEC 1-026A (galo driver, 7 channels)
m. CEC 5-124 (oscillograph, 12 channels)
n. Ballantine 320 (true rms meter)
p. Nonlinear systems 481 (digital voltmeter)

Signals

1. Sine voltage, at first mode frequency of model
2. (1) plus random
3. Current, proportional to (2)
4. Force, proportional to (3)
5. Velocity at spider beam
6. Voltage signal proportional to velocity
7. (6) filtered
8. (7) amplified
9. Currents proportional to (8) or (15)
10. Sine voltage, constant amplitude
11. Gaussian white noise (0 - 120 cps)
12. Gaussian, band limited white noise (3.5 - 5.5 cps, approximate)
13. dc voltage proportional to mean square input
14. ac, with plus voltage above 0.1895 volts converted to dB scale

Figure B-15 - Sine-Plus-Random Test Setup

Oscillograph records of the velocity signal were made for all above tests, and maximum response in two-minute runs were noted. Figure B-16 shows the pattern of response signals for various tests and damping values. Maximum responses in two minutes are plotted against model damping for each damping value in Figure B-17.

B.4.6.3 Mean Square Response

The relationship between mean square velocity response and spectral level of excitation was measured for the first bending mode of the model with all outer booster tanks on, empty and without internal pressurization. The test setup is shown in Figure B-18.

The model was excited by the band-limited Gaussian white noise (obtained from the random noise generator and the low-pass filter) and the excitation spectral level and the mean square response were measured by the true RMS voltmeter.

An excitation spectral level range of over 25 dB was tested. The results are shown in the curve Figure B-19.

B.4.7 Miscellaneous Tests and Results

Three additional tests were conducted to provide answers to specific questions concerning Saturn launches. The first of these tests was to investigate the effect of internal pressurization of the booster tanks on damping. Figure B-20 shows, for both conditions, free vibration decays of the first bending mode of the cantilevered model without fuel or LOX simulator. The effect is seen to be very small.

Figure 21 shows results of a test to investigate whether excitation in one mode has any effect on damping in another. In the test, damping of free vibration in the first mode was obtained with and without a sinusoidal excita-

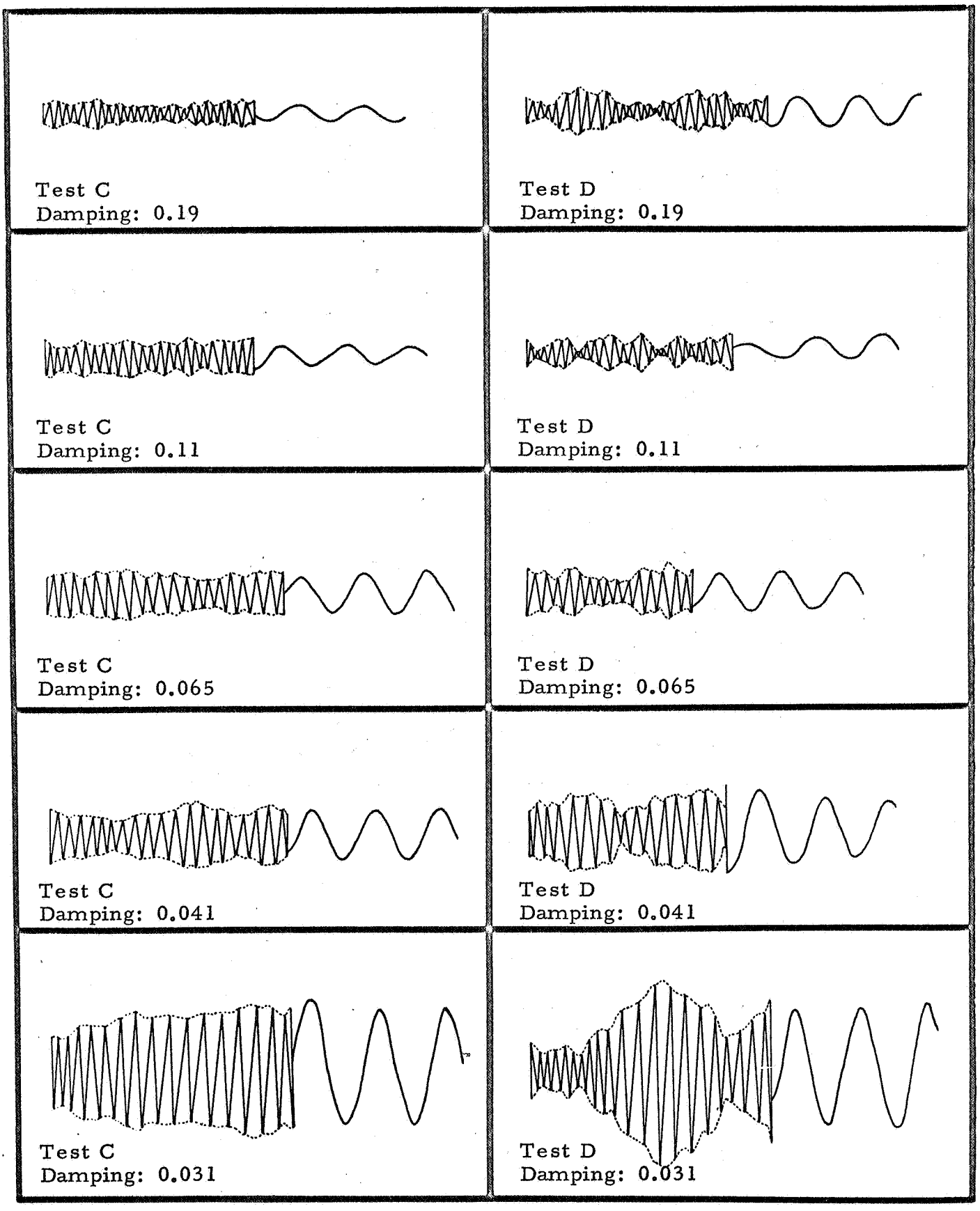

Figure B-16 - Response Patterns to Sine-Plus-Random Excitation at Different Modal Damping

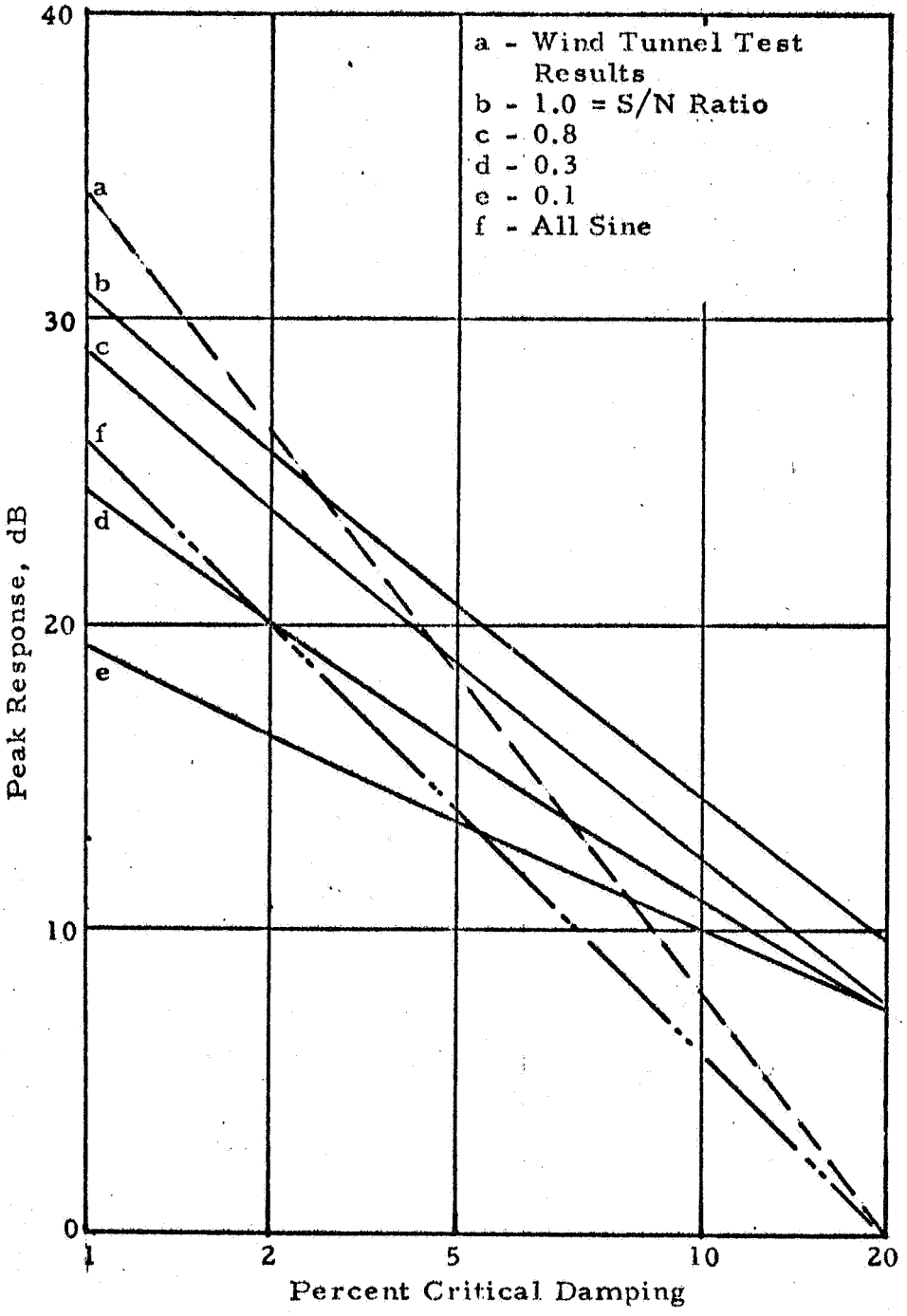

Figure B-17 - Theoretical Peak Response vs Damping

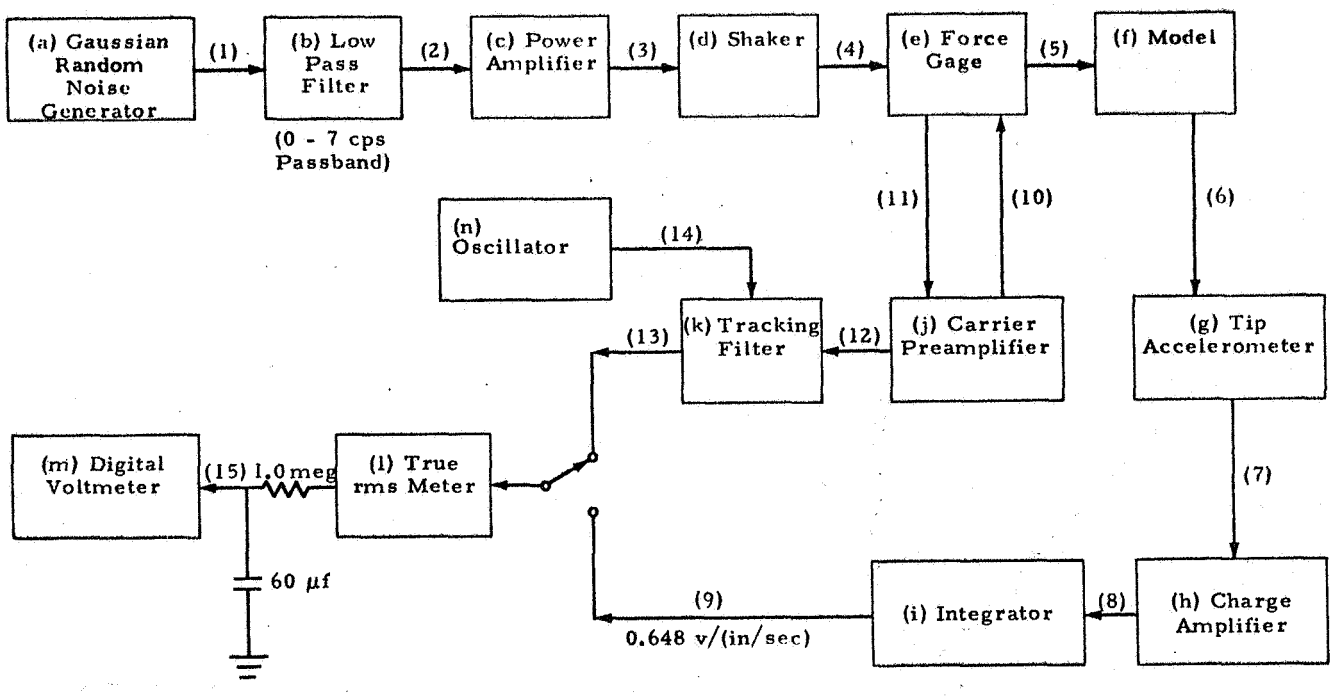

Equipment

a. Elgenco 312A (Gaussian white noise generator, 0 - 120 cps)
b. KRON HITE 350A (band rejection filter)
c. Ling TP 300 (power amplifier)
d. Ling-Goodman VG 50 (50 lb shaker)
e. Schaevitz-Bytrex JP 50 (force gage)
f. 1/5-scale Saturn SAI model
g. LMSC/HREC developed accelerometer
h. Endevco 2713A (charge amplifier)
i. Tektronics type "0" scope plug-in (operational amplifier)
j. Sanborn 350-1100B (carrier preamplifier)
k. Spectral Dynamics SD101A (dynamic analyzer with 2 cps tunable bandpass filter)
l. Ballantine 320 (true rms electronic voltmeter)
m. Nonlinear system 481 (digital voltmeter)
n. Spectral Dynamic SD104A-5 (oscillator)

Signals

1. Band limited (0 - 120 cps), Gaussian white noise voltage
2. Band limited (0 - 7 cps), Gaussian white noise voltage
3. Current proportional to (2)
4. Force proportional to (3)
5. Same force as (4)
6. Acceleration
7. Charge proportional to (6)
8. Voltage proportional to (7)
9. Velocity signal, voltage
10. Force gage excitation voltage
11. Modulated force signal
12. Demodulated force signal
13. (12) filtered (3.5 cps to 5.5 cps)
14. Tracking filter tuning signal
15. Mean square force or velocity

Figure B-18 - Mean Square Response Test Setup

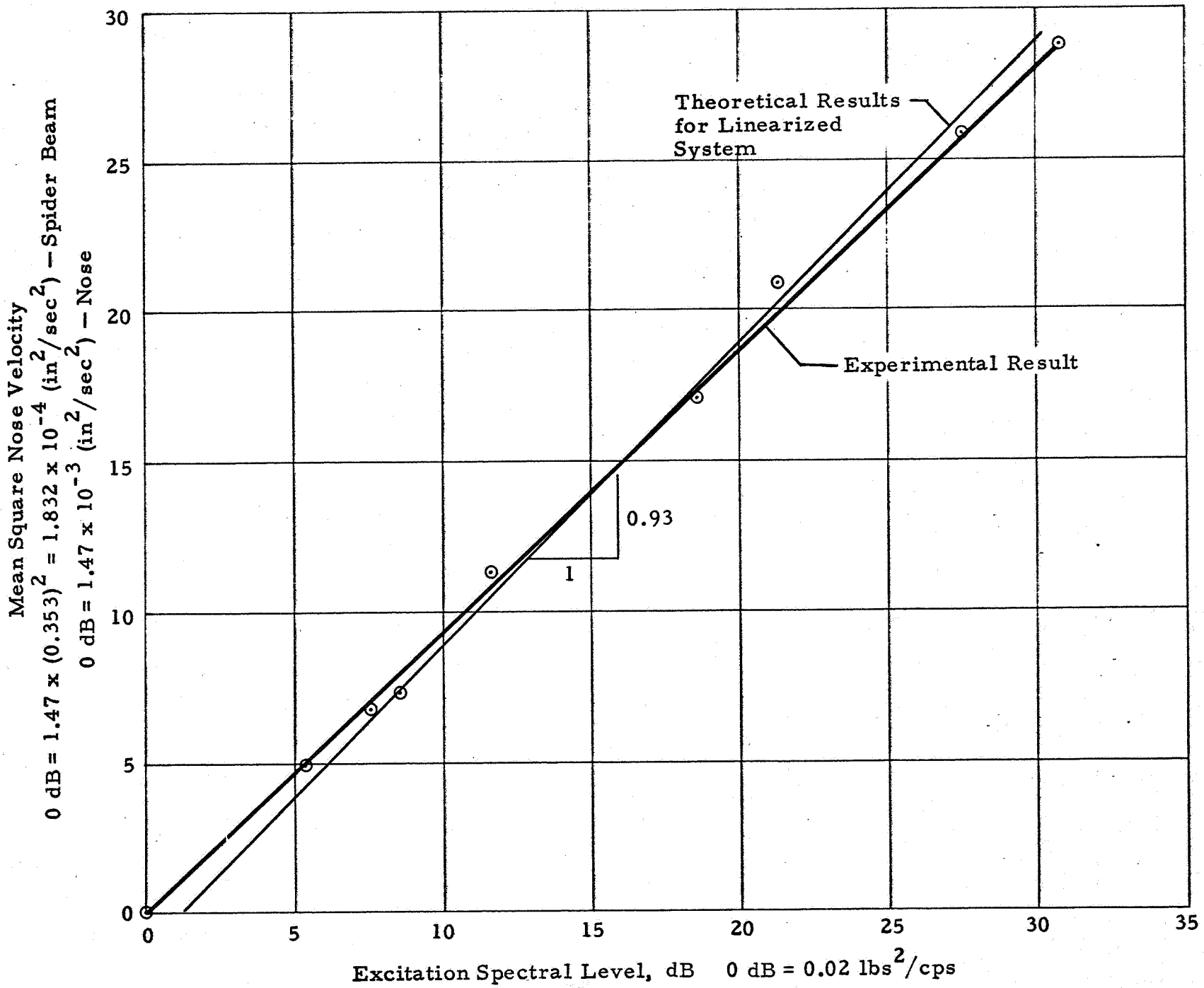

Figure B-19 - First Mode Mean Square Response, Configuration B-1

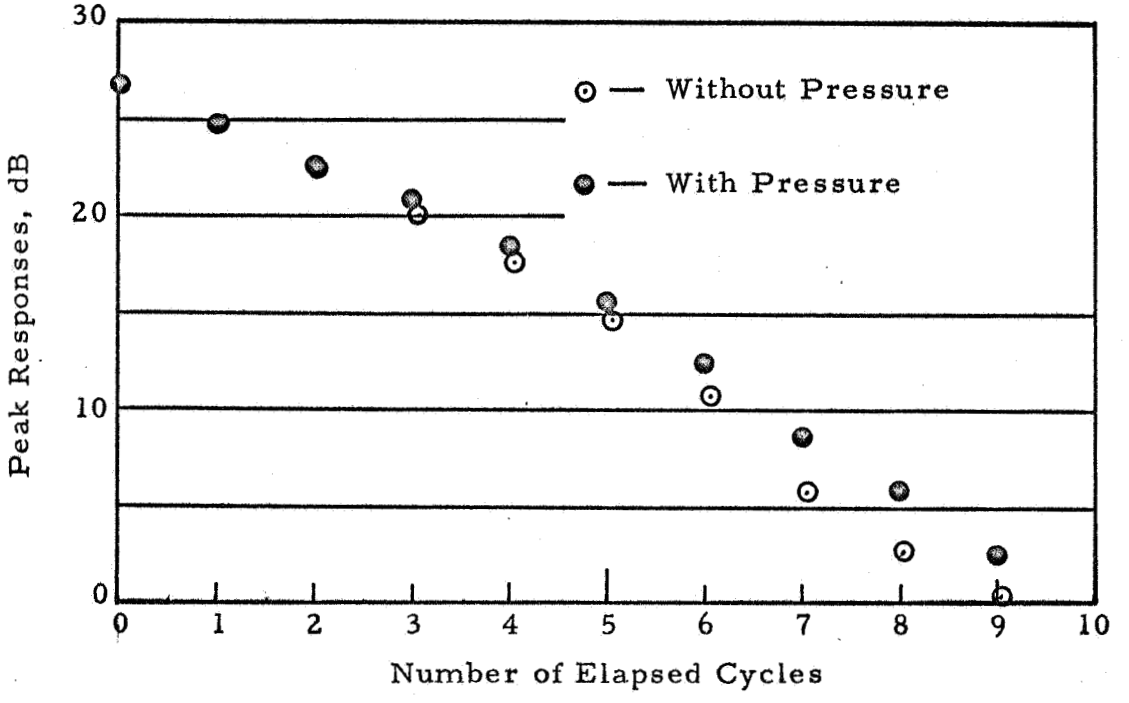

Figure B-20 - Effect of Internal Pressurization on Modal Damping

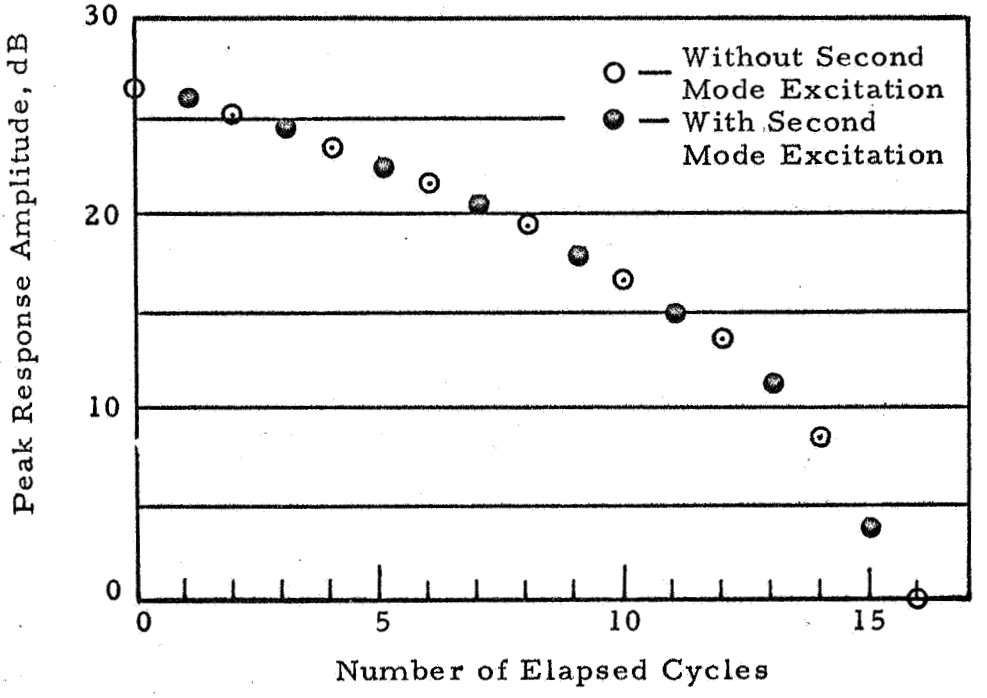

Figure B-21 - Effect of Second Mode Excitation on First Modal Damping

tion at the second mode frequency being applied. Comparative results in Figure B-21 indicate that response in one mode causes no observable effect on the damping in another.

The third test was an investigation of the effect of base stiffness on the cantilevered specimen damping, and on the response to sinusoidal excitations. The basic model configuration was B-1.

Base stiffness was altered by the removal of various numbers of holddowns from the original eight. Figure B-22 shows schematically the numbering system used to indicate holddown conditions.

Figure B-23 shows decay of free vibration for all holddown configurations investigated. It is seen that damping changes from a nonlinear one (A) to a relatively linear one, (E) as the holddown stiffness was decreased. The damping value also decreases with the stiffness. A visually evidenced reason of the noted change in damping is the following: as the holddown stiffness was decreased, the bending mode shape tends to approach one pivoting about the central LOX tank lower barrel. Large deformations took place due to straining of the material at this lower section while very little relative motion was noted for the complicated booster stage tanks. Damping became primarily due to material dissipation, and hence, tends toward linearity as the base stiffness was decreased.

Frequency response curves were obtained for the five base configurations investigated and are shown in Figures B-24 through B-28. Indications of frequency shifts, resonance response amplitude linearity, and bandwidths can all be obtained from these frequency sweep data.

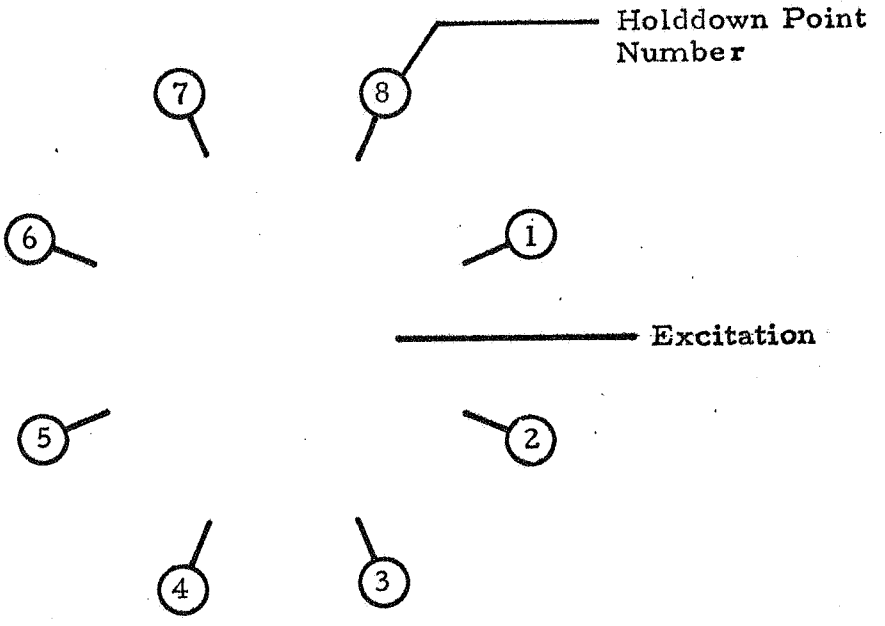

Holddowns Removed	Holddown Configuration Code
None	A
1, 2, 5, 6	B
3, 4, 7, 8	C
1, 2	D
1, 2, 4, 7	E

Figure B-22 - Schematic Showing Model Holddown Configuration Codes

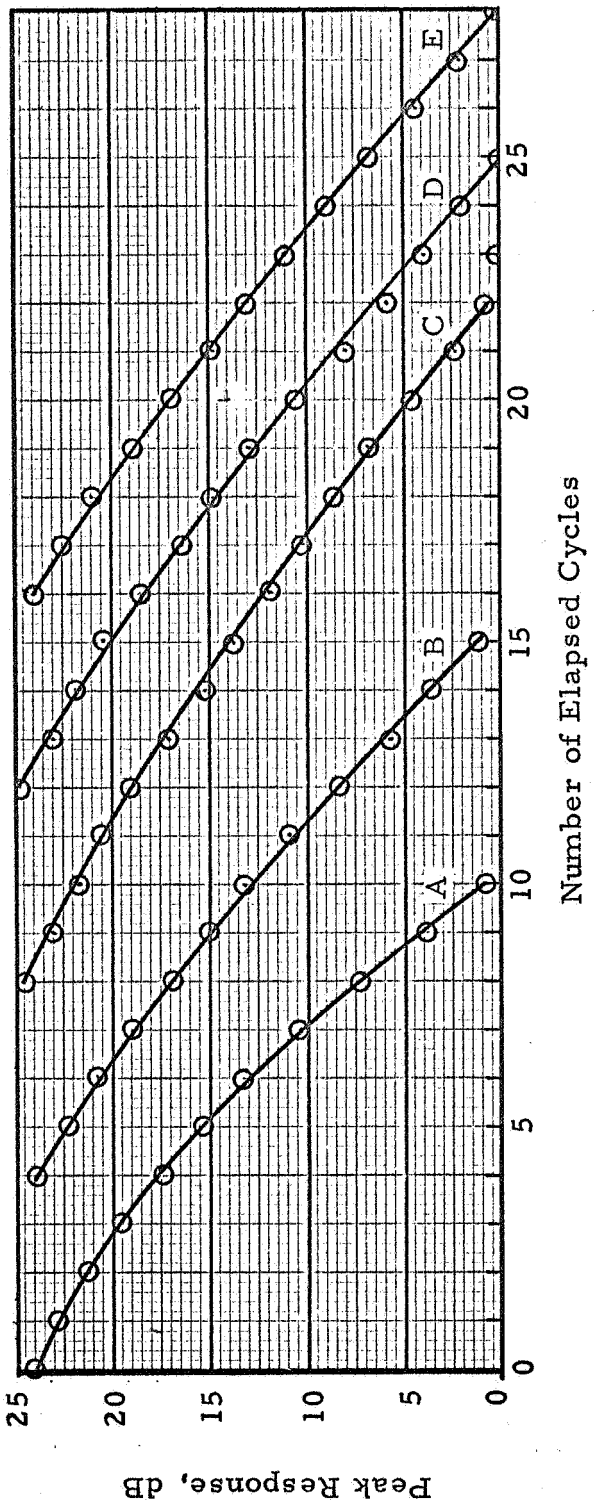

Figure B-23 - Damping of Free Vibrations for Various Base Configurations
(see Figure B-22 for definitions of base configurations)

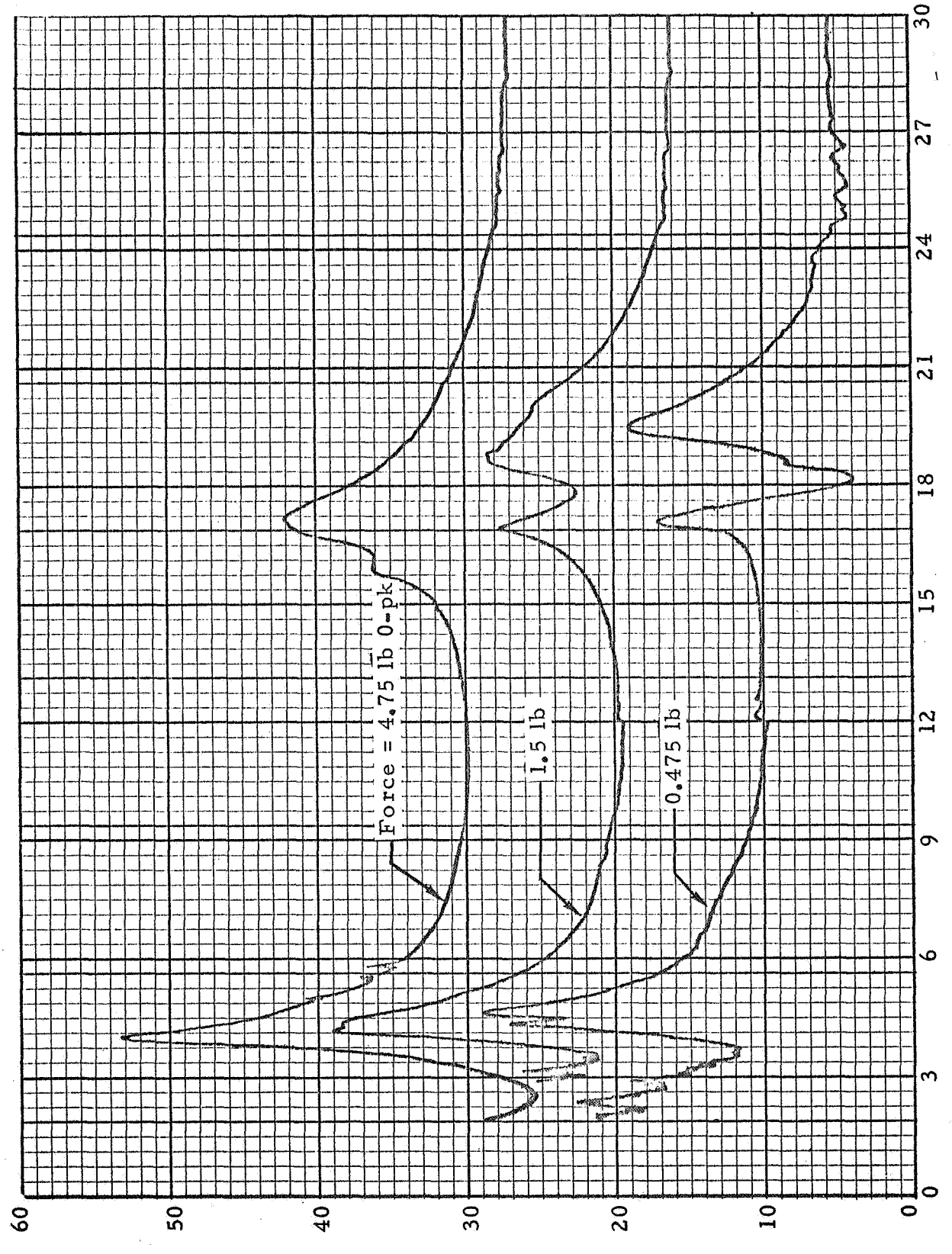

Figure B-24 - Nose Velocity vs Frequency, Configuration B-1A

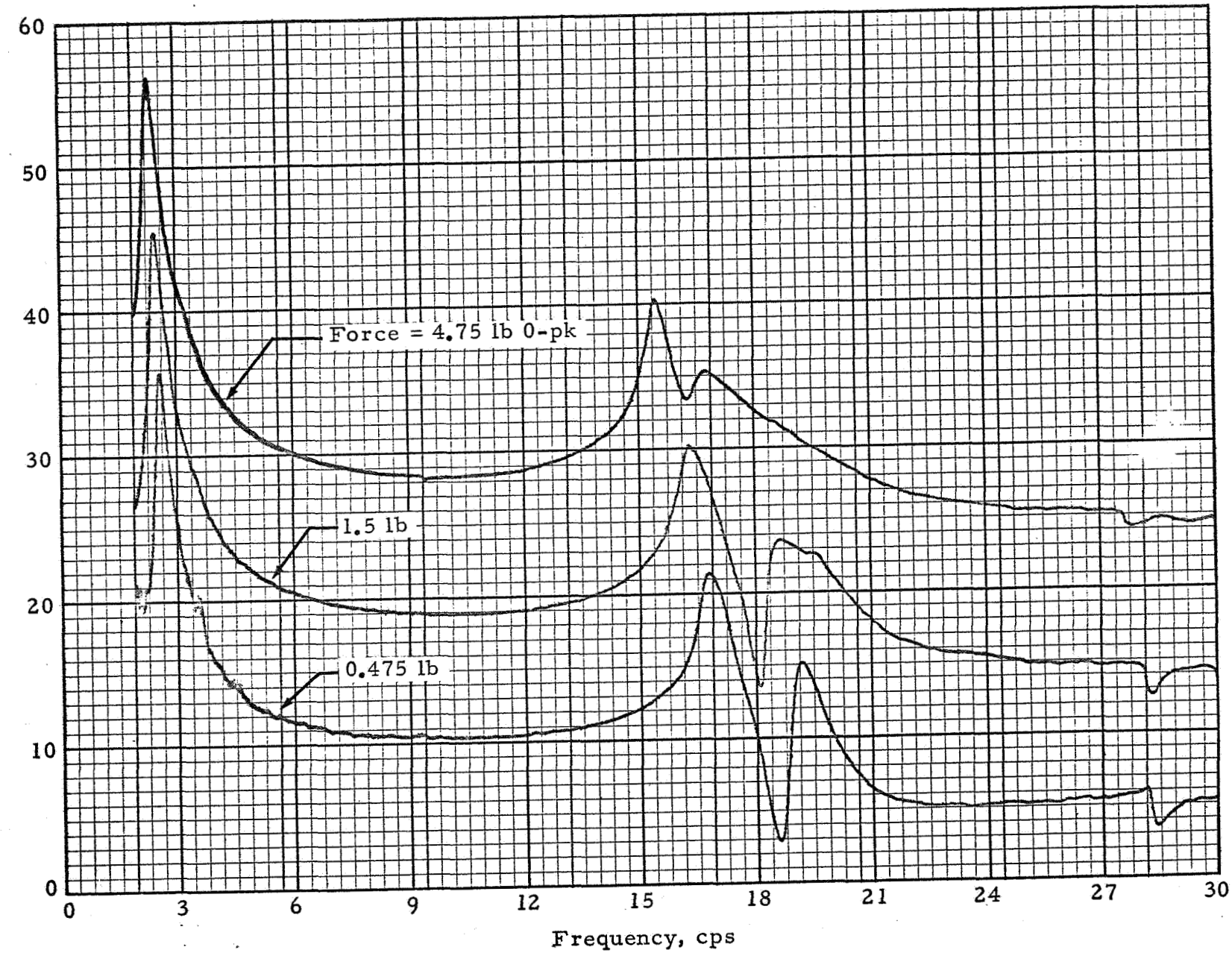

Figure B-25 - Nose Velocity vs Frequency, Configuration B-1B

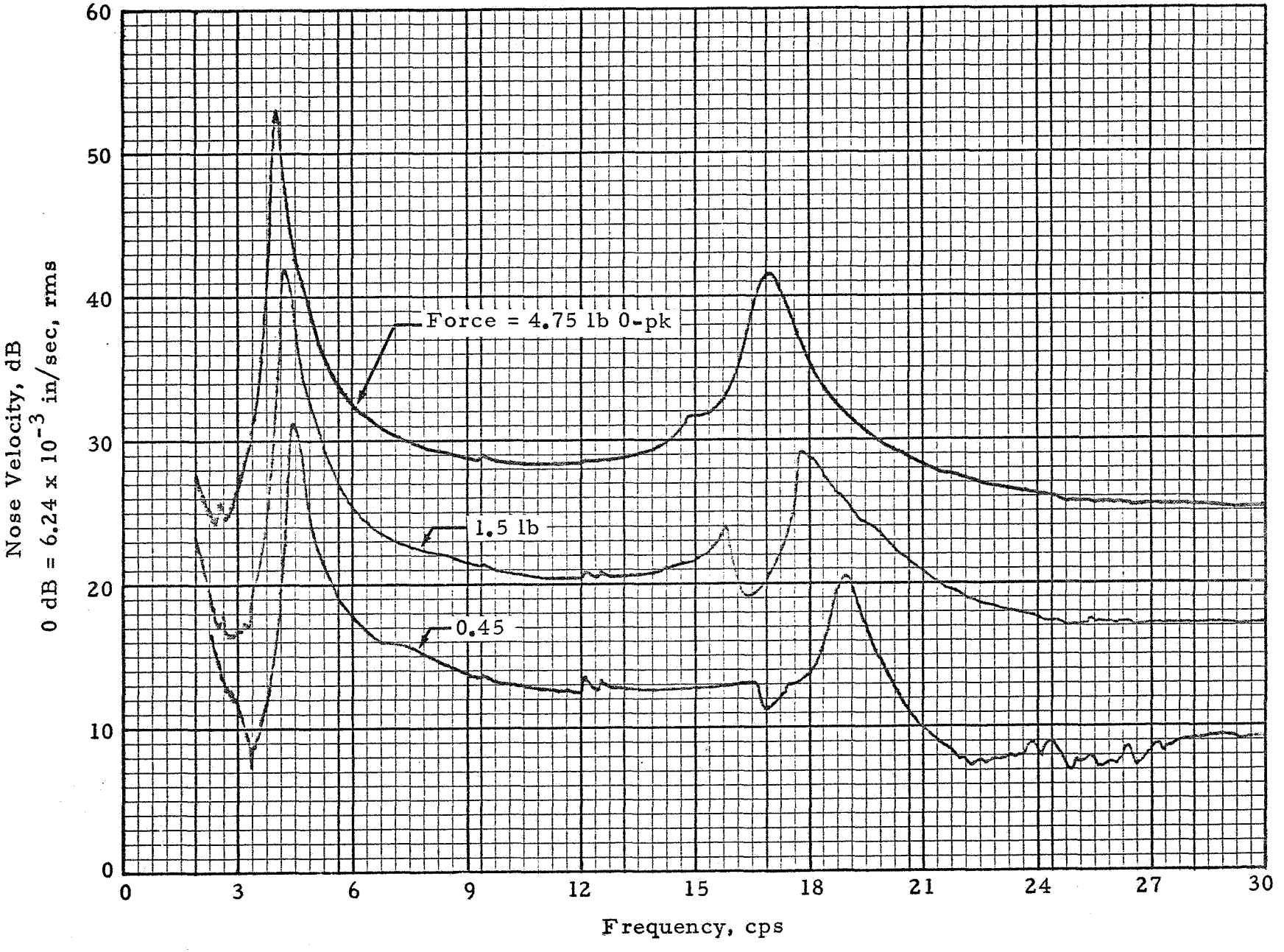

Figure B-26 - Nose Velocity vs Frequency, Configuration B-1C

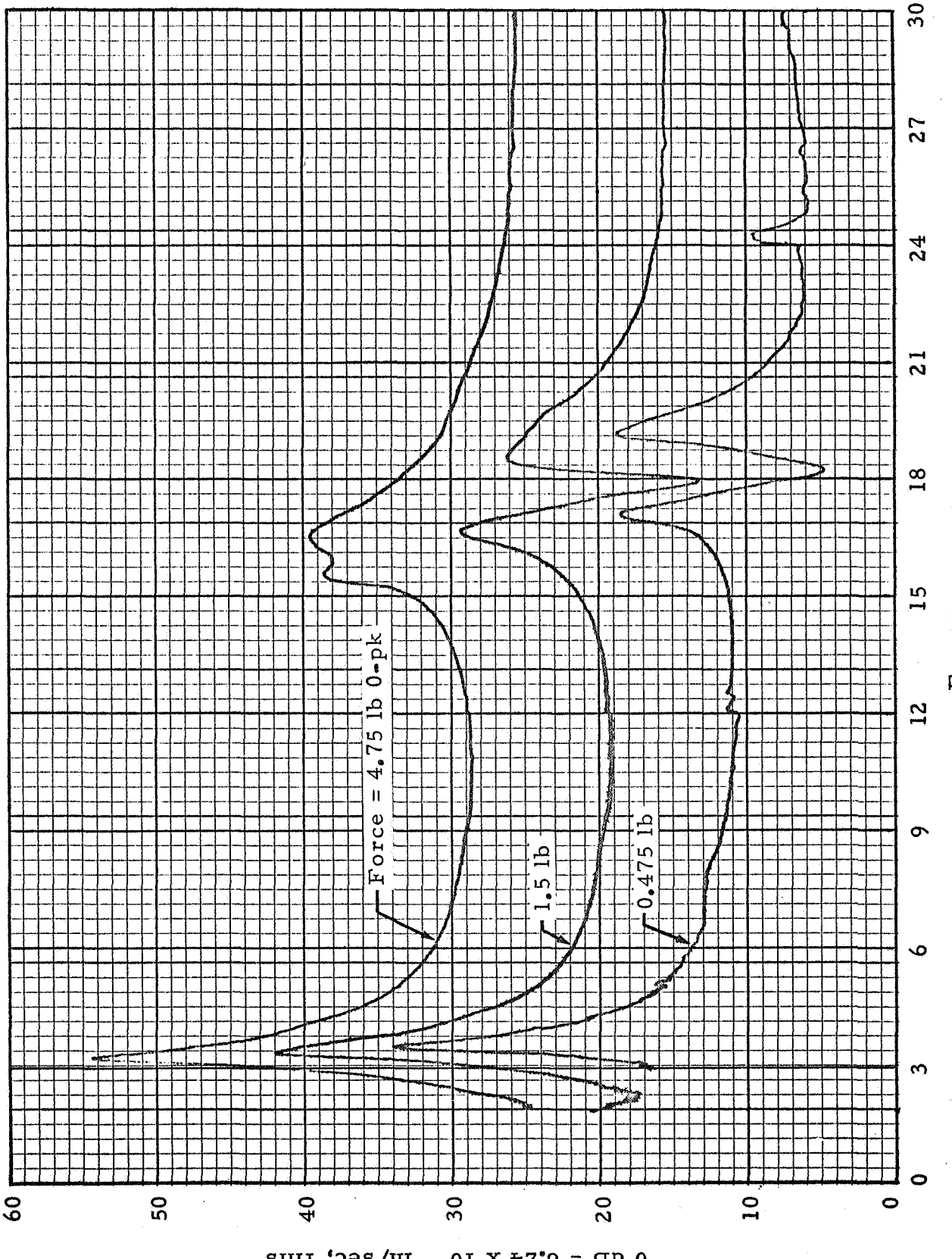

Figure B-27 - Nose Velocity vs Frequency, Configuration B-1D

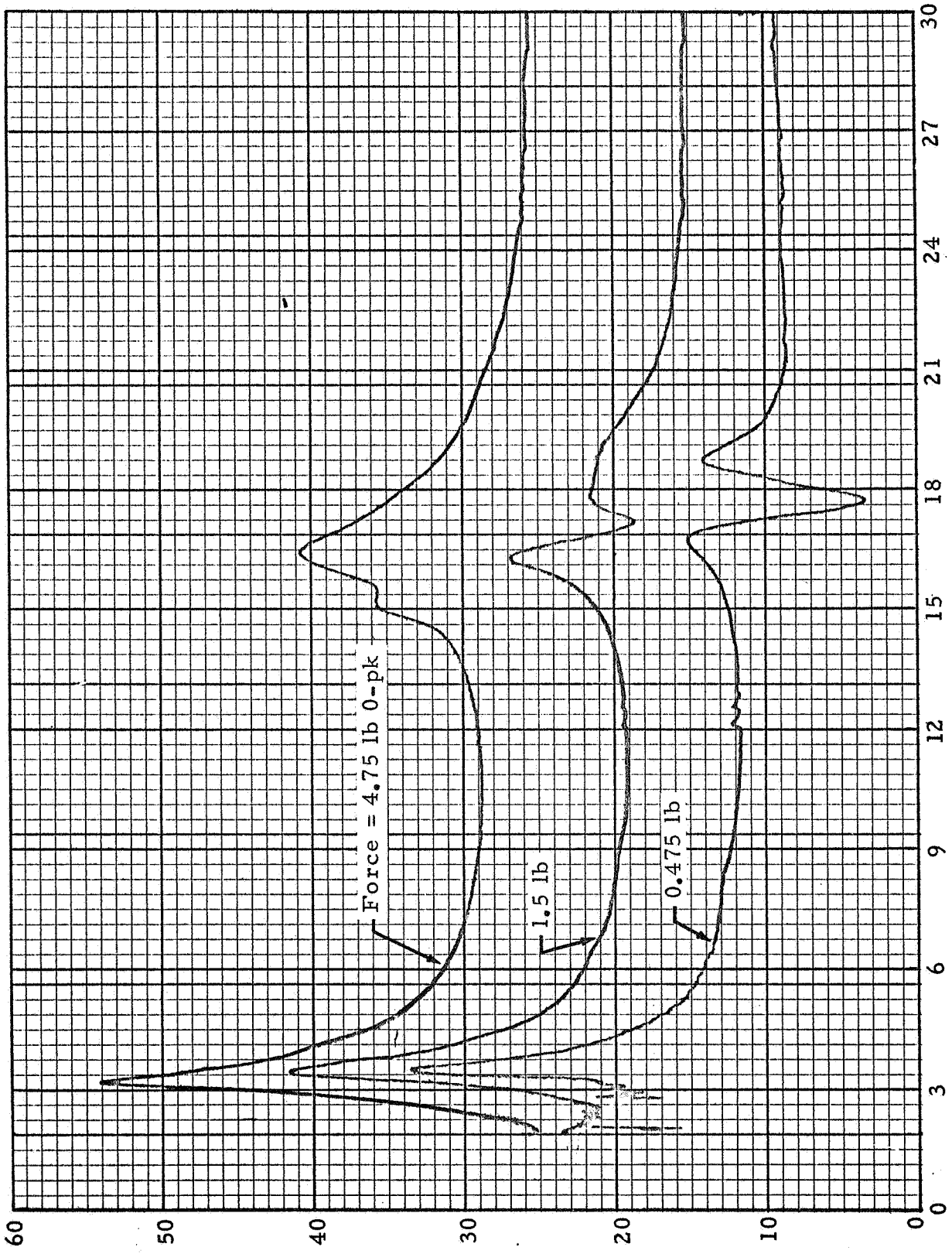

Figure B-28 - Nose Velocity vs Frequency, Configuration B-1E

APPENDIX C

TEST DATA

Appendix C
TEST DATA

All significant bending vibration test data obtained for the 1/5-scale model of Launch Vehicle Saturn SA-1 in the prelaunch (cantilevered) condition are included in this appendix. Data are grouped according to specimen configurations according to definitions of Appendix A.

For each test configuration, the following test data are shown: frequency sweep, mode shape survey, generalized mass test, resonant response, frequency shift, and damping, in that order. Random vibration data for Test Configuration B-1 and additional frequency sweep results are also presented.

TEST CONFIGURATION A
INDEX TO FIGURES

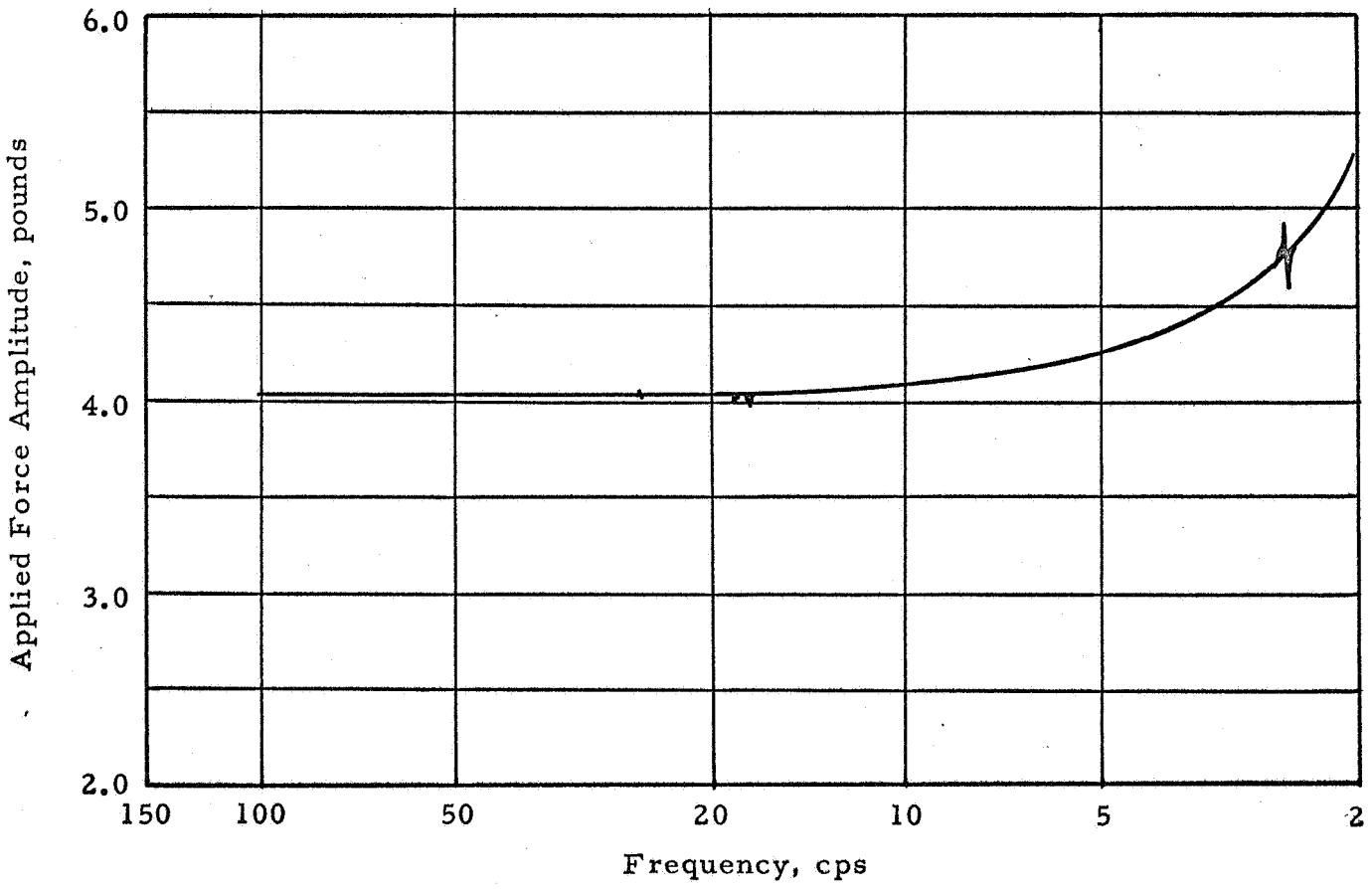

Figure C-A-1 - Variation of Applied Force Amplitude with Frequency (Configuration A)

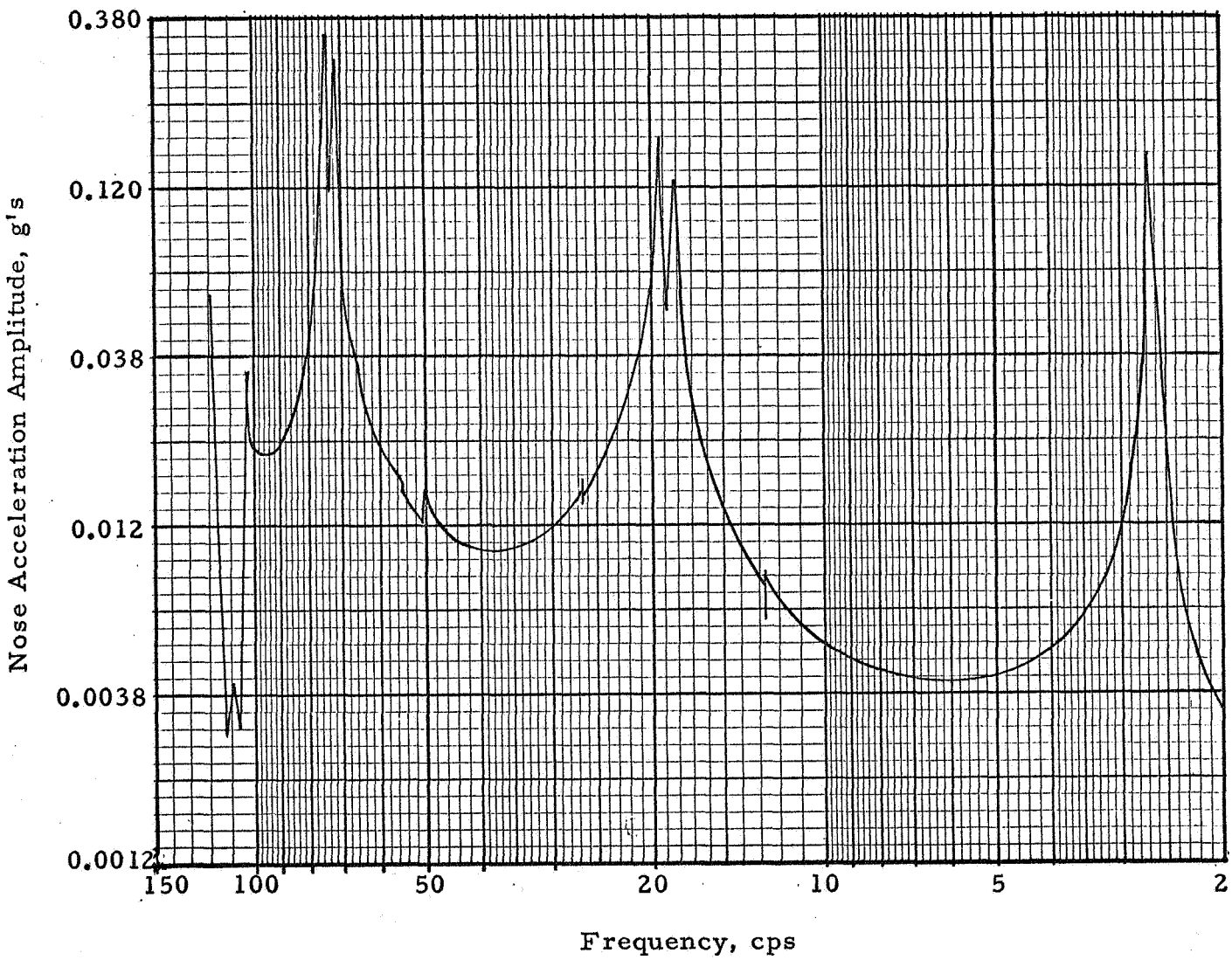

Figure C-A-2 - Frequency Response (Configuration A) Force Amplitude: 0.1262 lb at 40 cps

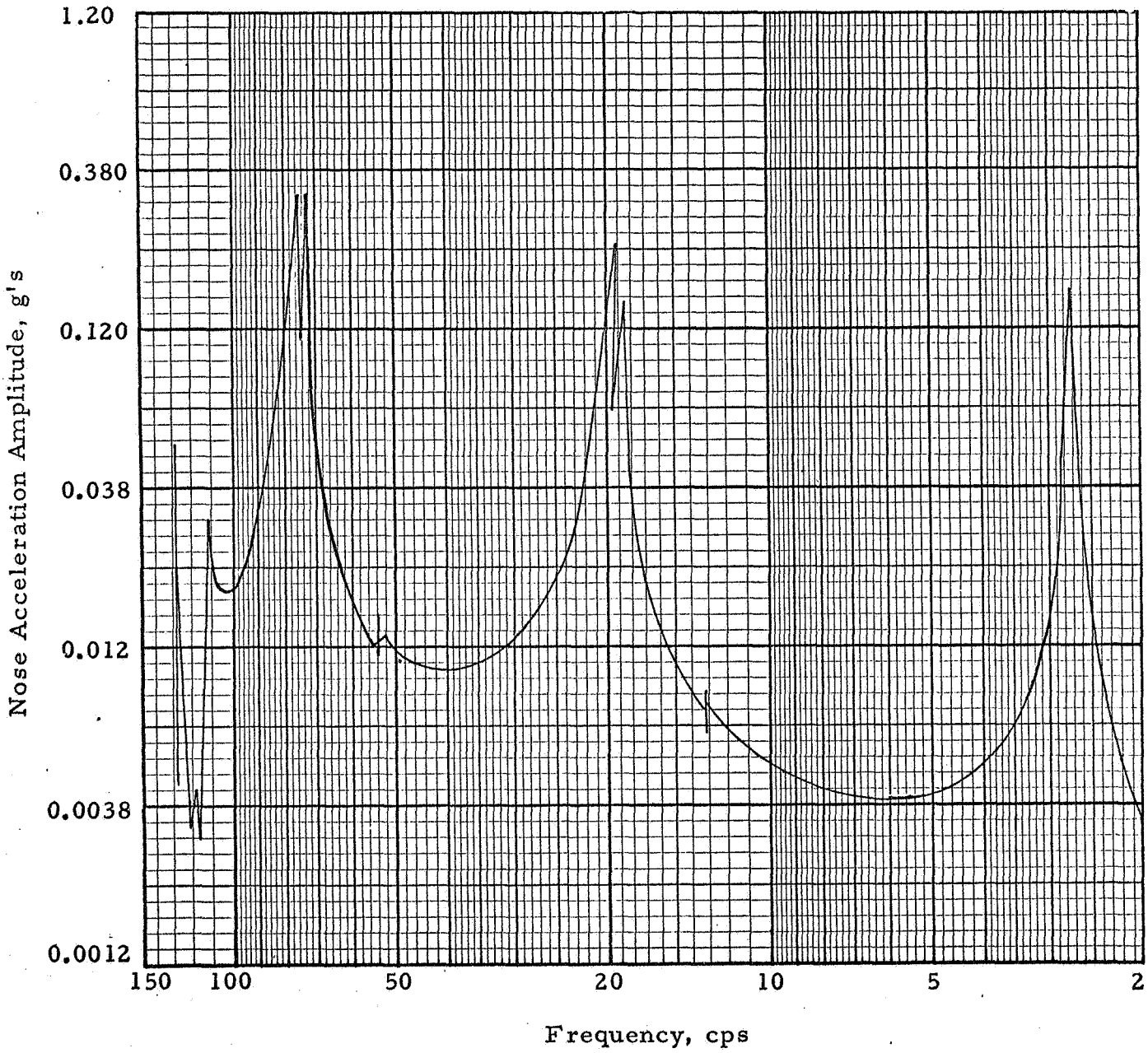

Figure C-A-3 - Frequency Response (Configuration A) Force Amplitude: 0.40 lb at 40 cps

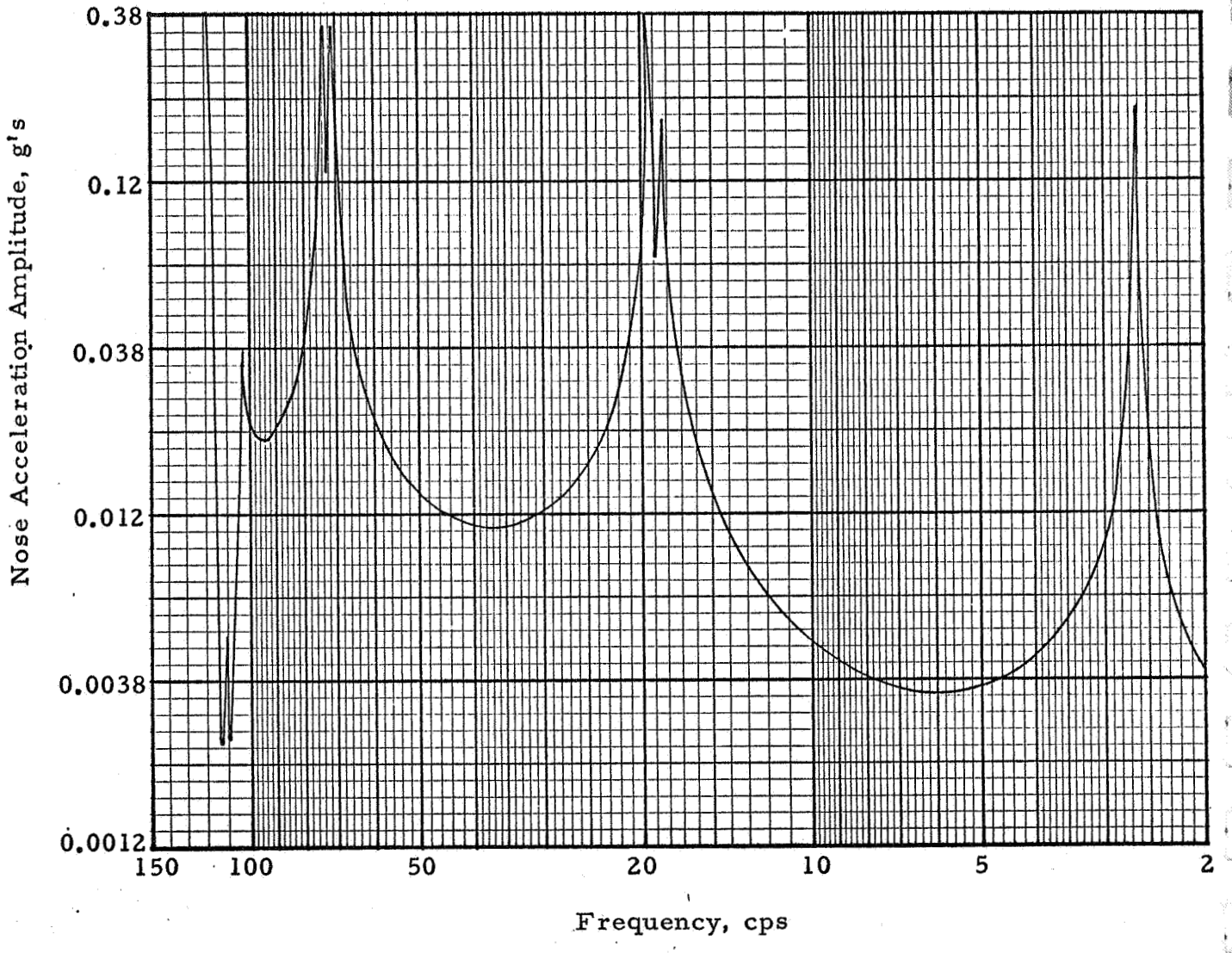

Figure C-A-4 - Frequency Response (Configuration A) Force Amplitude: 1.262 lb at 40 cps

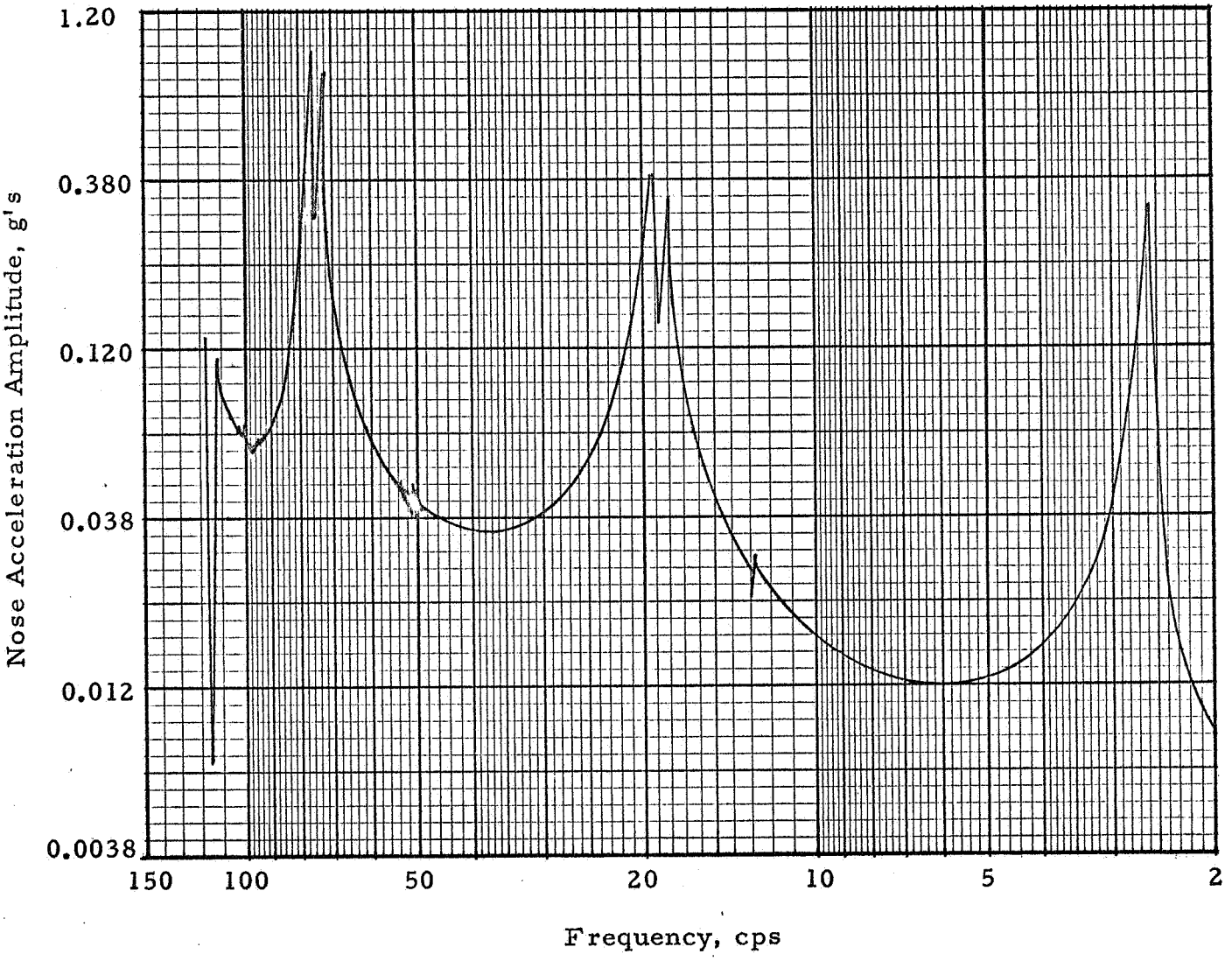

Figure C-A-5 - Frequency Response (Configuration A) Force Amplitude: 4.05 lb at 40 cps

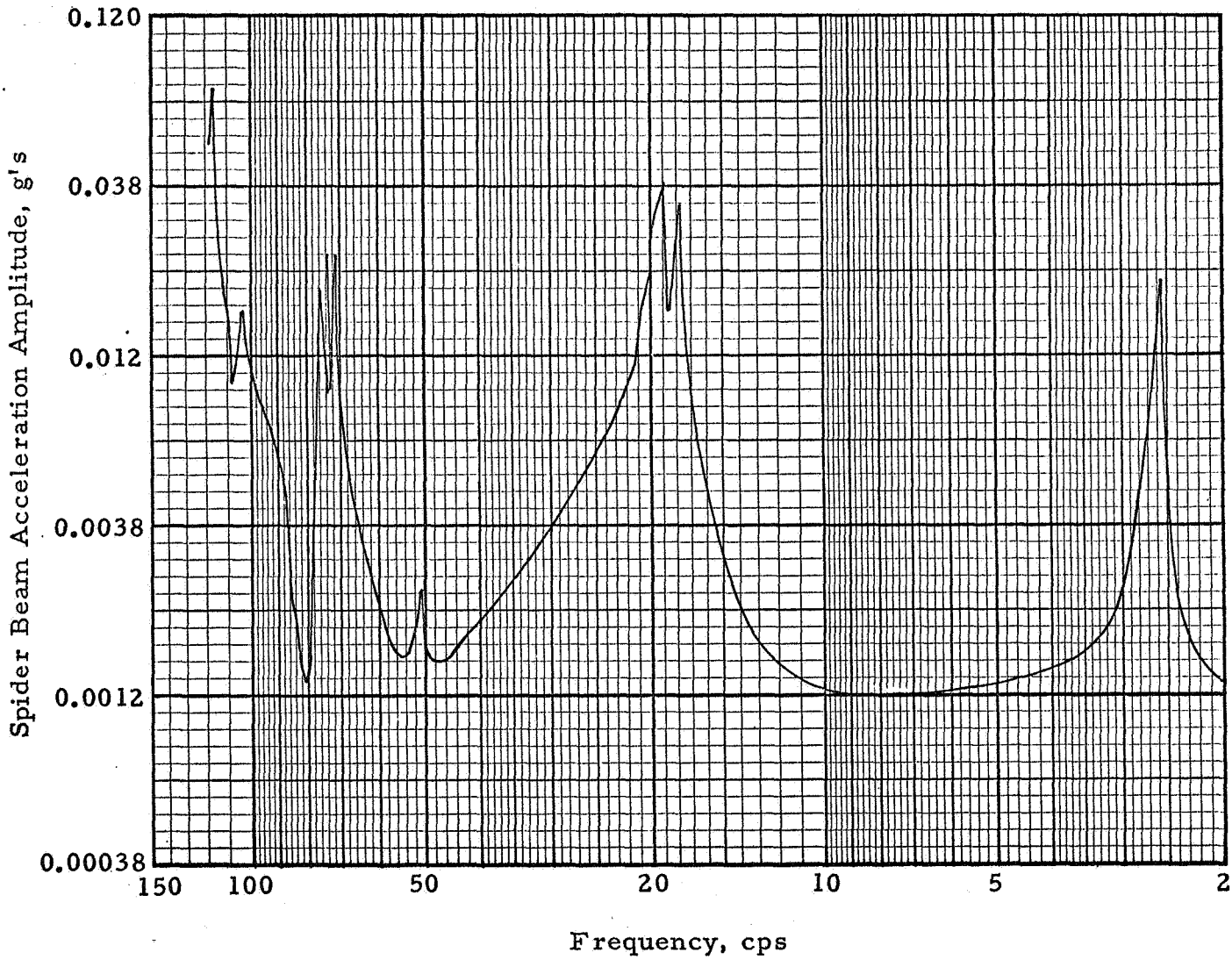

Figure C-A-6 - Frequency Response (Configuration A) Force Amplitude: 4.05 lb at 40 cps

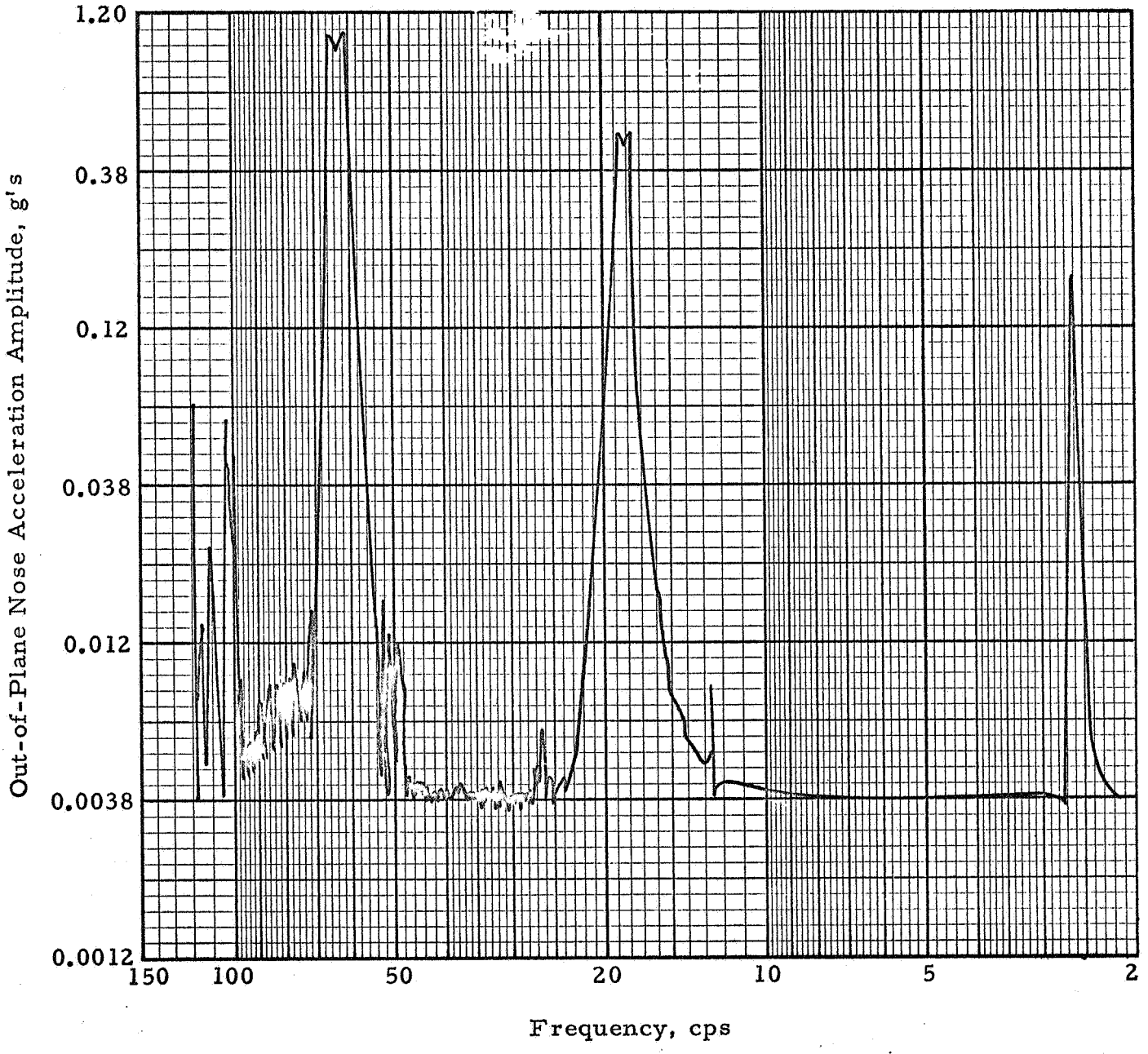

Figure C-A-7 - Frequency Response (Configuration A) Force Amplitude: 4.05 lb at 40 cps

CONFIGURATION: A

FREQUENCY: 2.639 cps

FORCE: 0.4 pounds, 0-pk

MODE NUMBER: 1

DAMPING: see Figure C-A-26

TIP ACCELERATION: 0.048 g (In-Plane)

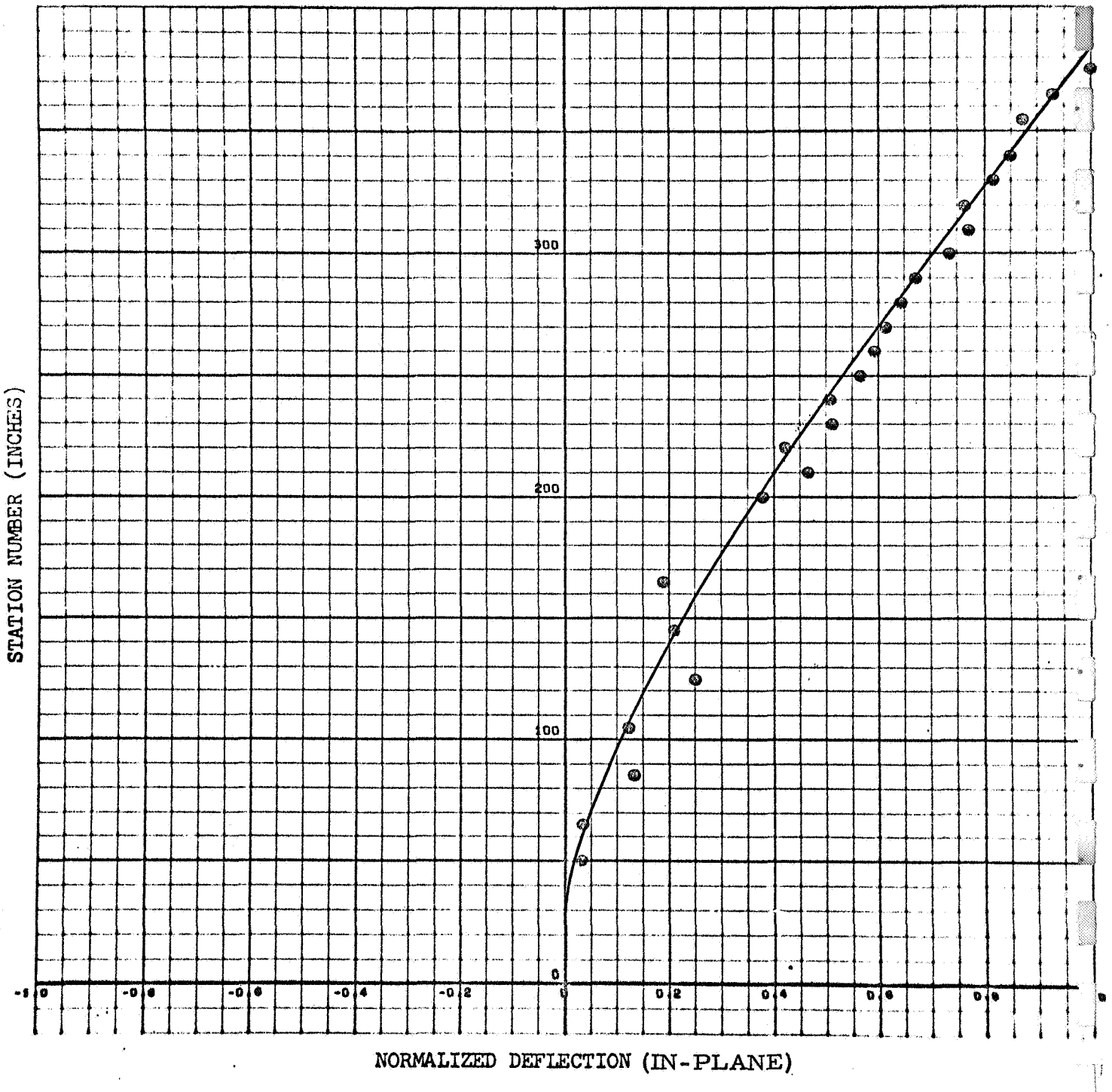

Figure C-A-8

CONFIGURATION: A

FREQUENCY: 2.639 cps

FORCE: 0.4 pounds, 0-pk

MODE NUMBER: 1

DAMPING: see Figure C-A-26

TIP ACCELERATION: 0.014 g (Out-of-Plane)

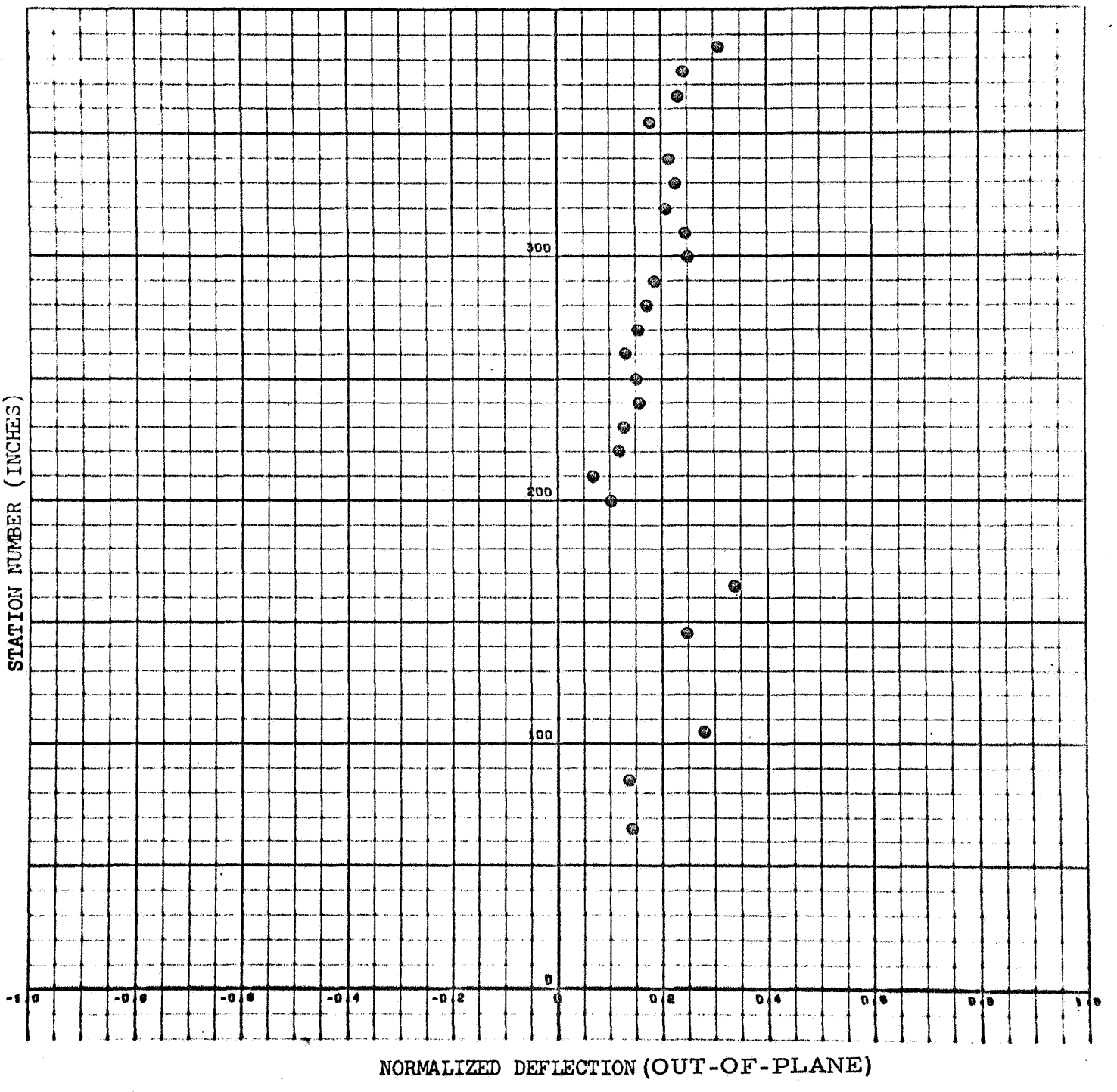

Figure C-A-9

CONFIGURATION: A

FREQUENCY: 19.28 cps

FORCE: 0.4 pounds, 0-pk

MODE NUMBER: 2

DAMPING: See Figure C-A-27

TIP ACCELERATION: 0.073 g (In-Plane)

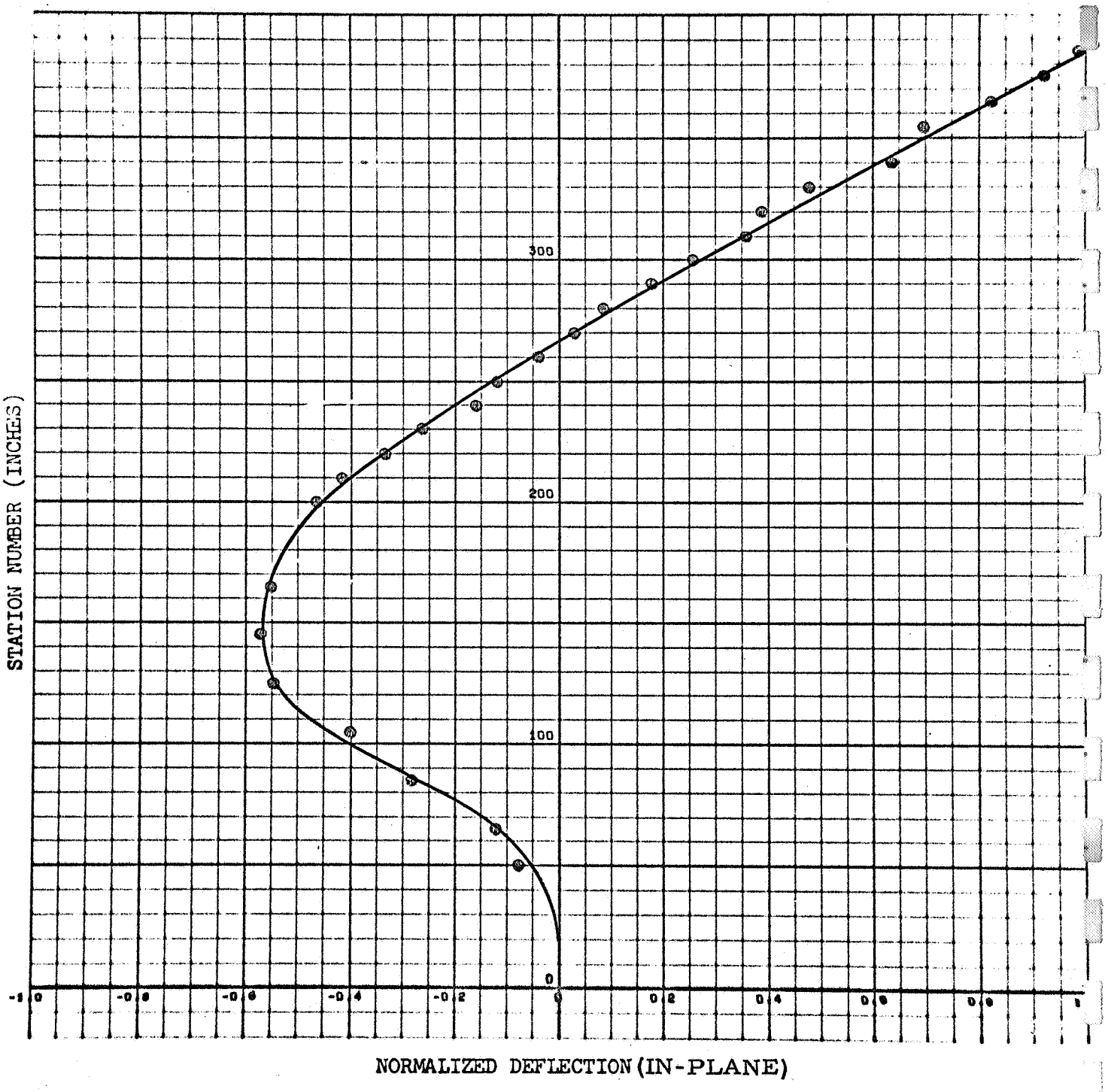

Figure C-A-10

CONFIGURATION: A

FREQUENCY: 19.28 cps

FORCE: 0.4 pounds, 0-pk

MODE NUMBER: 2

DAMPING: see Figure C-A-27

TIP ACCELERATION: 0.072 g (Out-of-Plane)

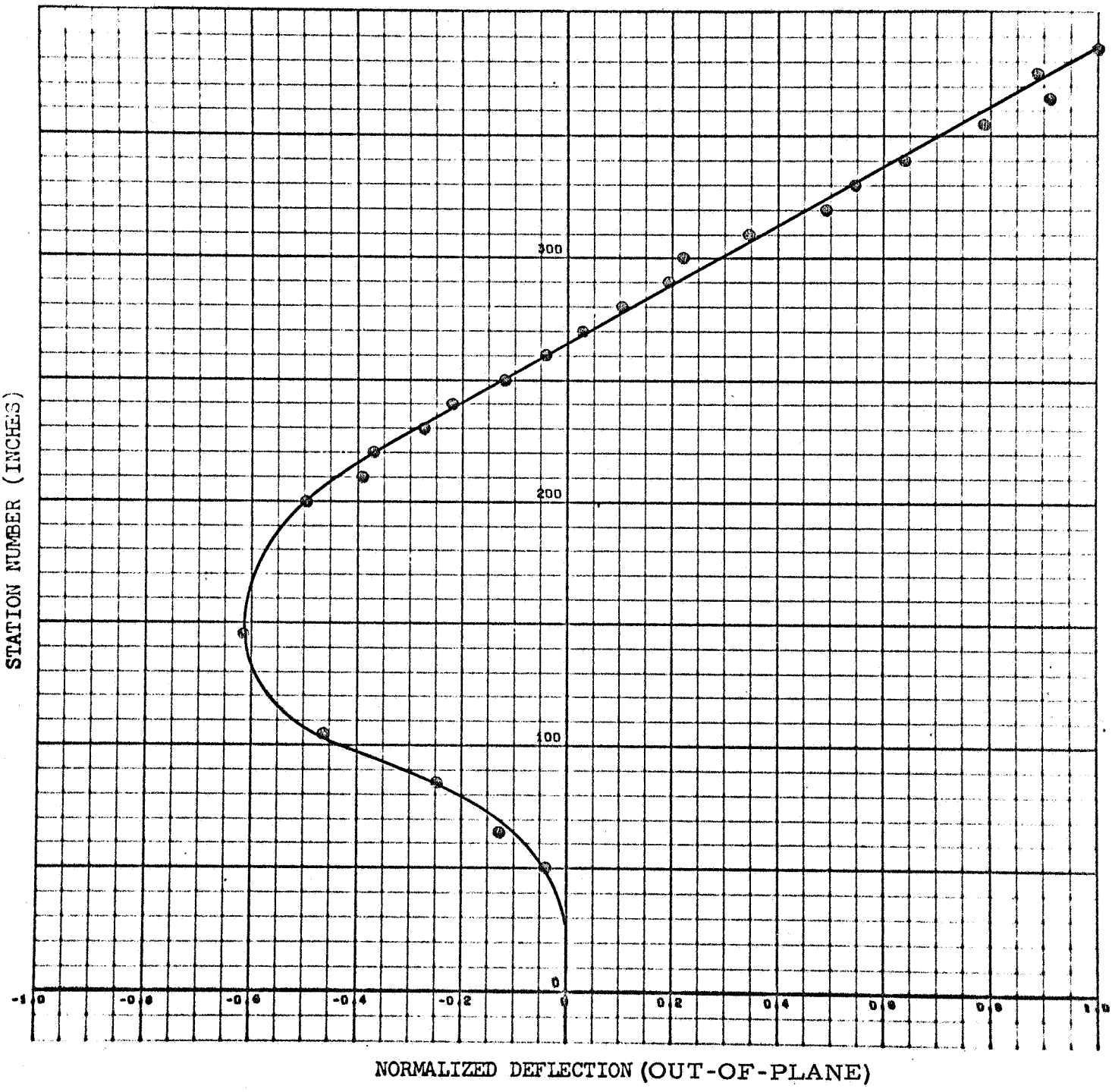

Figure C-A-11

CONFIGURATION: A

FREQUENCY: 72.25 cps

FORCE: 0.4 pounds, 0-pk

MODE NUMBER: 3

DAMPING: see Figure C-A-27

TIP ACCELERATION: 0.119 g (In-Plane)

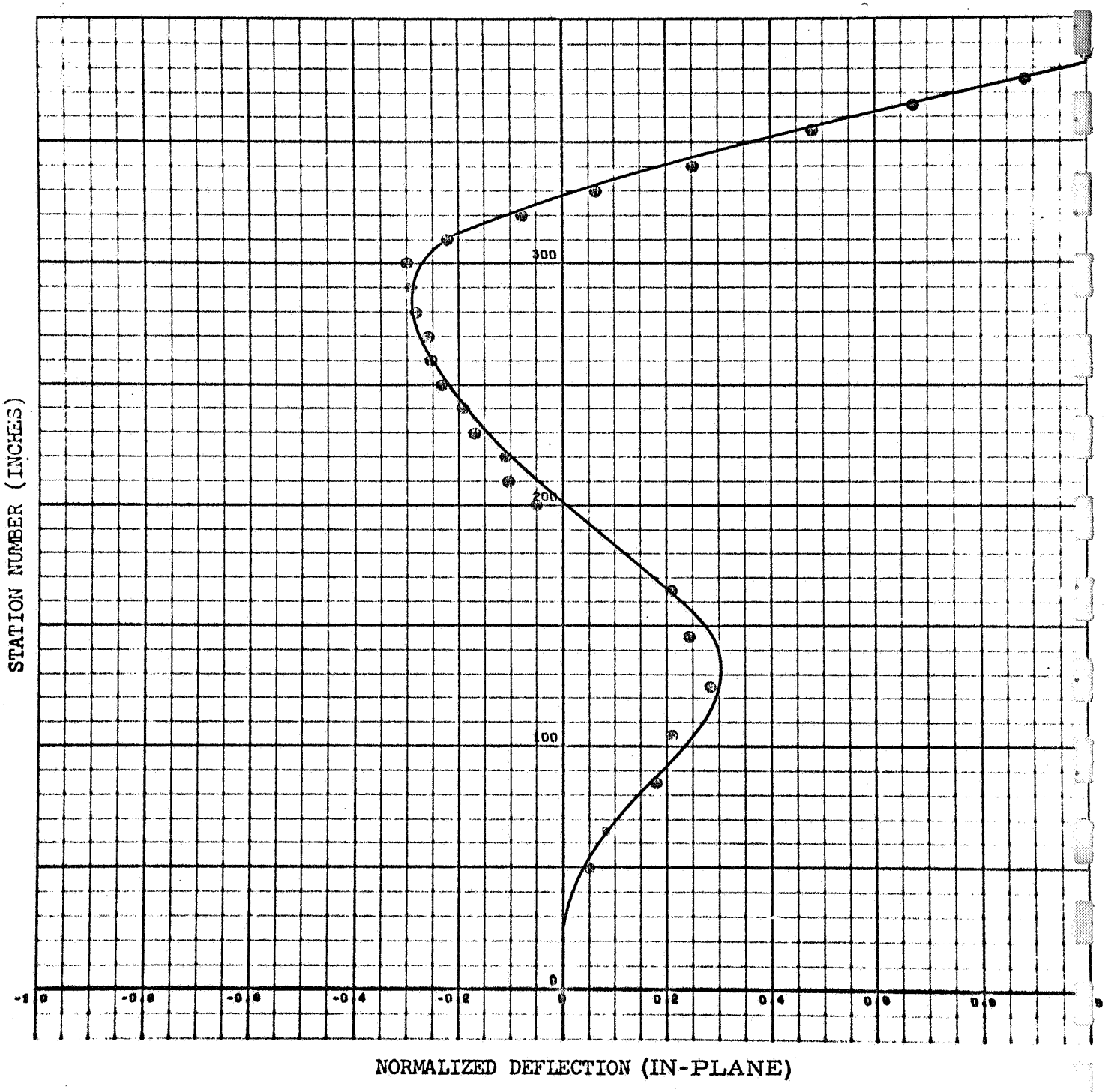

Figure C-A-12

CONFIGURATION: A

FREQUENCY: 72.25 cps

FORCE: 0.4 pounds, 0-pk

MODE NUMBER: 3

DAMPING: see Figure C-A-27

TIP ACCELERATION: 0.098 g (Out-of-Plane)

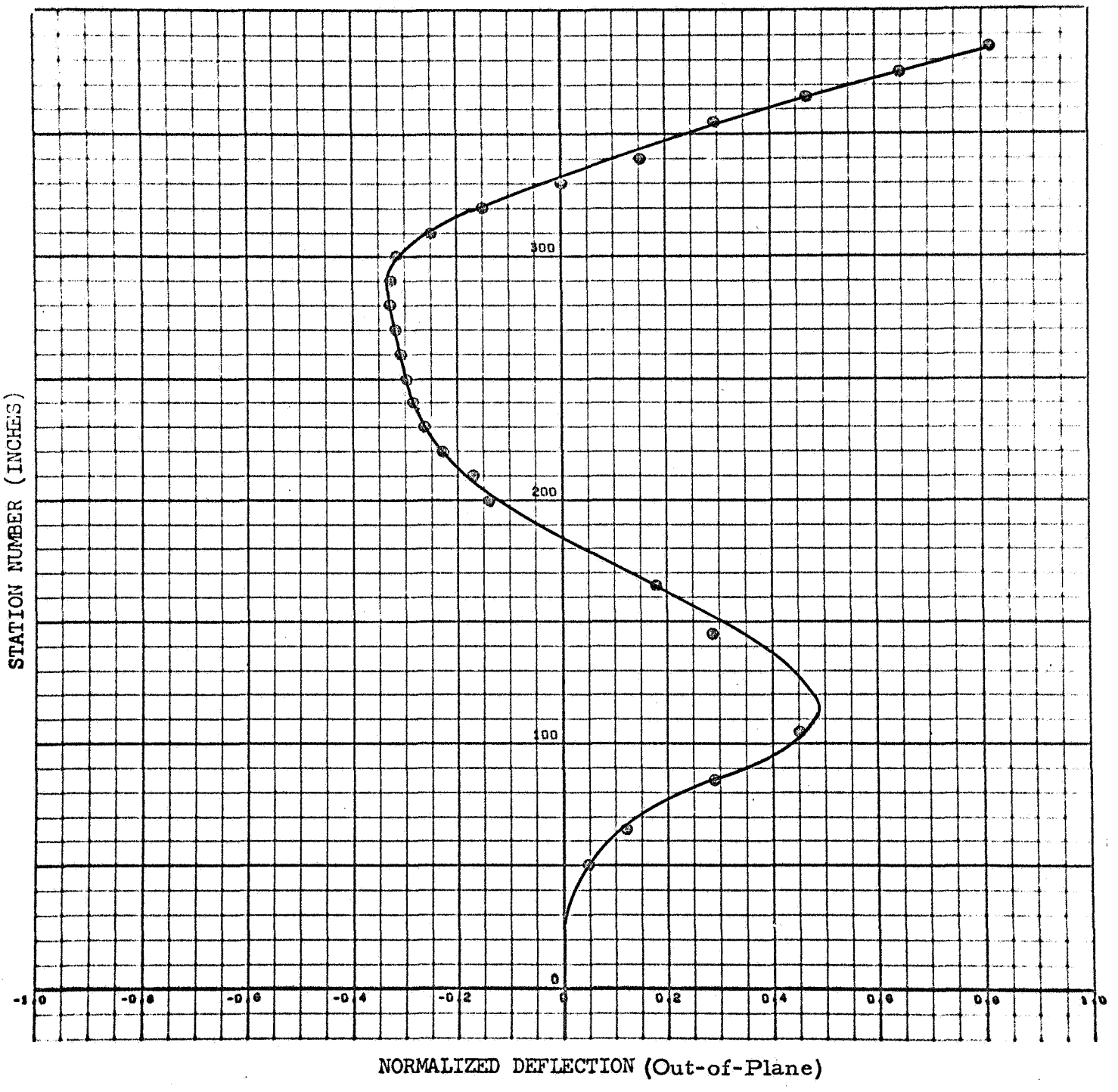

Figure C-A-13

CONFIGURATION: A

FREQUENCY: 2.548 cps

MODE NUMBER: 1

FORCE: 4.0 pounds, 0-pk

DAMPING: see Figure C-A-26

GENERALIZED WEIGHT: 1516.3 pounds

TIP ACCELERATION: 0.065 g (Out-of-Plane)

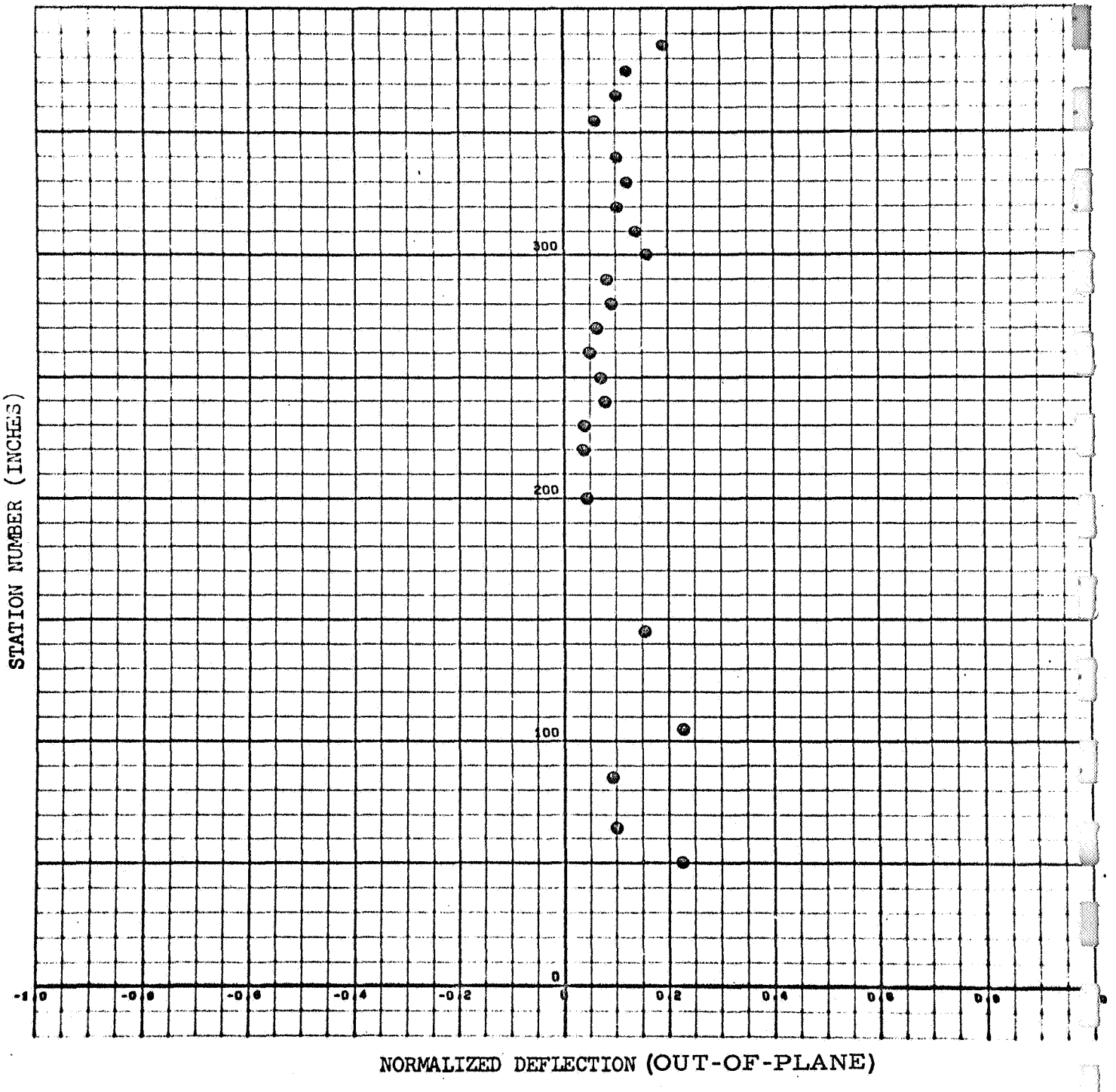

Figure C-A-14

CONFIGURATION: A

FREQUENCY: 18.91 cps

FORCE: 2.25 pounds, 0-pk

MODE NUMBER: 2

DAMPING: see Figure C-A-27

TIP ACCELERATION: 0.269 g (In-Plane)

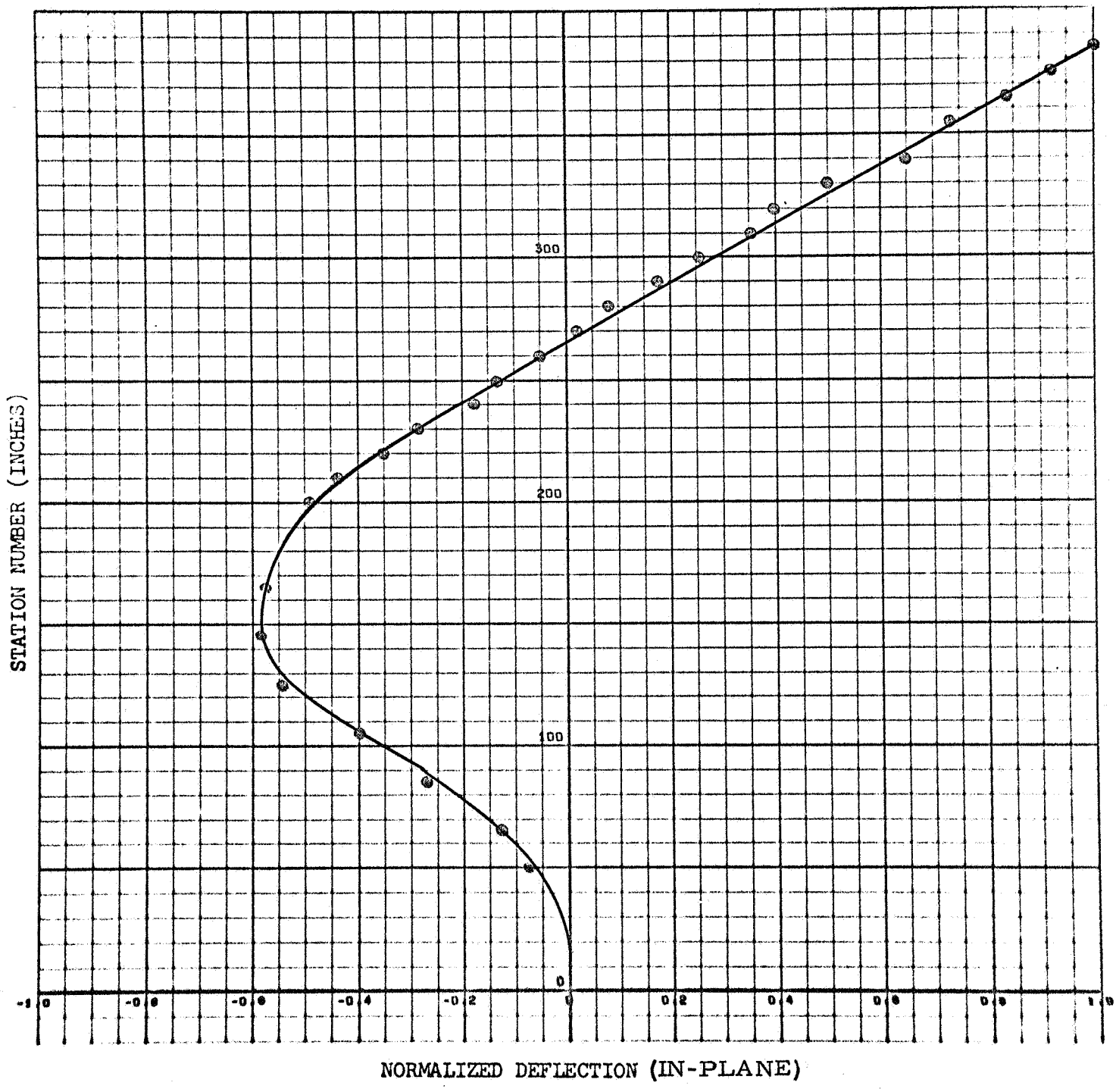

Figure C-A-15

CONFIGURATION: A

FREQUENCY: 18.91 cps

FORCE: 2.25 pounds, 0-pk

MODE NUMBER: 2

DAMPING: see Figure C-A-27

TIP ACCELERATION: 0.256 g (Out-of-Plane)

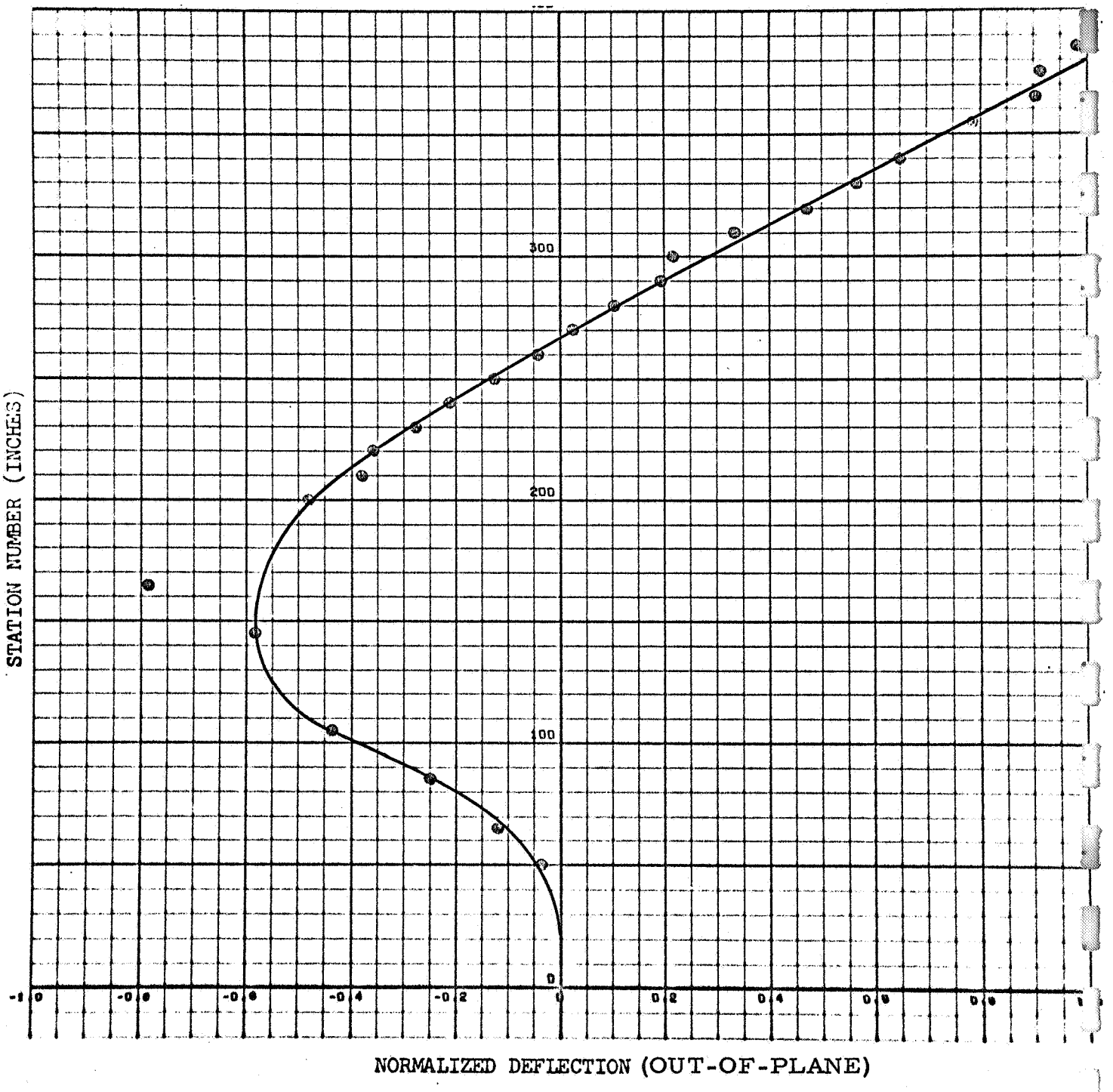

Figure C-A-16

CONFIGURATION: A

FREQUENCY: 73.8 cps

FORCE: 2.25 pounds, 0-pk

MODE NUMBER: 3

DAMPING: see Figure C-A-27

TIP ACCELERATION: 0.585 g (In-Plane)

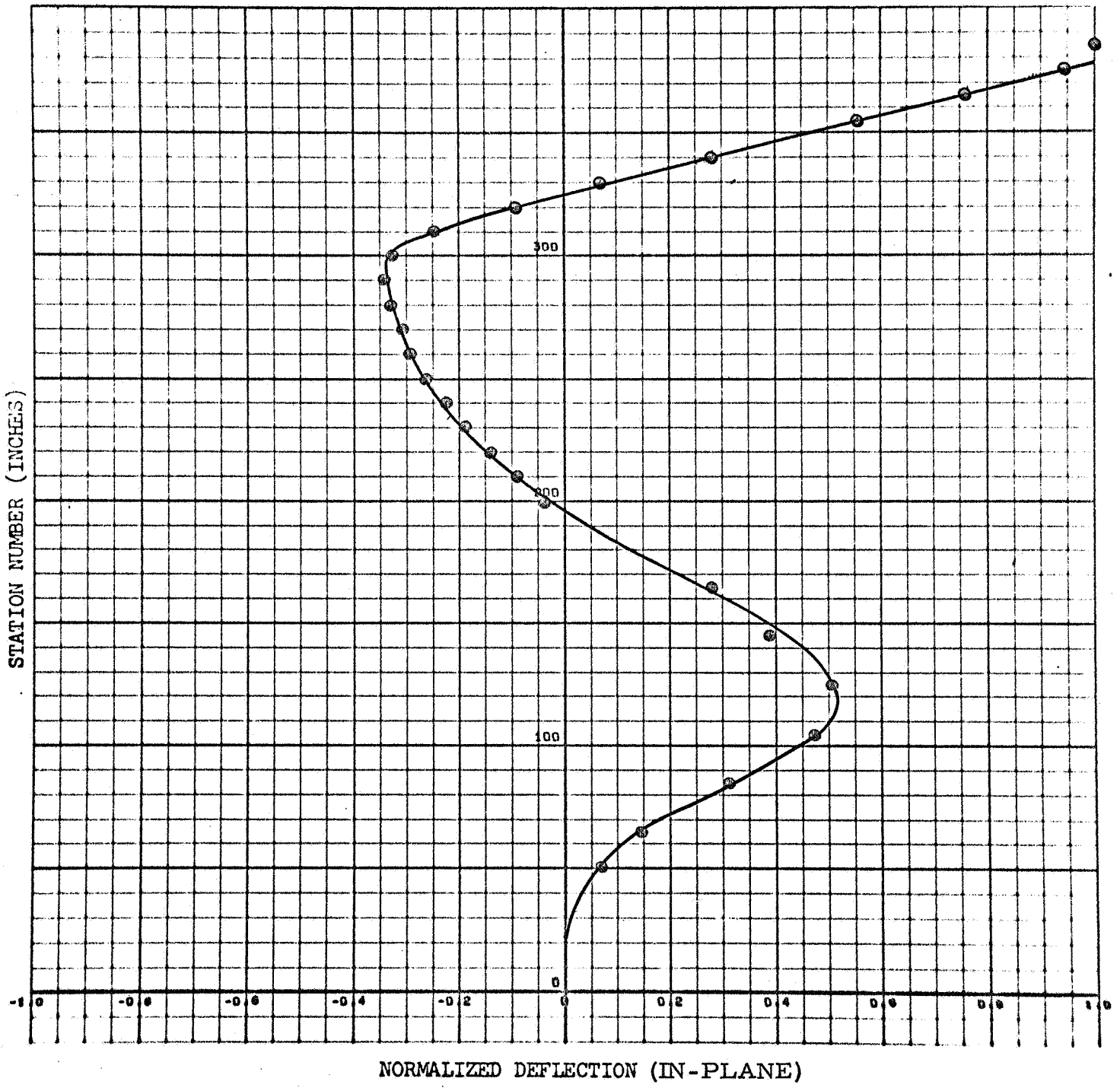

Figure C-A-17

CONFIGURATION: A

FREQUENCY: 73.8 cps

FORCE: 2.25 pounds, 0-pk

MODE NUMBER: 3

DAMPING: see Figure C-A-27

TIP ACCELERATION: 0.450 g (Out-of-Plane)

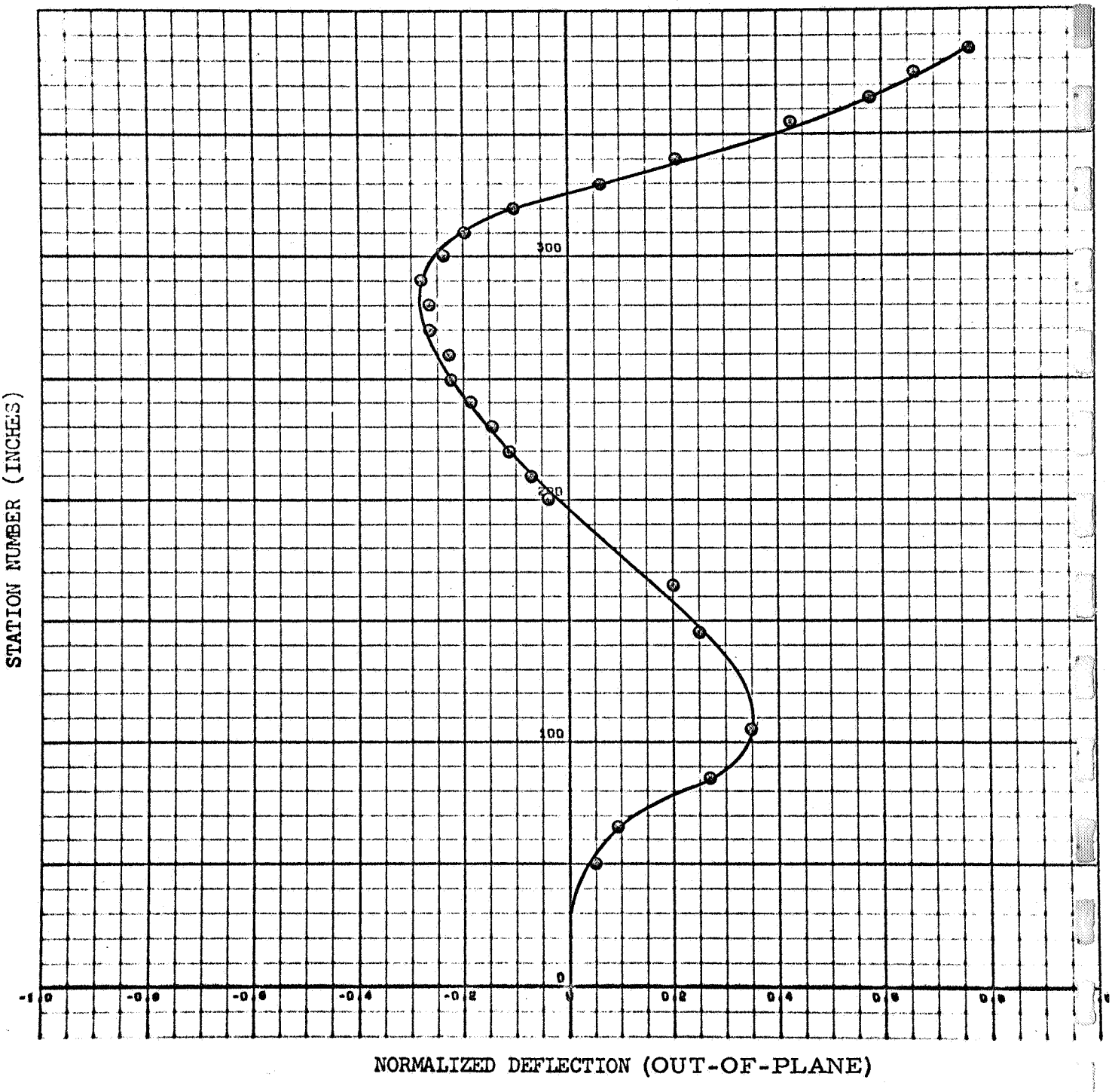

Figure C-A-18

CONFIGURATION: A

FREQUENCY: 2.548 cps

FORCE: 4.0 pounds, 0-pk

MODE NUMBER: 1

DAMPING: see Figure C-A-26

TIP ACCELERATION: 0.374 g (In-Plane)

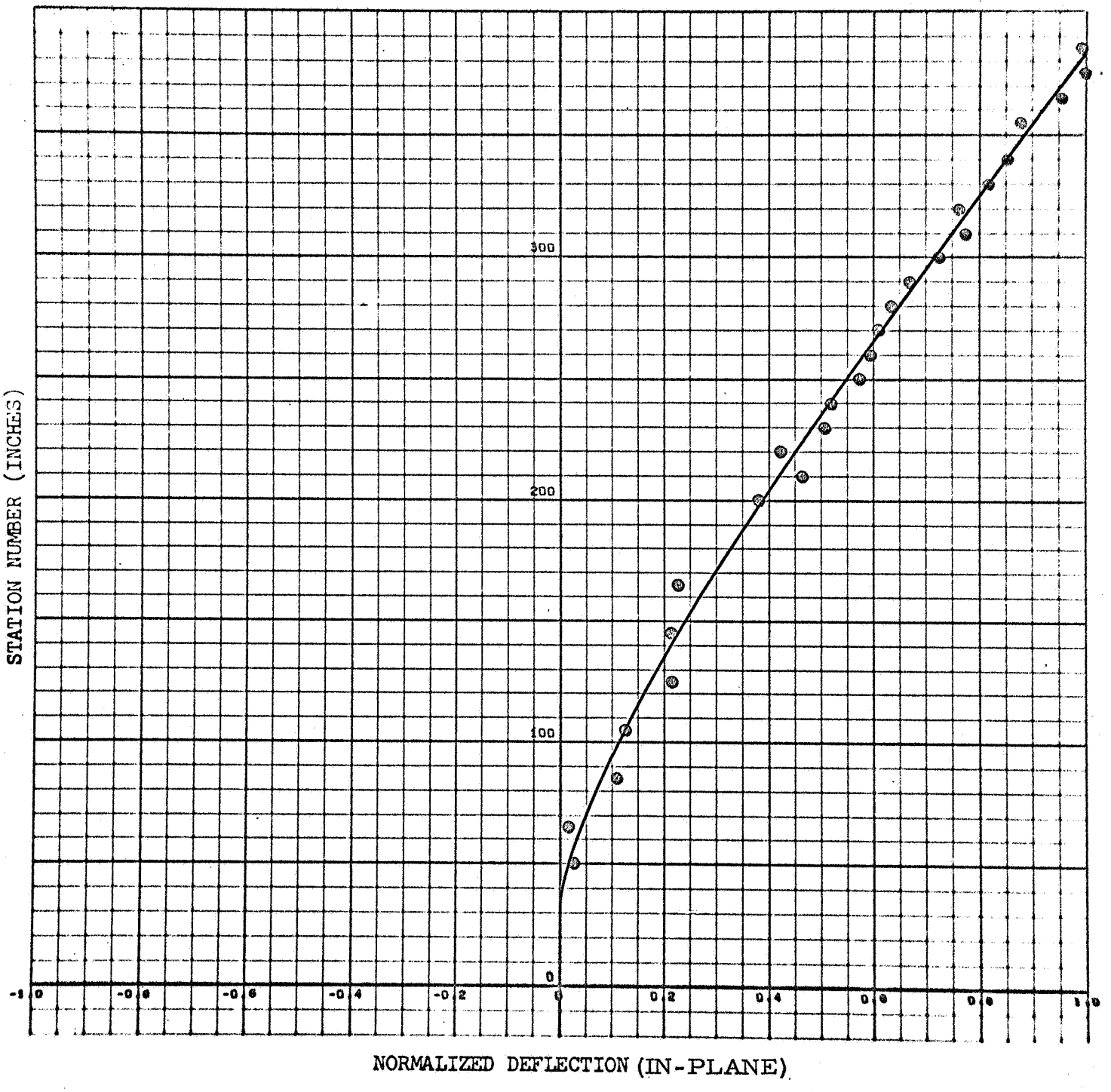

Figure C-A-19

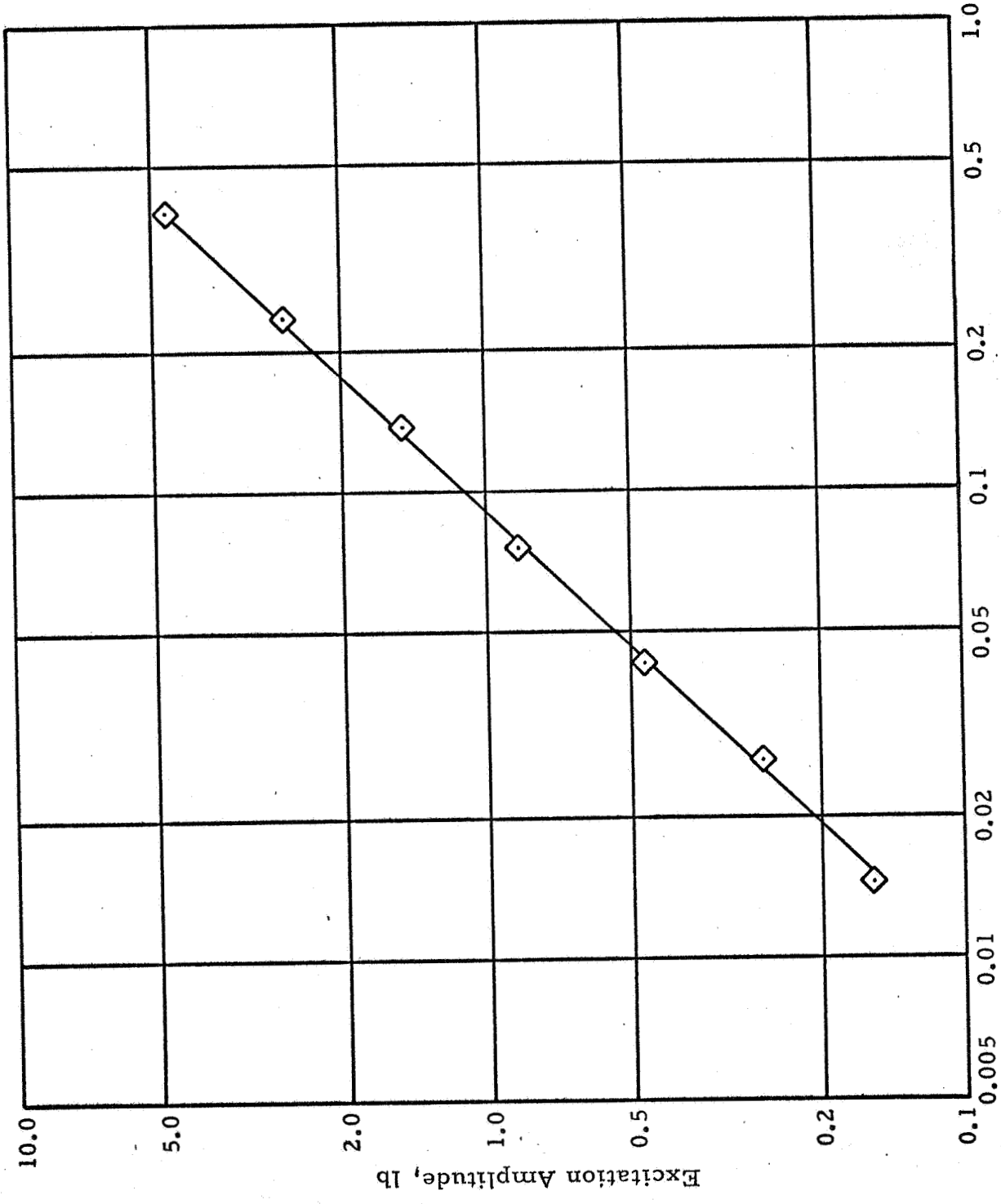

Figure C-A-20 - First Mode Resonant Response (Configuration A)

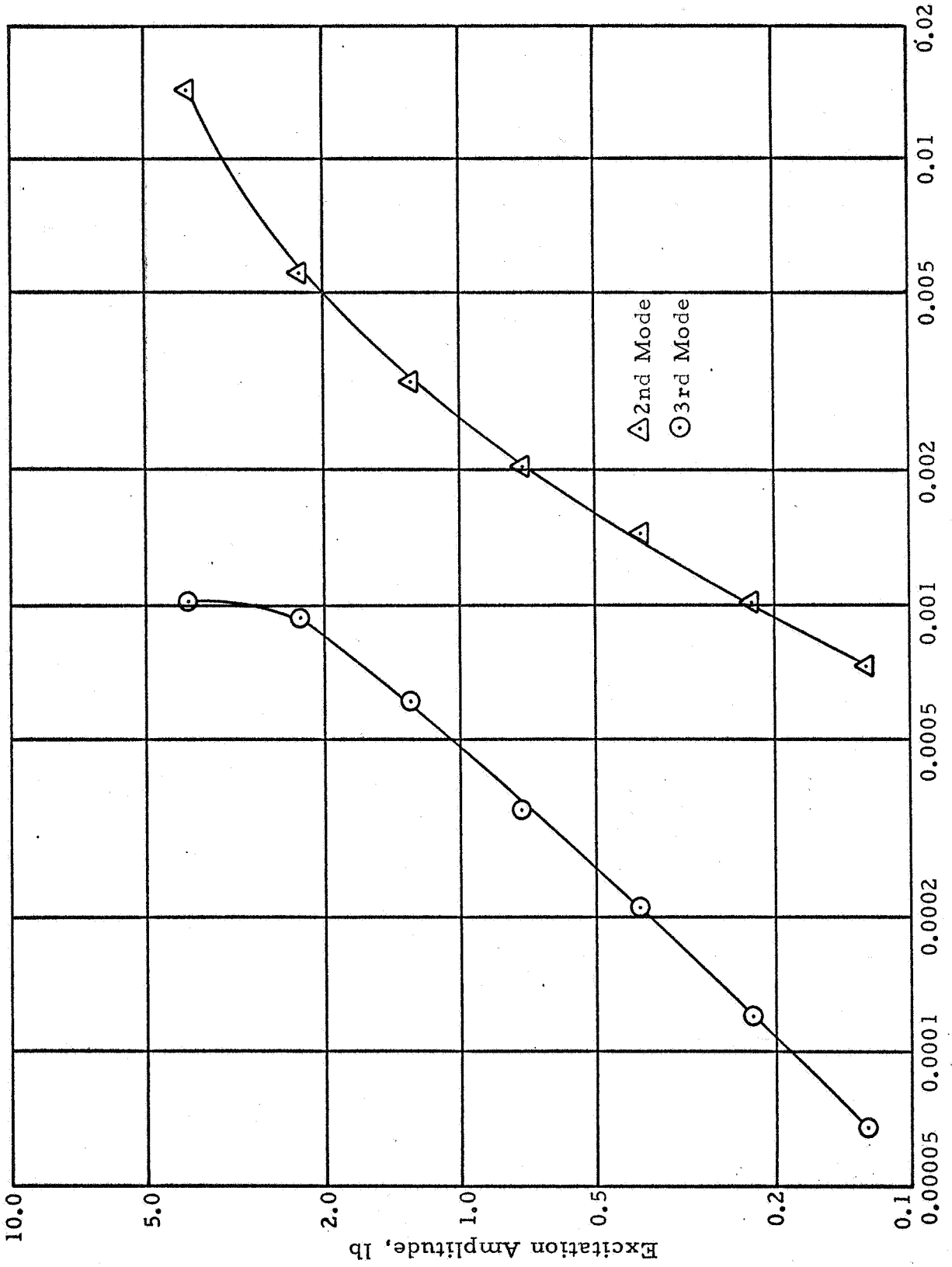

Figure C-A-21 - Second and Third Mode Resonant Responses (Configuration A)

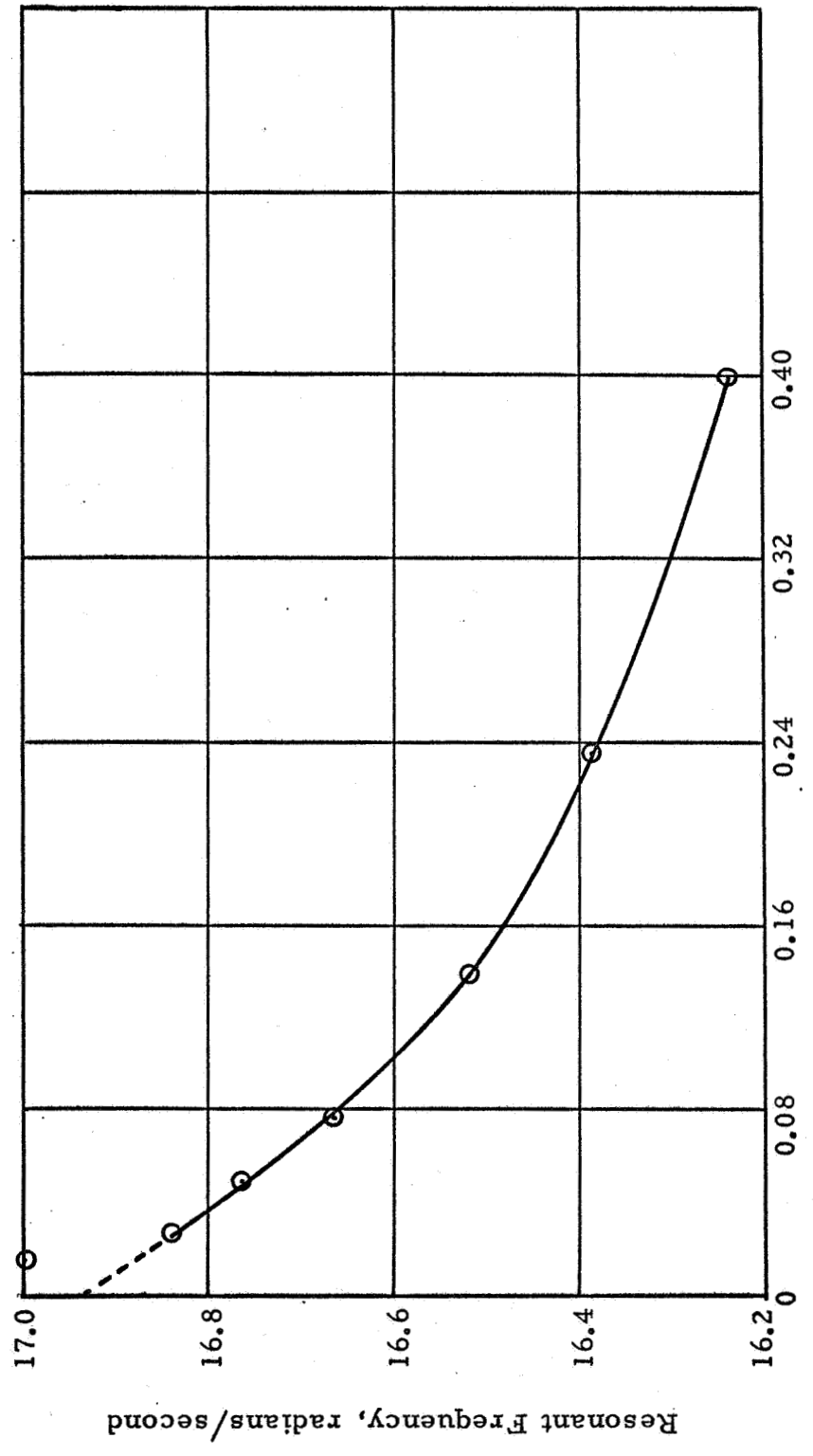

Figure C-A-22 - Variation of First Mode Frequency with Displacement Amplitude (Configuration A)

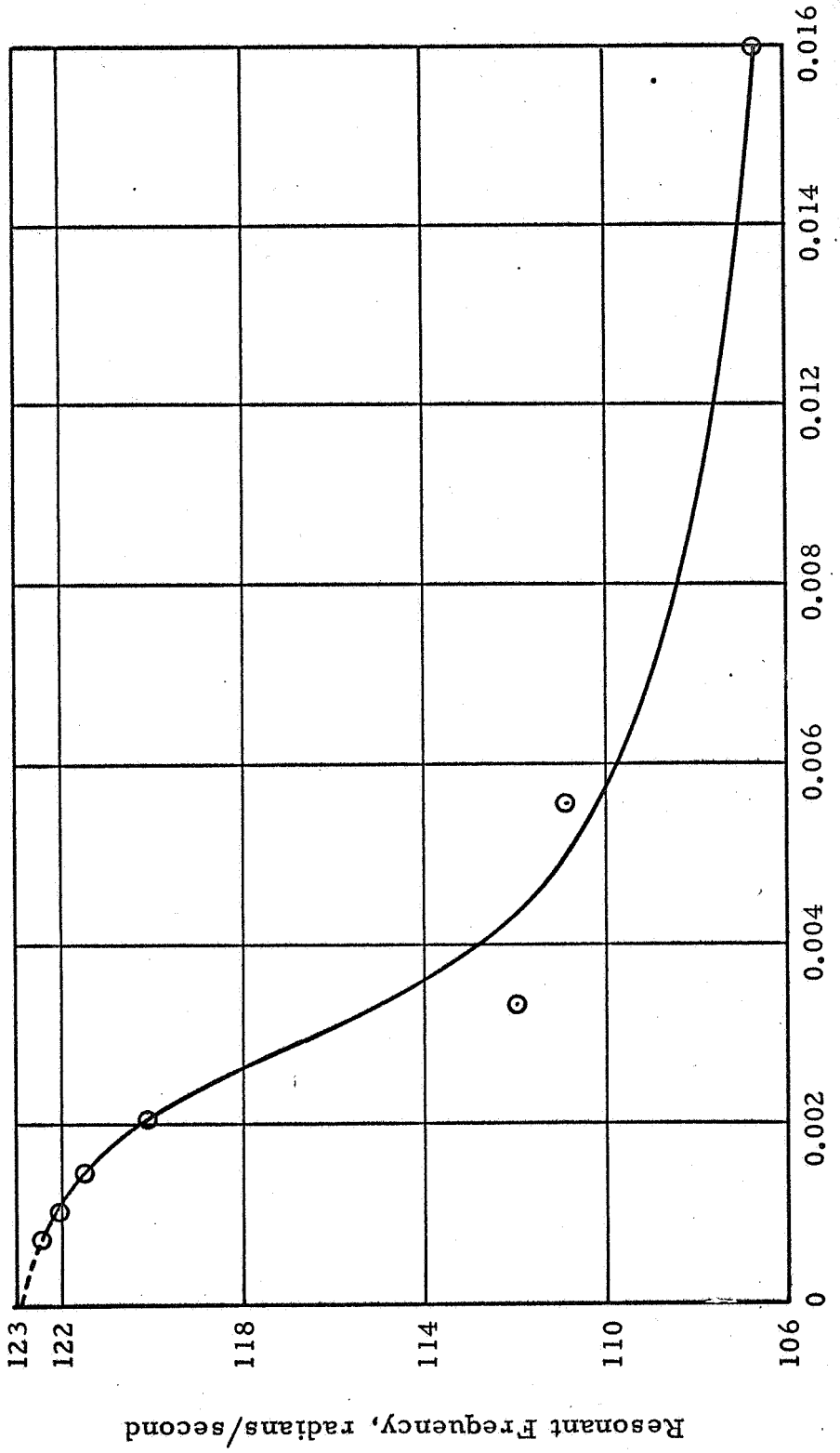

Figure C-A-23 - Variation of Second Mode Frequency with Displacement Amplitude (Configuration A)

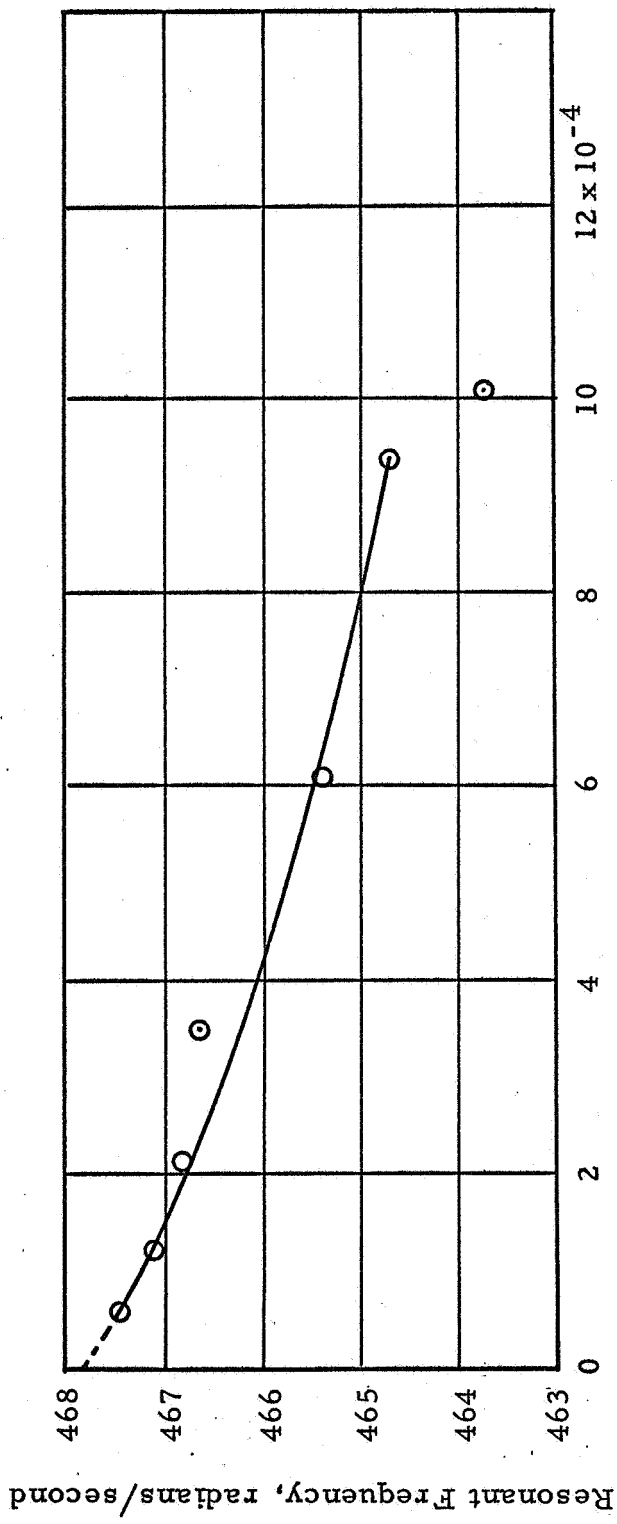

Figure C-A-24 - Variation of Third Mode Frequency with Displacement Amplitude (Configuration A)

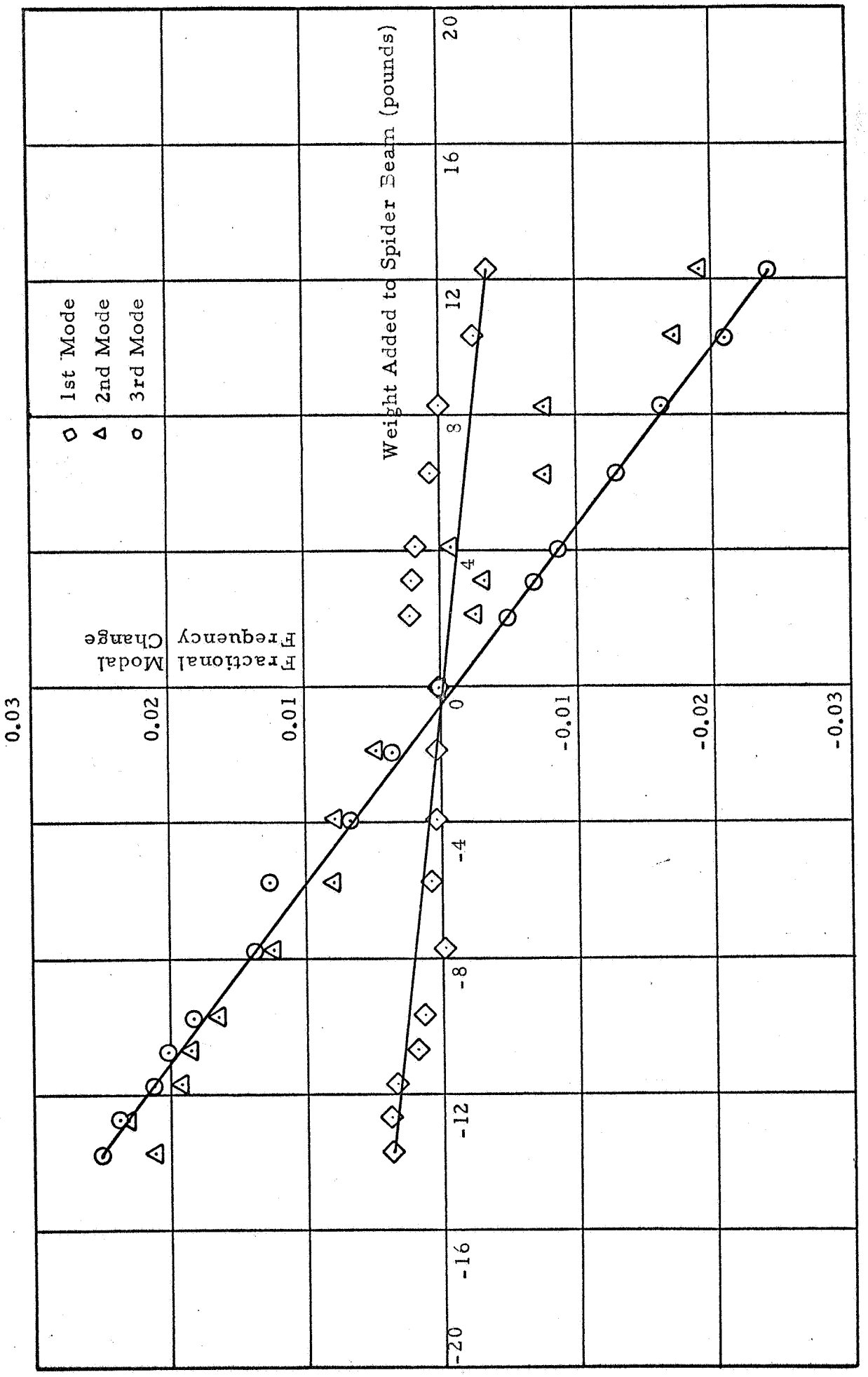

Figure C-A-25 - Generalized Mass Tests (Configuration A)

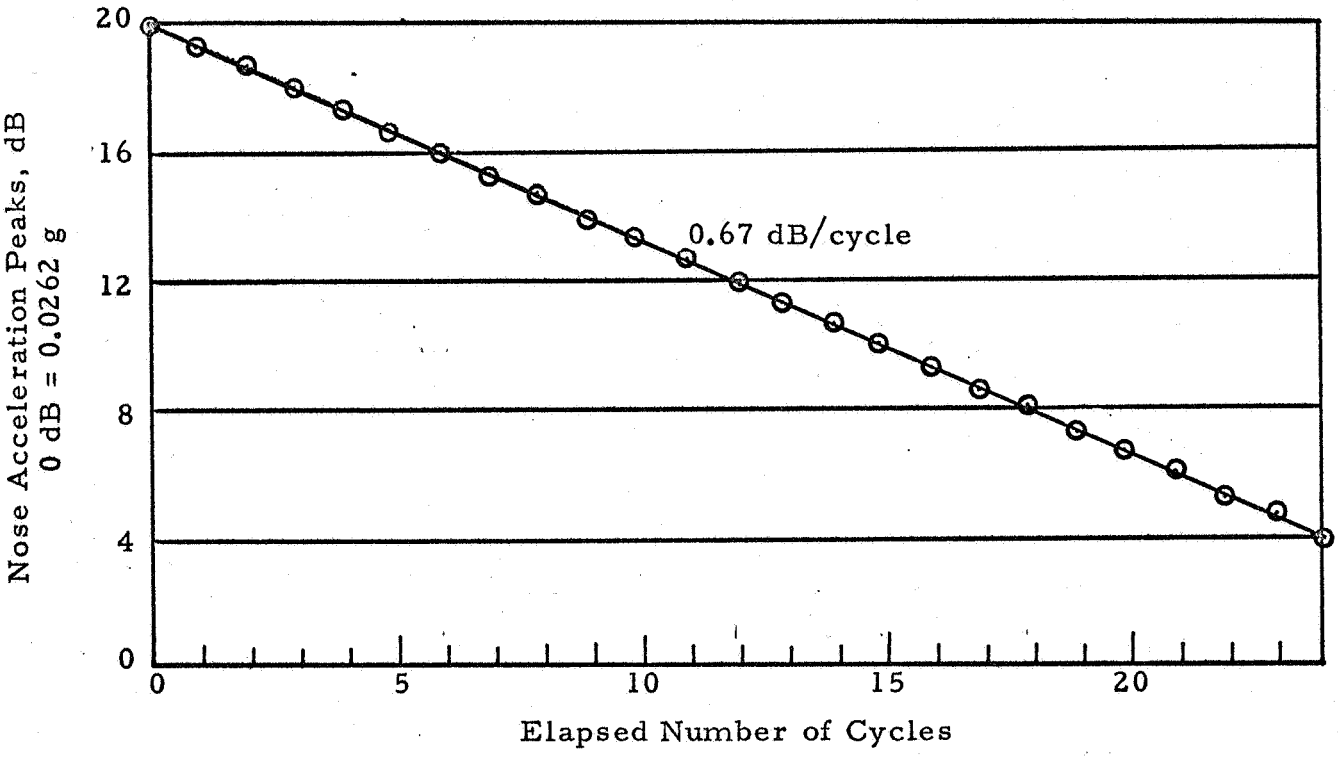

Figure C-A-26 - Decay of First Mode Free Vibration (Configuration A)

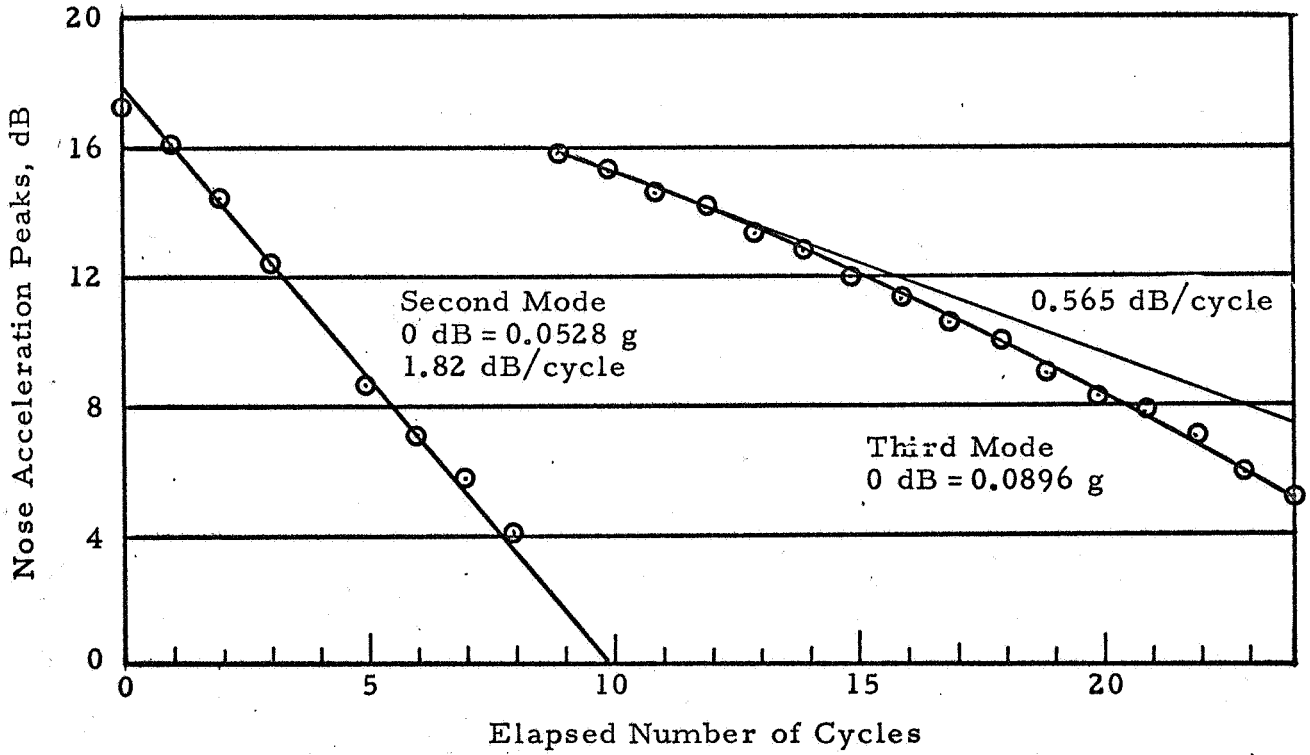

Figure C-A-27 - Decay of Second and Third Mode Free Vibration (Configuration A)

TEST CONFIGURATION B
INDEX TO FIGURES

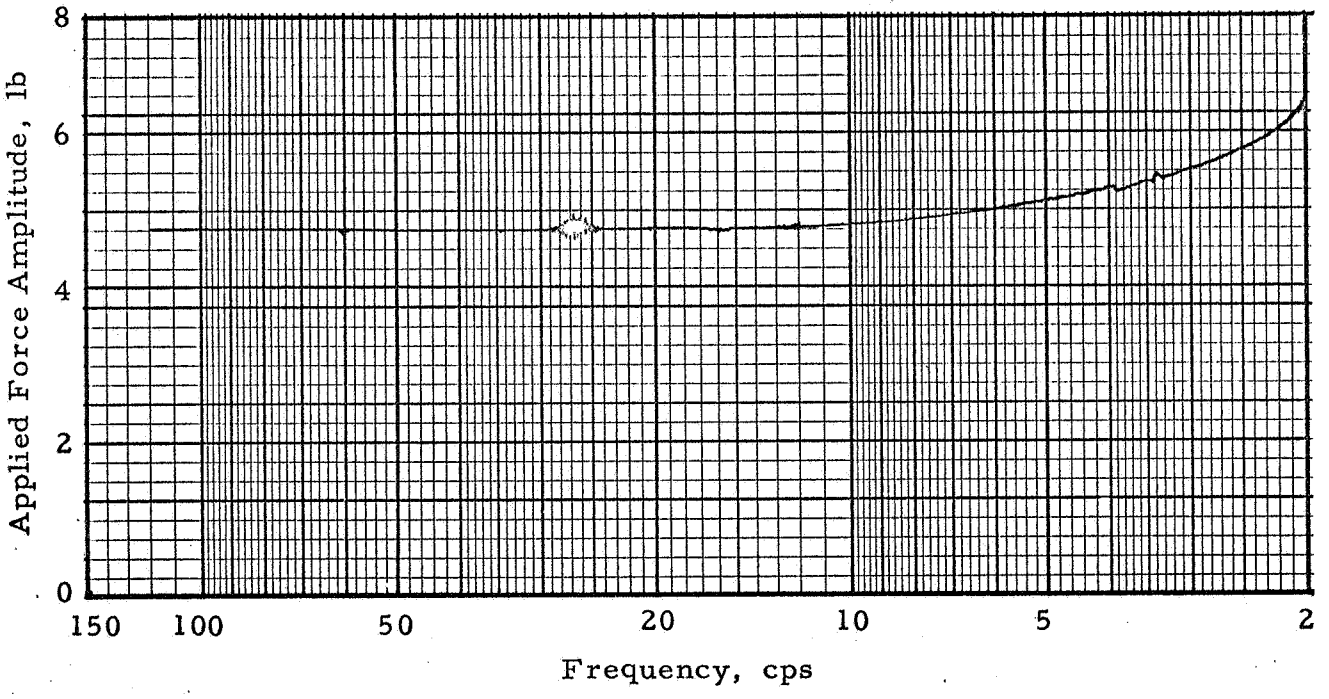

Figure C-B-1 - Variation of Applied Force Amplitude with Frequency (Configuration B)

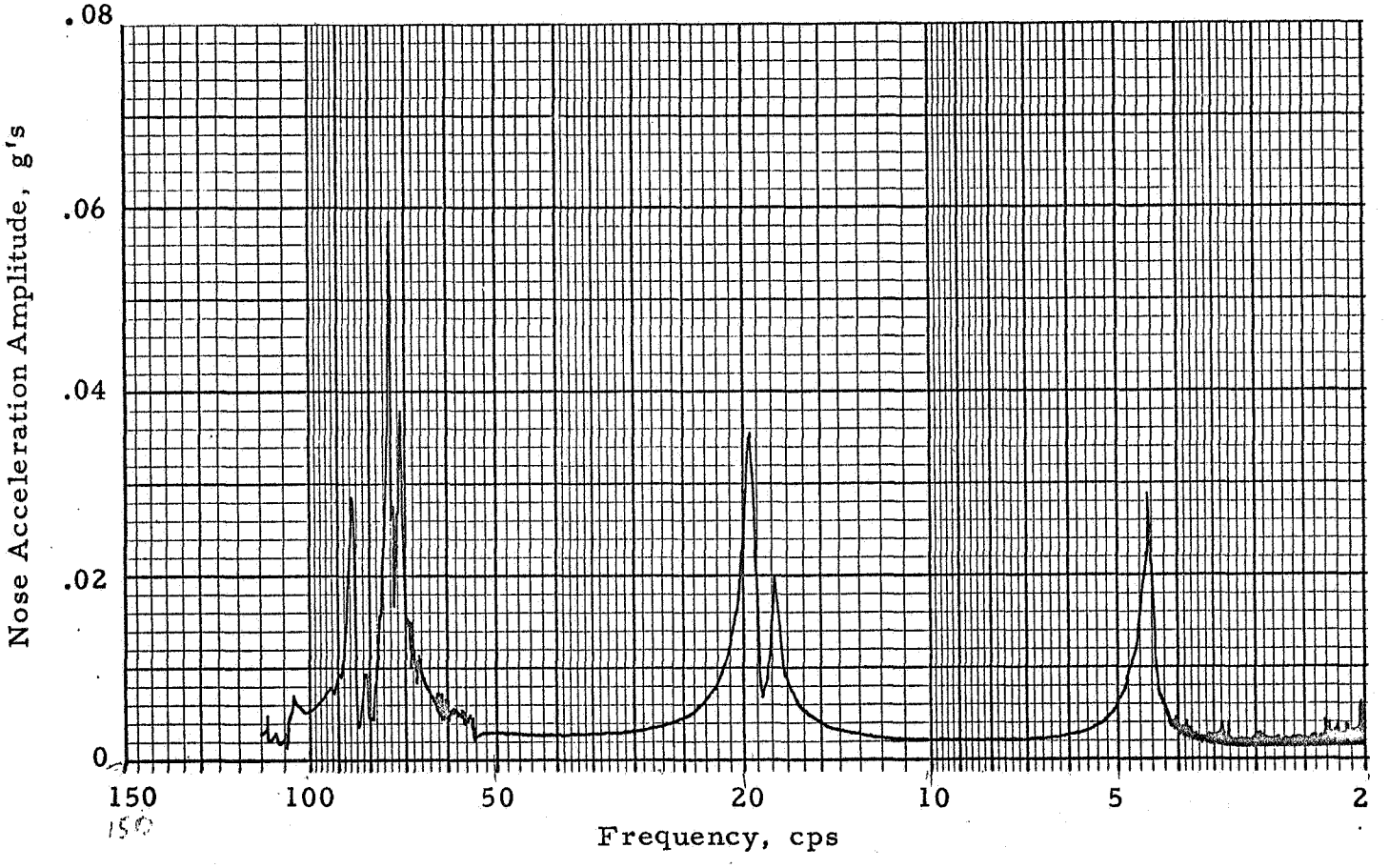

Figure C-B-2 - Frequency Response (Configuration B) Force Amplitude: 0.475 lb at 40 cps

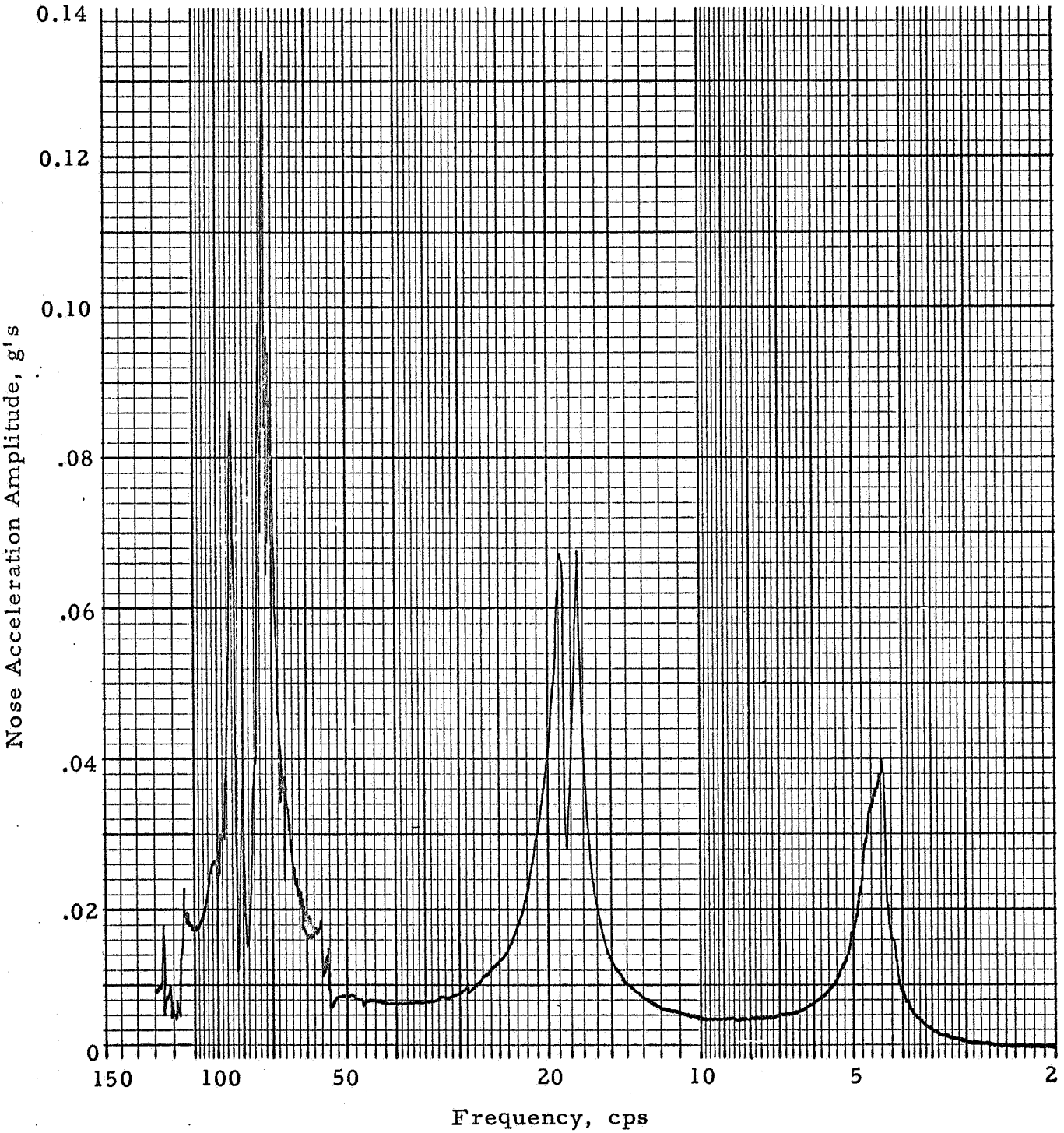

Figure C-B-3 - Frequency Response (Configuration B) Force Amplitude: 1.5 lb at 40 cps

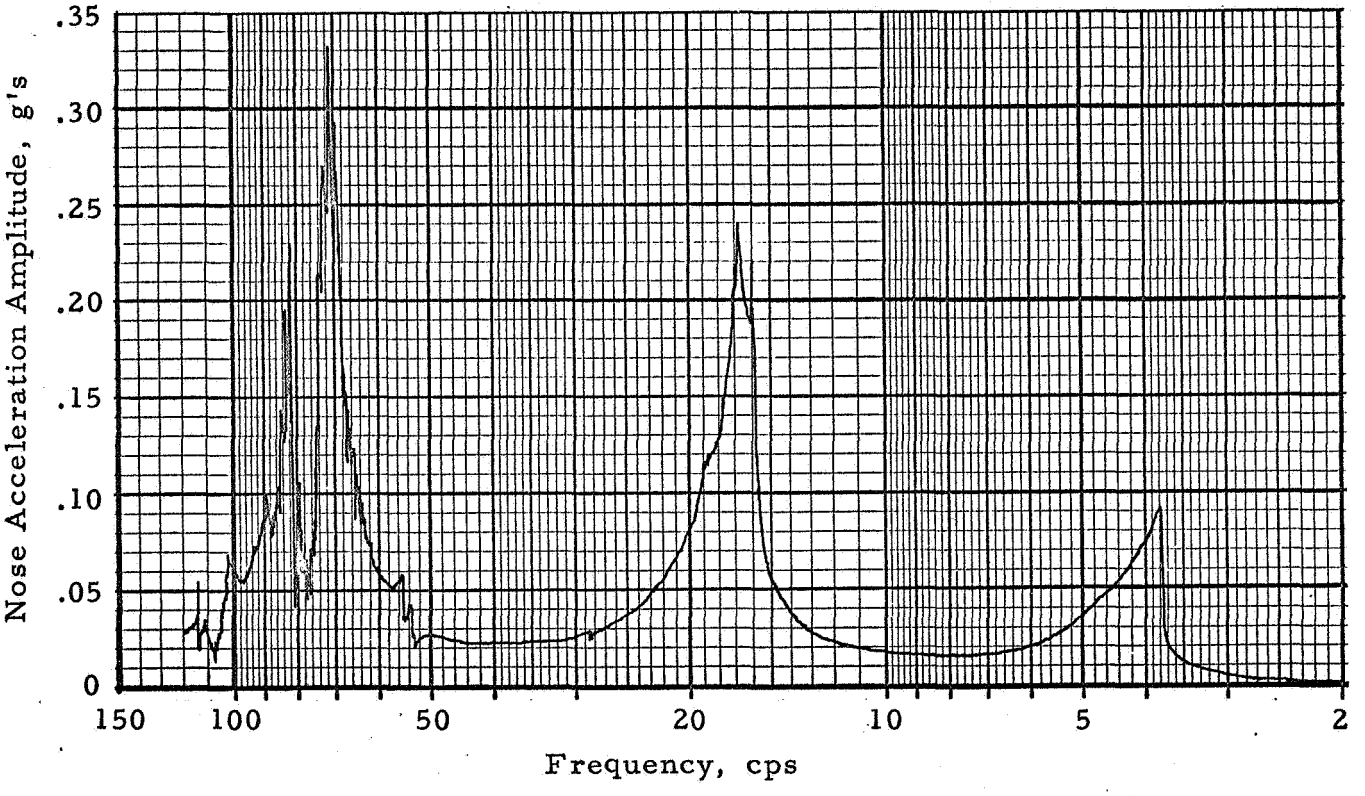

Figure C-B-4 - Frequency Response (Configuration B) Force Amplitude: 4.75 lb at 40 cps

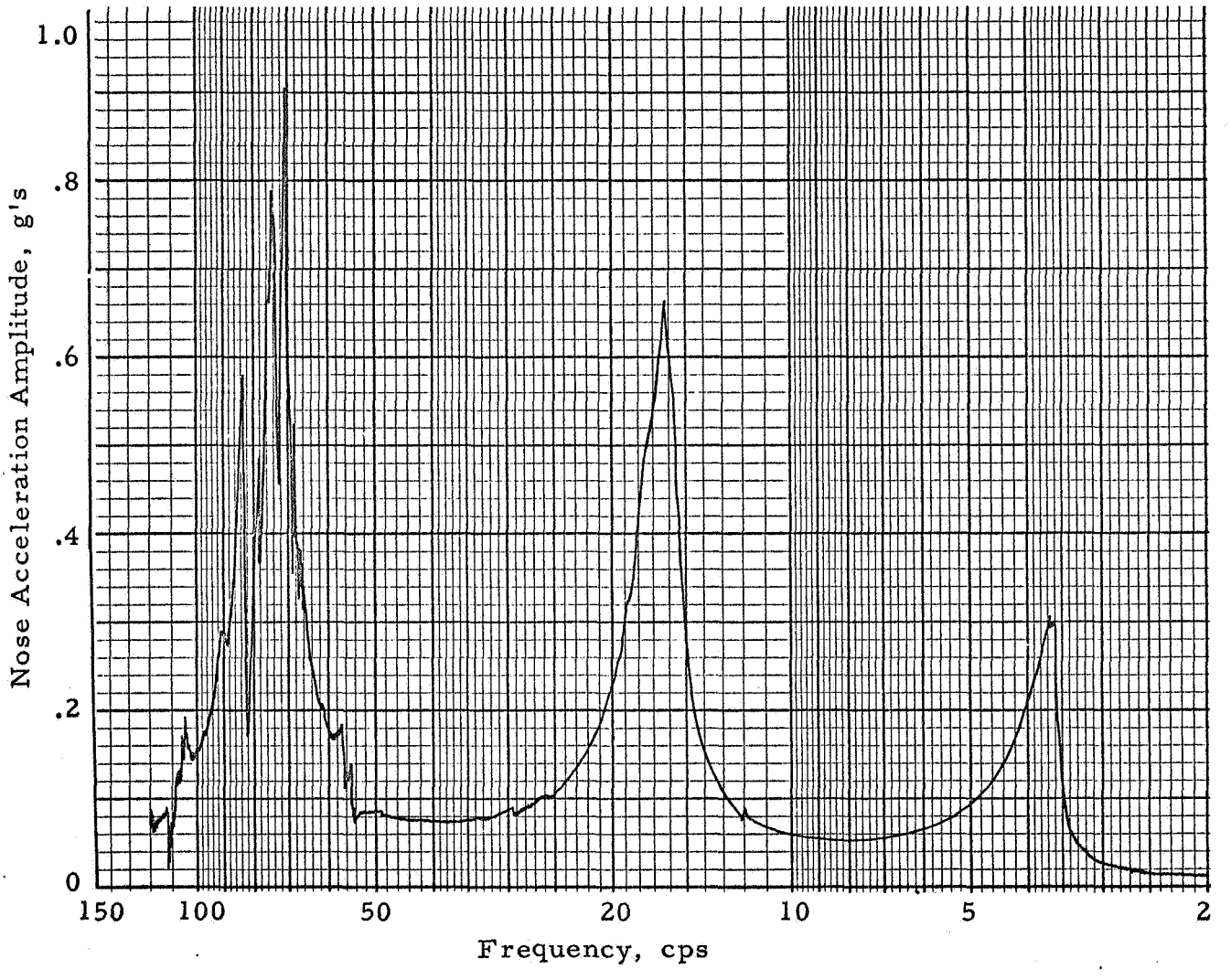

Figure C-B-5 - Frequency Response (Configuration B) Force Amplitude: 15 lb at 40 cps

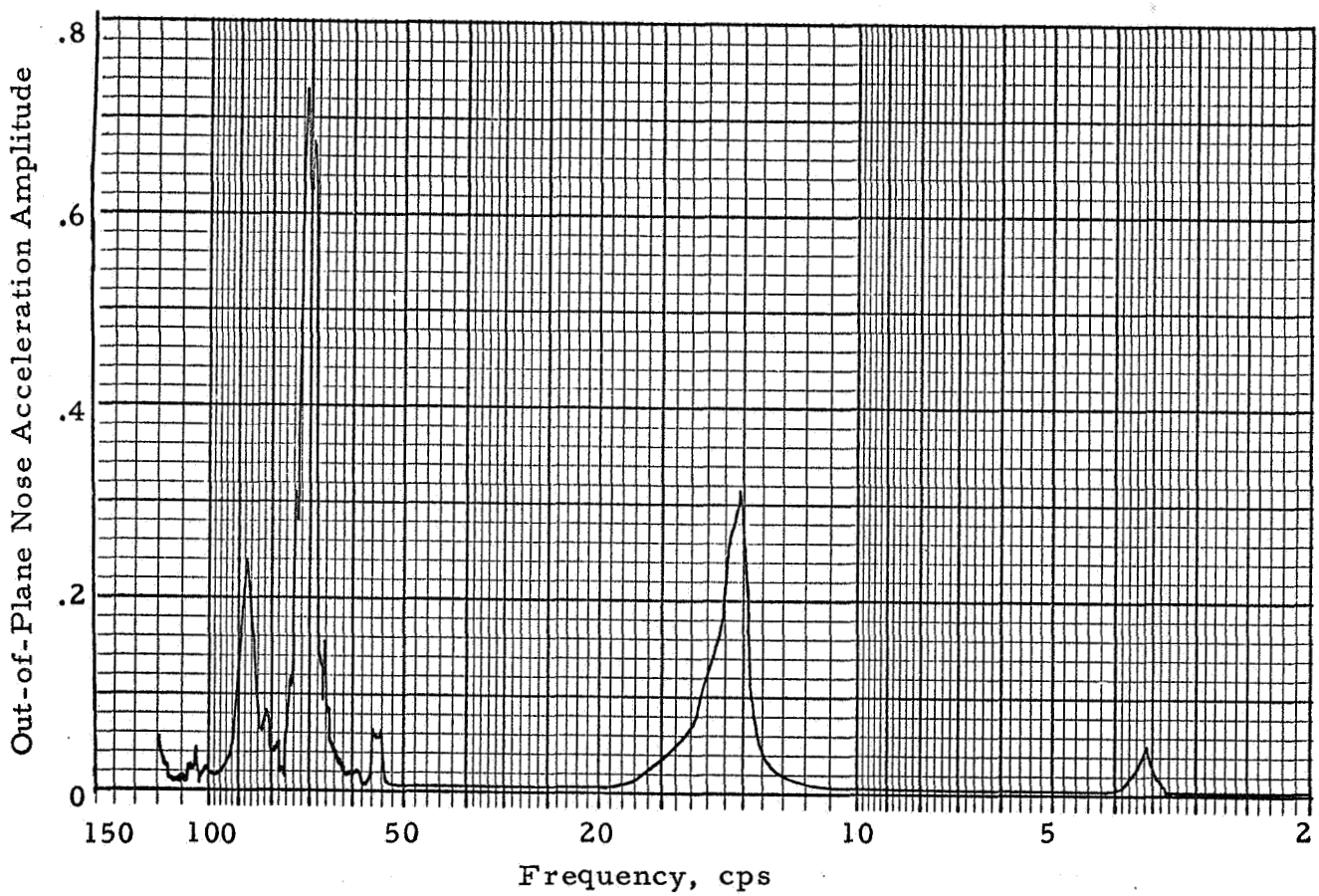

Figure C-B-6 - Frequency Response (Configuration B) Force Amplitude: 15 lb at 40 cps

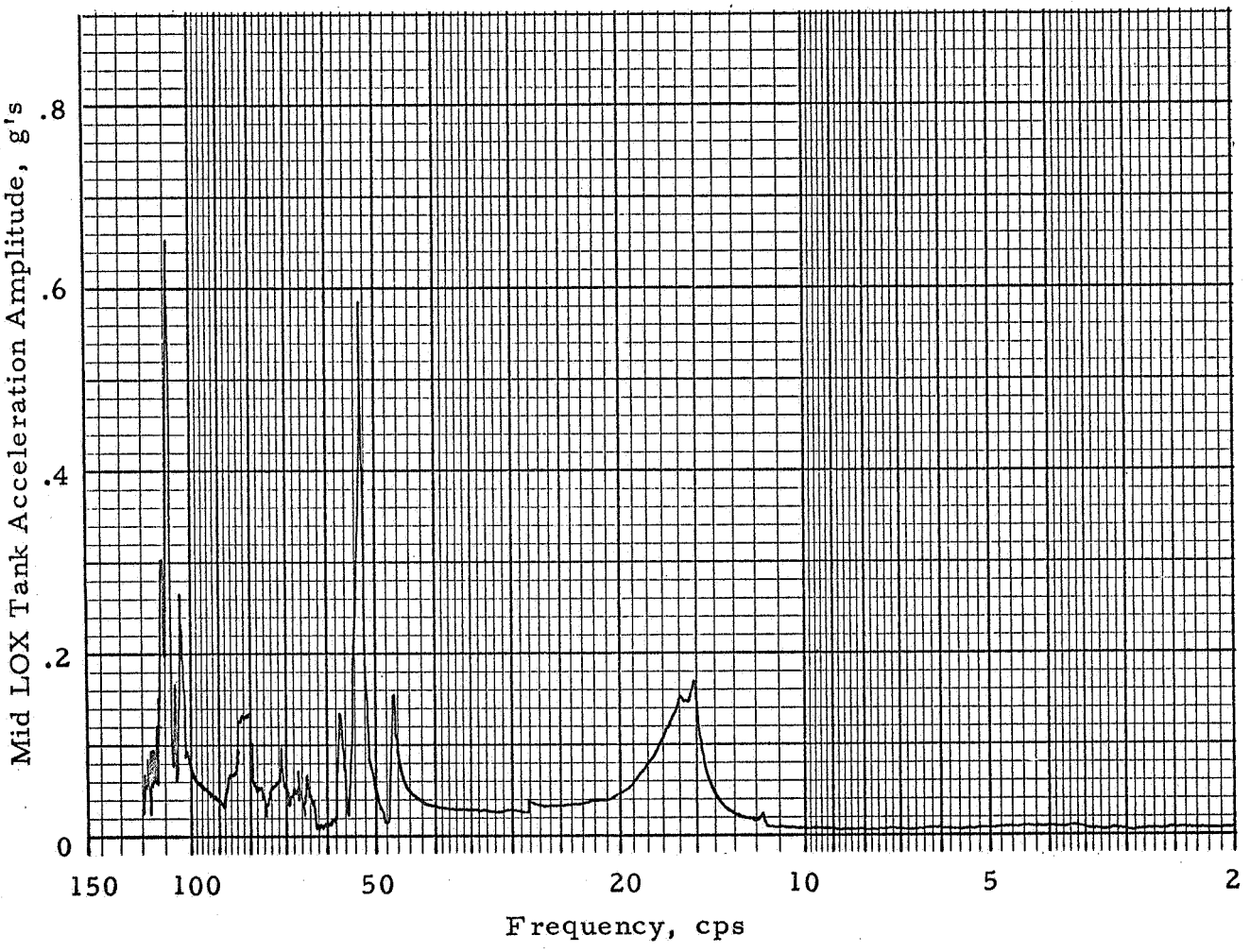

Figure C-B-7 - Frequency Response (Configuration B) Force Amplitude: 15 lb at 40 cps

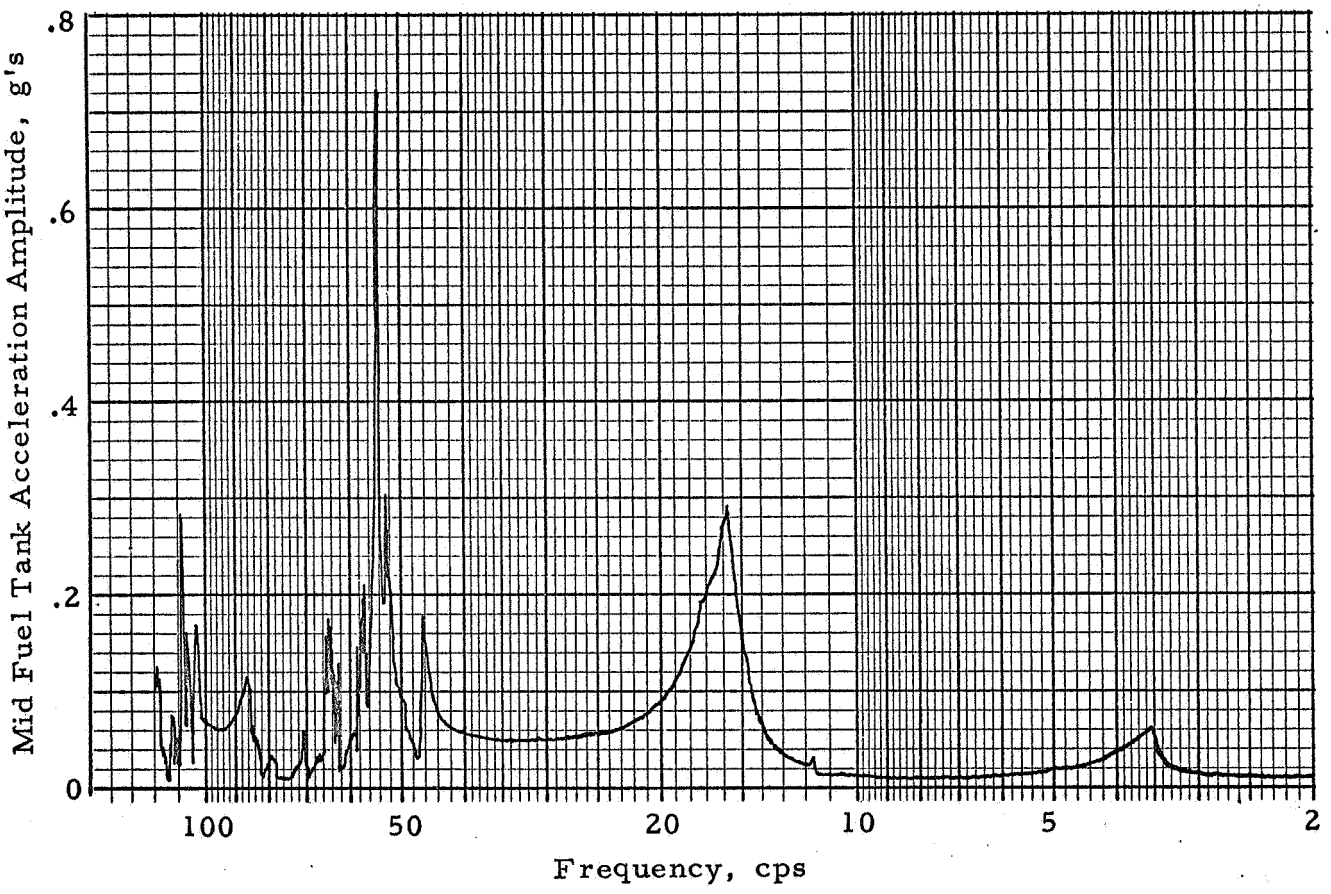

Figure C-B-8 - Frequency Response (Configuration B) Force Amplitude: 15 lb at 40 cps

CONFIGURATION: B

FREQUENCY: 4.29 cps

FORCE: 1.5 pounds, 0-pk

MODE NUMBER: 1

DAMPING:

TIP ACCELERATION: .057 g (In-Plane)

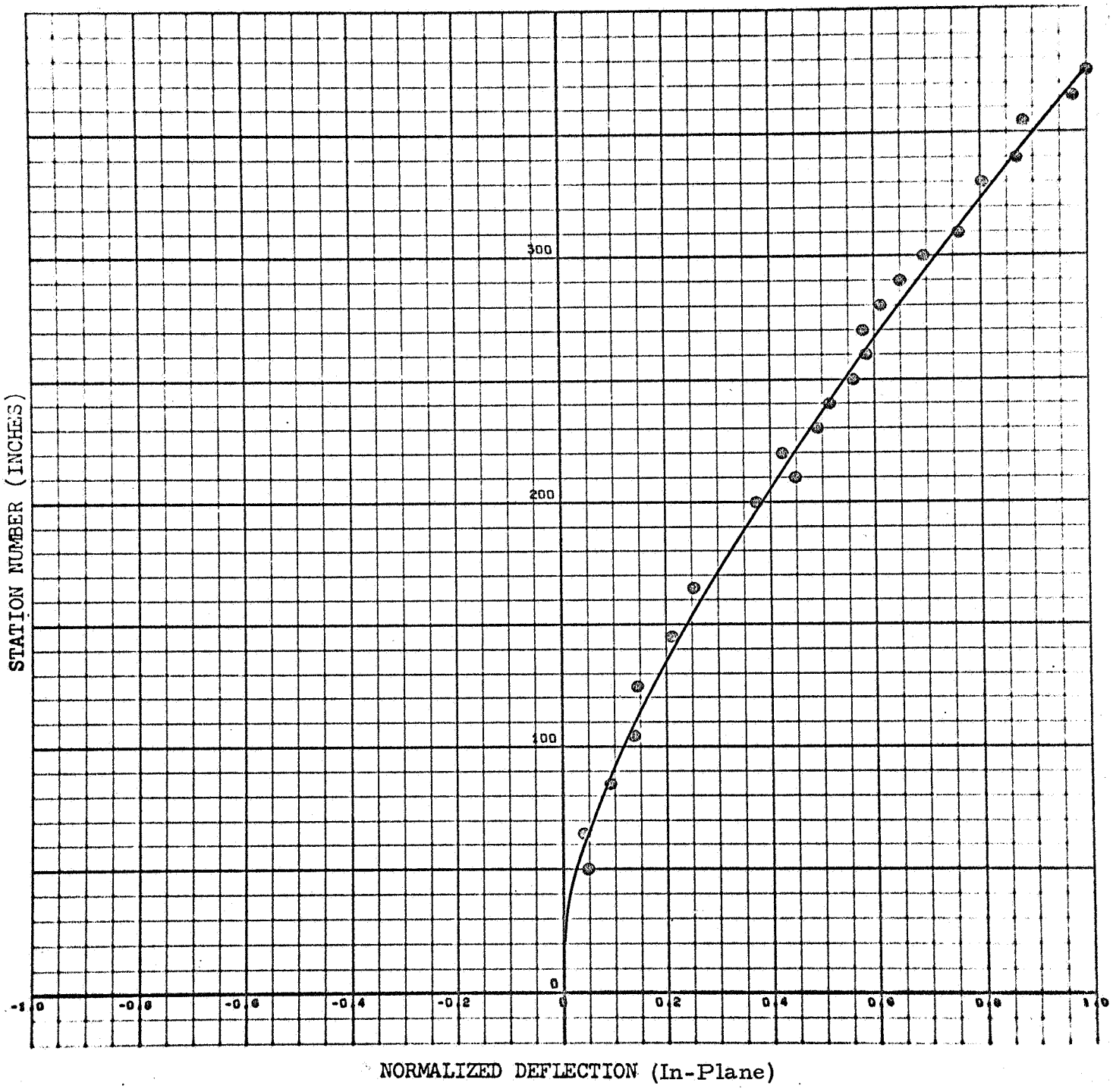

Figure C-B-9

CONFIGURATION: B

FREQUENCY: 4.29 cps

FORCE: 1.5 pounds, 0-pk

MODE NUMBER: 1

DAMPING:

TIP ACCELERATION: .005 g (Out-of-Plane)

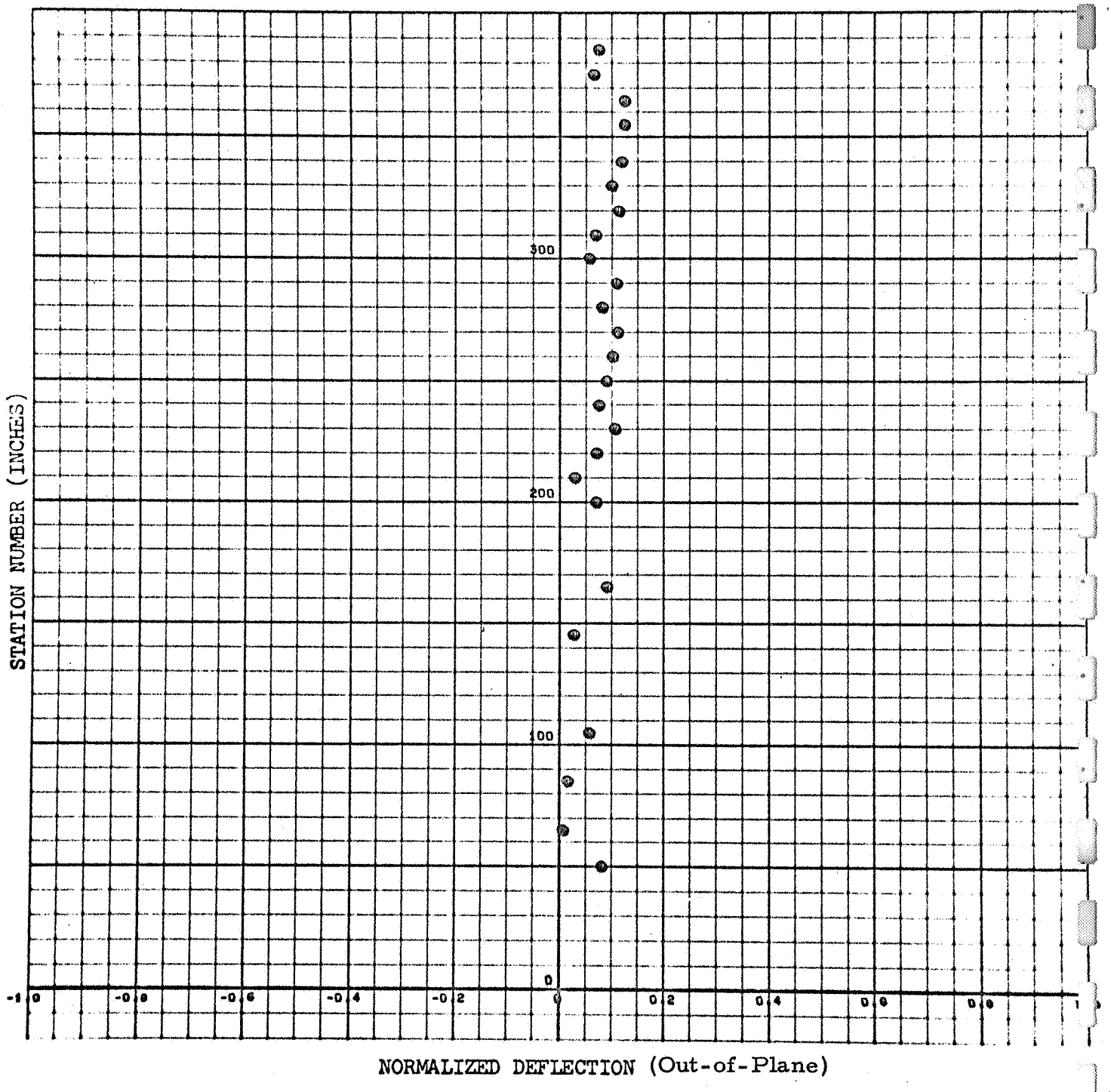

Figure C-B-10

CONFIGURATION: B

FREQUENCY: 4.21 cps

FORCE: 1.5 pounds, 0-pk

MODE NUMBER: 1

DAMPING:

TIP ACCELERATION: .057 g (In-Plane)

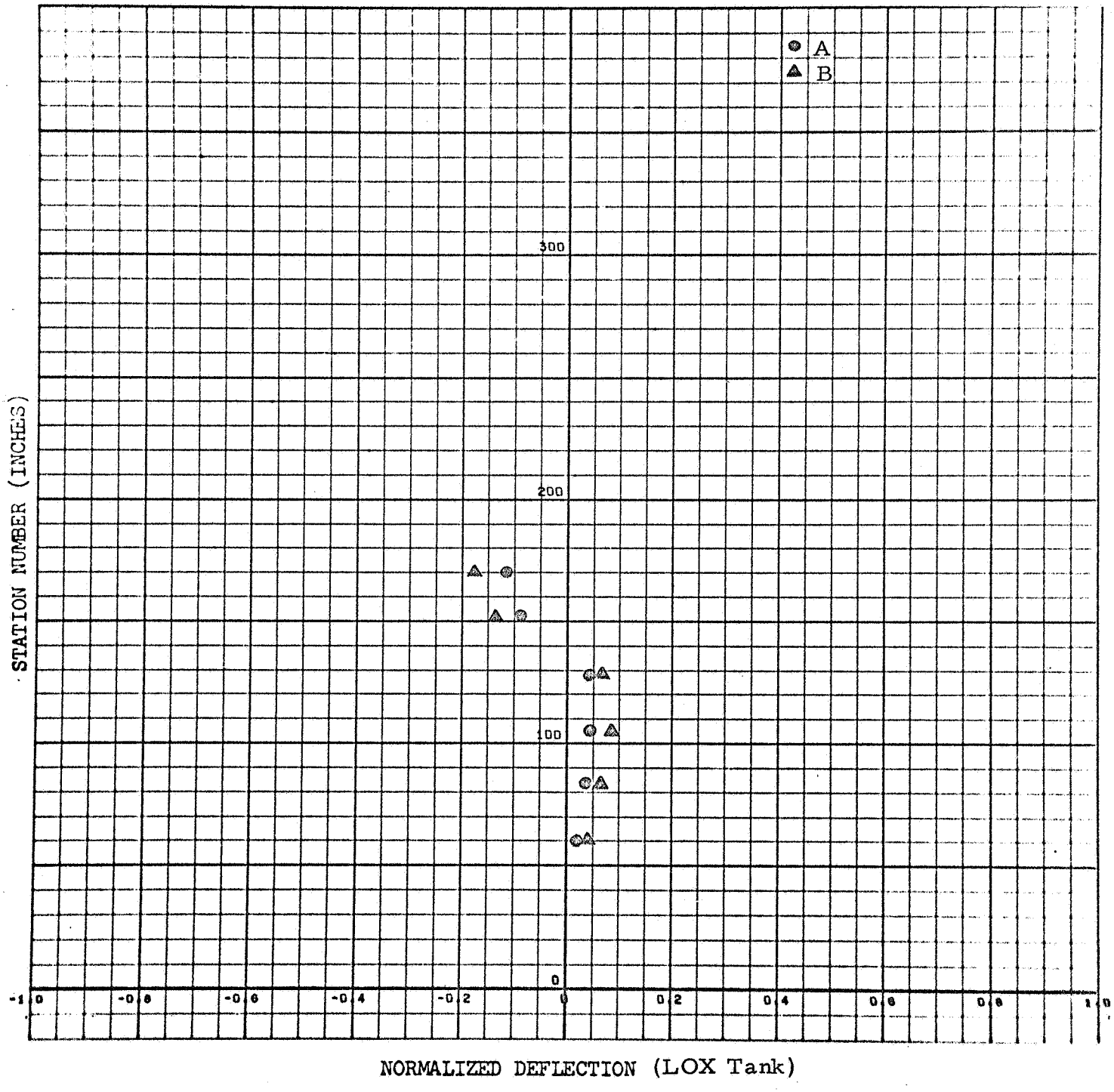

Figure C-B-11

CONFIGURATION: B

FREQUENCY: 4.21 cps

FORCE: 1.5 pounds, 0-pk

MODE NUMBER: 1

DAMPING:

TIP ACCELERATION: .057 g (In-Plane)

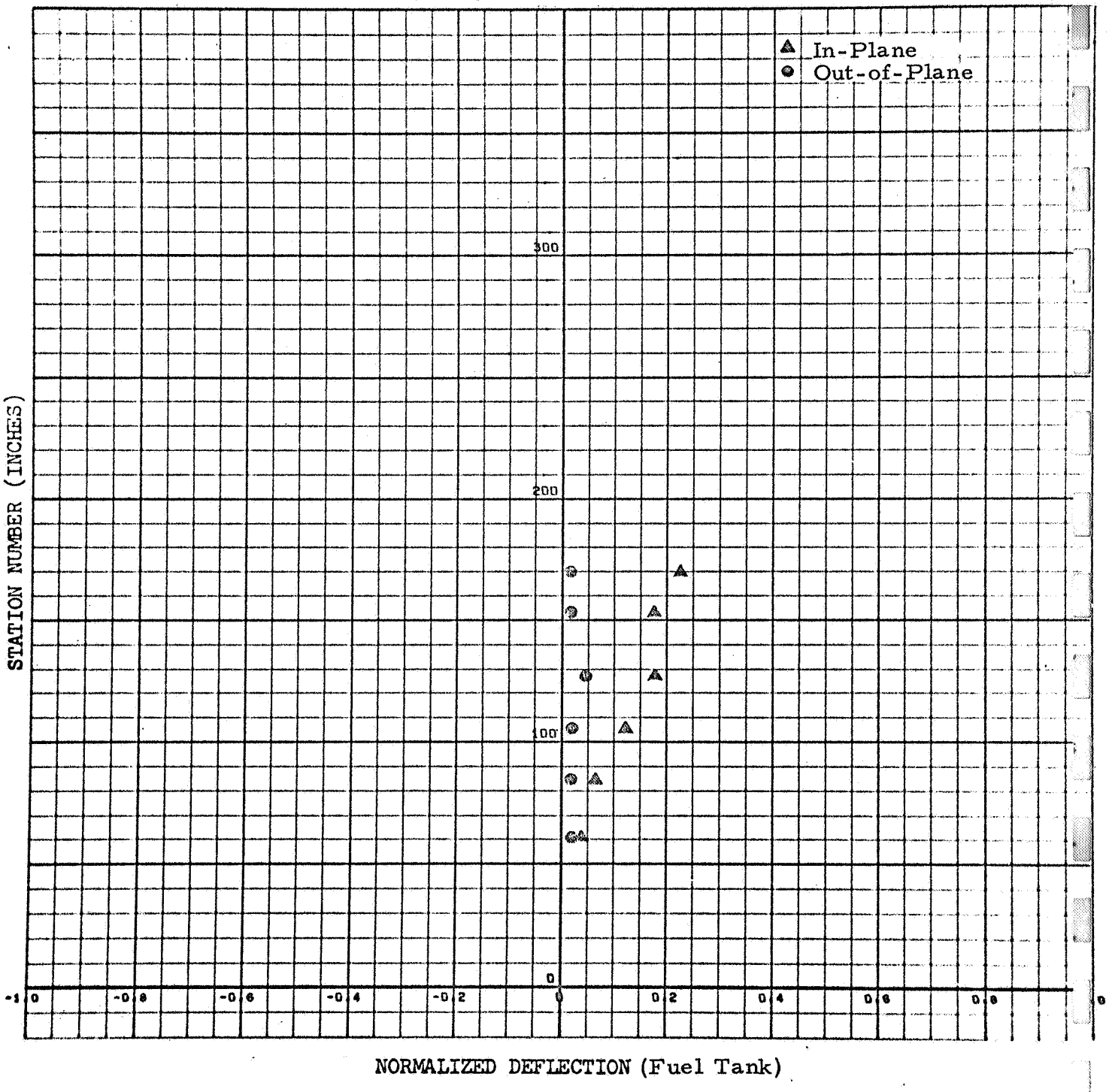

Figure C-B-12

CONFIGURATION: B

FREQUENCY: 16.51 cps

FORCE: 1.5 pounds, 0-pk

MODE NUMBER: 2

DAMPING: (See Figure C-B-41)

TIP ACCELERATION: .080 g (In-Plane)

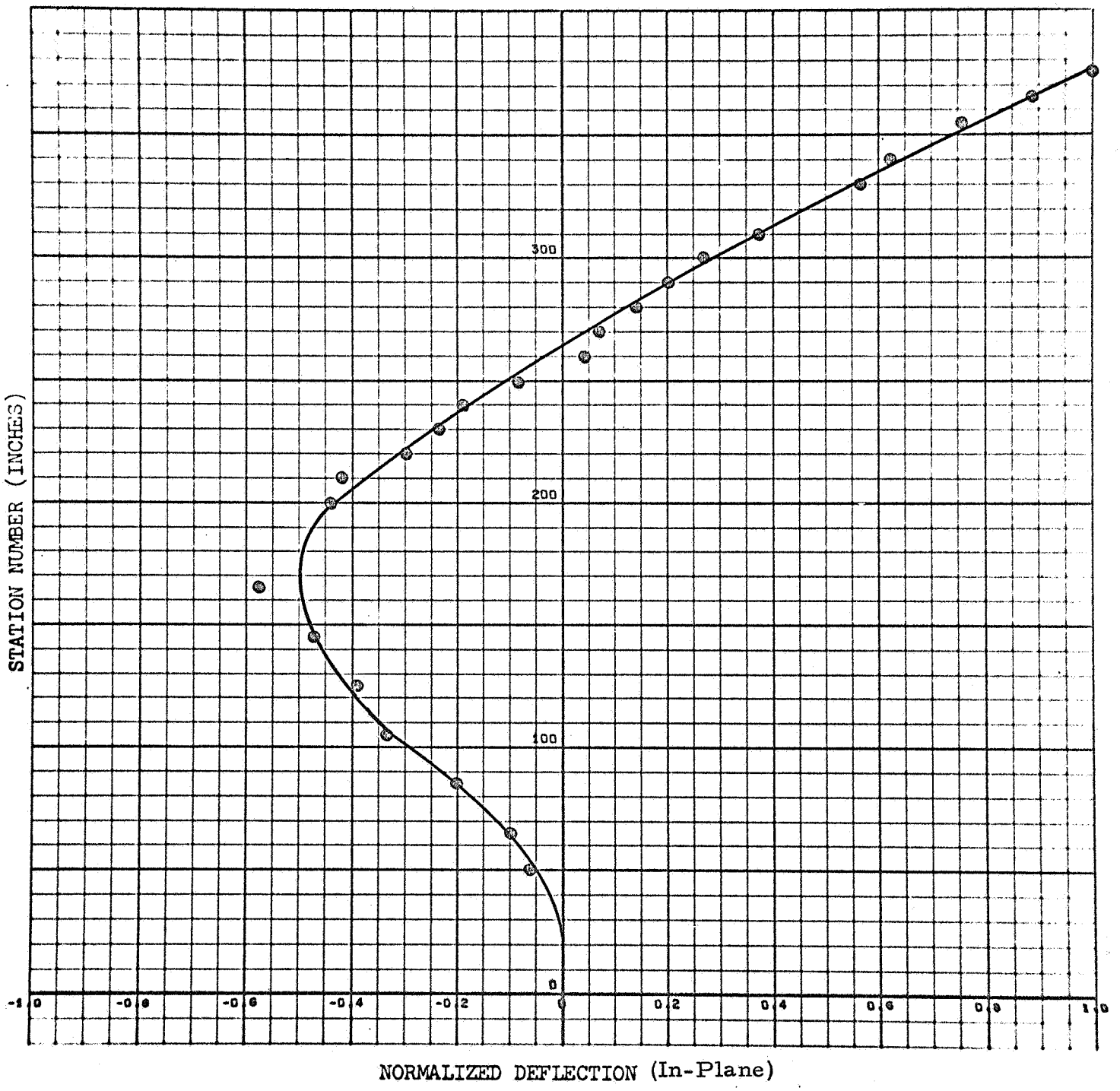

Figure C-B-13

CONFIGURATION: B

FREQUENCY: 16.51 cps

FORCE: 1.5 pounds, 0-pk

MODE NUMBER: 2

DAMPING:

TIP ACCELERATION: .079 g (Out-of-Plane)

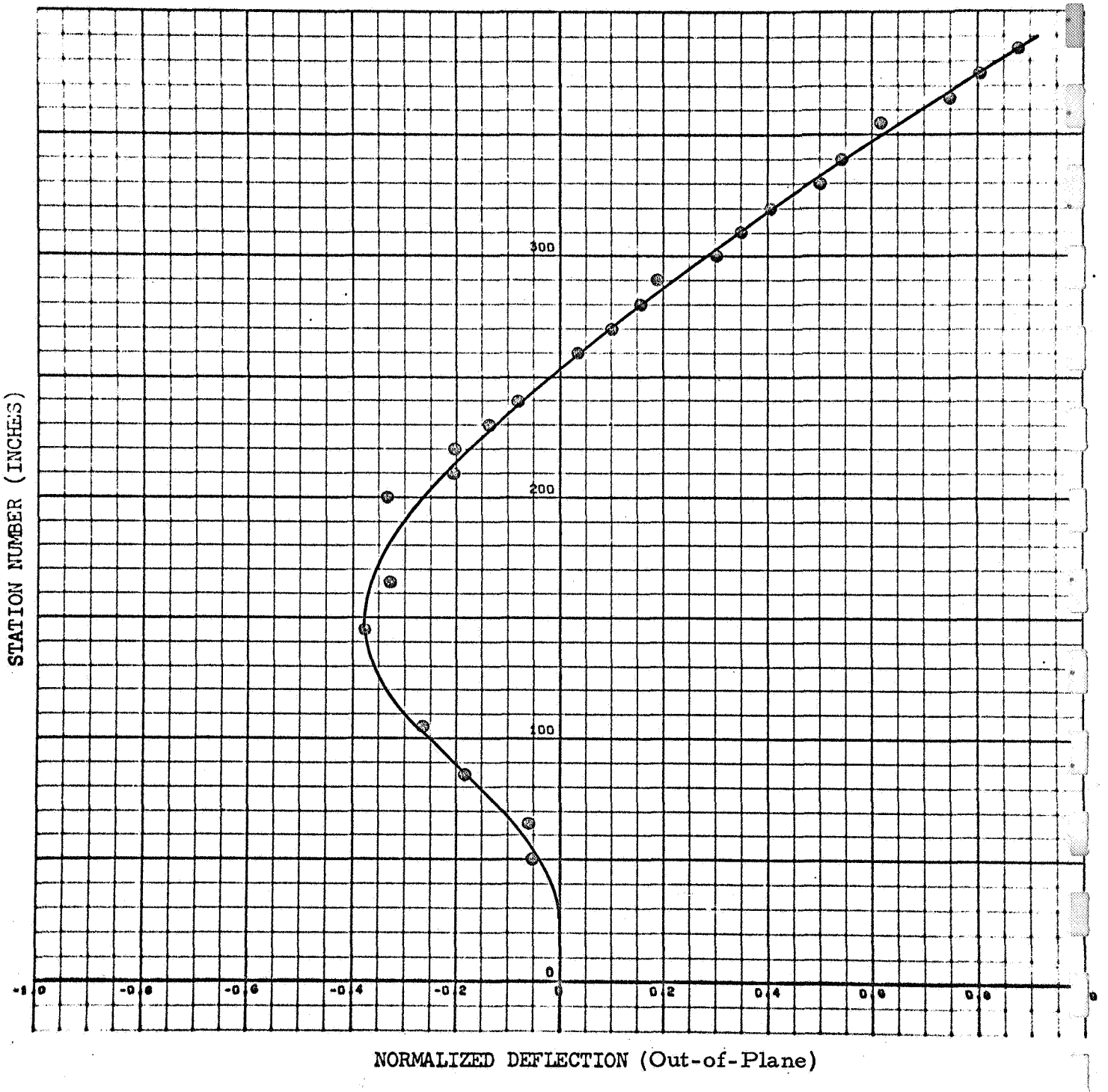

Figure C-B-14

CONFIGURATION: B

FREQUENCY: 16.55 cps

FORCE: 1.5 pounds, 0-pk

MODE NUMBER: 2

DAMPING: (See Figure C-B-43)

TIP ACCELERATION: .080 g (In-Plane)

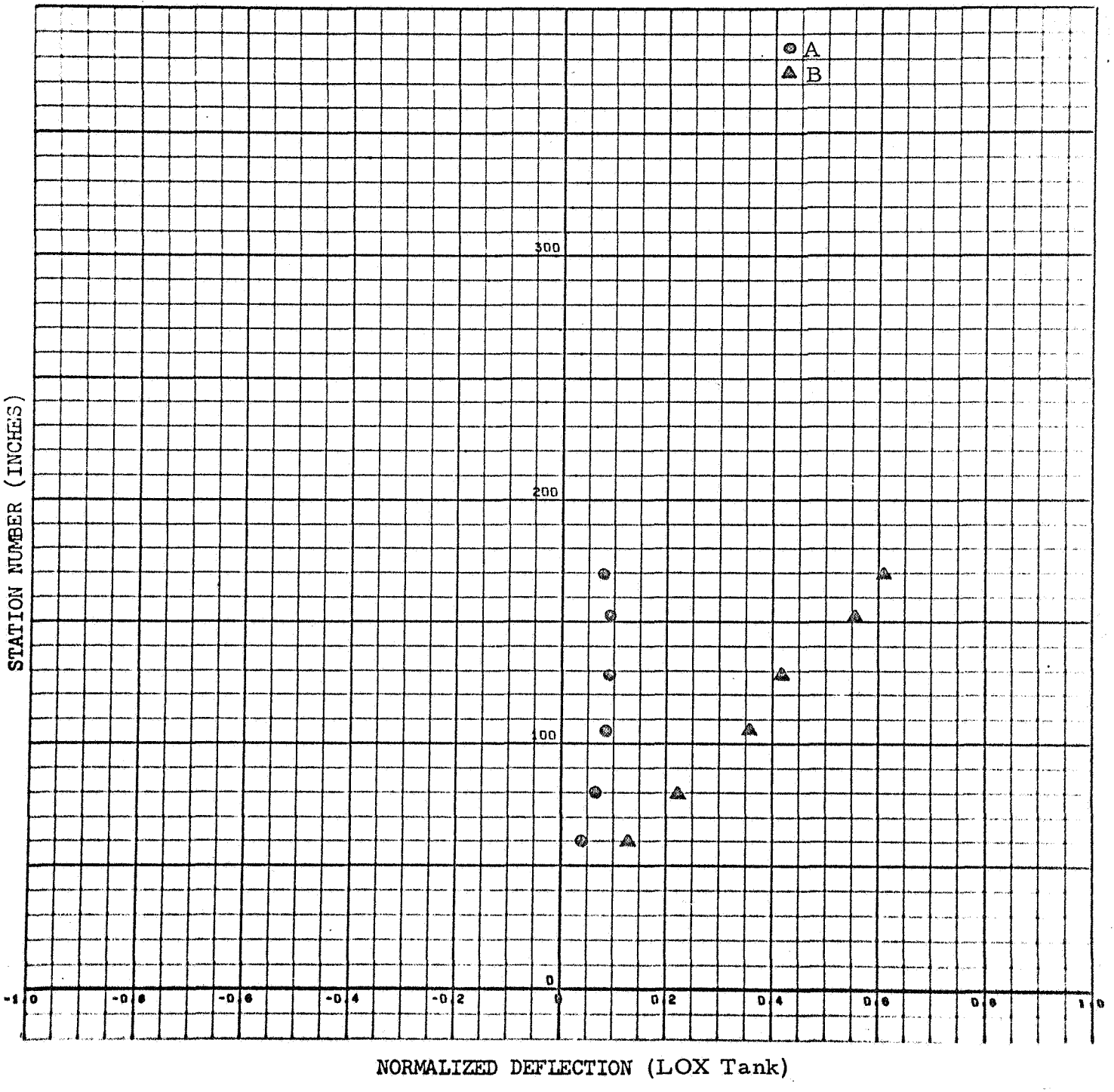

Figure C-B-15

CONFIGURATION: B

FREQUENCY: 16.55 cps

FORCE: 1.5 pounds, 0-pk

MODE NUMBER: 2

DAMPING: (See Figure C-B-45)

TIP ACCELERATION: .080 g (In-Plane)

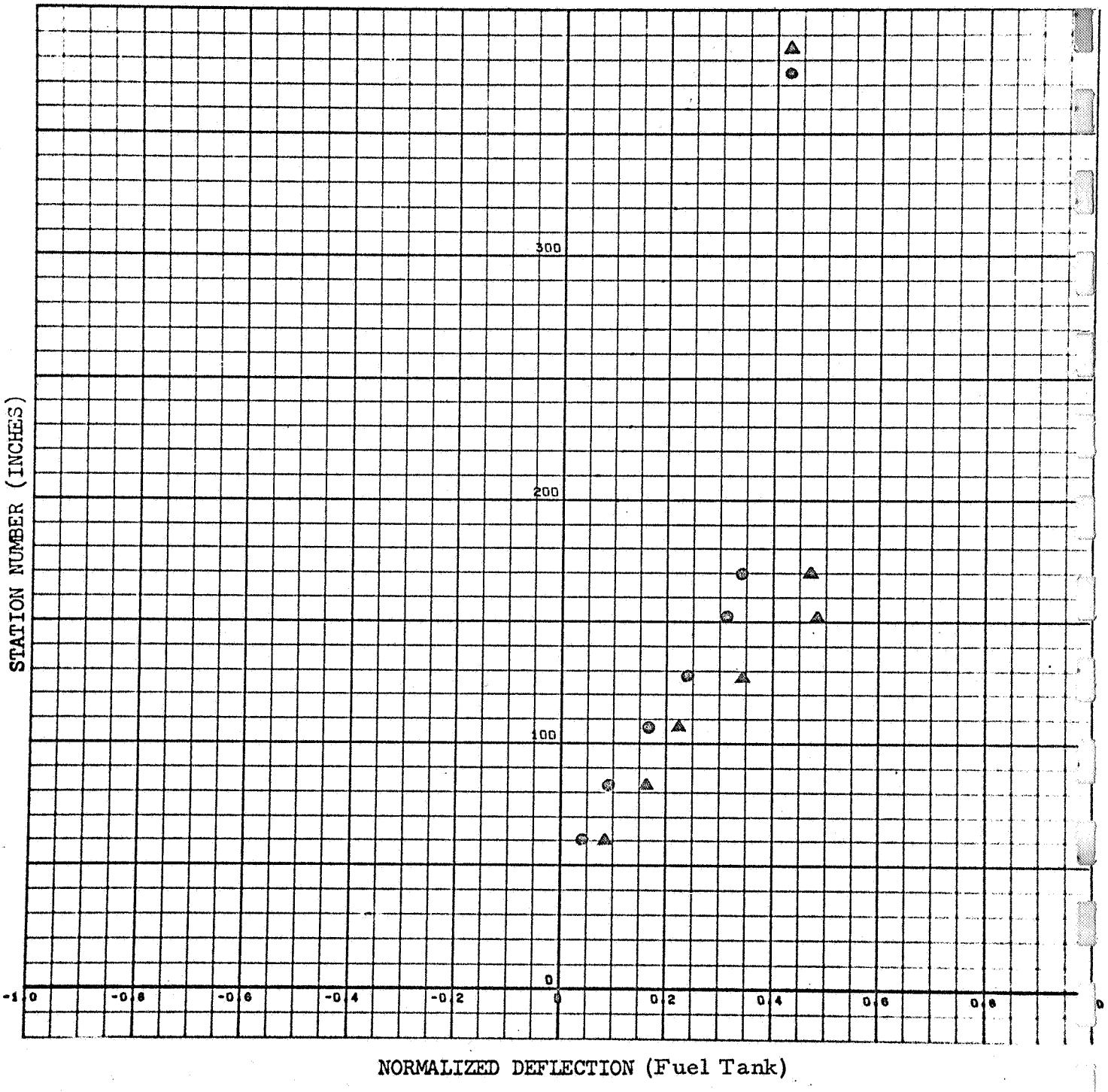

Figure C-B-16

CONFIGURATION: B

FREQUENCY: 68.8 cps

FORCE: 1.5 pounds, 0-pk

MODE NUMBER: 3

DAMPING: (See Figure C-B-42)

TIP ACCELERATION: .090 g (In-Plane)

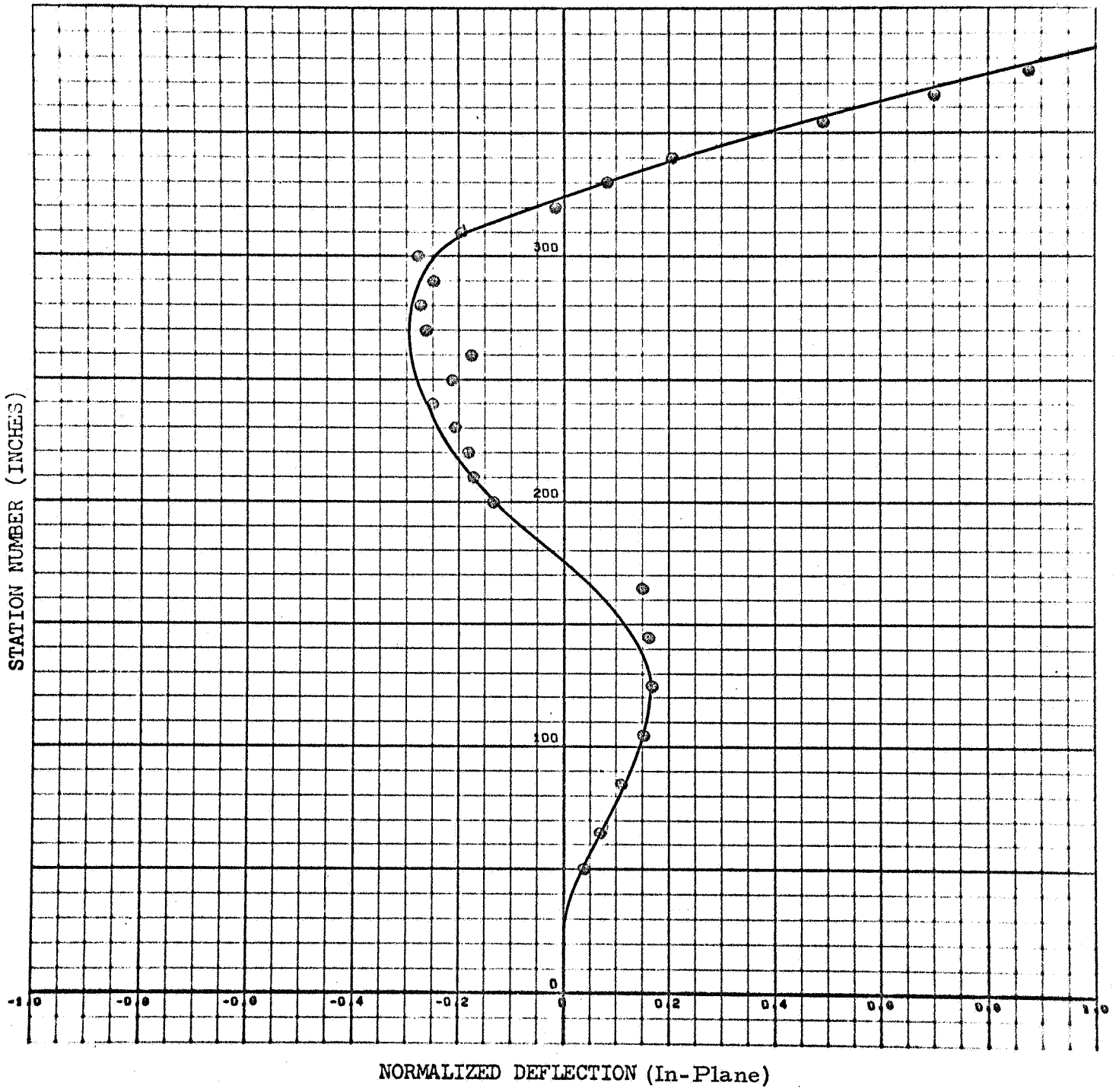

Figure C-B-17

CONFIGURATION: B

FREQUENCY: 68.8 cps

FORCE: 1.5 pounds, 0-pk

MODE NUMBER: 3

DAMPING:

TIP ACCELERATION: .107 g(Out-of-Plane)

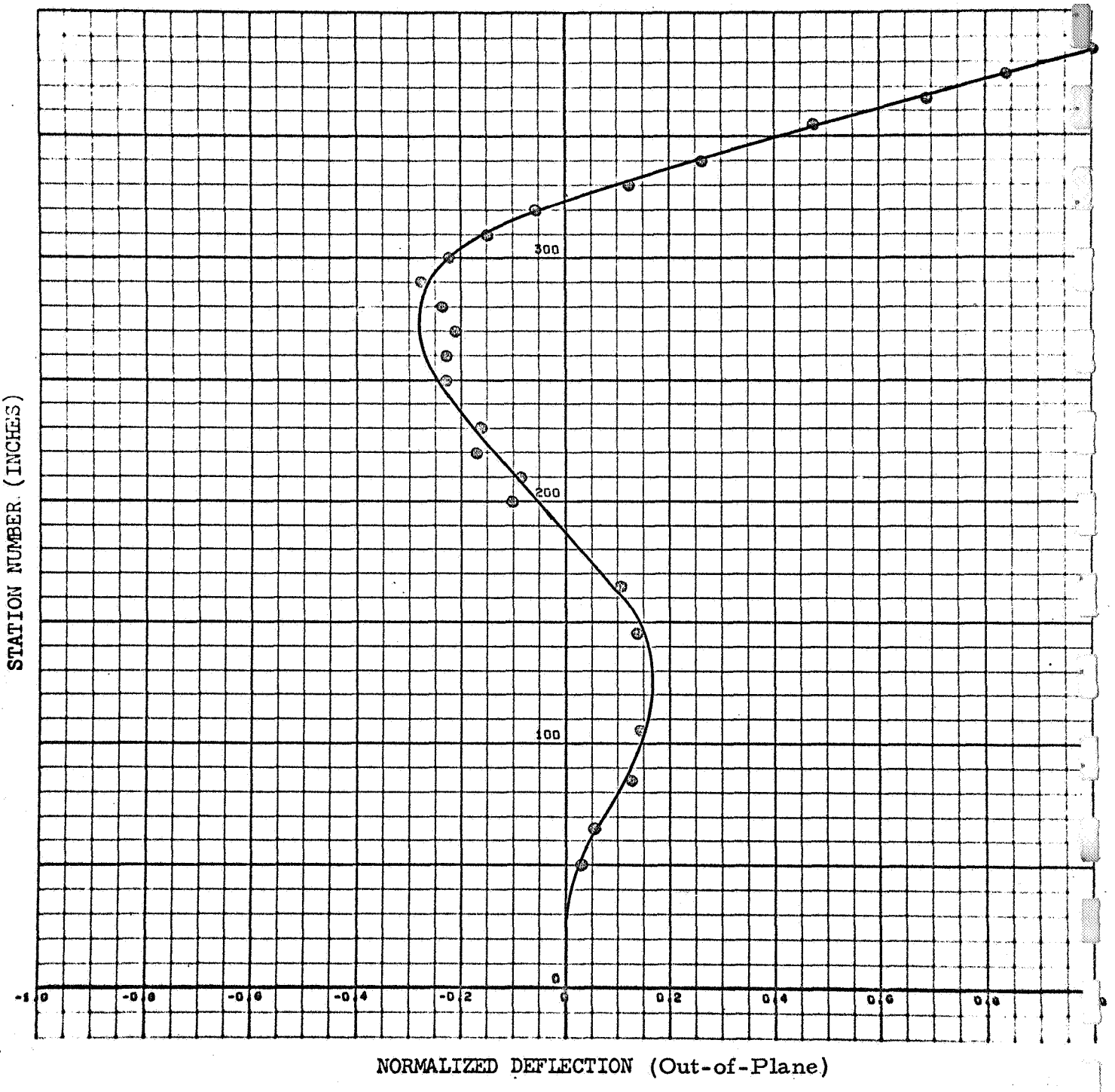

Figure C-B-18

CONFIGURATION: B

FREQUENCY: 69.1 cps

FORCE: 1.5 pounds, 0-pk

MODE NUMBER: 3

DAMPING: (See Figure C-B-44)

TIP ACCELERATION: .090 g (In-Plane)

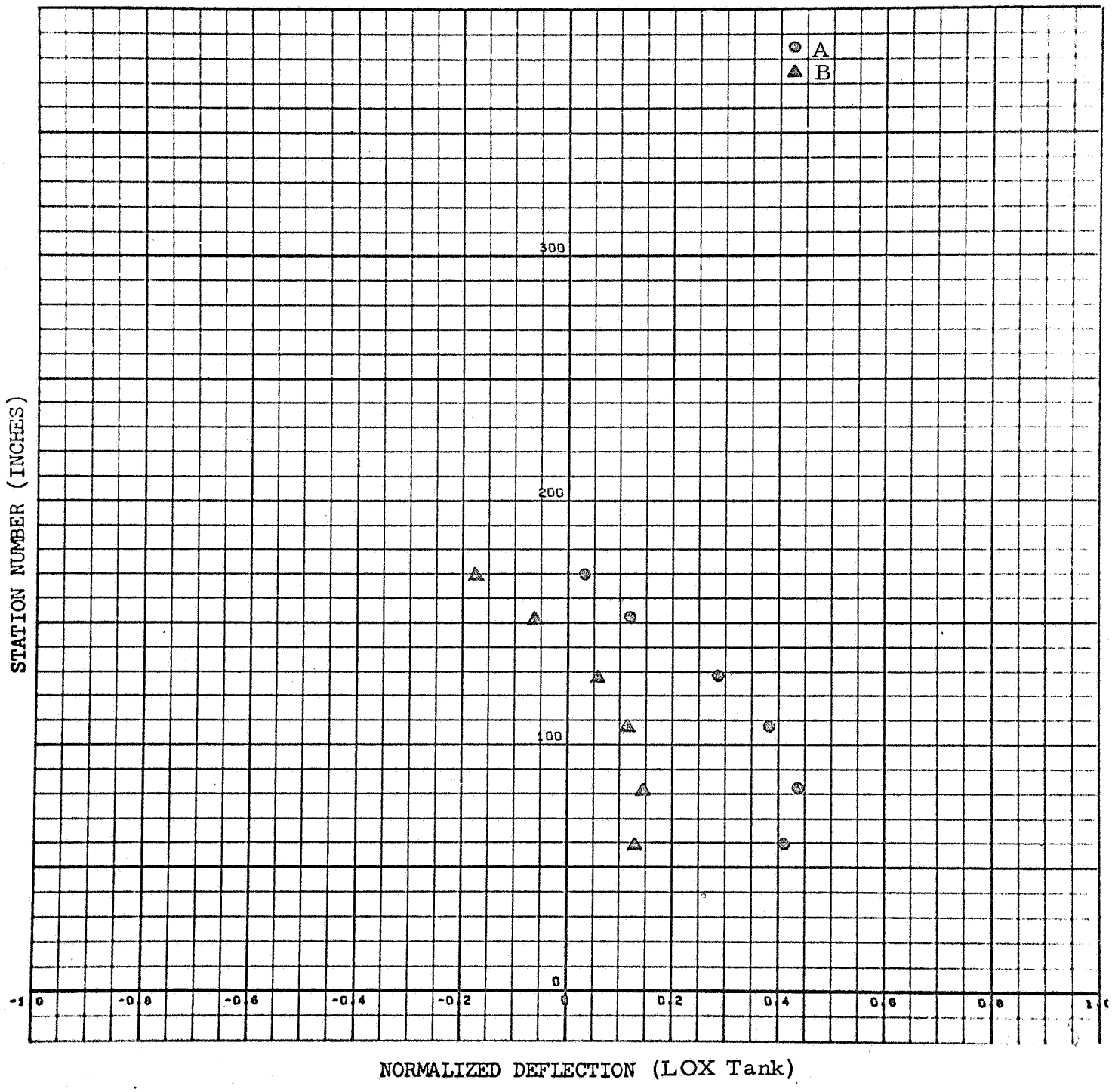

Figure C-B-19

CONFIGURATION: B

FREQUENCY: 69.1 cps

FORCE: 1.5 pounds, 0-pk

MODE NUMBER: 3

DAMPING: (Not Available)

TIP ACCELERATION: .090 g (In-Plane)

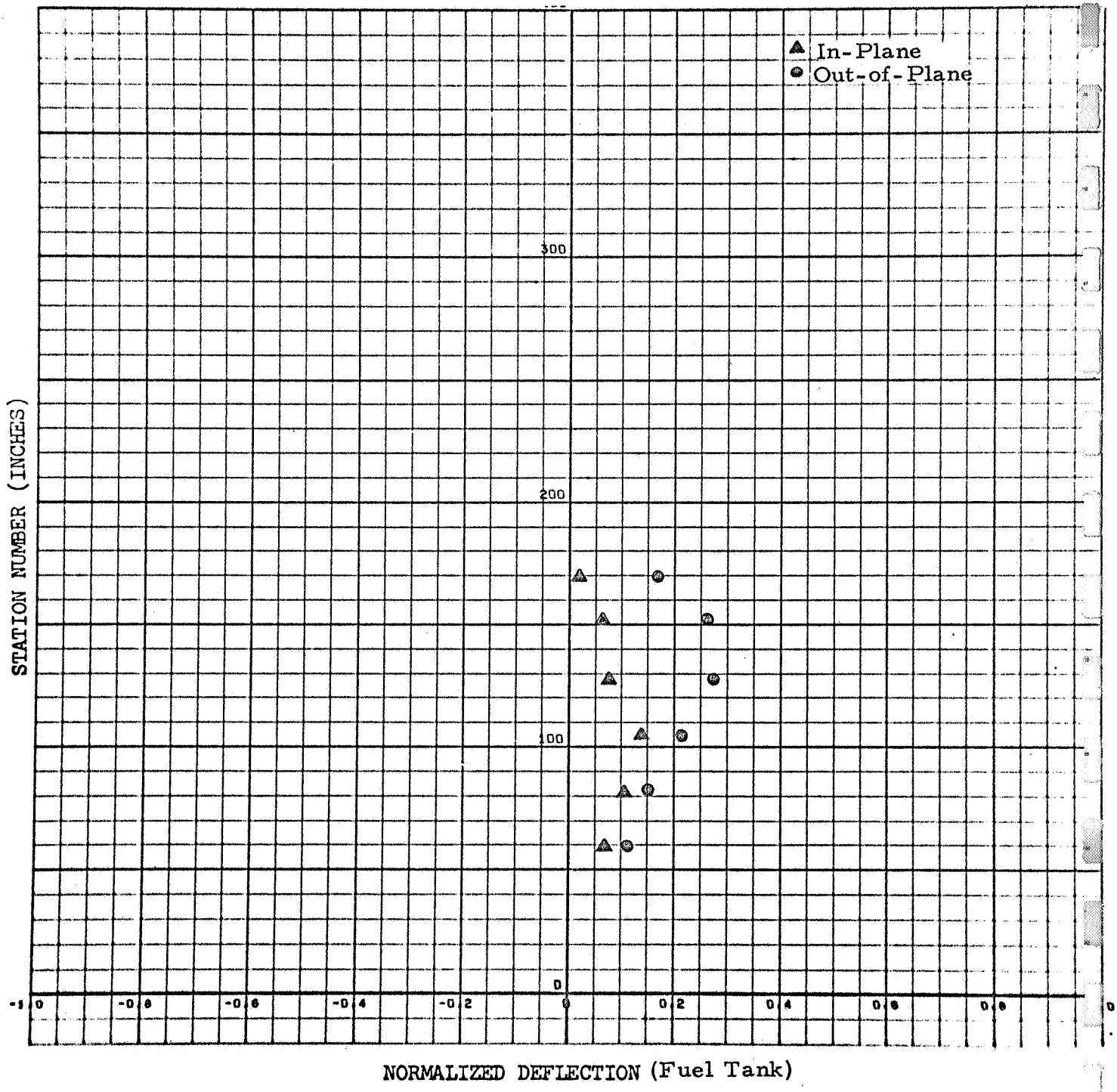

Figure C-B-20

CONFIGURATION: B

FREQUENCY: 3.75 cps

FORCE: 10 pounds, 0-pk

MODE NUMBER: 1

DAMPING: (See Figure C-B-40)

TIP ACCELERATION: .230 g (In-Plane)

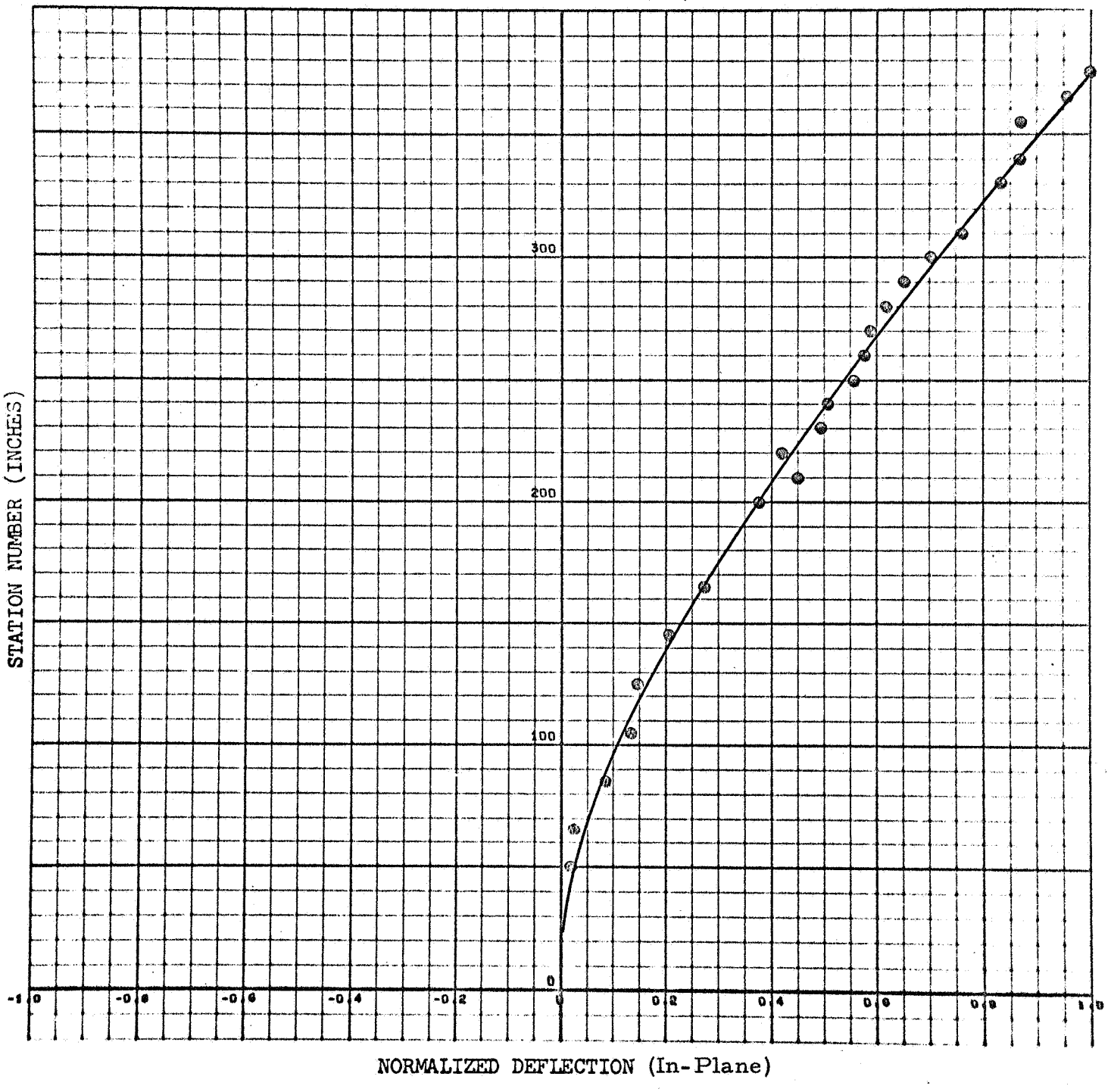

Figure C-B-21

CONFIGURATION: B

FREQUENCY: 3.75 cps

FORCE: 10 pounds, 0-pk

MODE NUMBER: 1

DAMPING:

TIP ACCELERATION: .016 g (Out-of-Plane)

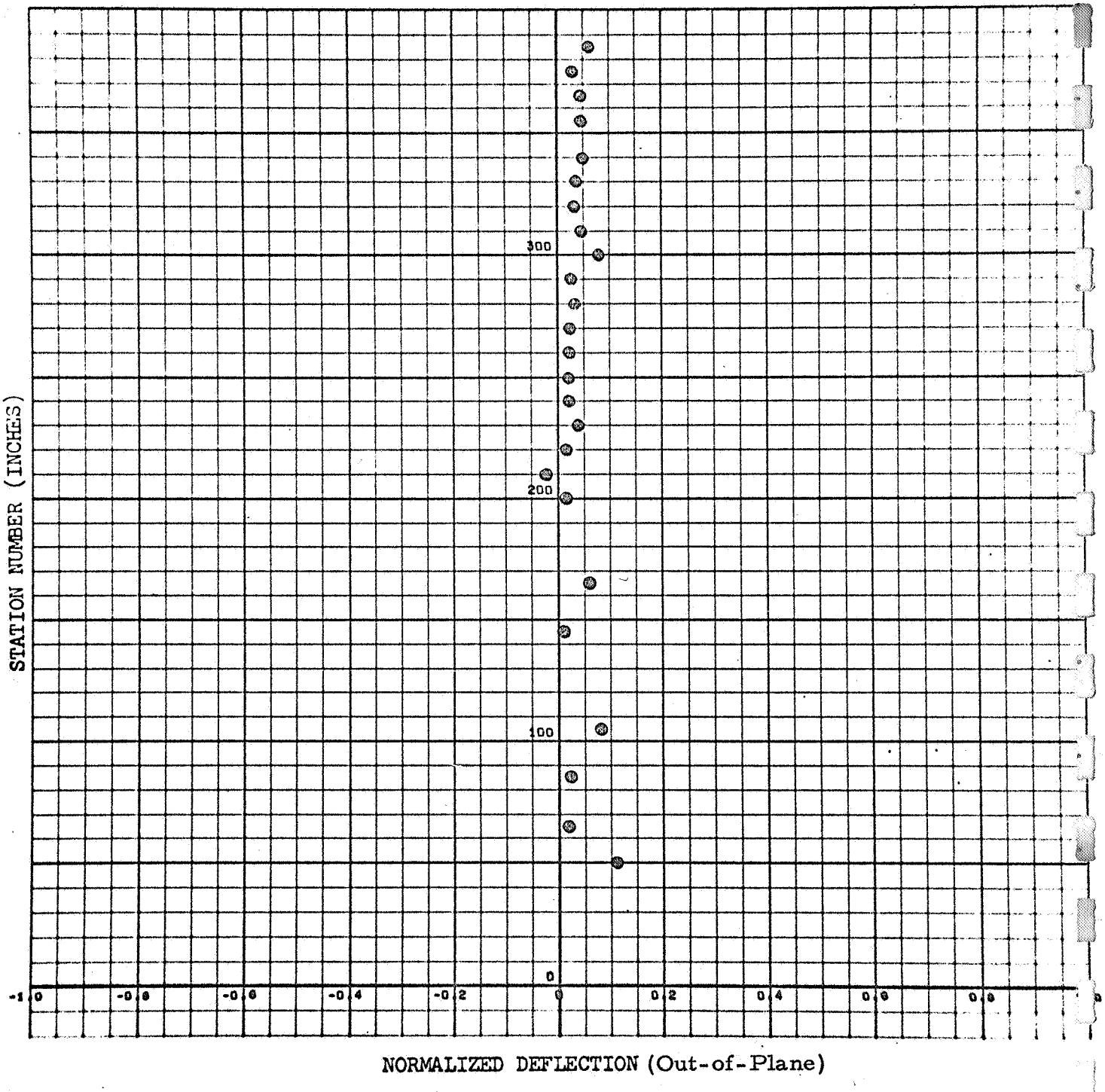

Figure C-B-22

CONFIGURATION: B

FREQUENCY: 3.57 cps

FORCE: 10 pounds, 0-pk

MODE NUMBER: 1

DAMPING:

TIP ACCELERATION: .230 g (In-Plane)

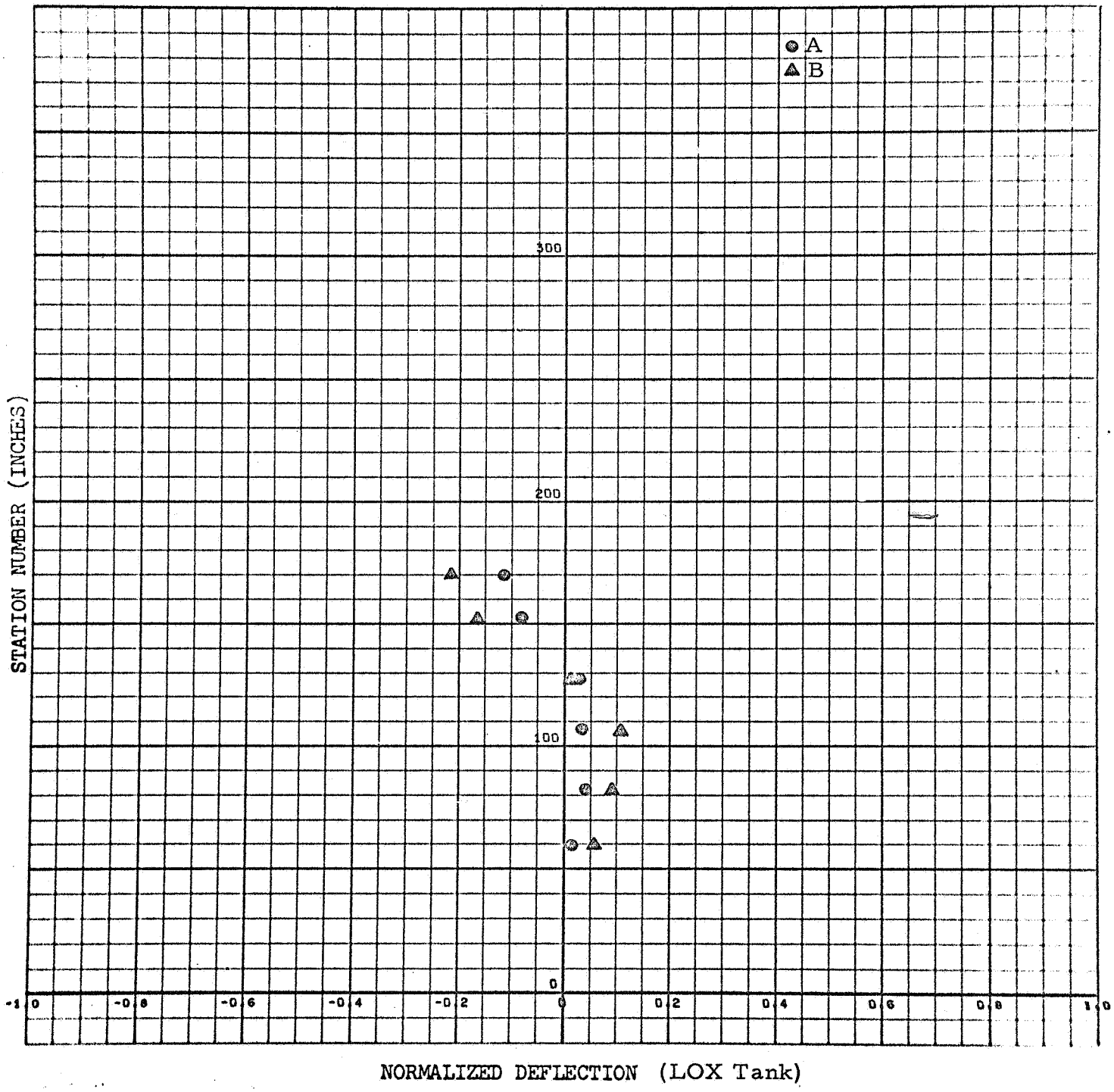

Figure C-B-23

CONFIGURATION: B

FREQUENCY: 3.57 cps

FORCE: 10 pounds, 0-pk

MODE NUMBER: 1

DAMPING:

TIP ACCELERATION:.230 g (In-Plane)

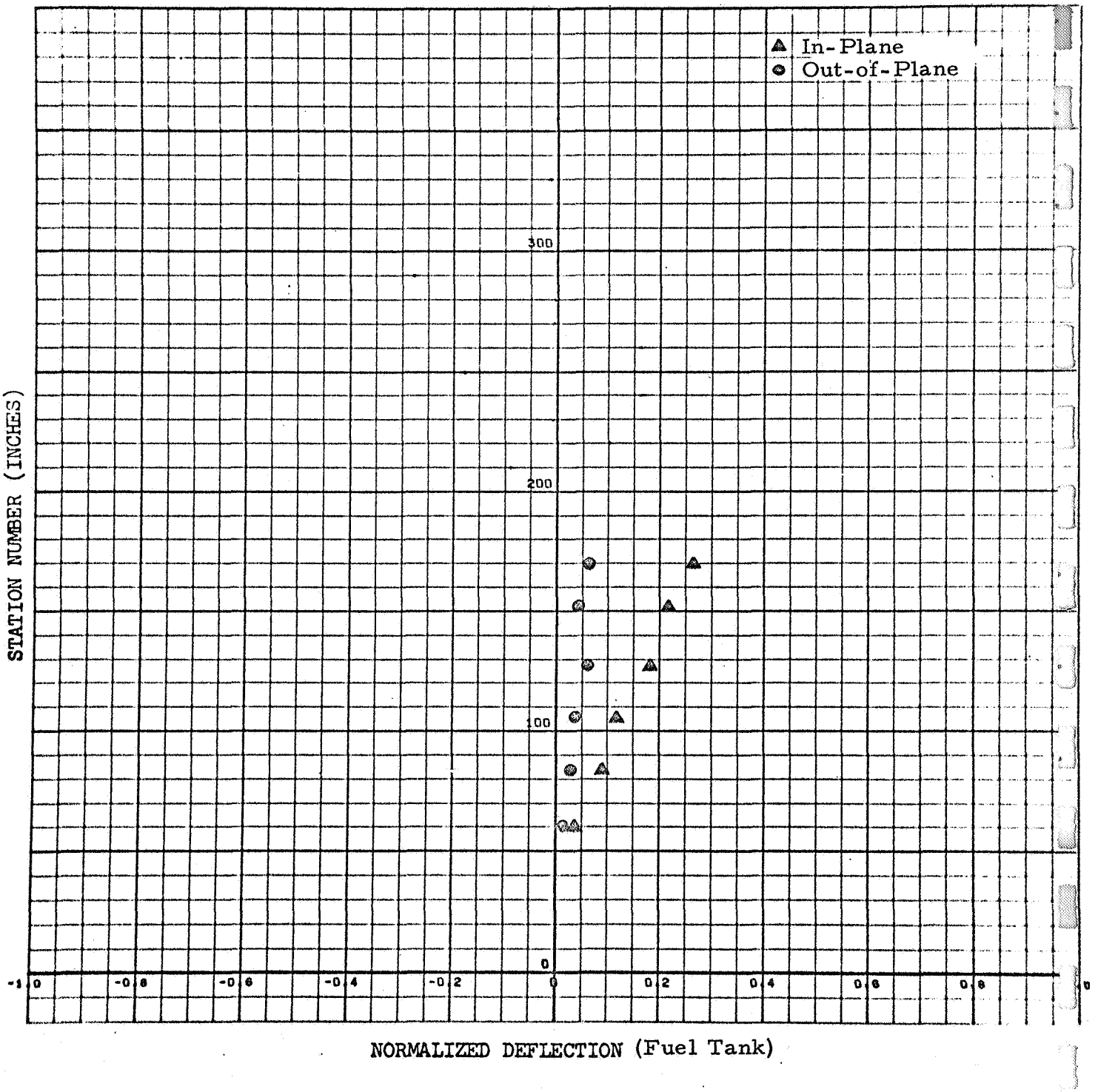

Figure C-B-24

CONFIGURATION: B

FREQUENCY: 16.42 cps

FORCE: 10 pounds, 0-pk

MODE NUMBER: 2

DAMPING: (See Figure C-B-41)

TIP ACCELERATION: .580 g (In-Plane)

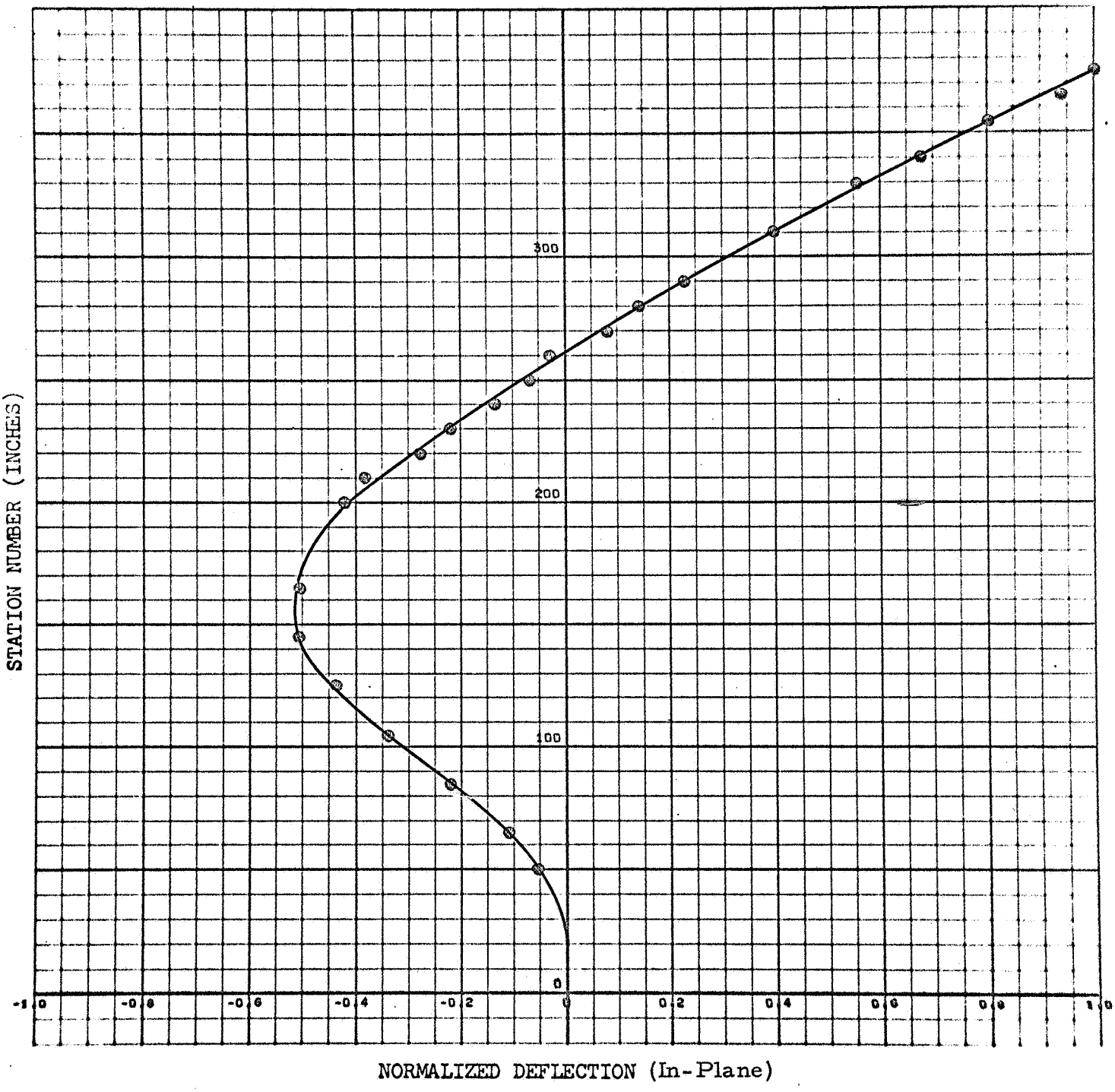

Figure C-B-25

CONFIGURATION: B

FREQUENCY: 16.42 cps

FORCE: 10 pounds, 0-pk

MODE NUMBER: 2

DAMPING:

TIP ACCELERATION: .254 g (Out-of-Plane)

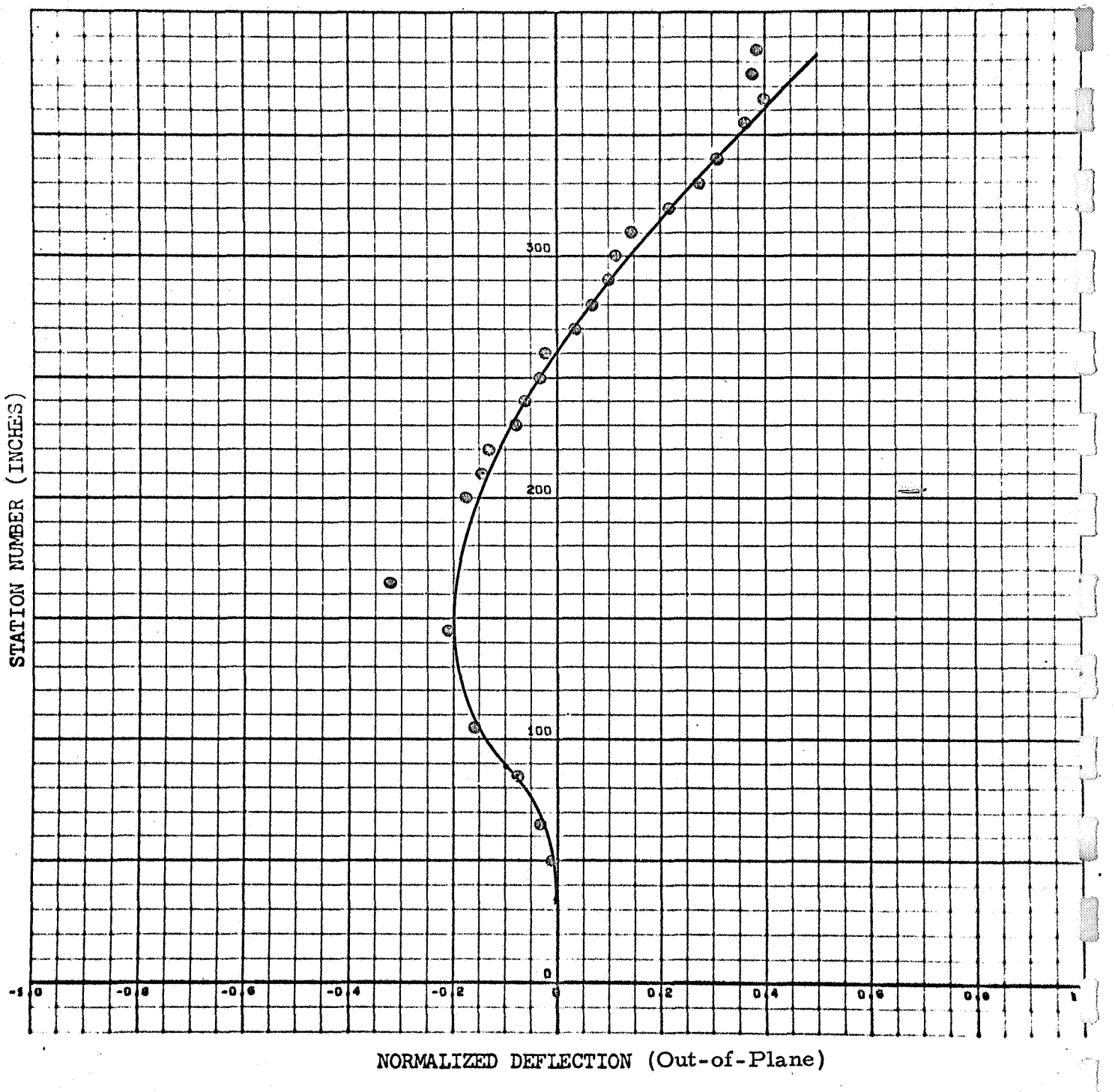

Figure C-B-26

CONFIGURATION: B

FREQUENCY: 16.4 cps

FORCE: 10 pounds, 0-pk

MODE NUMBER: 2

DAMPING: (See Figure C-B-43)

TIP ACCELERATION: .580 g (In-Plane)

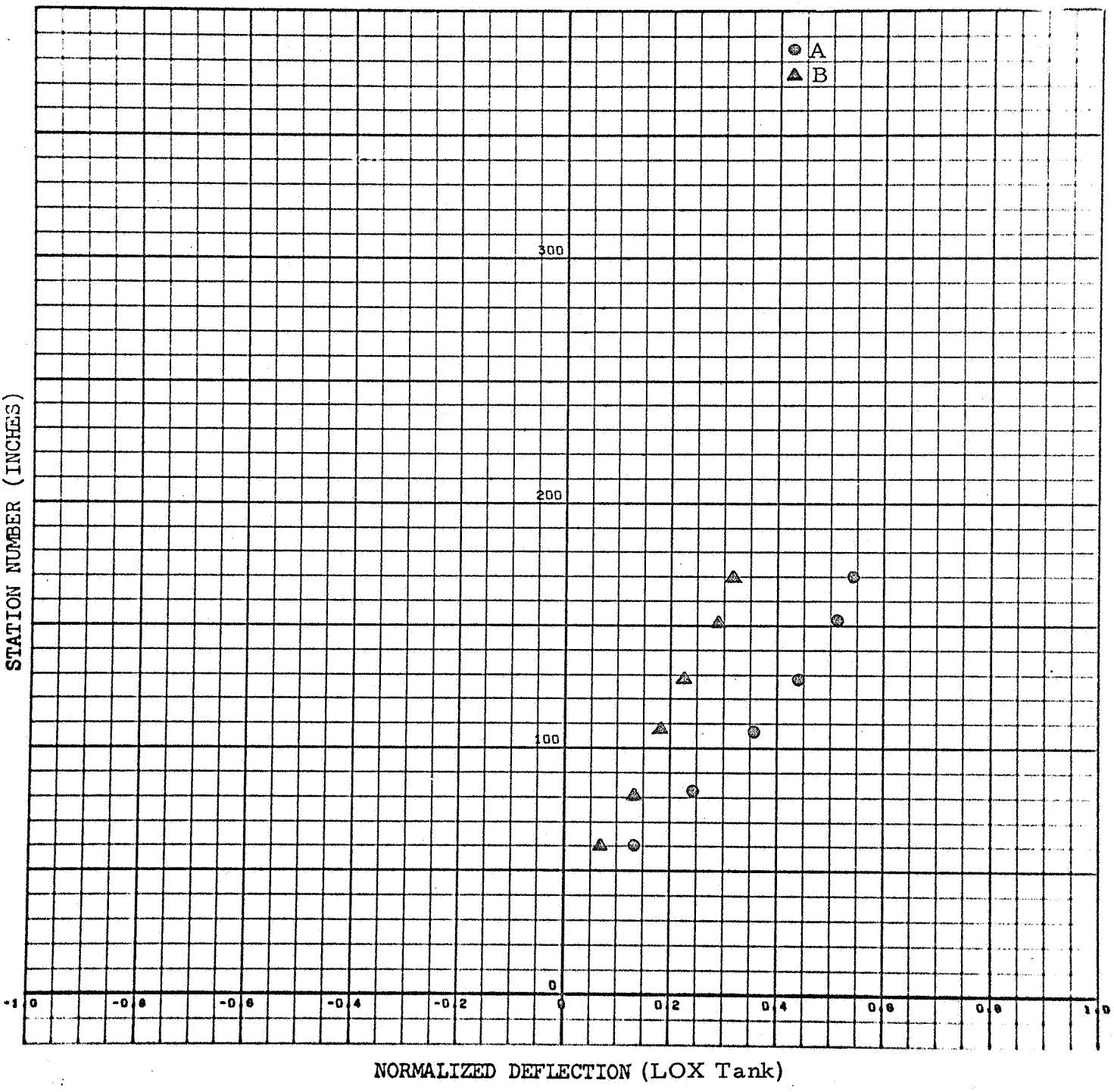

Figure C-B-27

CONFIGURATION: B

FREQUENCY: 16.4 cps

FORCE: 10 pounds, 0-pk

MODE NUMBER: 2

DAMPING: (See Figure C-B-45)

TIP ACCELERATION: .580 g (In-Plane)

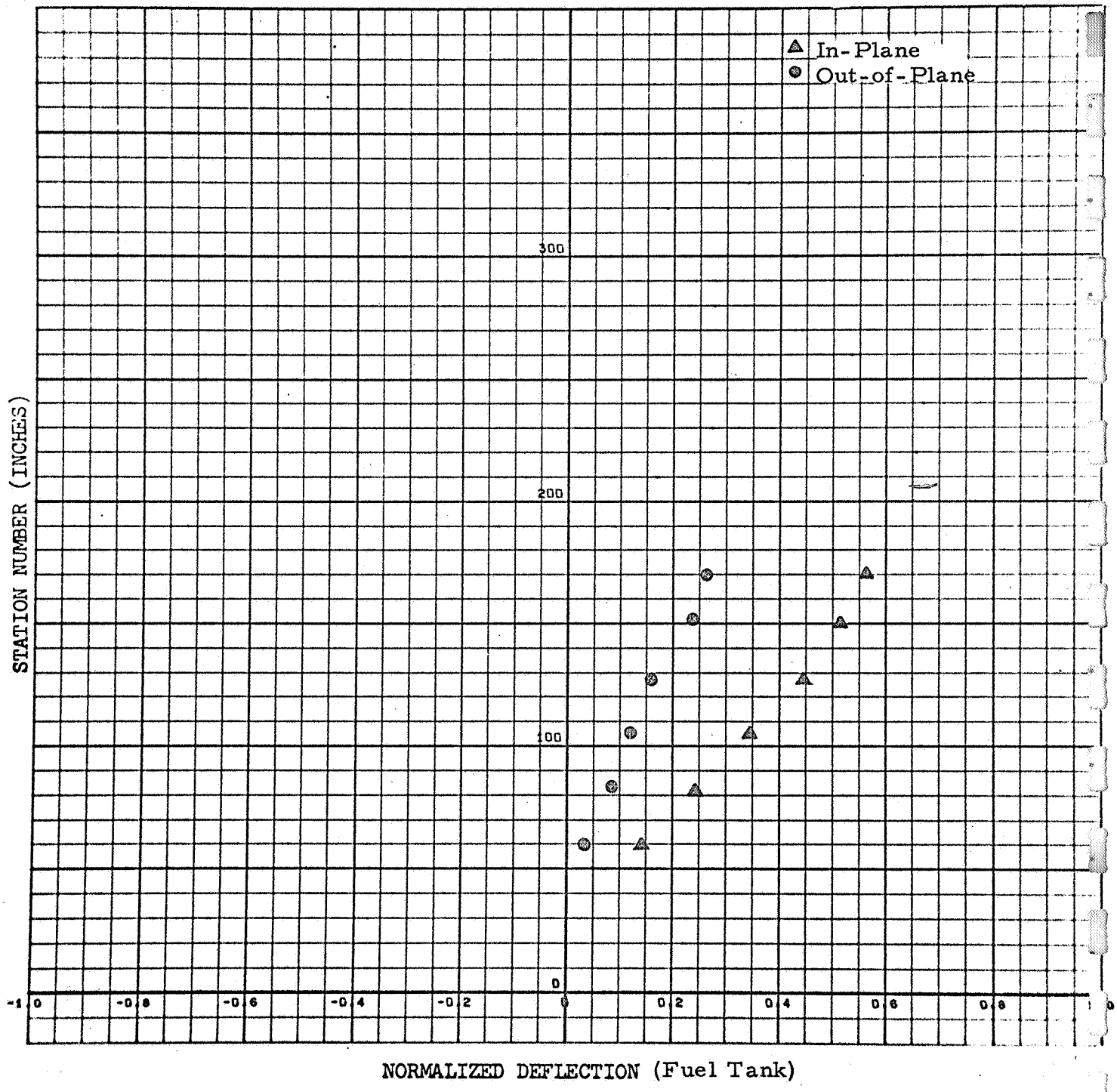

Figure C-B-28

CONFIGURATION: B

FREQUENCY: 69.4 cps

FORCE: 10 pounds, 0-pk

MODE NUMBER: 3

DAMPING: (See Figure C-B-42)

TIP ACCELERATION: .522 g (In-Plane)

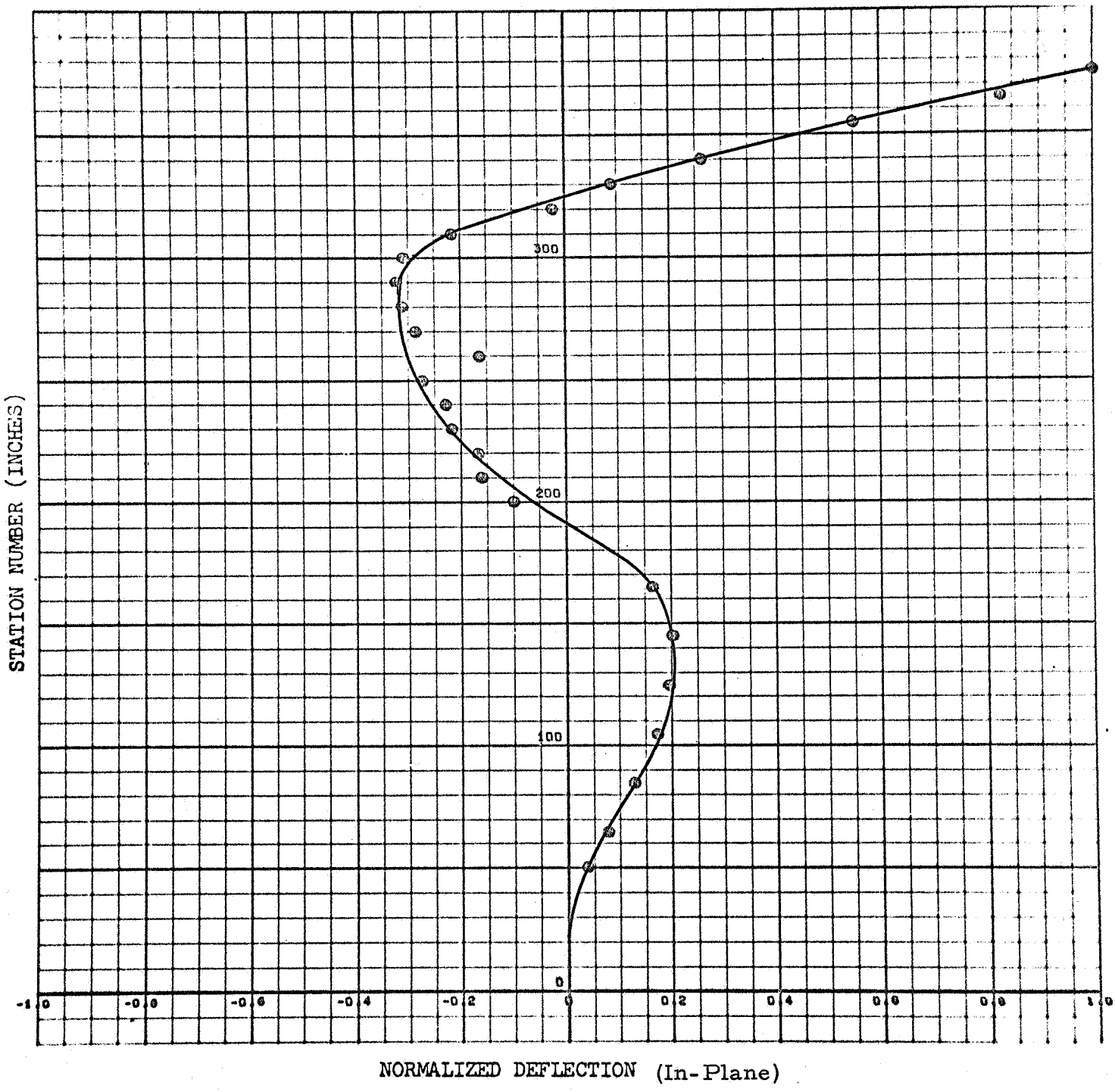

Figure C-B-29

CONFIGURATION: B

FREQUENCY: 69.4 cps

FORCE: 10 pounds, 0-pk

MODE NUMBER: 3

DAMPING:

TIP ACCELERATION: .270 g (Out-of-Plane)

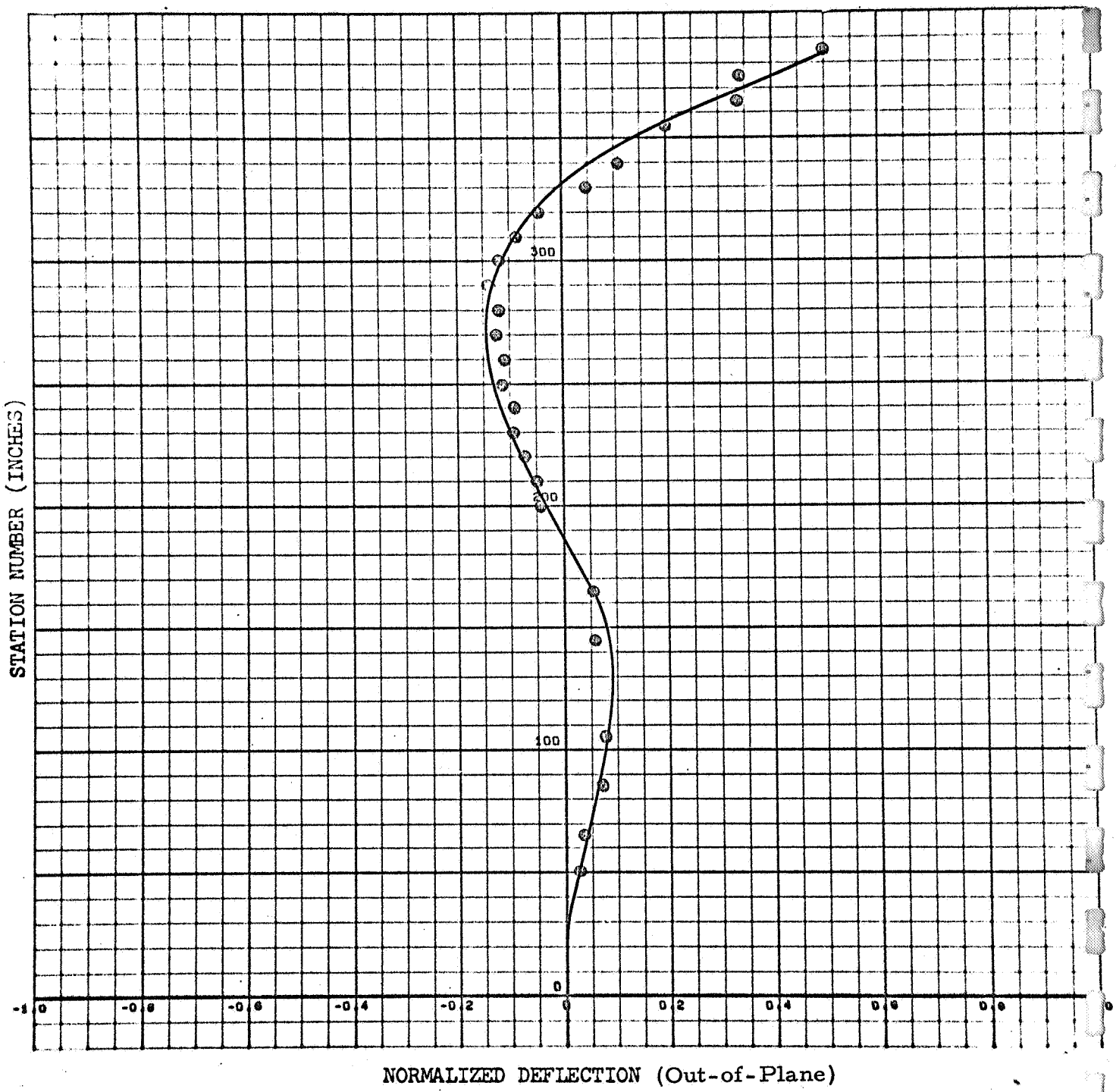

Figure C-B-30

CONFIGURATION: B

FREQUENCY: 69.1 cps

FORCE: 10 pounds, 0-pk

MODE NUMBER: 3

DAMPING: (See Figure C-B-44)

TIP ACCELERATION: .522 g (In-Plane)

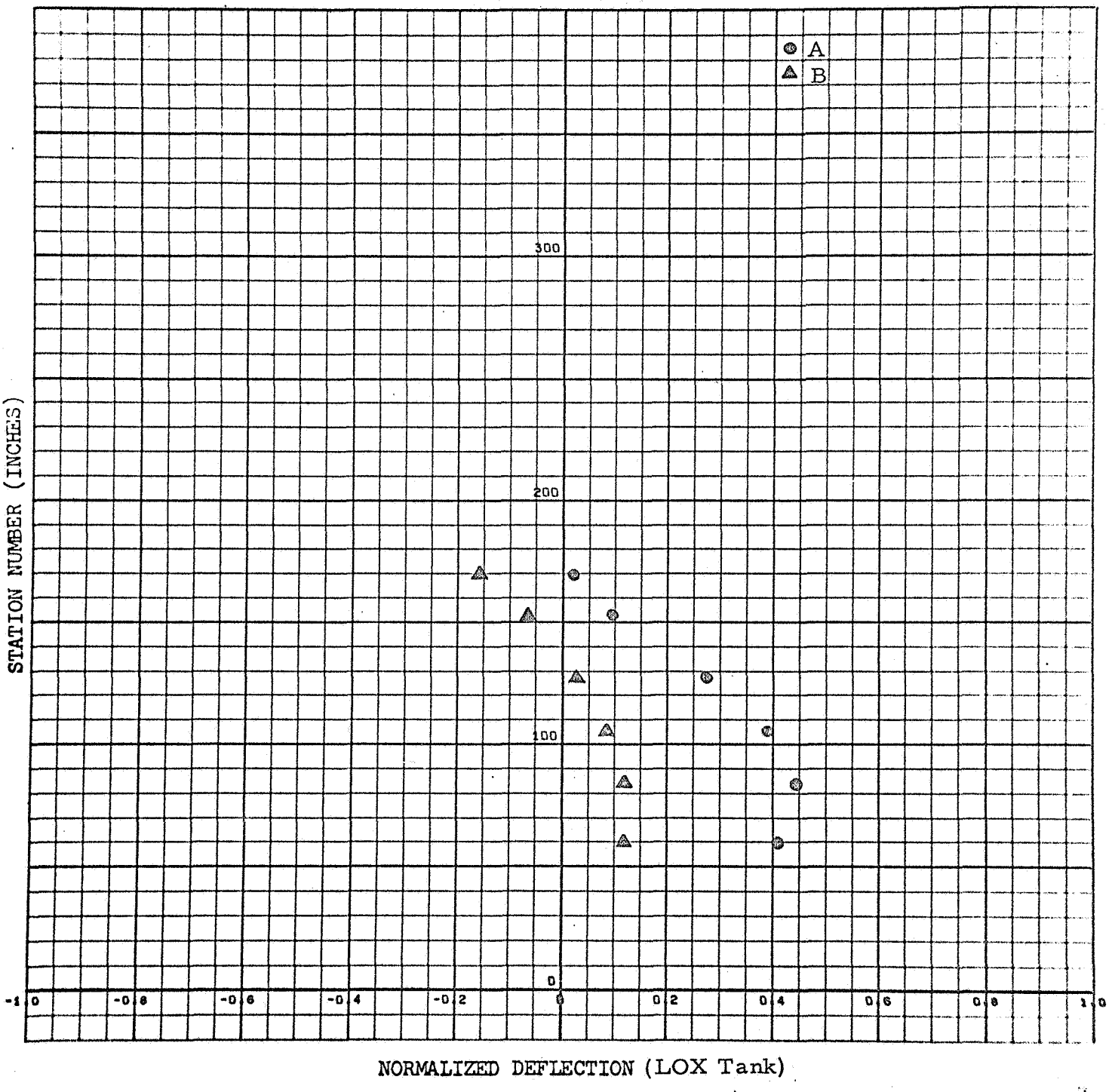

Figure C-B-31

CONFIGURATION: B

FREQUENCY: 69.1 cps

FORCE: 10 pounds, 0-pk

MODE NUMBER: 3

DAMPING: (Not Available)

TIP ACCELERATION: .522 g (In-Plane)

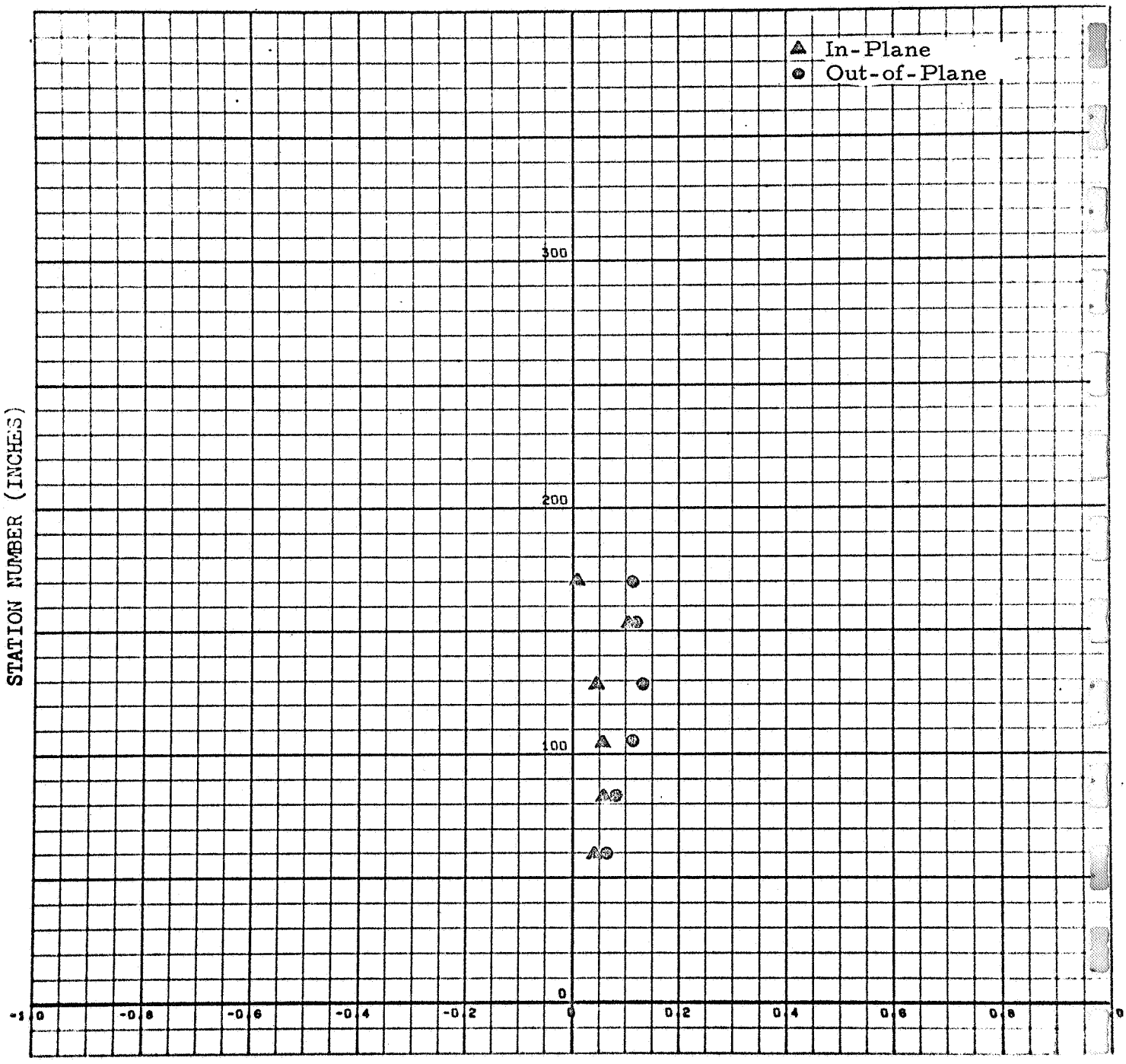

Figure C-B-32

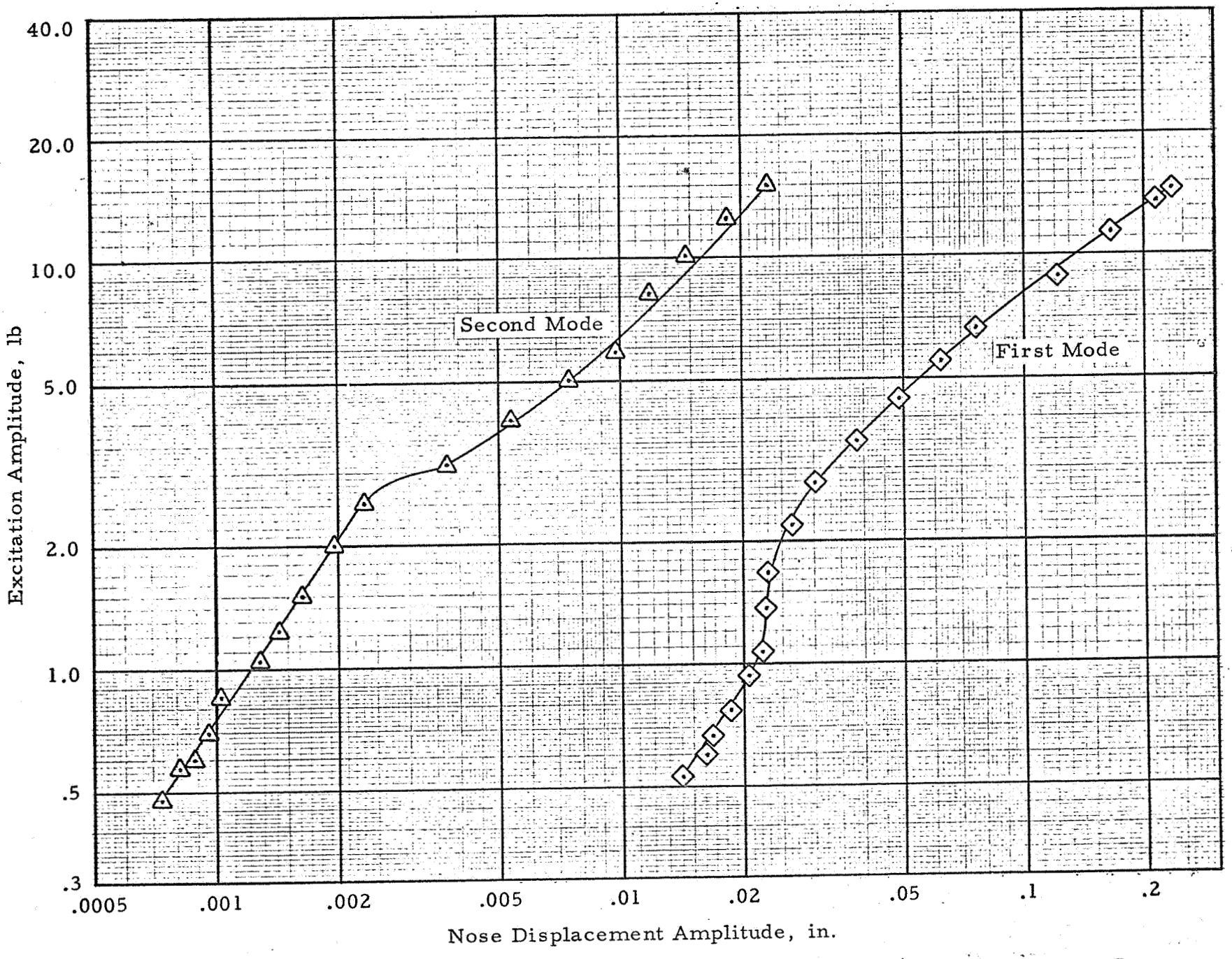

Figure C-B-33 - First and Second Mode Resonant Response (Configuration B)

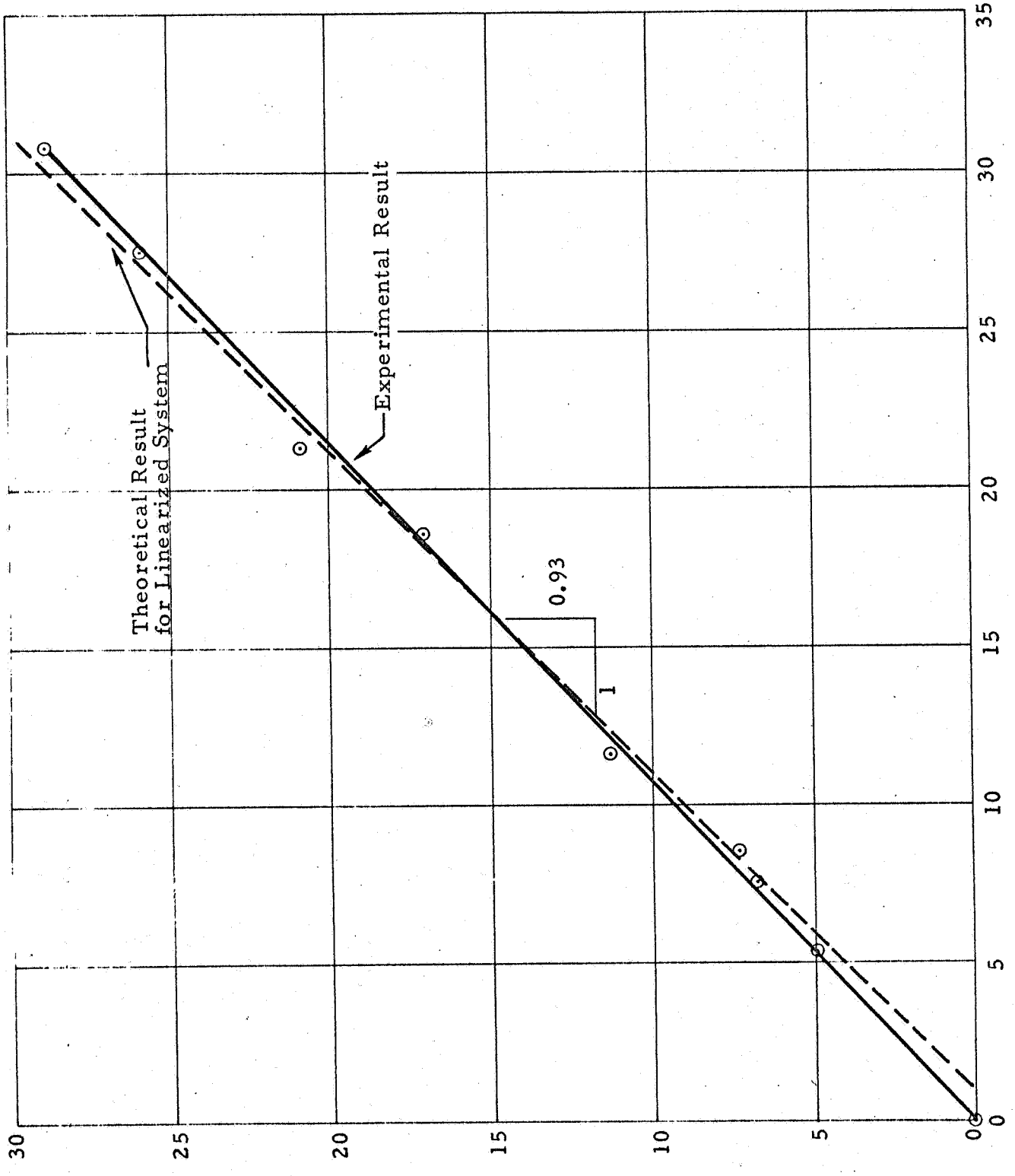

Figure C-B-33a-First Mode Mean Square Response, Configuration B-1

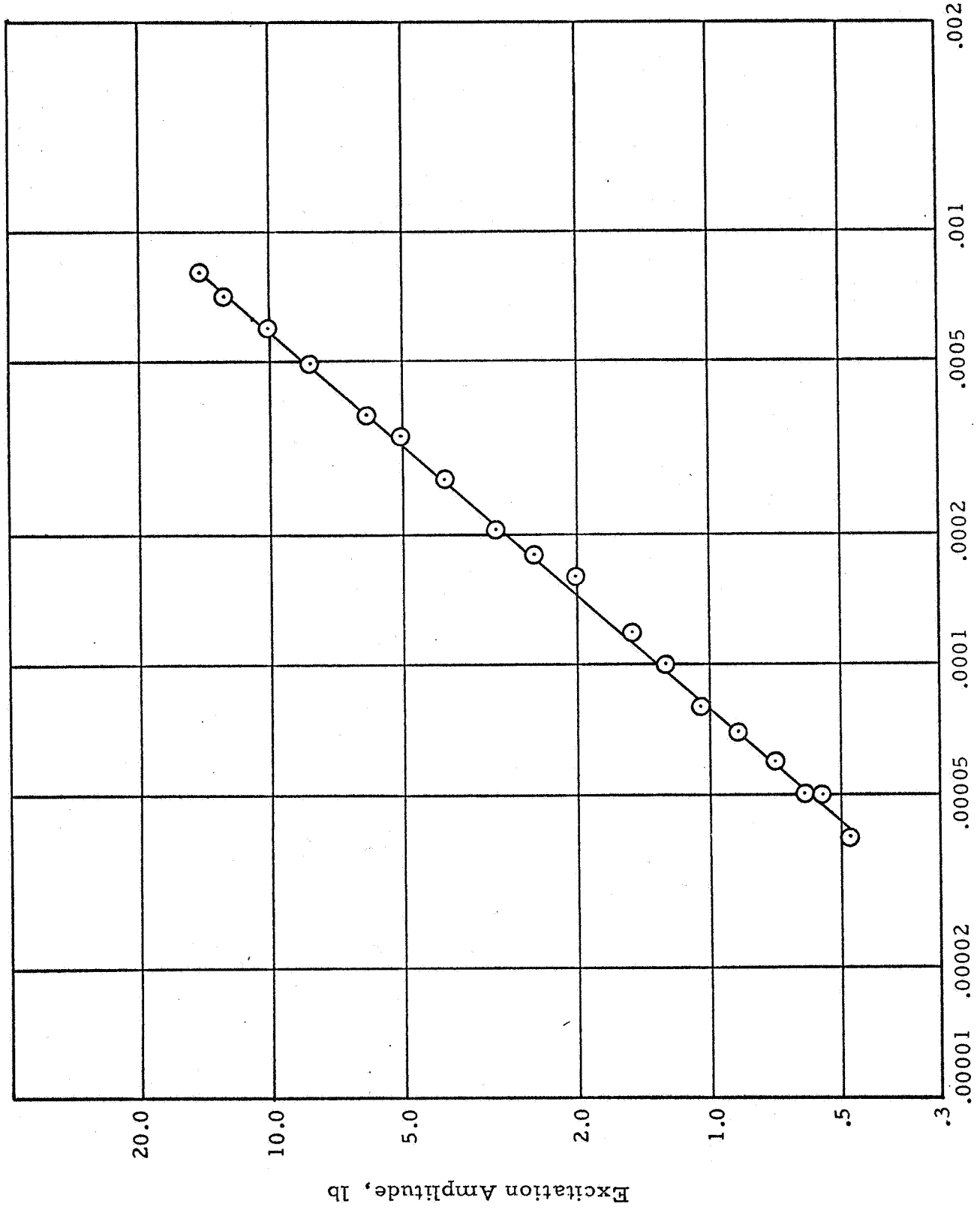

Figure C-B-34 - Third Mode Resonant Response (Configuration B)

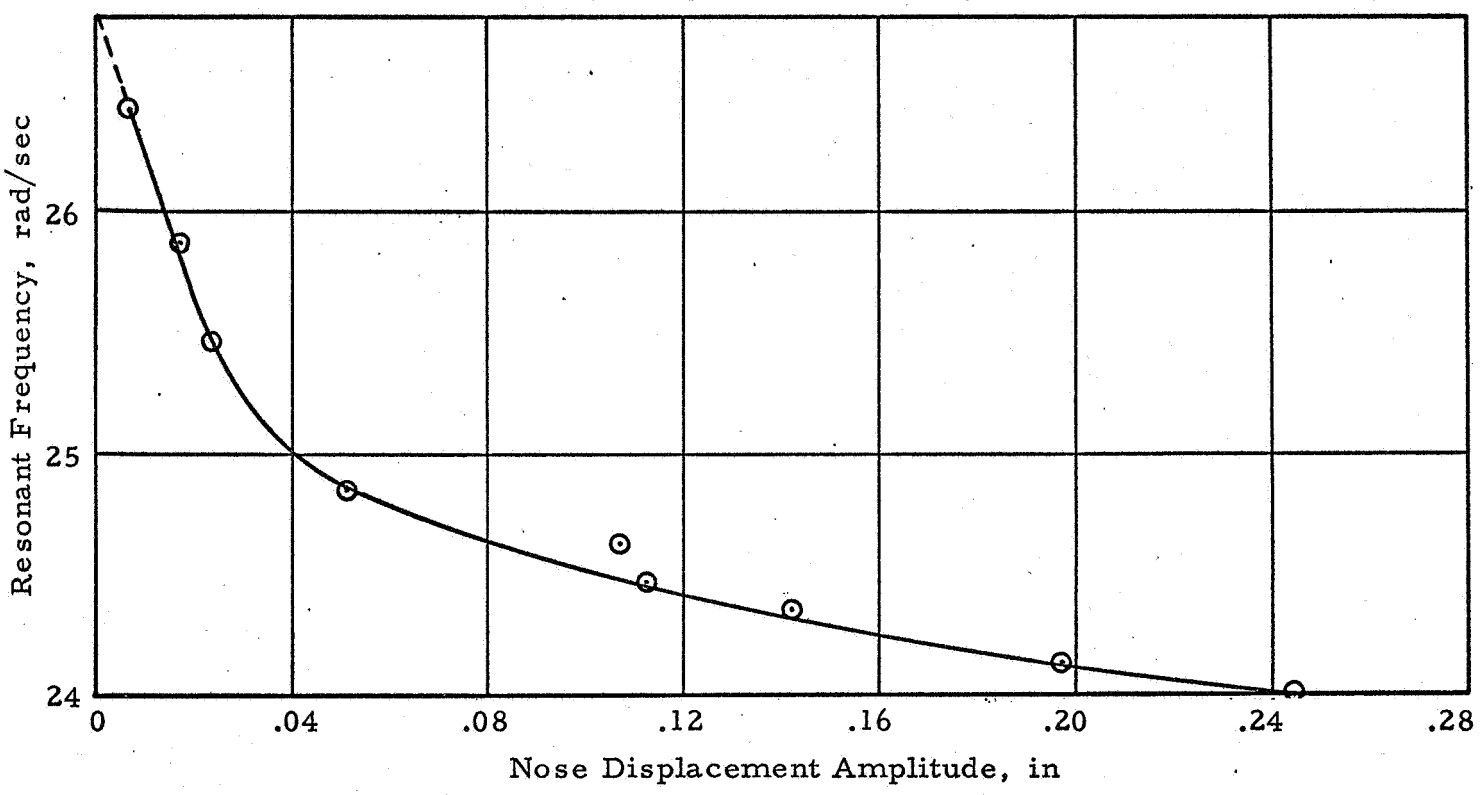

Figure C-B-35 - Variation of First Mode Frequency with Displacement Amplitude (Configuration B-1).

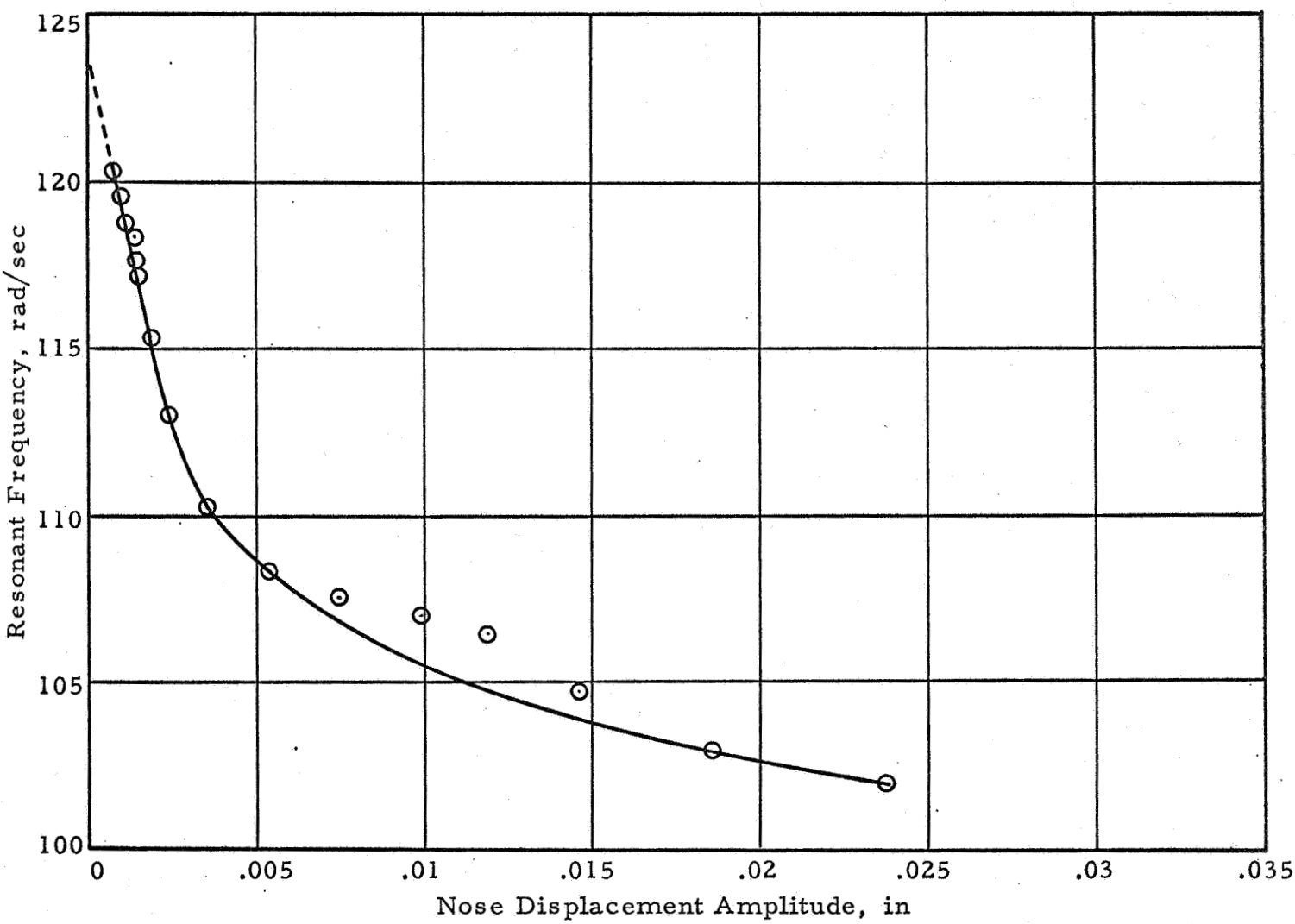

Figure C-B-36 - Variation of Second Mode Frequency with Displacement Amplitude (Configuration B)

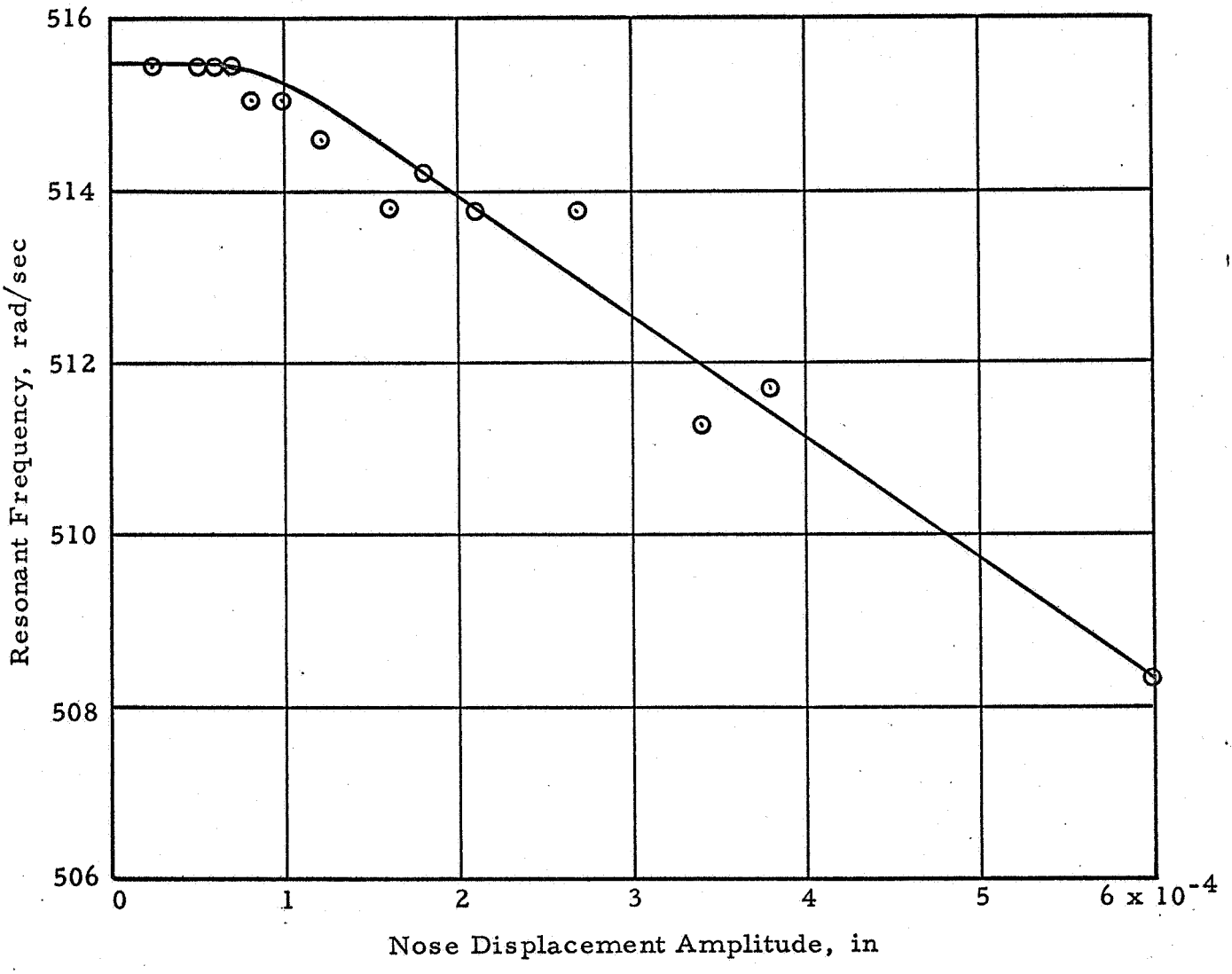

Figure C-B-37 - Variation of Third Mode Frequency with Displacement Amplitude (Configuration B)

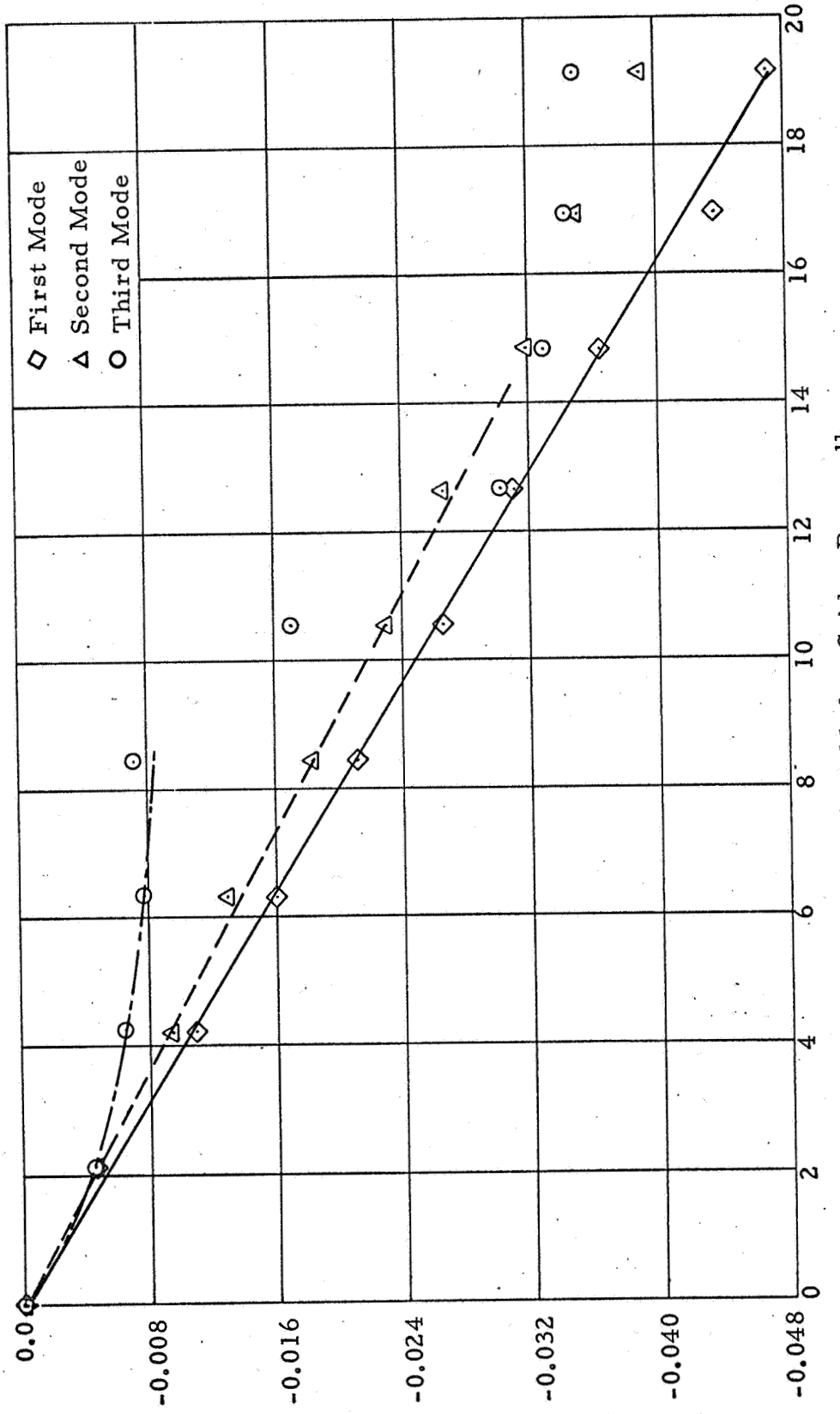

Figure C-B-38 - Generalized Mass Tests (Configuration B) Low Amplitude Tests

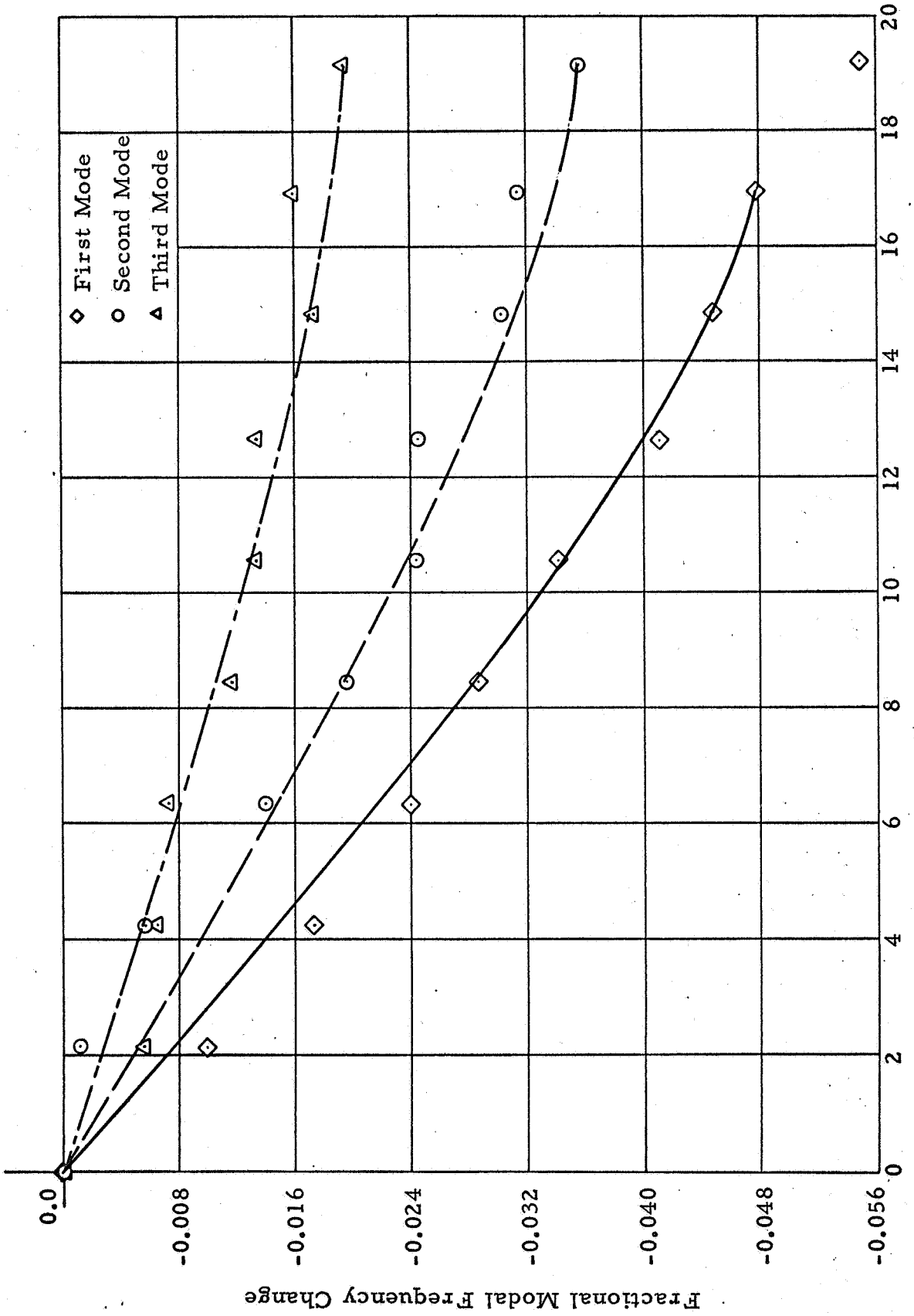

Figure C-B-39 - Generalized Mass Tests (Configuration B) High Amplitude Tests

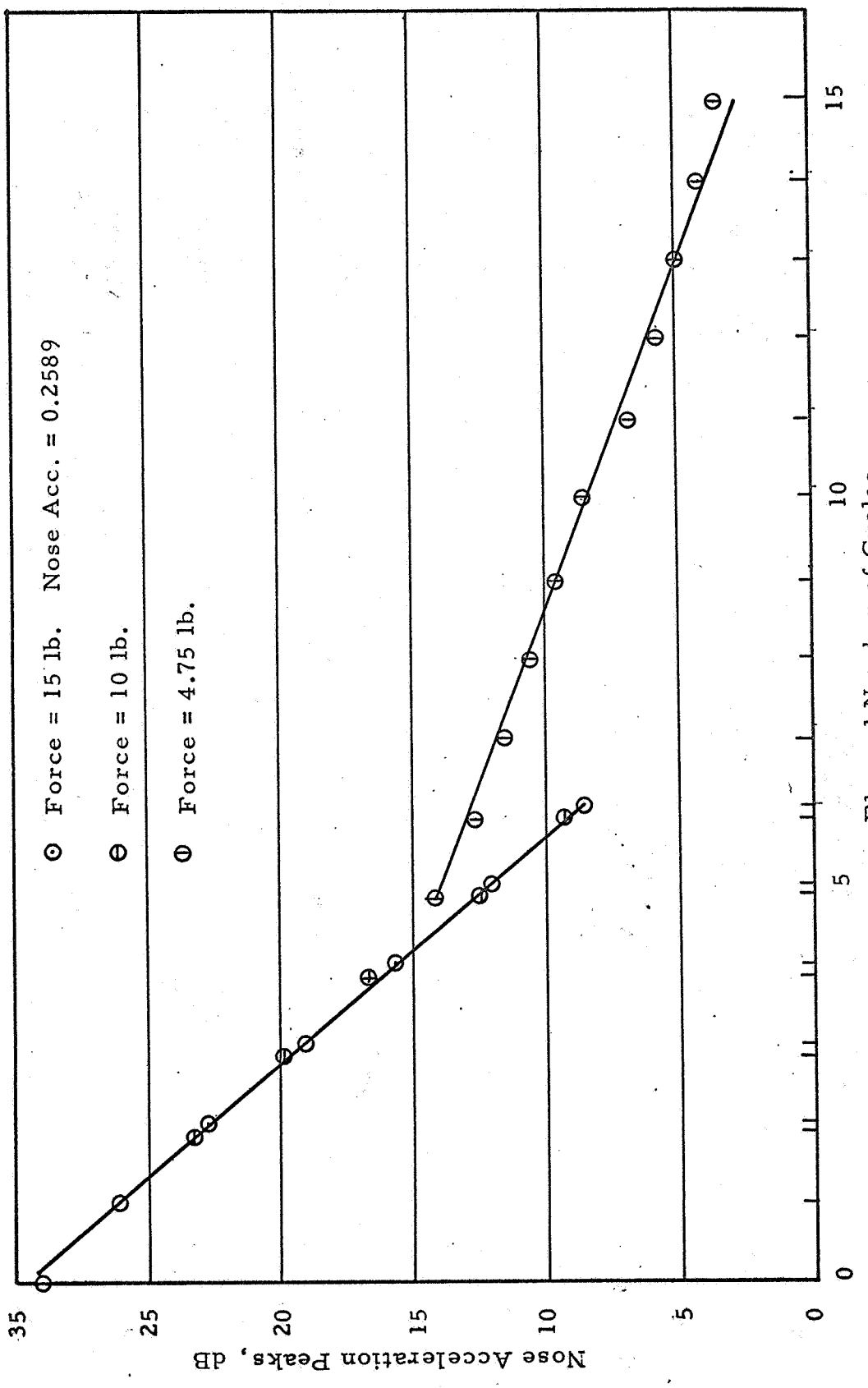

Figure C-B-40 - Decay of First Mode Free Vibration Peaks (Configuration B)

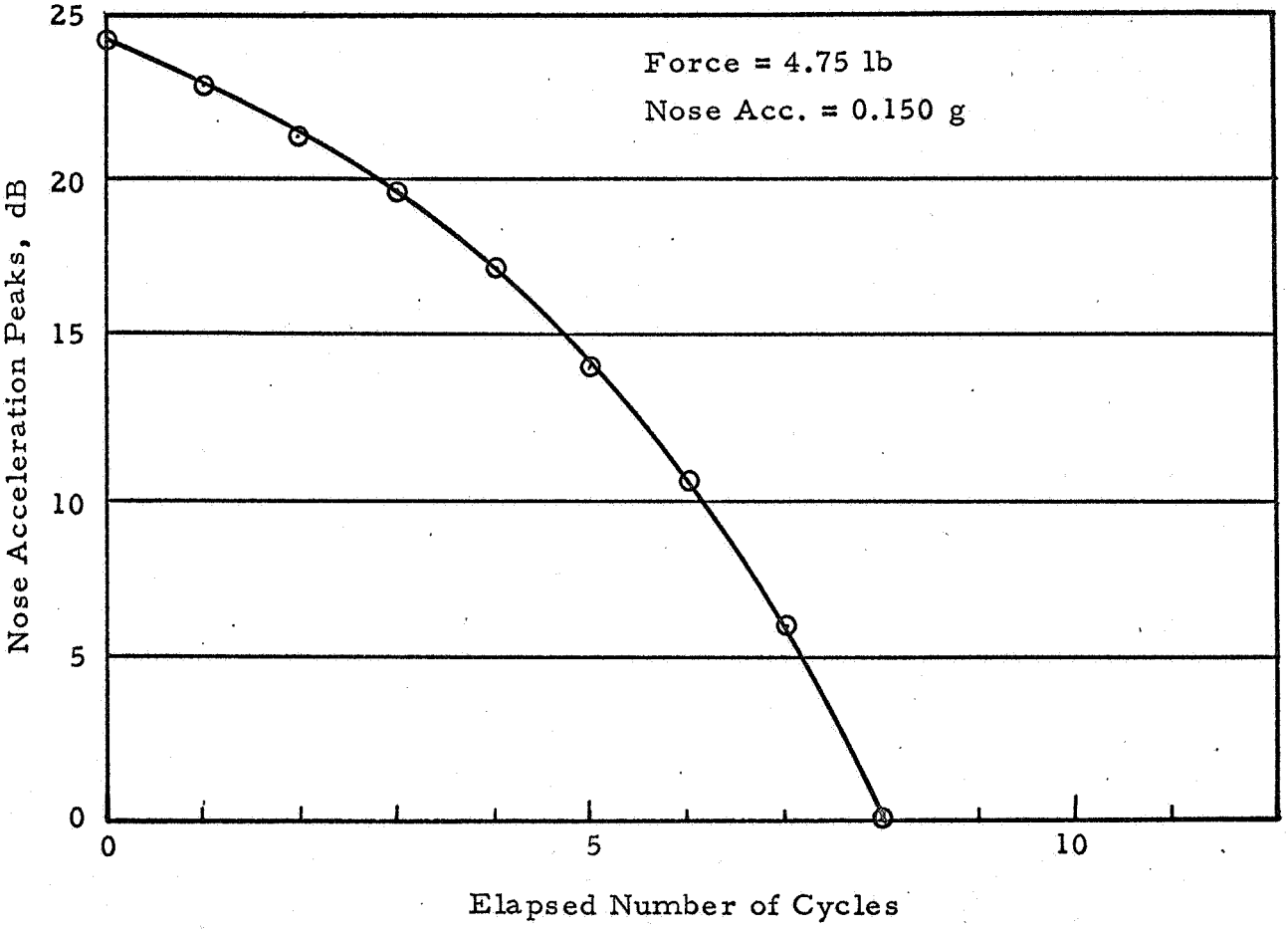

Figure C-B-40(a) - Decay of First Mode Free Vibration Peaks (Configuration B-1)

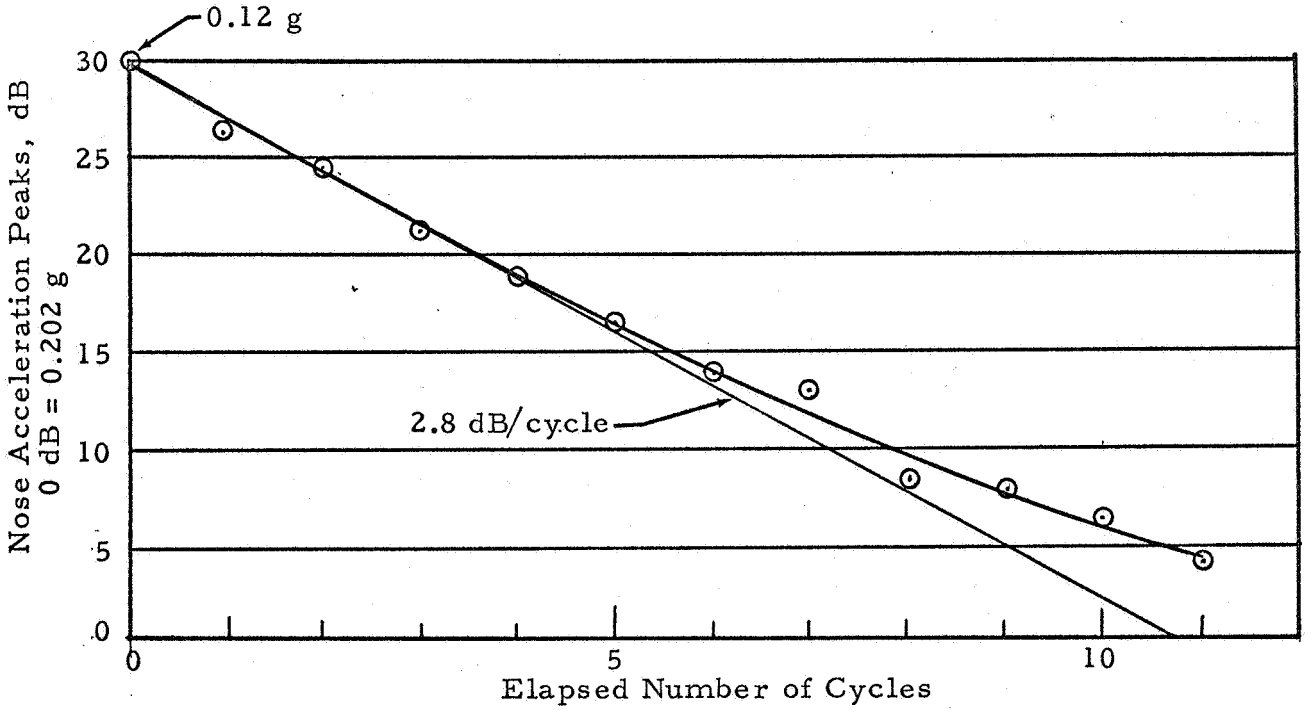

Figure C-B-41 - Decay of 2nd Mode Free Vibration (Configuration B)

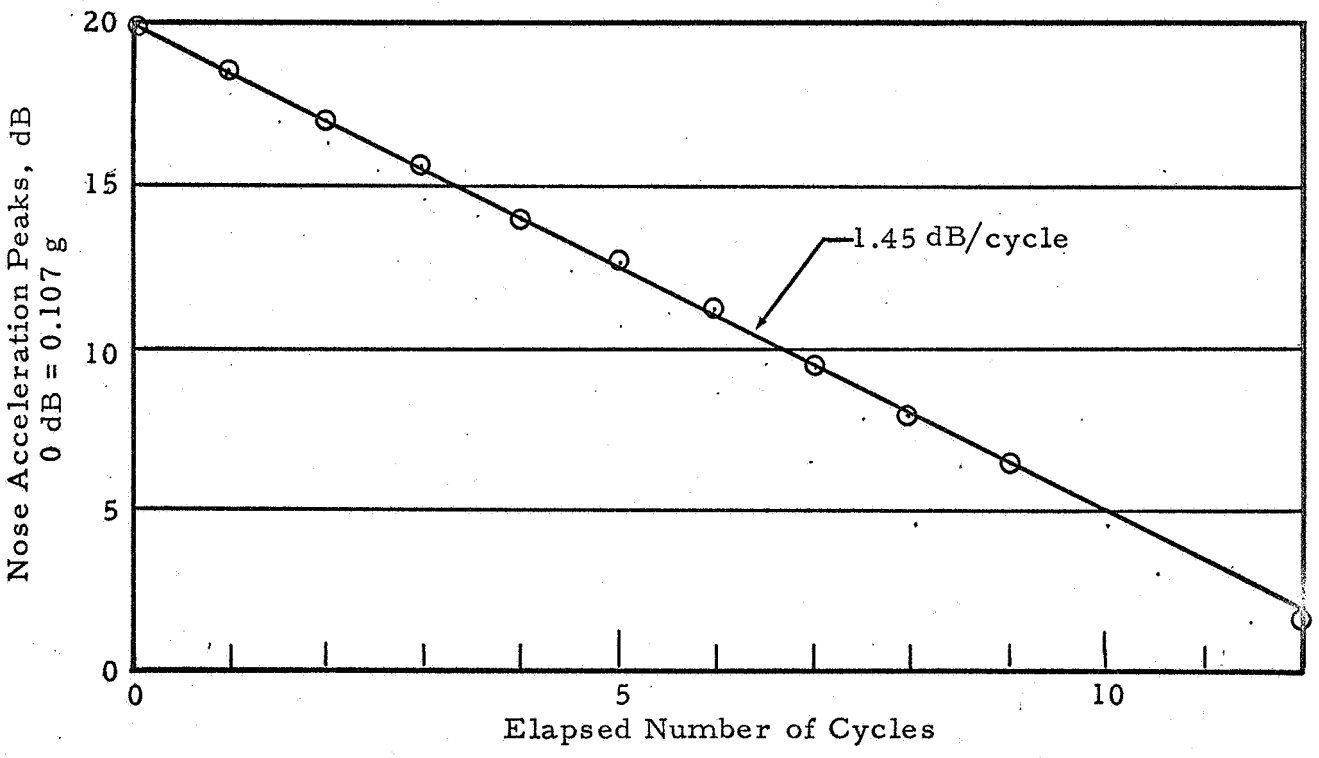

Figure C-B-42 - Decay of 3rd Mode Free Vibration (Configuration B)

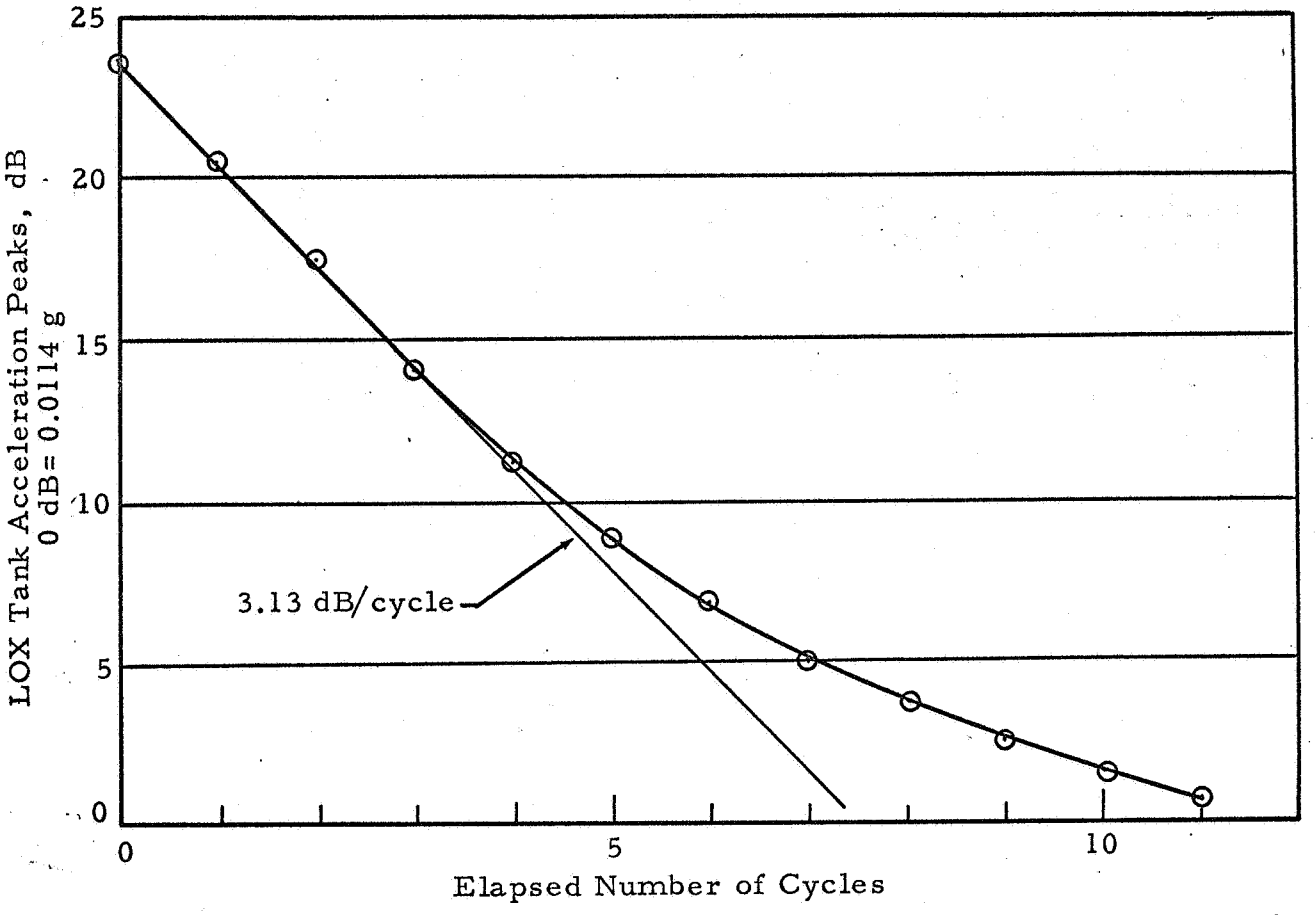

Figure C-B-43 - Decay of 2nd Mode Free Vibration (Configuration B)

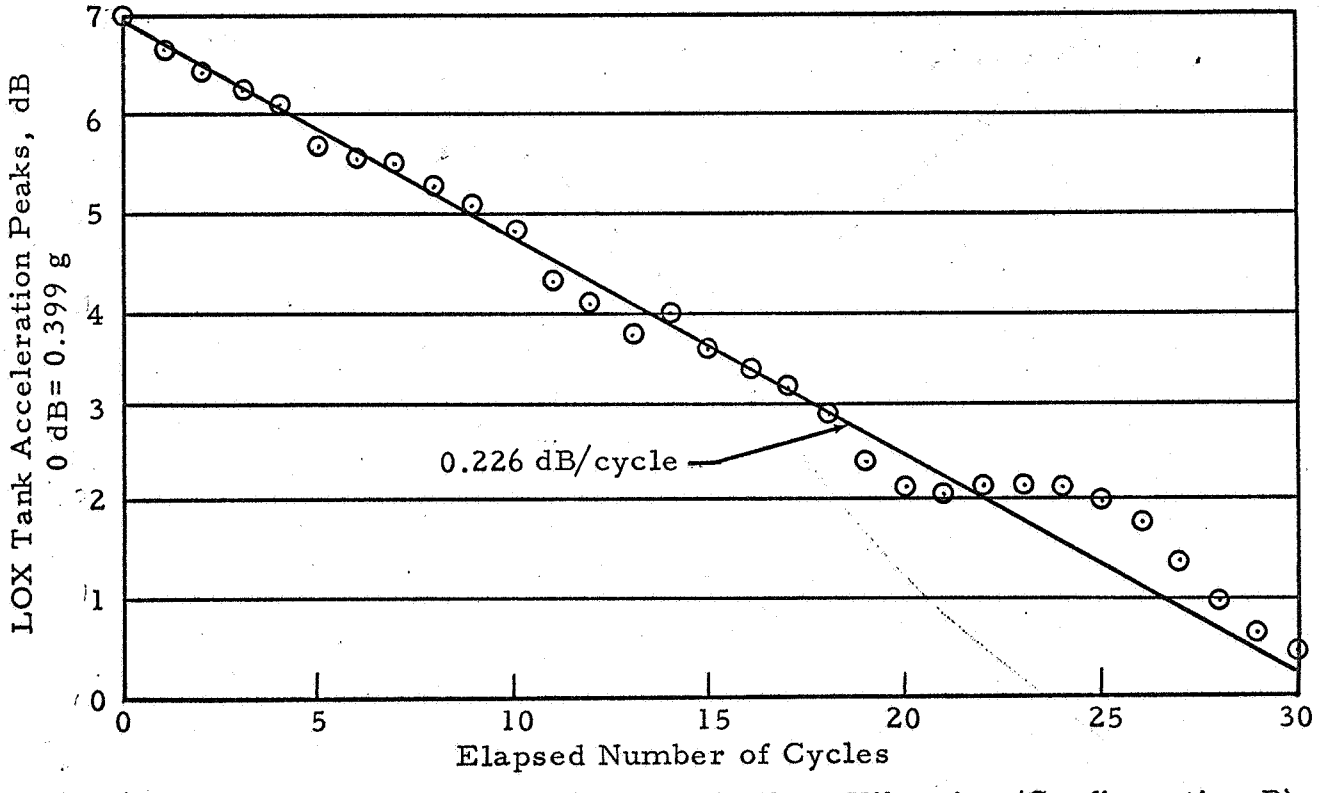

Figure C-B-44 - Decay of 3rd Mode Free Vibration (Configuration B)

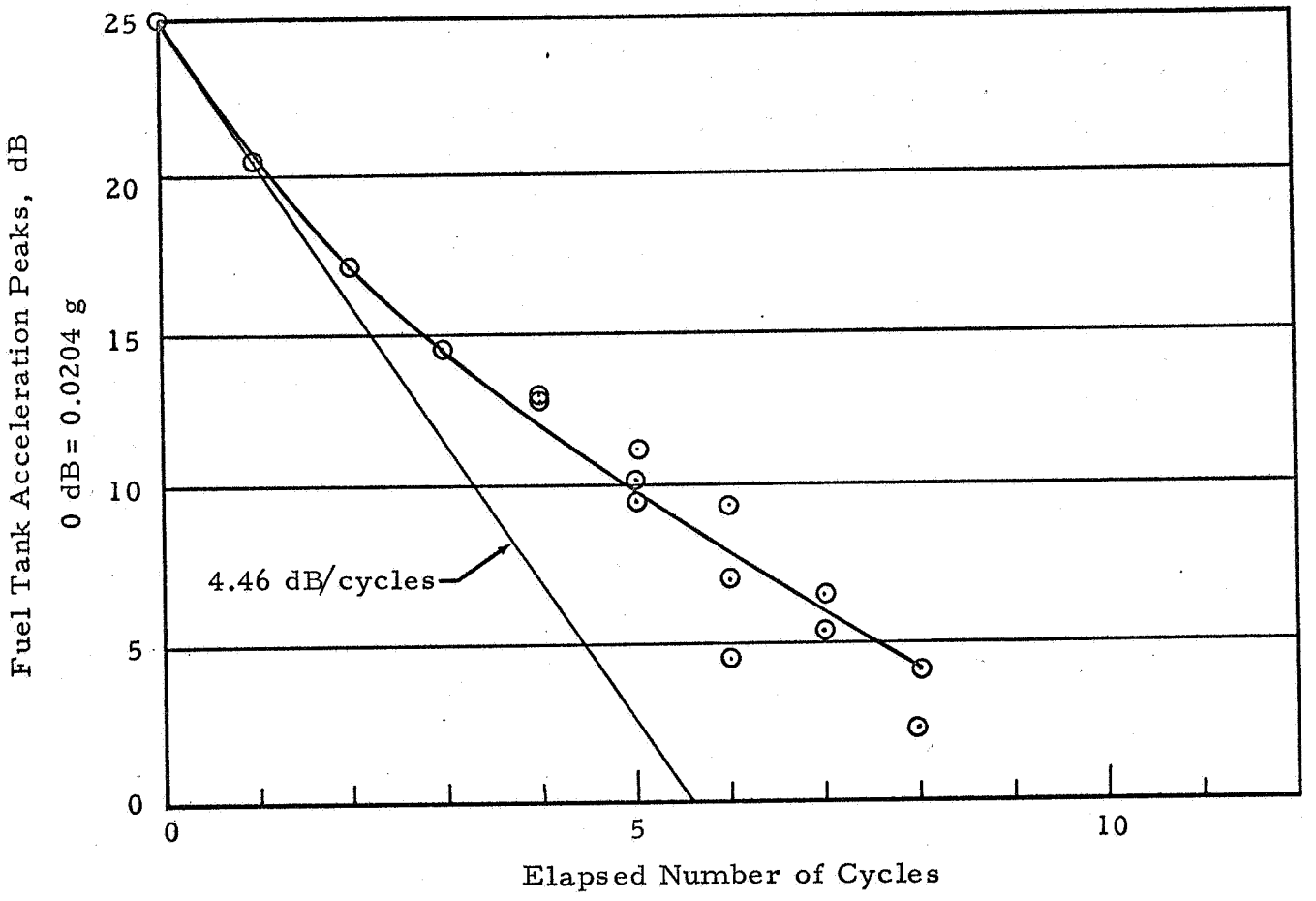

Figure C-B-45 - Decay of 2nd Mode Free Vibration (Configuration B)

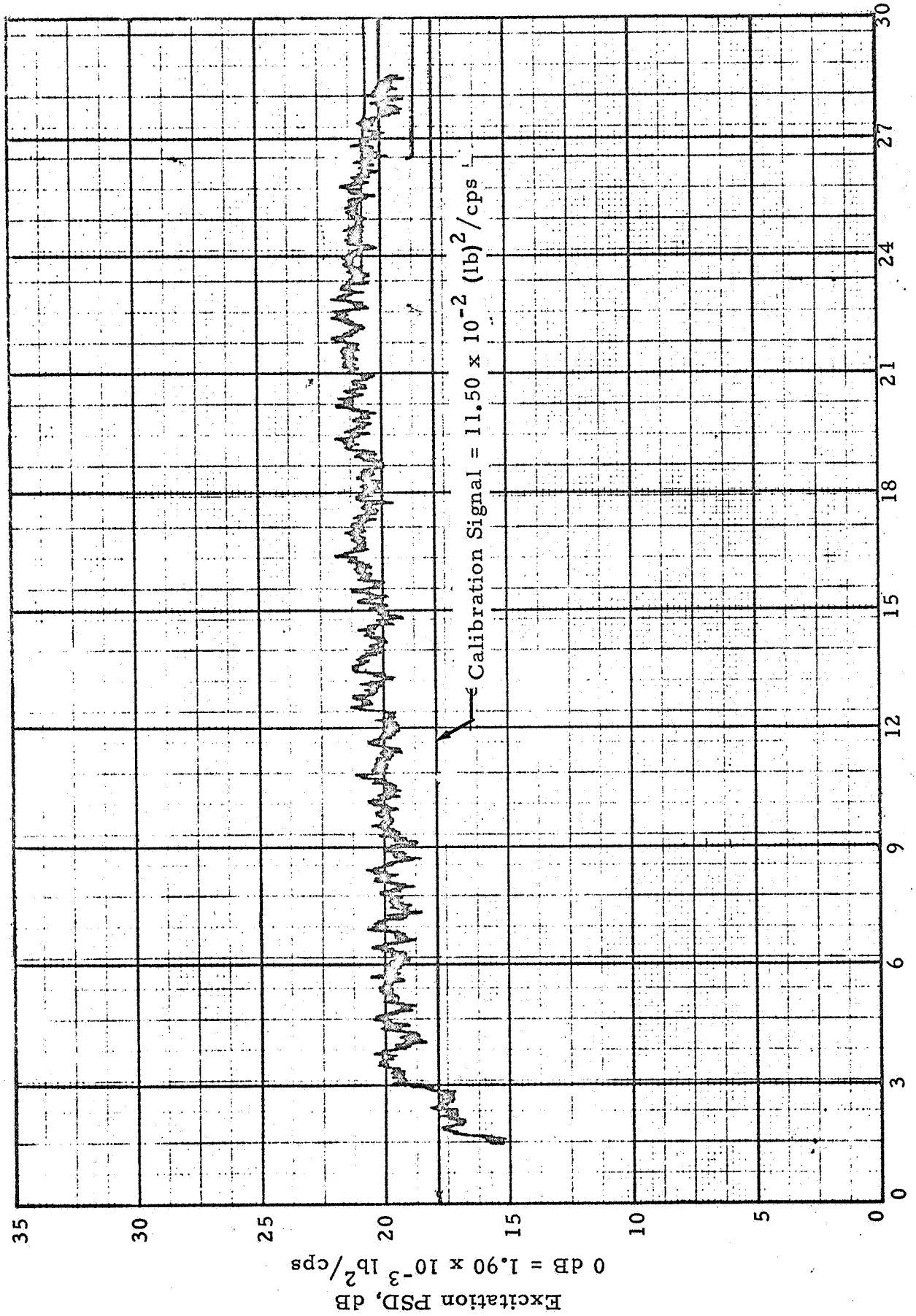

Figure C-B-46 - Excitation PSD (Configuration B-1)

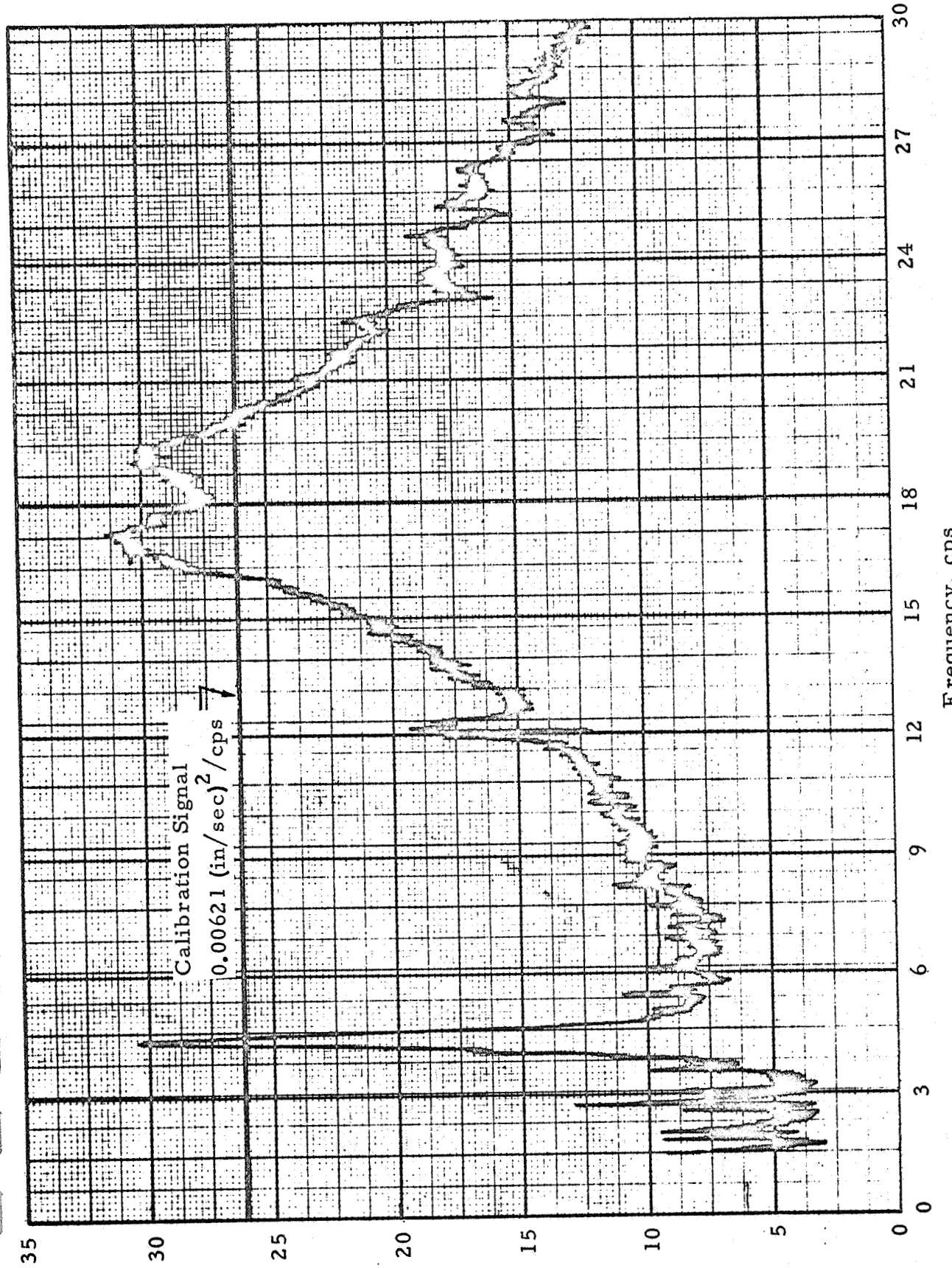

Figure C-B-47 - Response PSD (Configuration B-1)

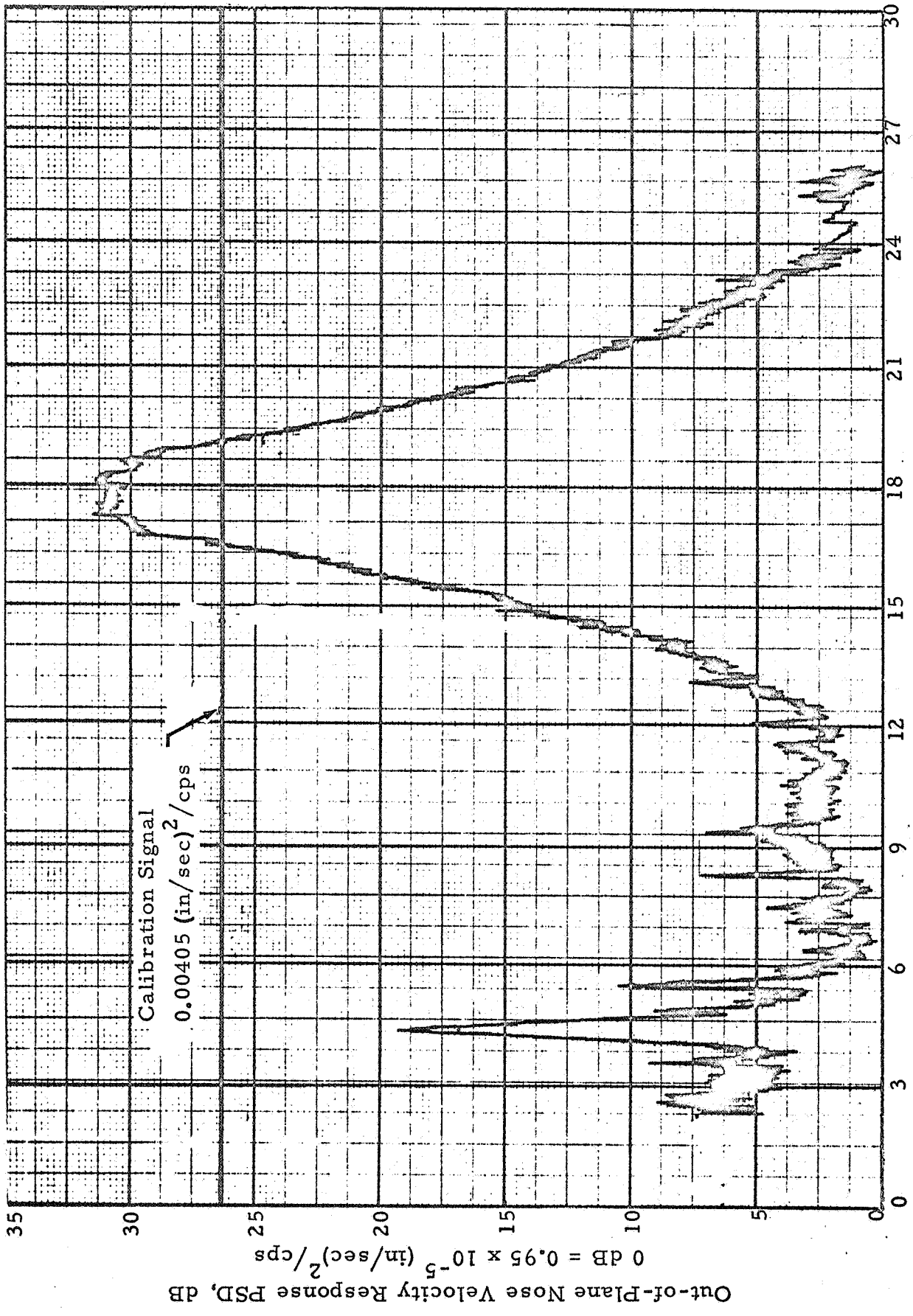

Figure C-B-48 - Response PSD (Configuration B-1)

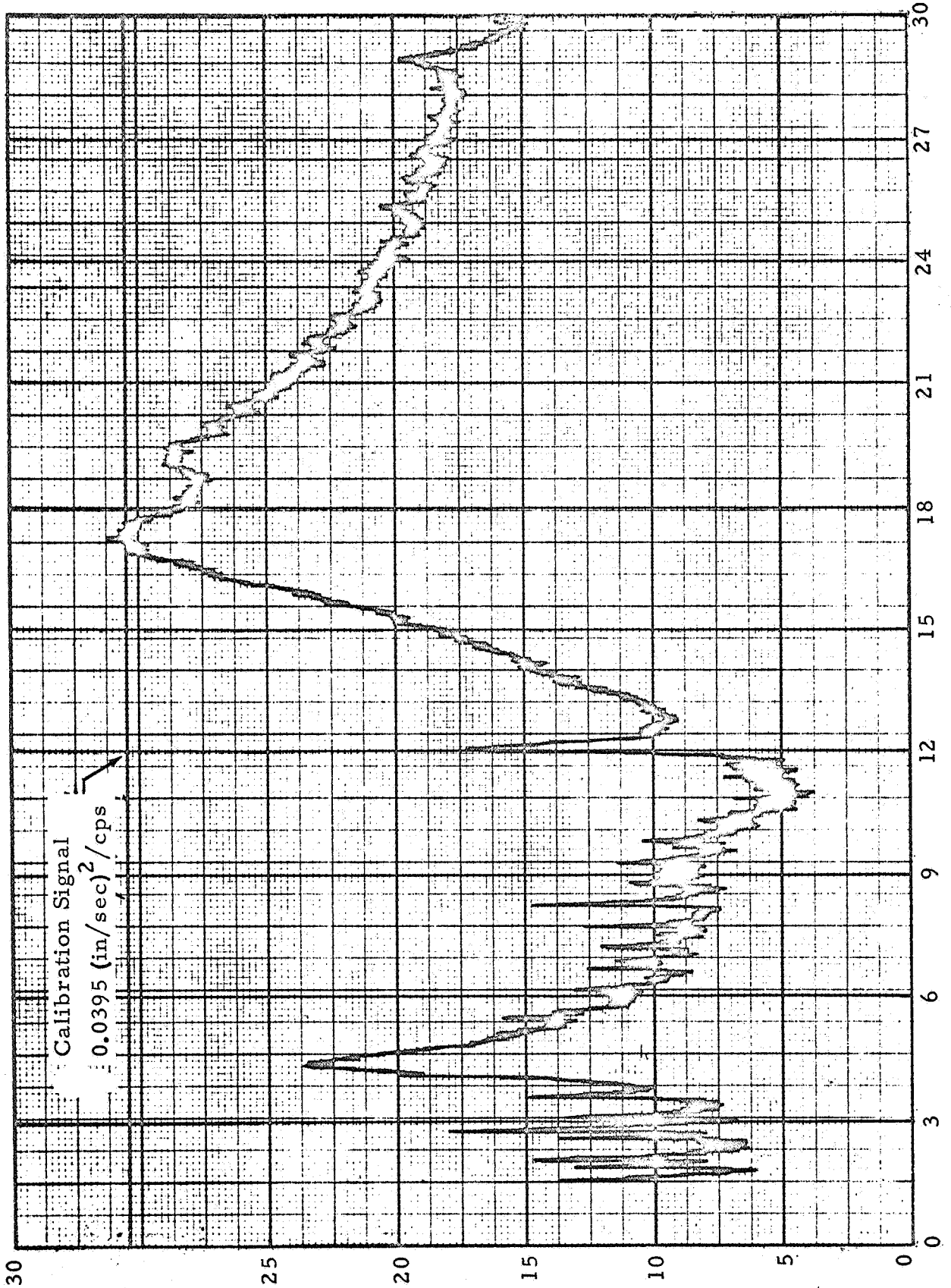

Figure C-B-49 - Response PSD (Configuration B-1)

TEST CONFIGURATION C
INDEX TO FIGURES

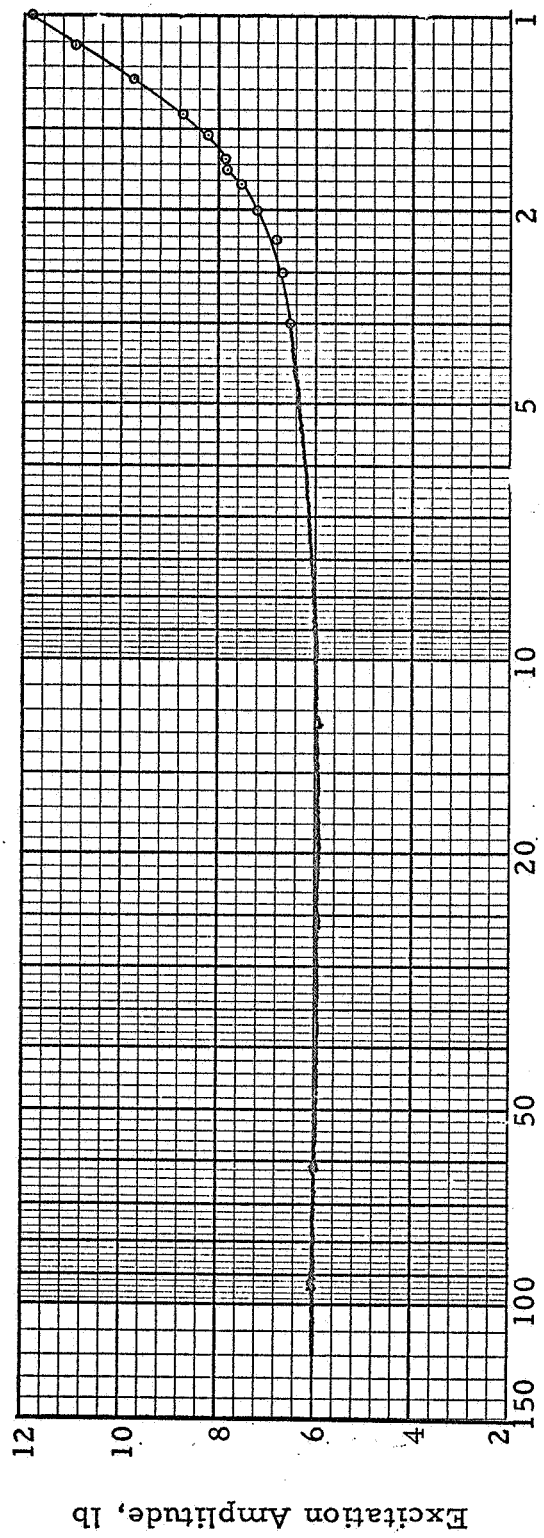

Figure C-C-1 - Variation of Applied Force Amplitude with Frequency (Configuration C)

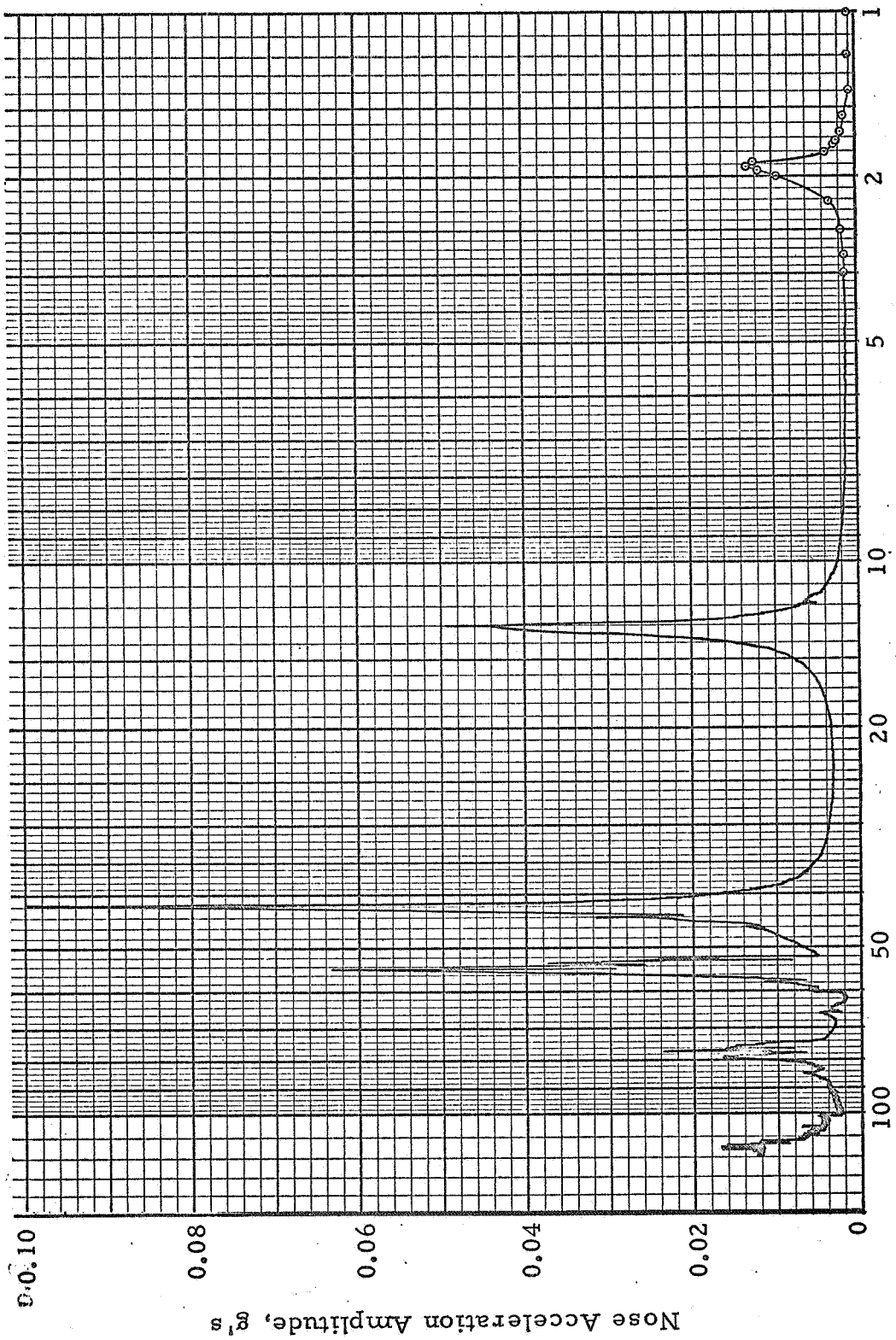

Figure C-C-2 - Frequency Response (Configuration C) Force Amplitude: 1.0 lb at 25 cps

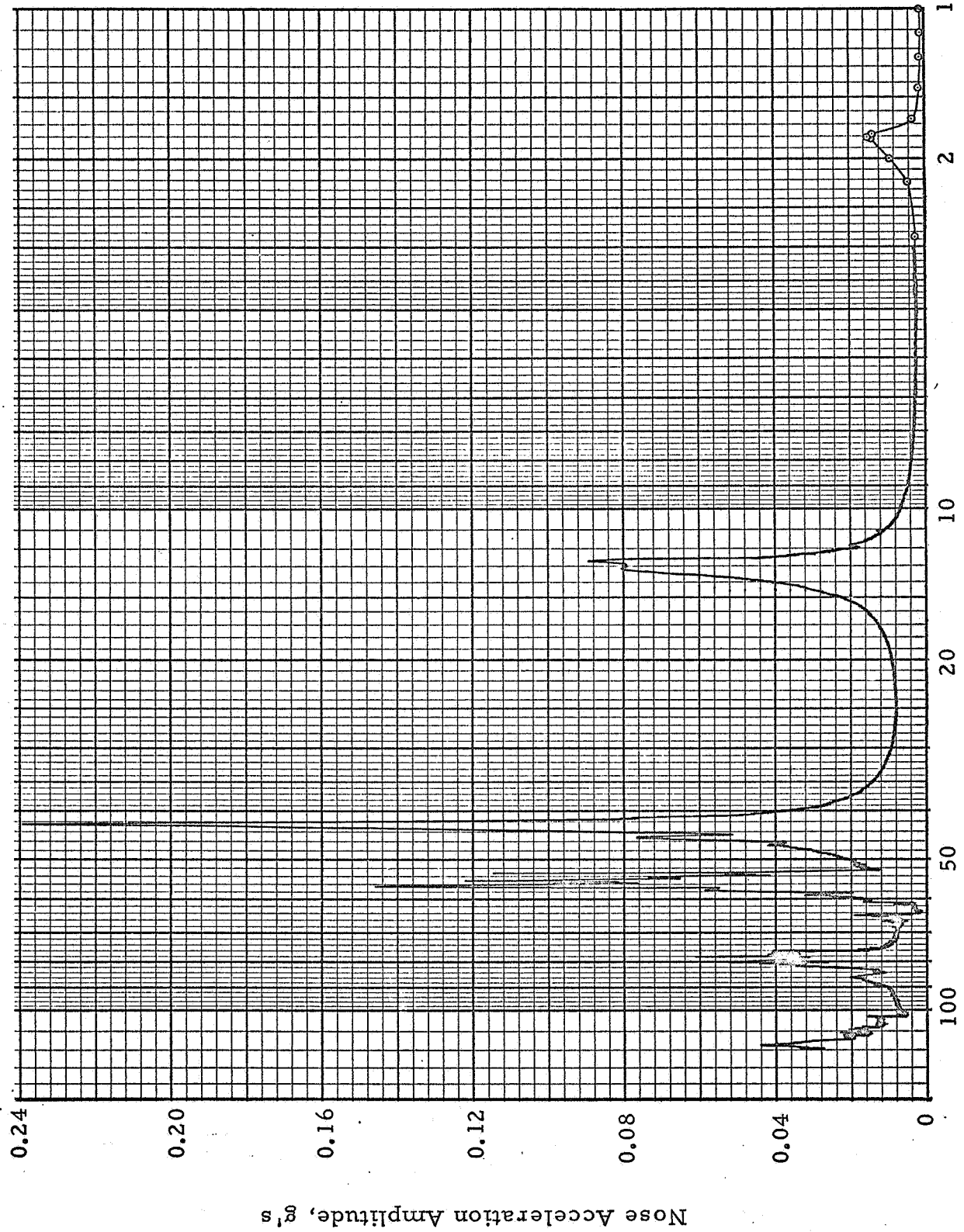

Figure C-C-3 - Frequency Response (Configuration C) Force Amplitude: 3.0 lb at 25 cps

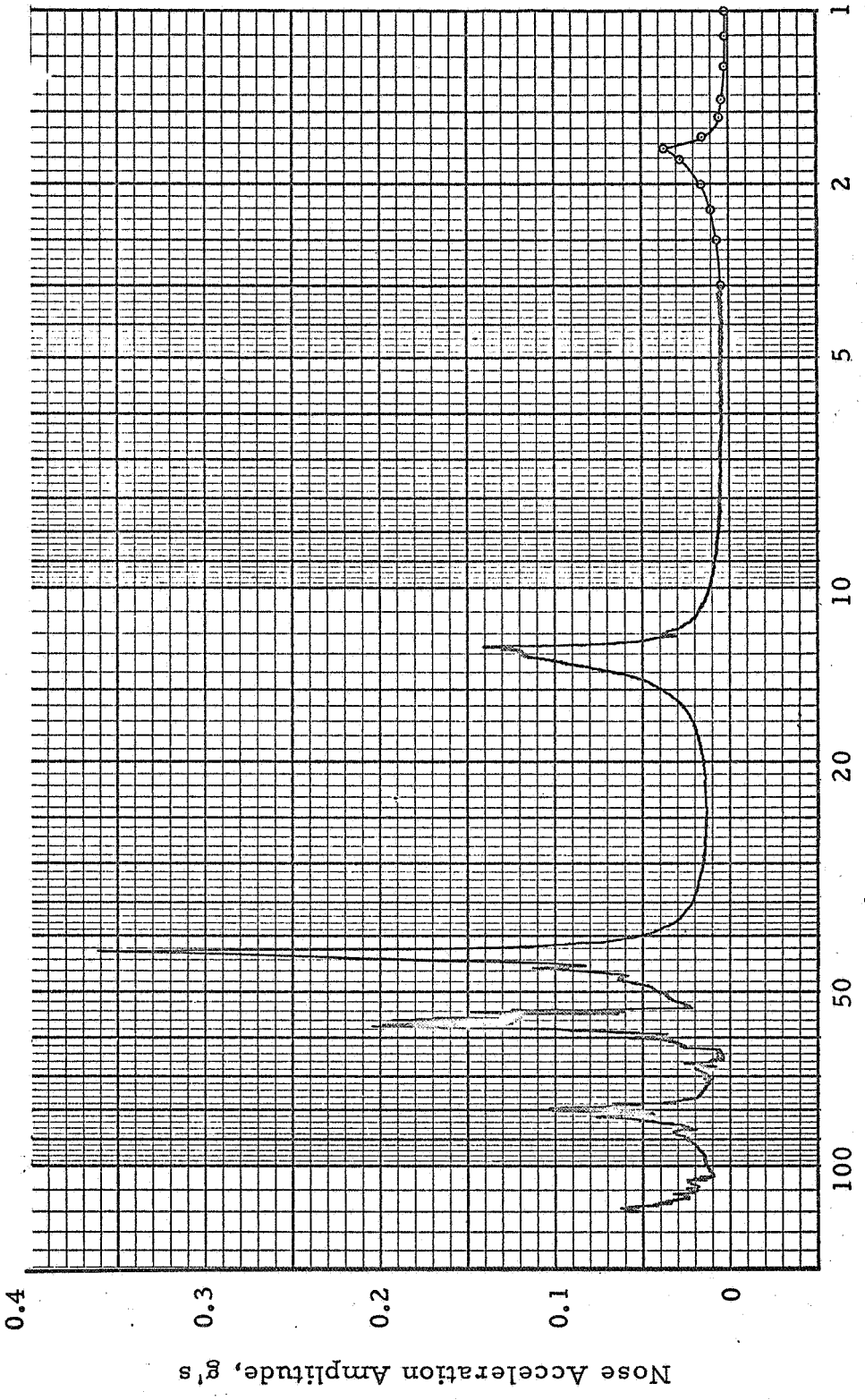

Figure C-C-4 - Frequency Response (Configuration C) Force Amplitude: 4.75 lb at 25 cps

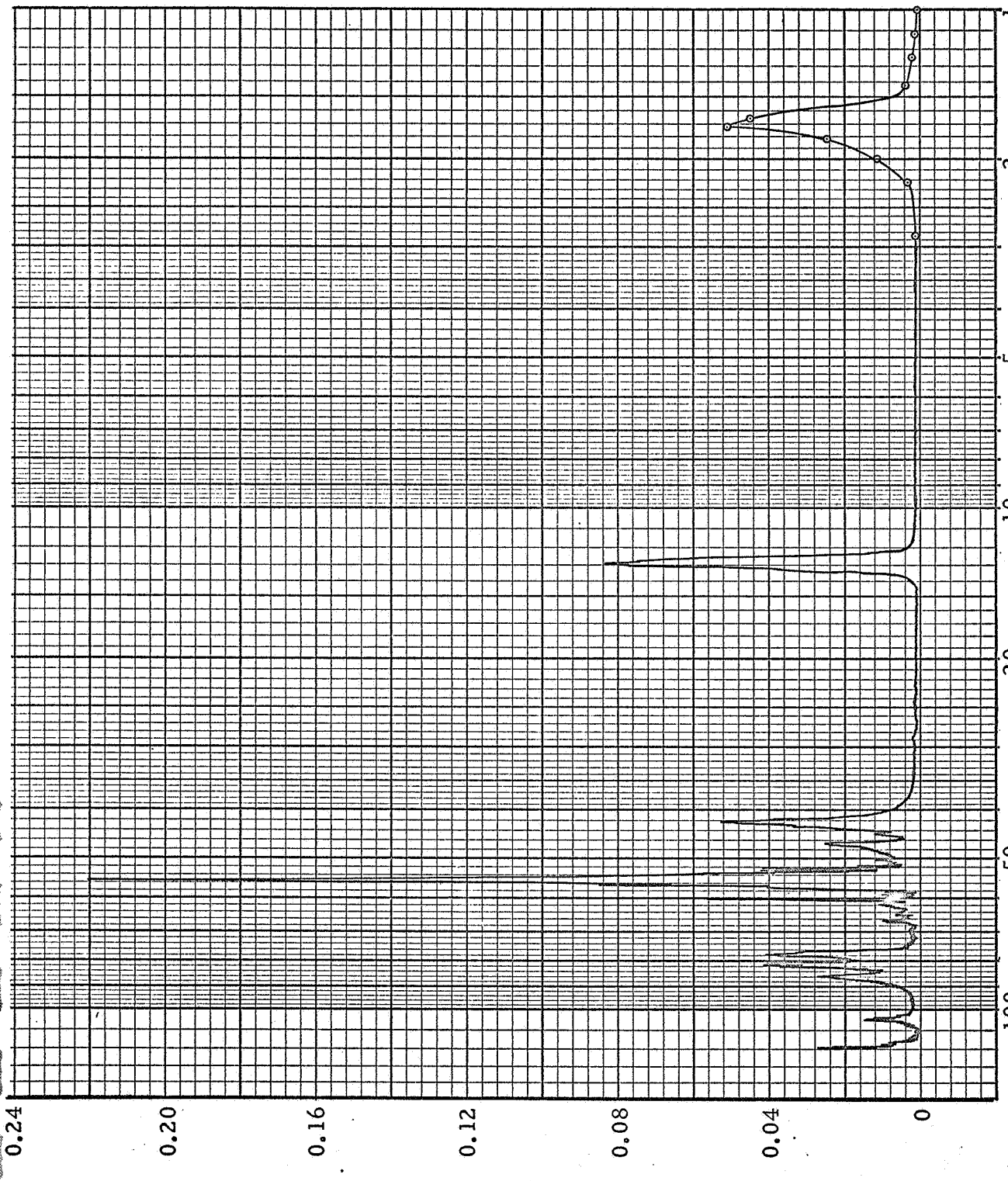

Figure C-C-5 - Frequency Response (Configuration C) Force Amplitude: 4.75 lb at 25 cps

Accel. No. 6 Fuel, 19 LOX
Accel. Type Chang
Shaker Force, 4.75 lb at 25 cps
Configuration C

SD101A Multiplier: 1.0
SD101A Range: 1.0
Plotter Range: 1 v/in.

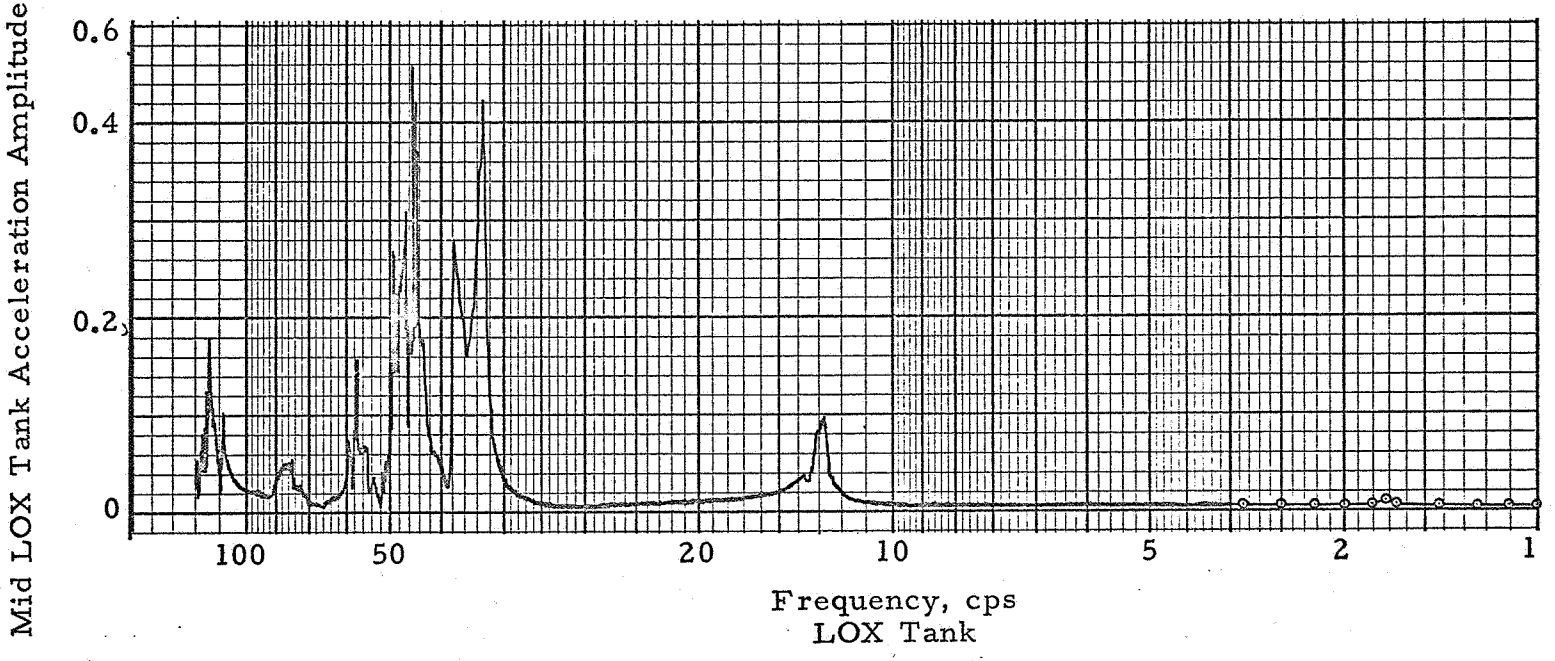

Figure C-C-6 - Frequency Response (Configuration C) Force Amplitude: 4.75 lb at 25 cps

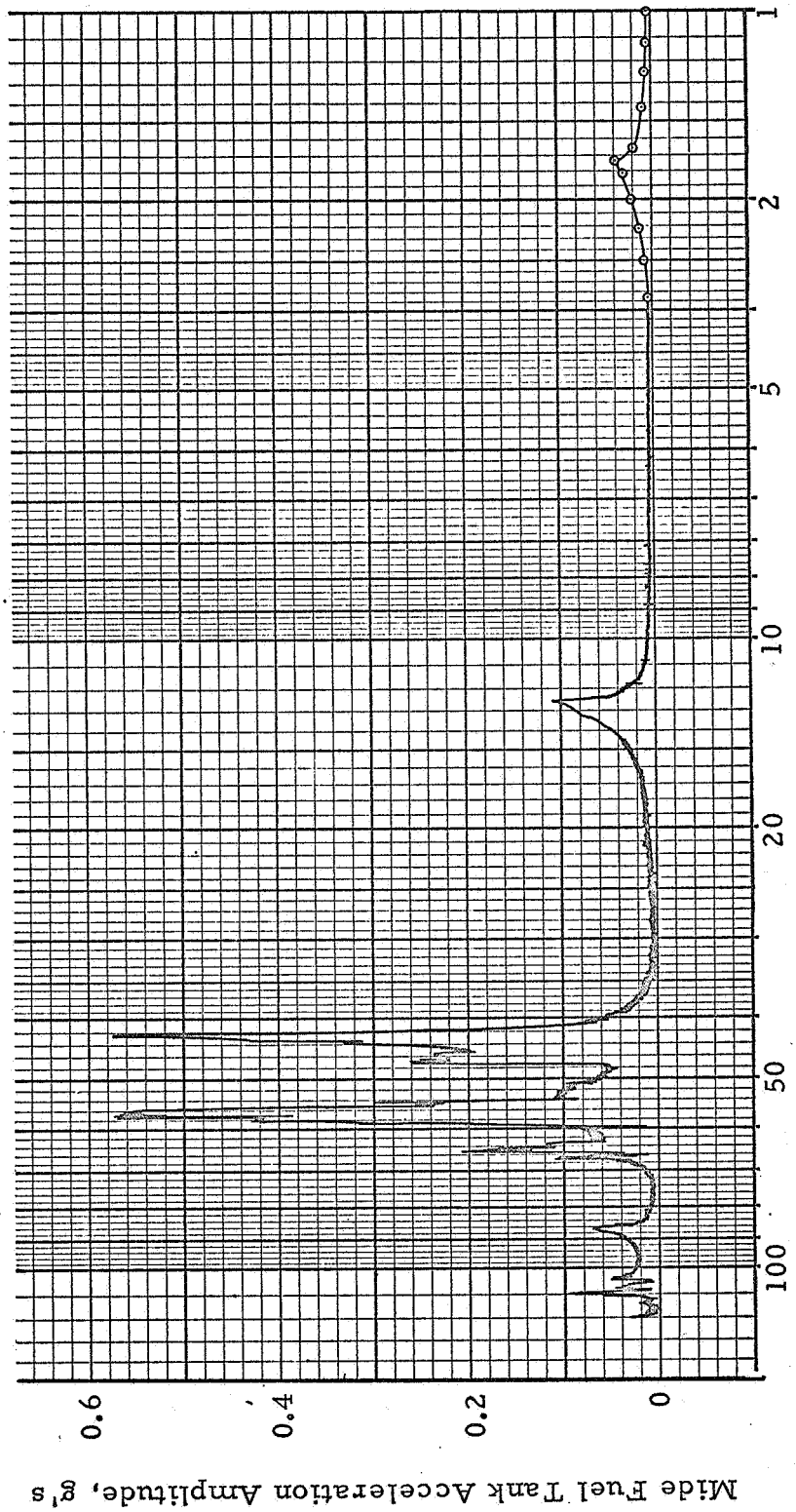

Figure C-C-7 - Frequency Response (Configuration C) Force Amplitude: 4.75 lb at 25 cps

CONFIGURATION: C

FREQUENCY: 1.918 cps

FORCE: 1.0 pounds, 0-pk

MODE NUMBER: 1

DAMPING: (See Figure C-C-35)

TIP ACCELERATION: .007 g (In-Plane)

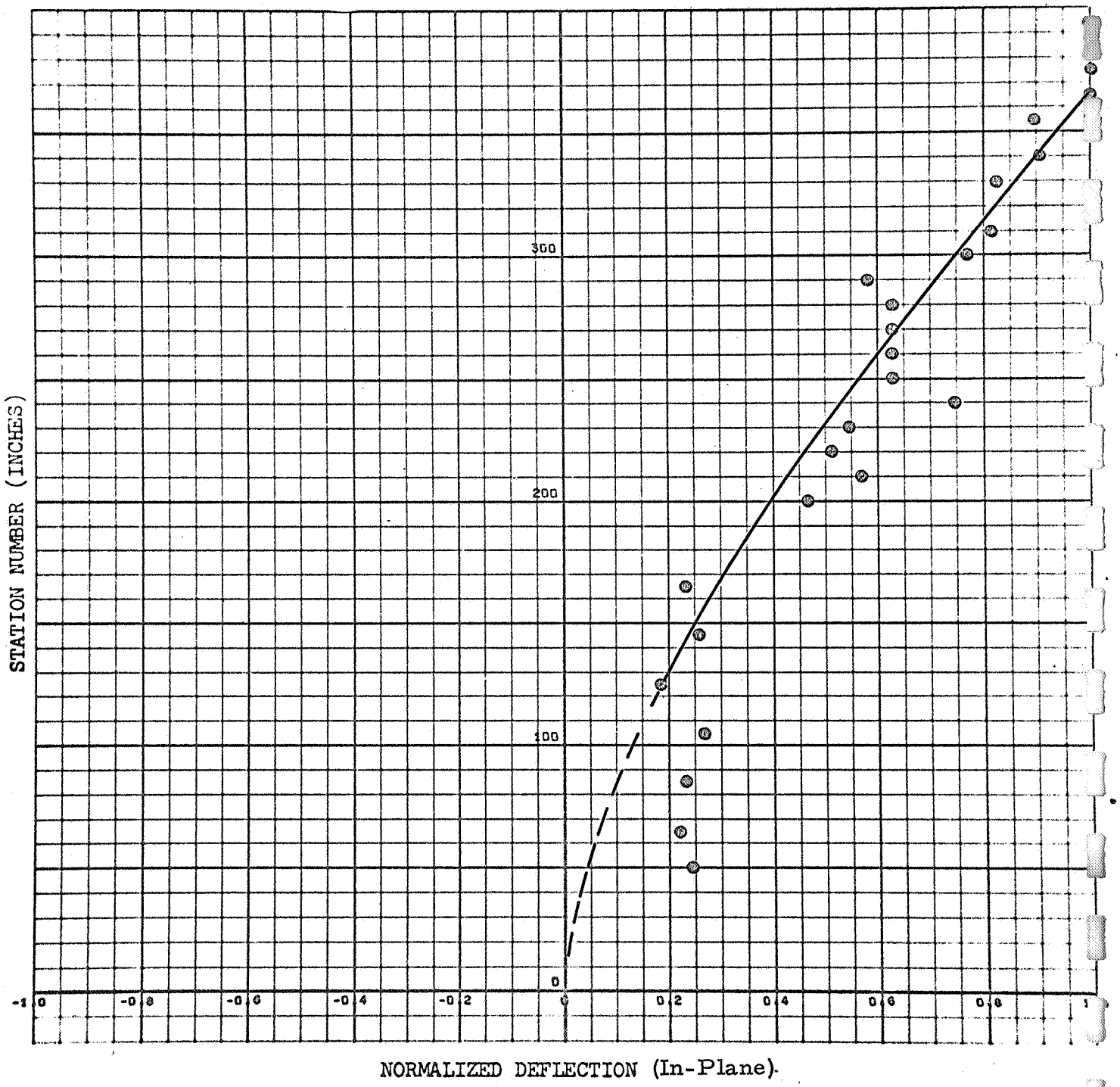

Figure C-C-8

CONFIGURATION: C

FREQUENCY: 1.918 cps

FORCE: 1.0 pounds, 0-pk

MODE NUMBER: 1

DAMPING:

TIP ACCELERATION: .003 g (Out-of-Plane)

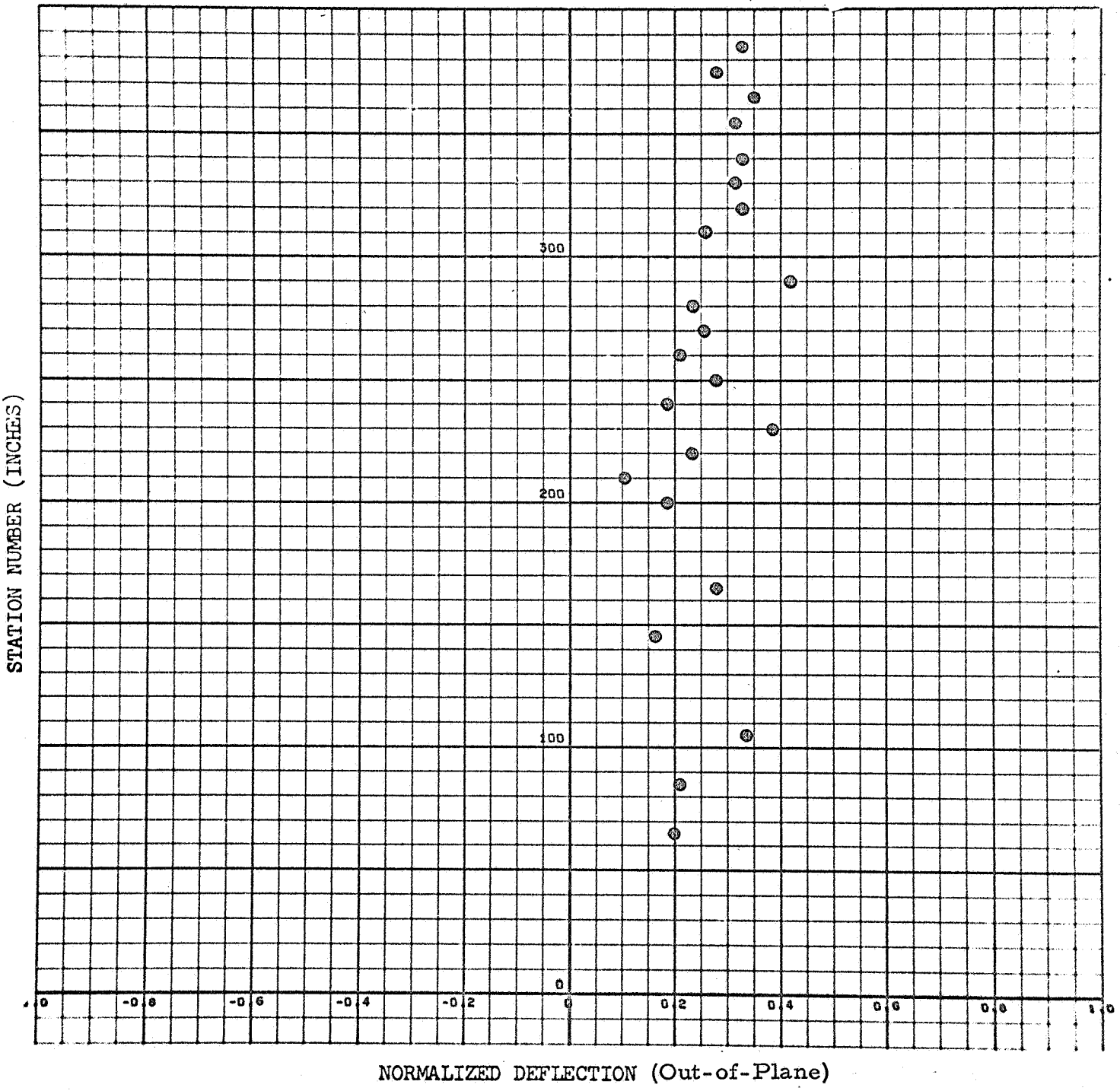

Figure C-C-9

CONFIGURATION: C

FREQUENCY: 13.1 cps

FORCE: 1.0 pounds, 0-pk

MODE NUMBER: 2

DAMPING: (See Figure C-C-36)

TIP ACCELERATION: .057 g (In-Plane)

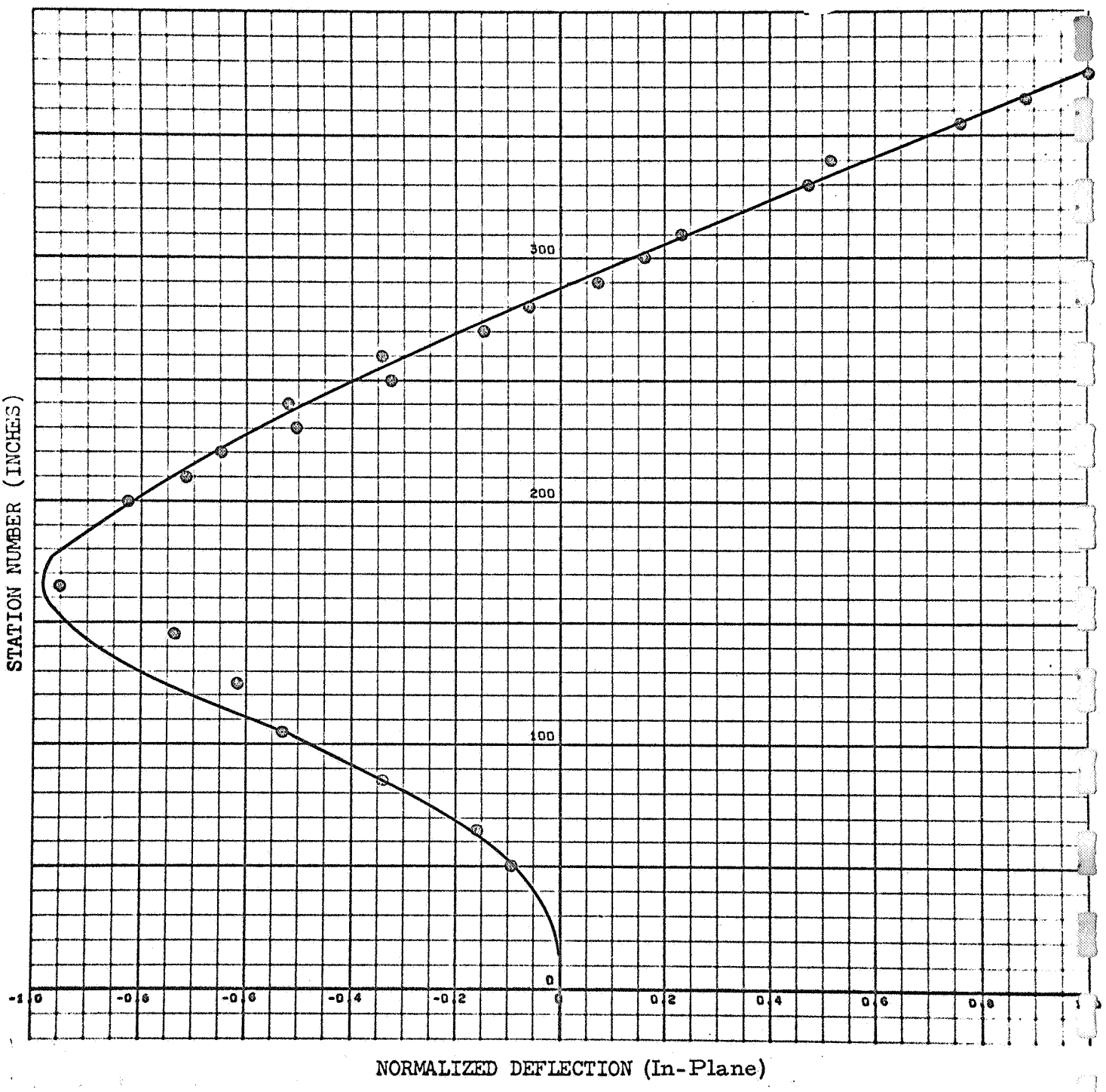

Figure C-C-10

CONFIGURATION: C

FREQUENCY: 13.1 cps

FORCE: 1.0 pounds, 0-pk

MODE NUMBER: 2

DAMPING:

TIP ACCELERATION: .028 g (Out-of-Plane)

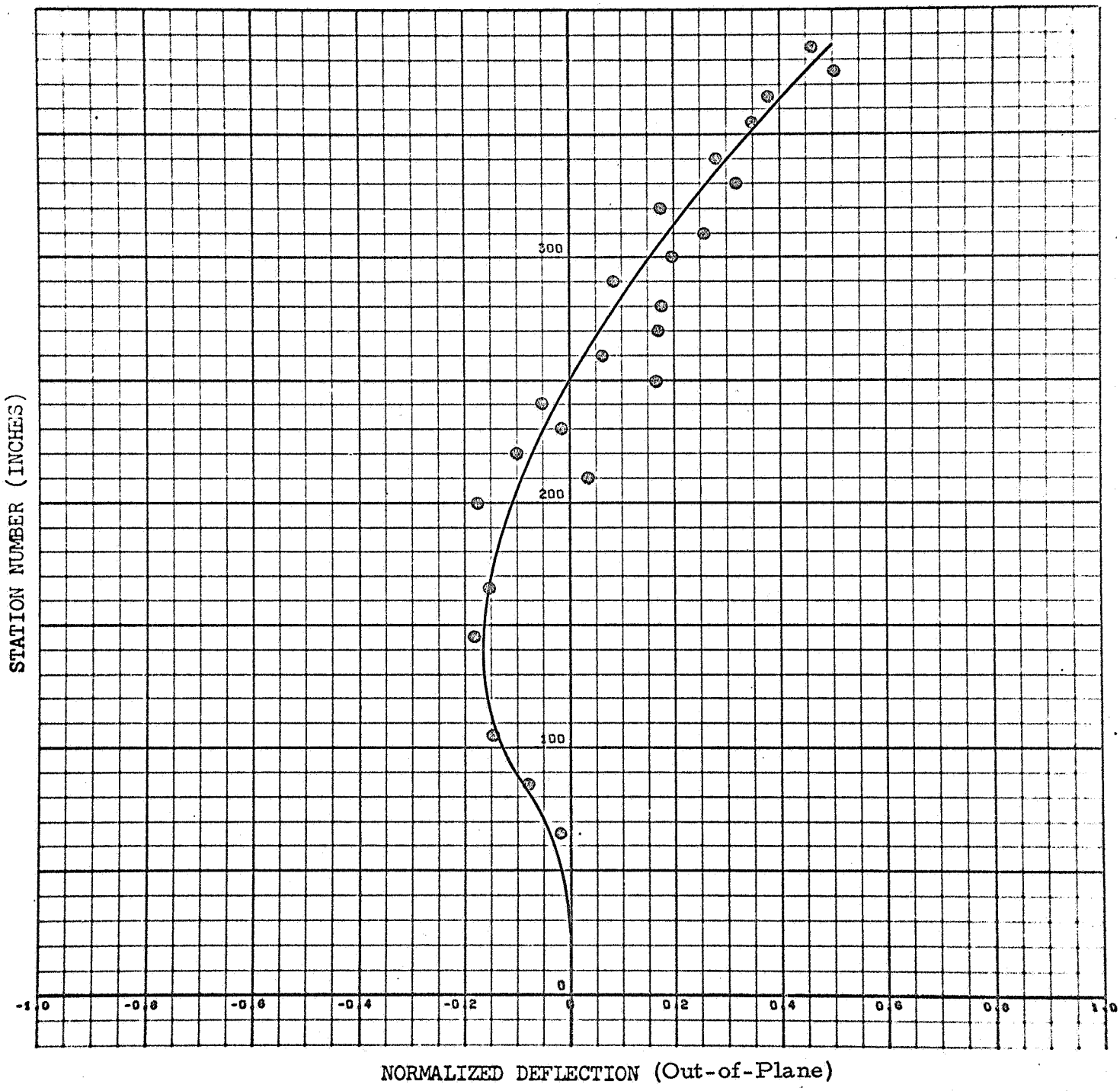

Figure C-C-11

CONFIGURATION: C

FREQUENCY: 13.16 cps

FORCE: 1.0 pounds, 0-pk

MODE NUMBER: 2

DAMPING: (See Figure C-C-38)

TIP ACCELERATION: .057 g (In-Plane)

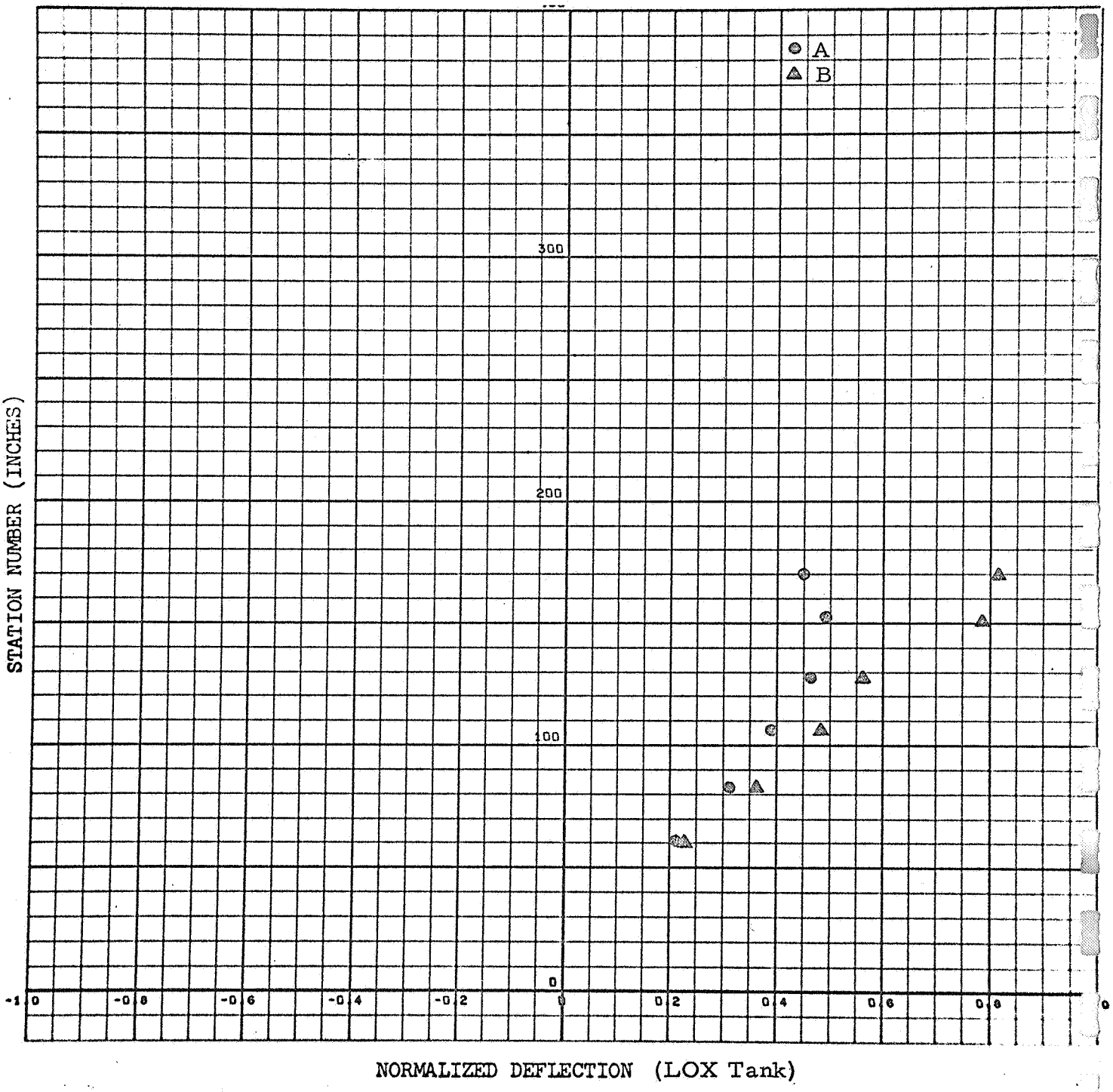

Figure C-C-12

CONFIGURATION: C

FREQUENCY: 13.16 cps

FORCE: 1.0 pounds, 0-pk

MODE NUMBER: 2

DAMPING: (See Figure C-C-39)

TIP ACCELERATION: .057 g (In-Plane)

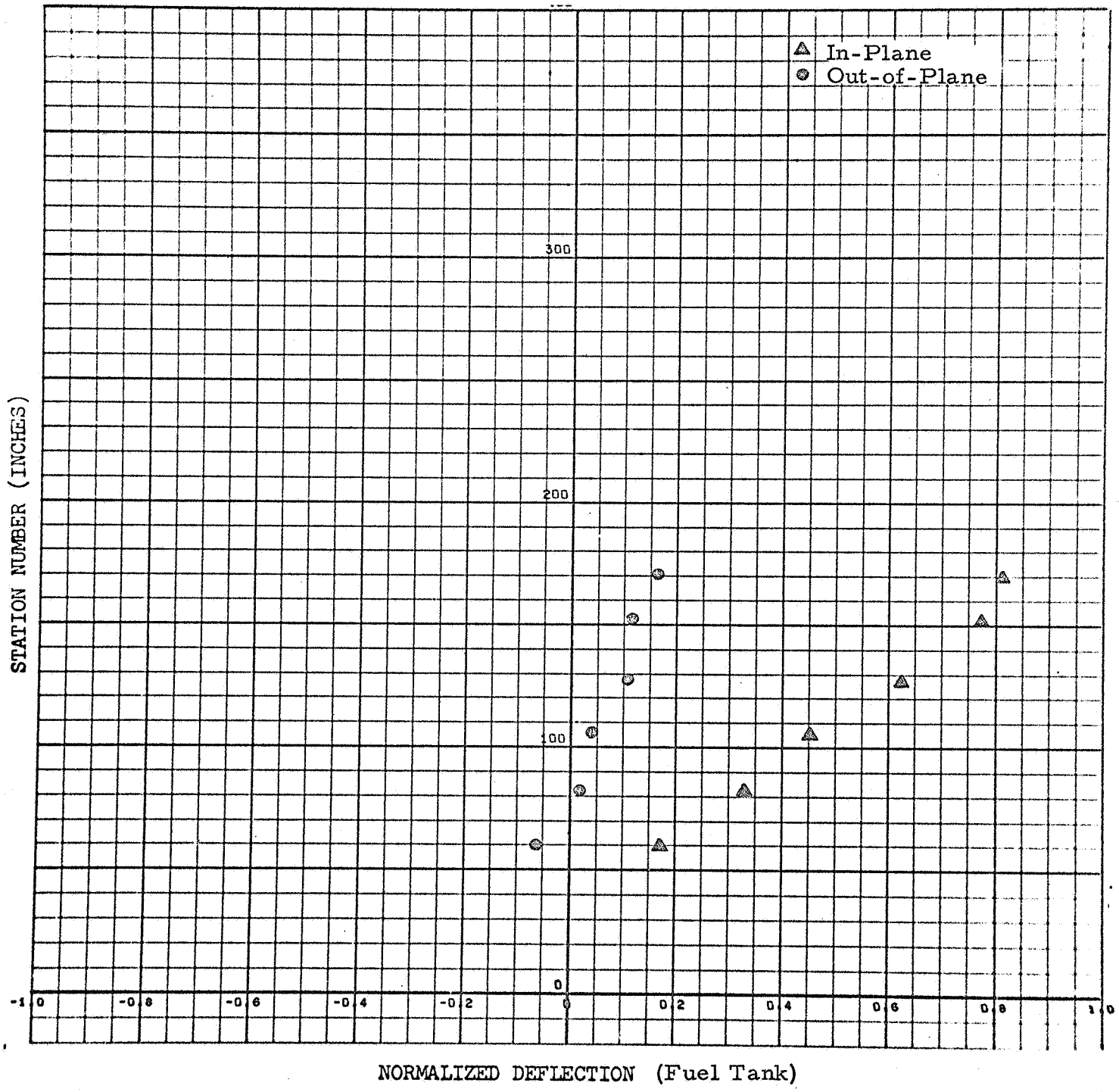

Figure C-C-13

CONFIGURATION: C

FREQUENCY: 43.0 cps

FORCE: 1.0 pounds, 0-pk

MODE NUMBER: 3

DAMPING: (See Figure C-C-37)

TIP ACCELERATION: .111 g (In-Plane)

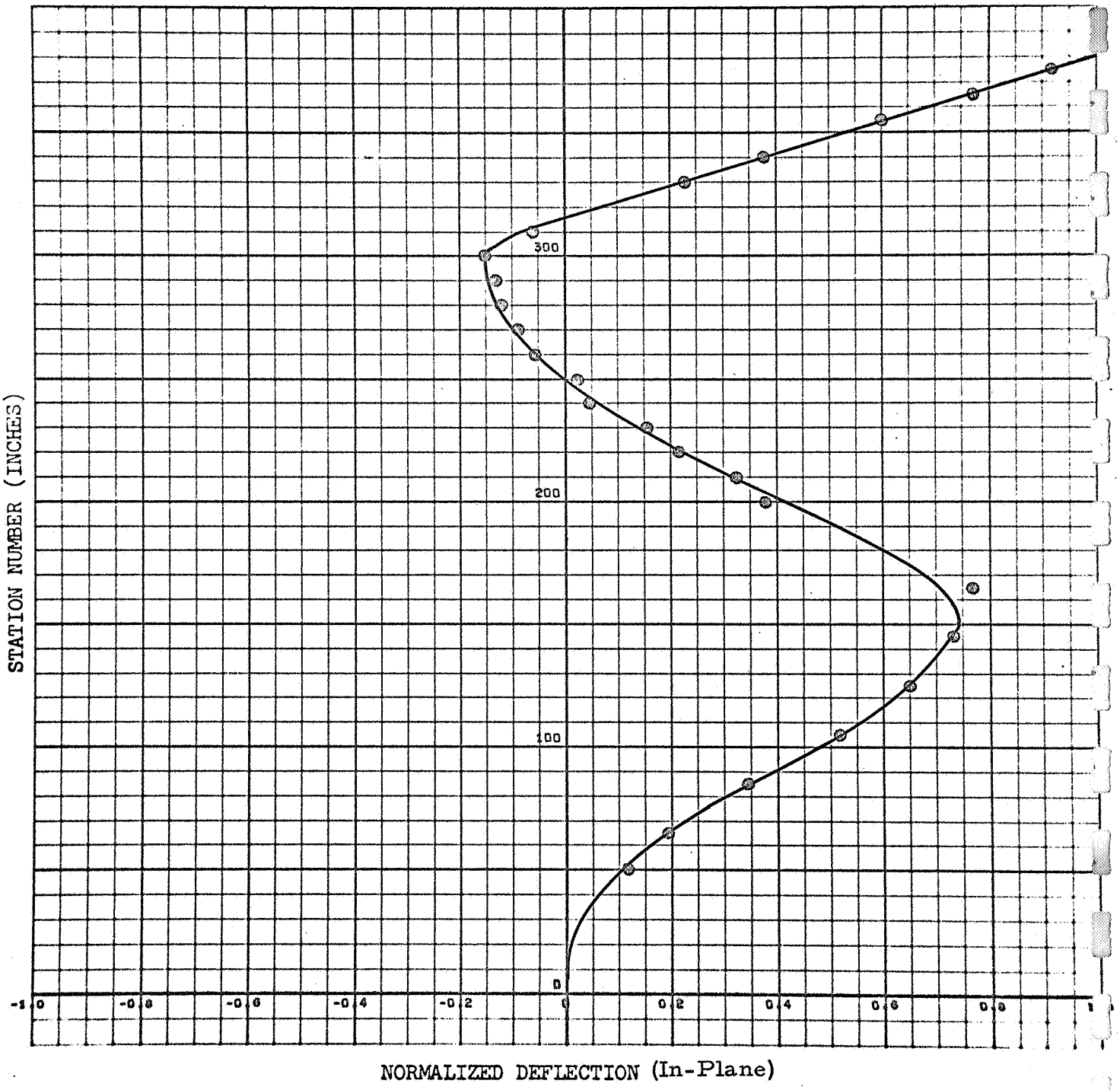

Figure C-C-14

CONFIGURATION: C

FREQUENCY: 43.0 cps

FORCE: 1.0 pounds, 0-pk

MODE NUMBER: 3

DAMPING:

TIP ACCELERATION: .007 g (Out-of-Plane)

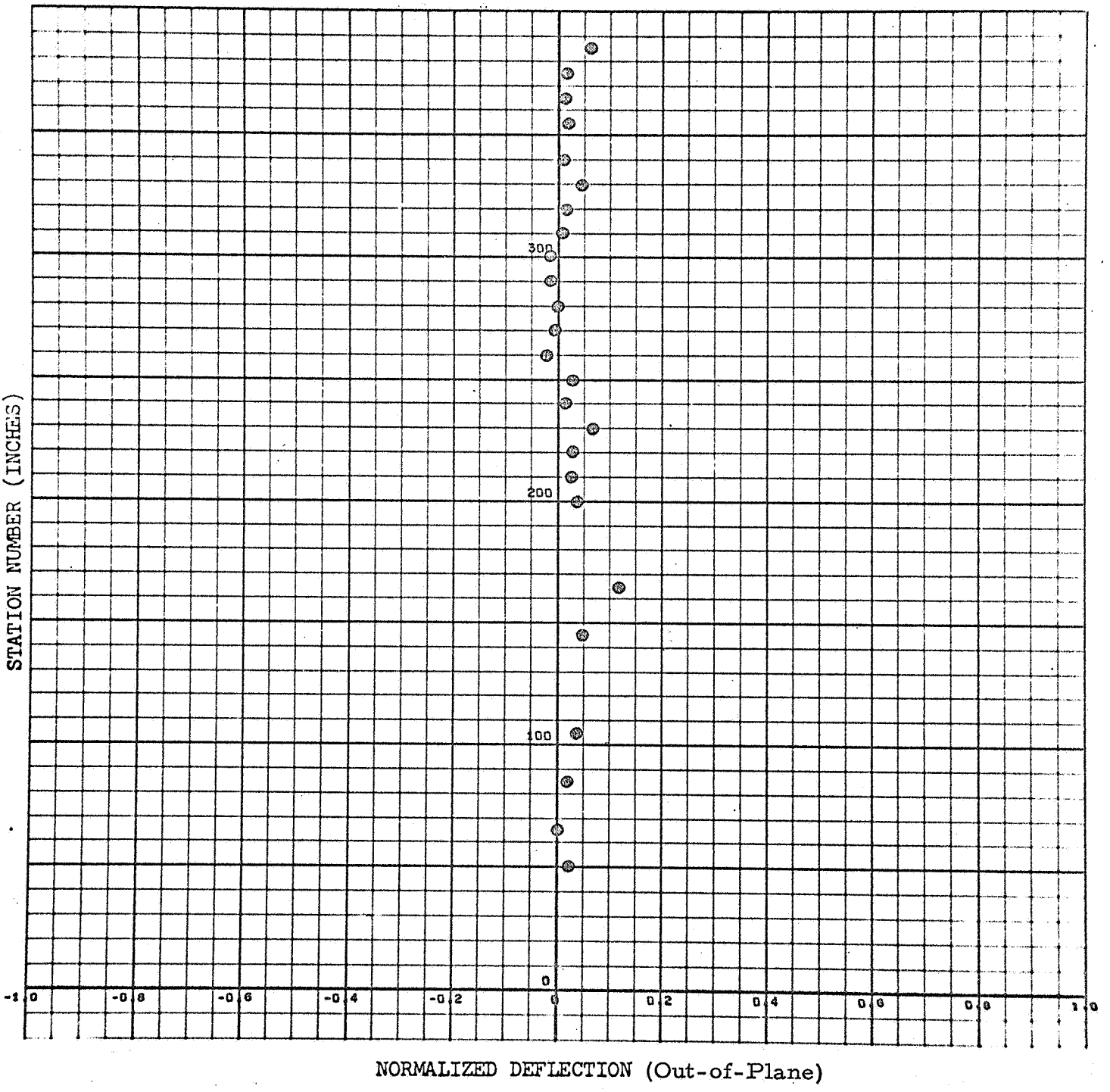

Figure C-C-15

CONFIGURATION: C

FREQUENCY: 43.18 cps

FORCE: 1.0 pounds, 0-pk

MODE NUMBER: 3

DAMPING: (Not Available)

TIP ACCELERATION: .111 g (In-Plane)

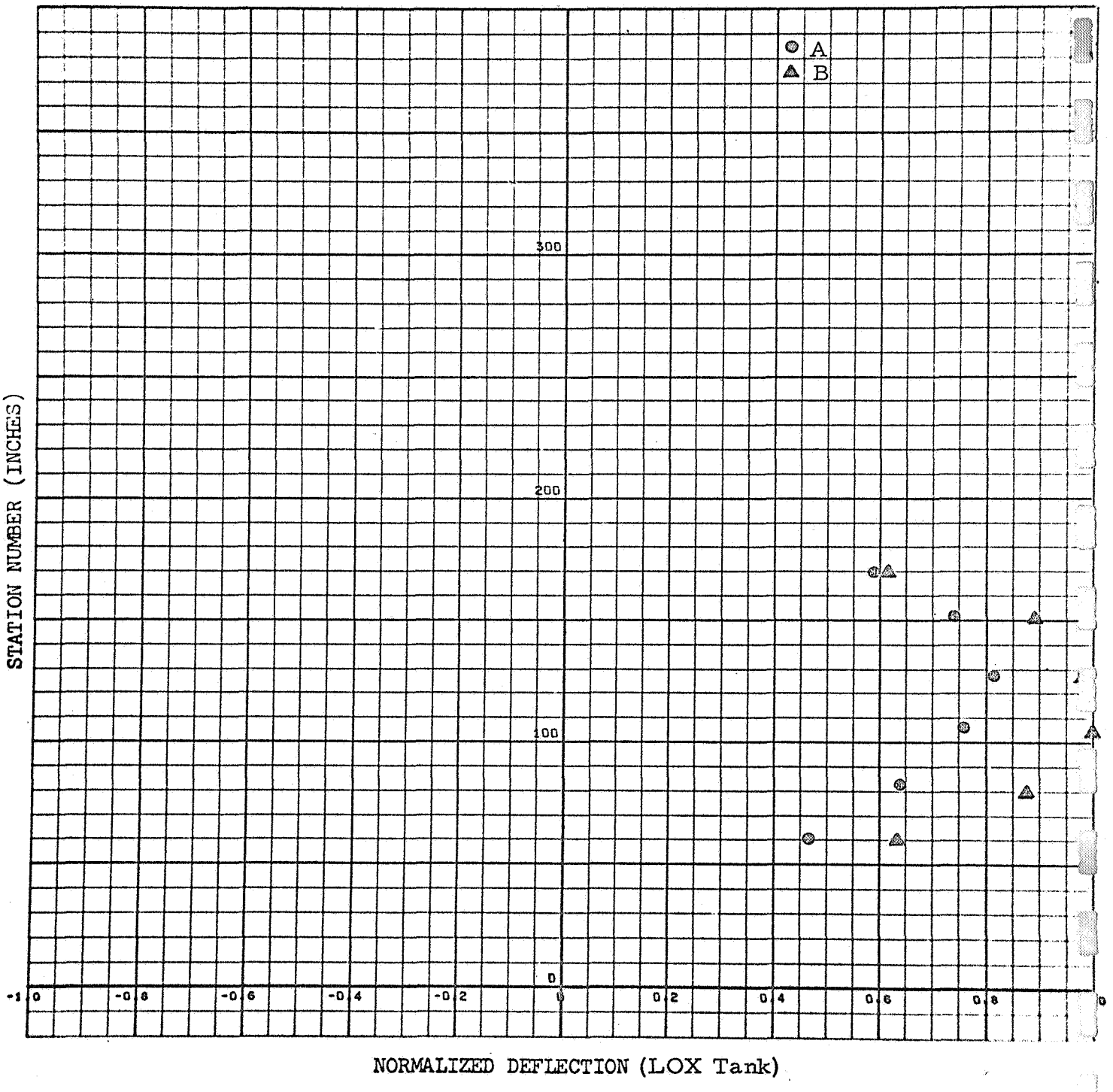

Figure C-C-16

CONFIGURATION: C

FREQUENCY: 43.18 cps

FORCE: 1.0 pounds, 0-pk

MODE NUMBER: 3

DAMPING: (Not Available)

TIP ACCELERATION: .111 g (In-Plane)

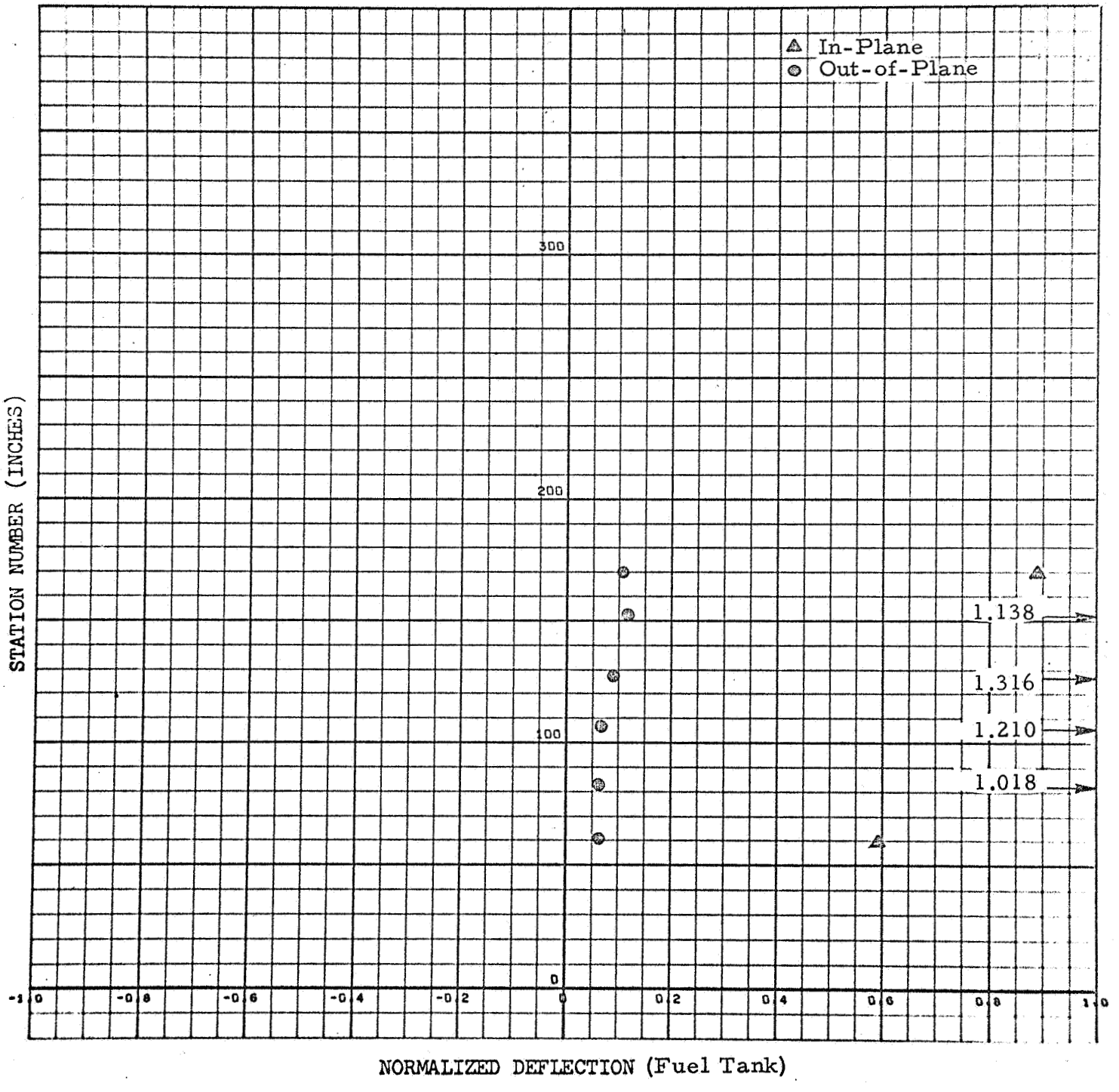

Figure C-C-17

CONFIGURATION: C

FREQUENCY: 1.803 cps

FORCE: 4.75 pounds, 0-pk

MODE NUMBER: 1

DAMPING: (See Figure C-C-35)

TIP ACCELERATION: .021 g (In-Plane)

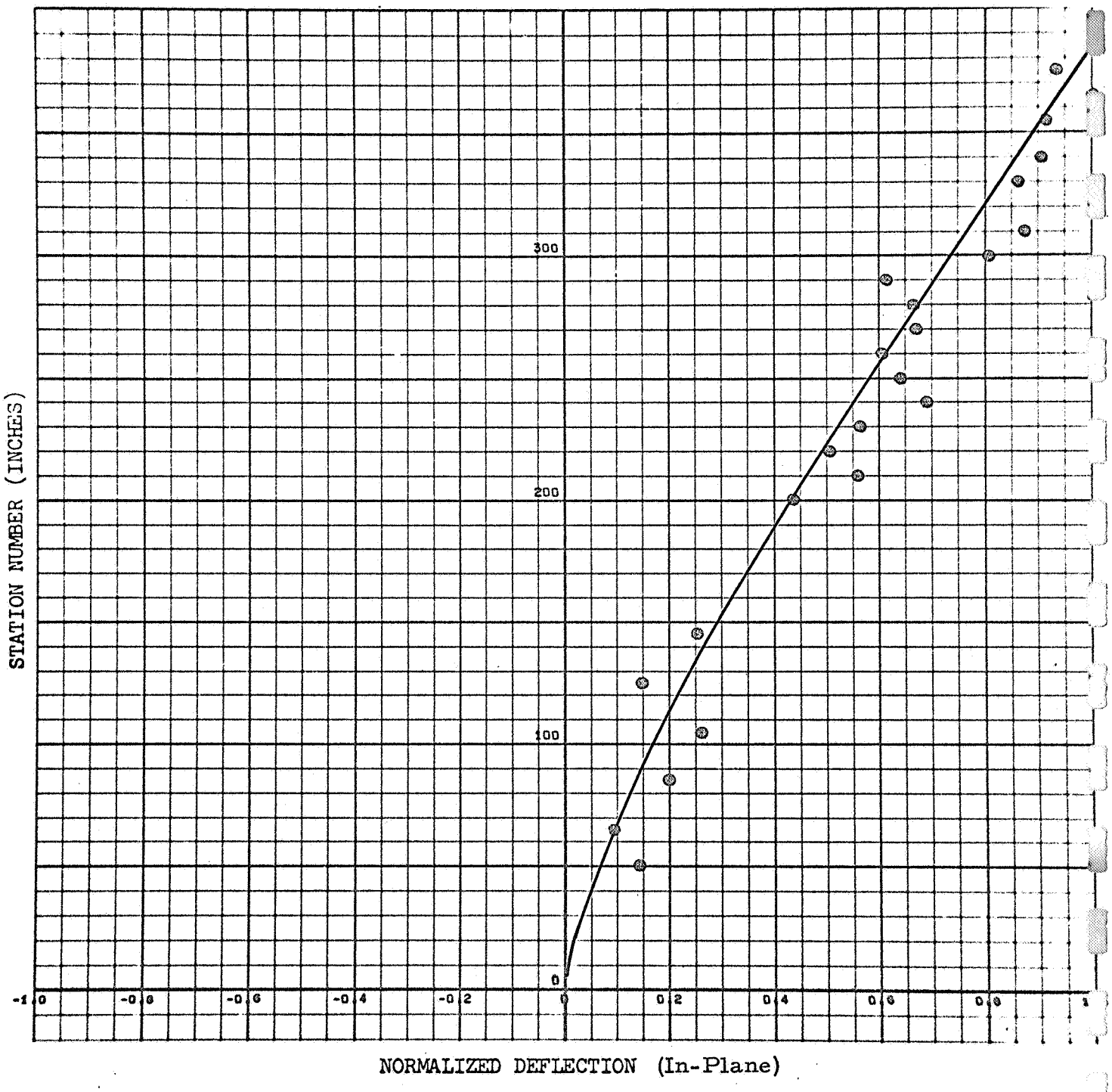

Figure C-C-18

CONFIGURATION: C

FREQUENCY: 1.803 , cps

FORCE: 4.75 , pounds, 0-pk

MODE NUMBER: 1

DAMPING:

TIP ACCELERATION: .005 g (Out-of-Plane)

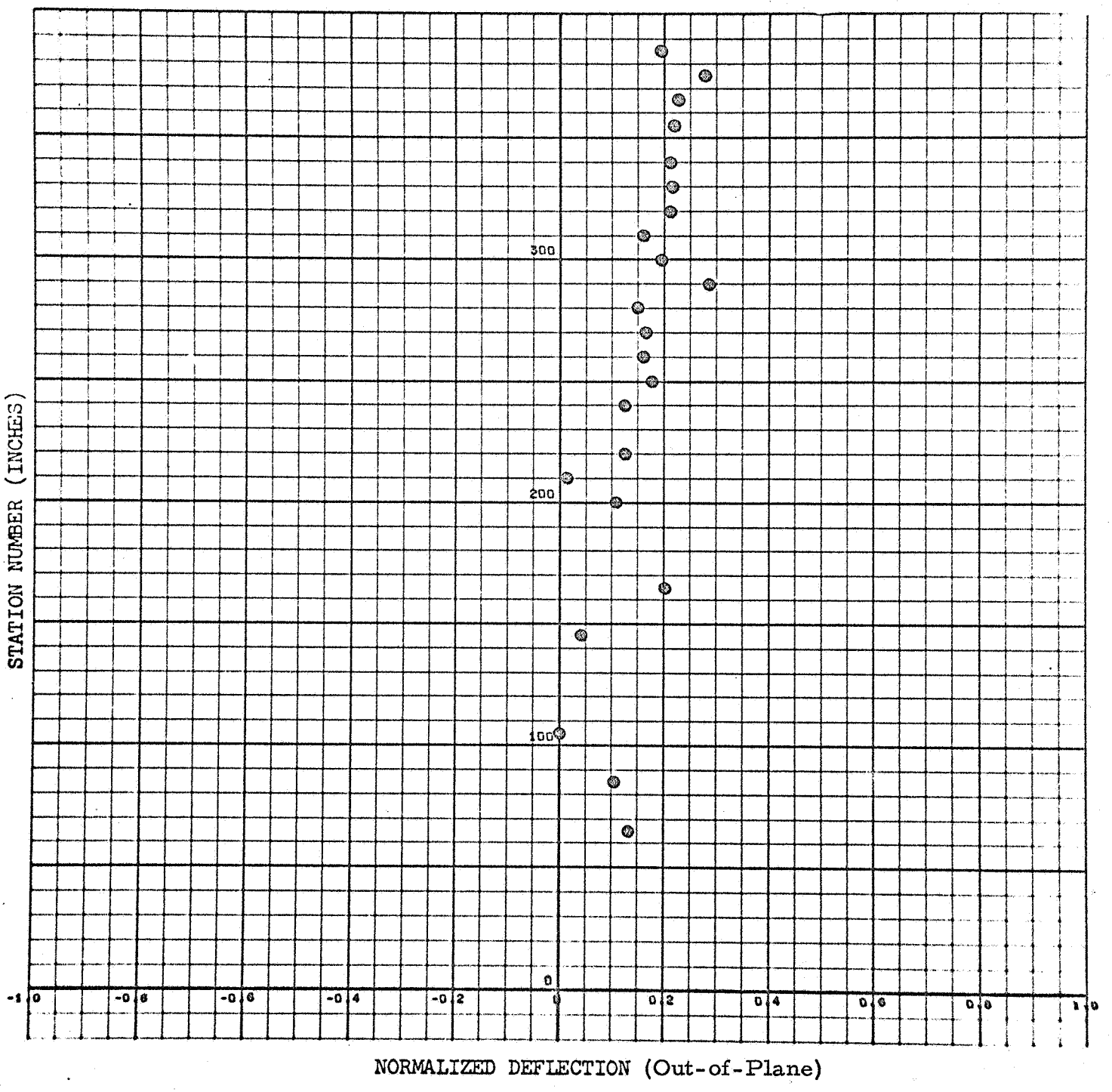

Figure C-C-19

CONFIGURATION: C

FREQUENCY: 1.777 cps

FORCE: 4.75 pounds, O-pk

MODE NUMBER: 1

DAMPING:

TIP ACCELERATION: .021 g (In-Plane)

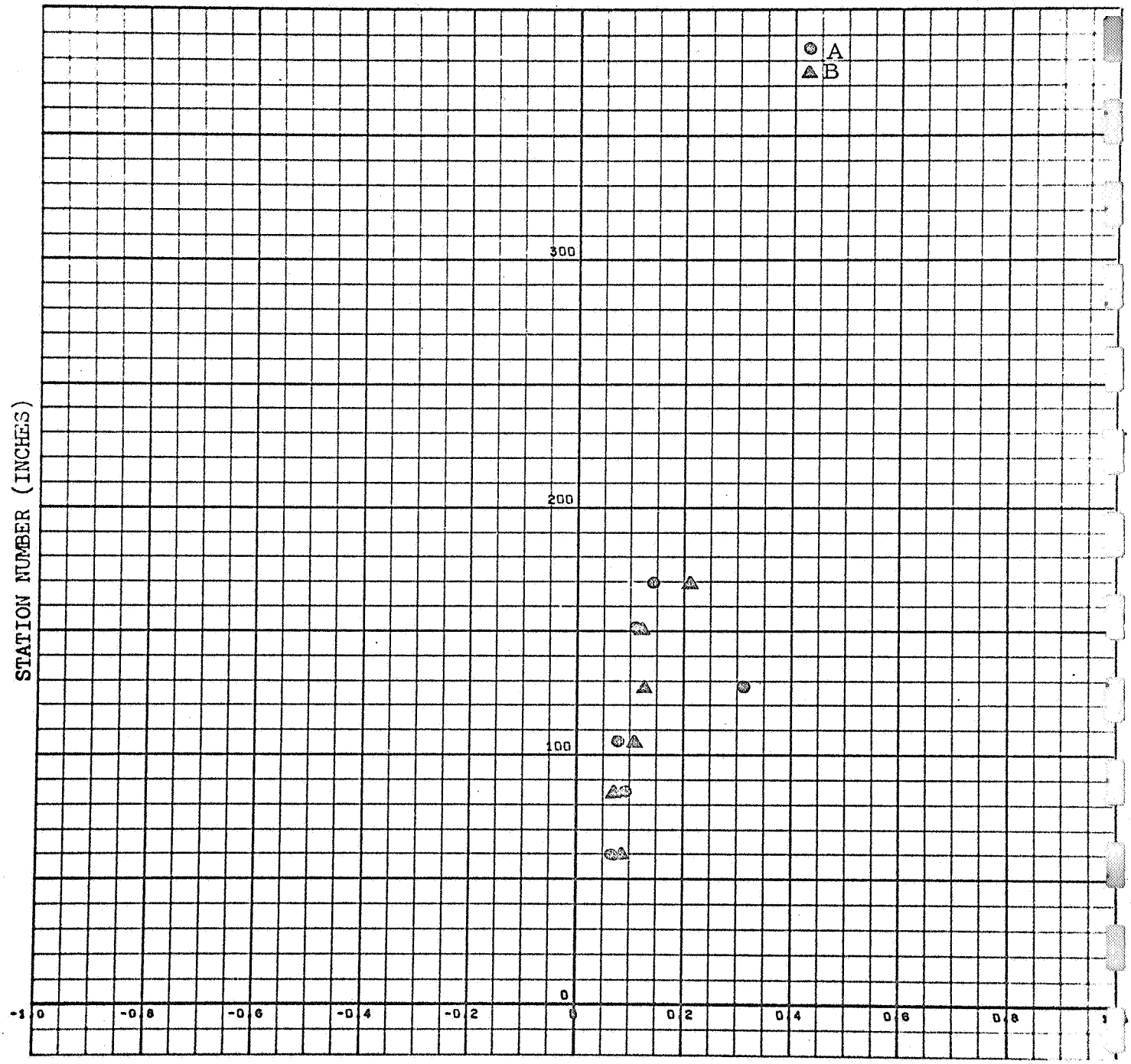

Figure C-C-20

CONFIGURATION: C

FREQUENCY: 1.777 cps

FORCE: 4.75 pounds, 0-pk

MODE NUMBER: 1

DAMPING:

TIP ACCELERATION: .021 g (In-Plane)

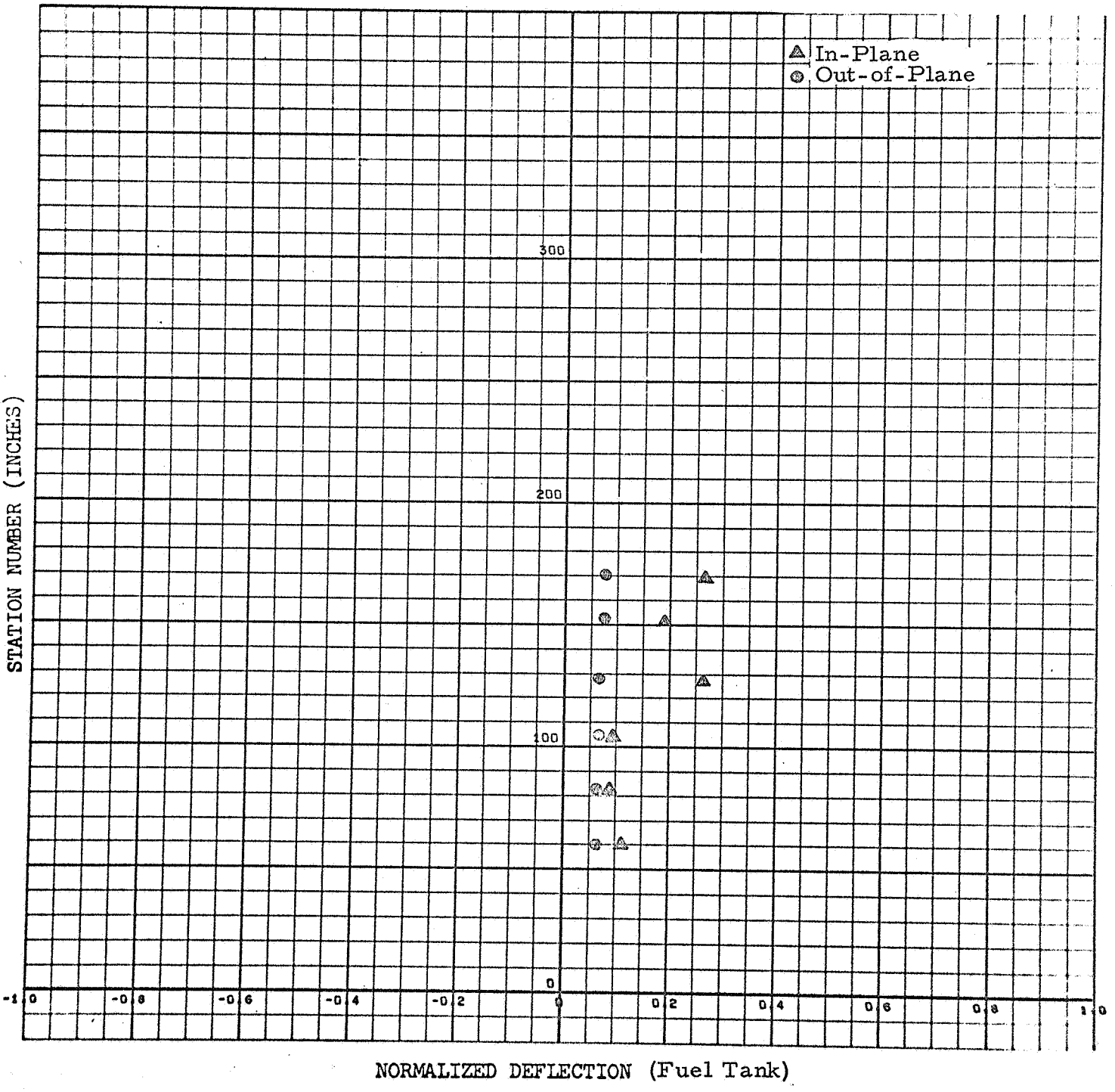

Figure C-C-21

CONFIGURATION: C

FREQUENCY: 12.54 cps

FORCE: 4.75 pounds, 0-pk

MODE NUMBER: 2

DAMPING: (See Figure C-C-36)

TIP ACCELERATION: .143 g (In-Plane)

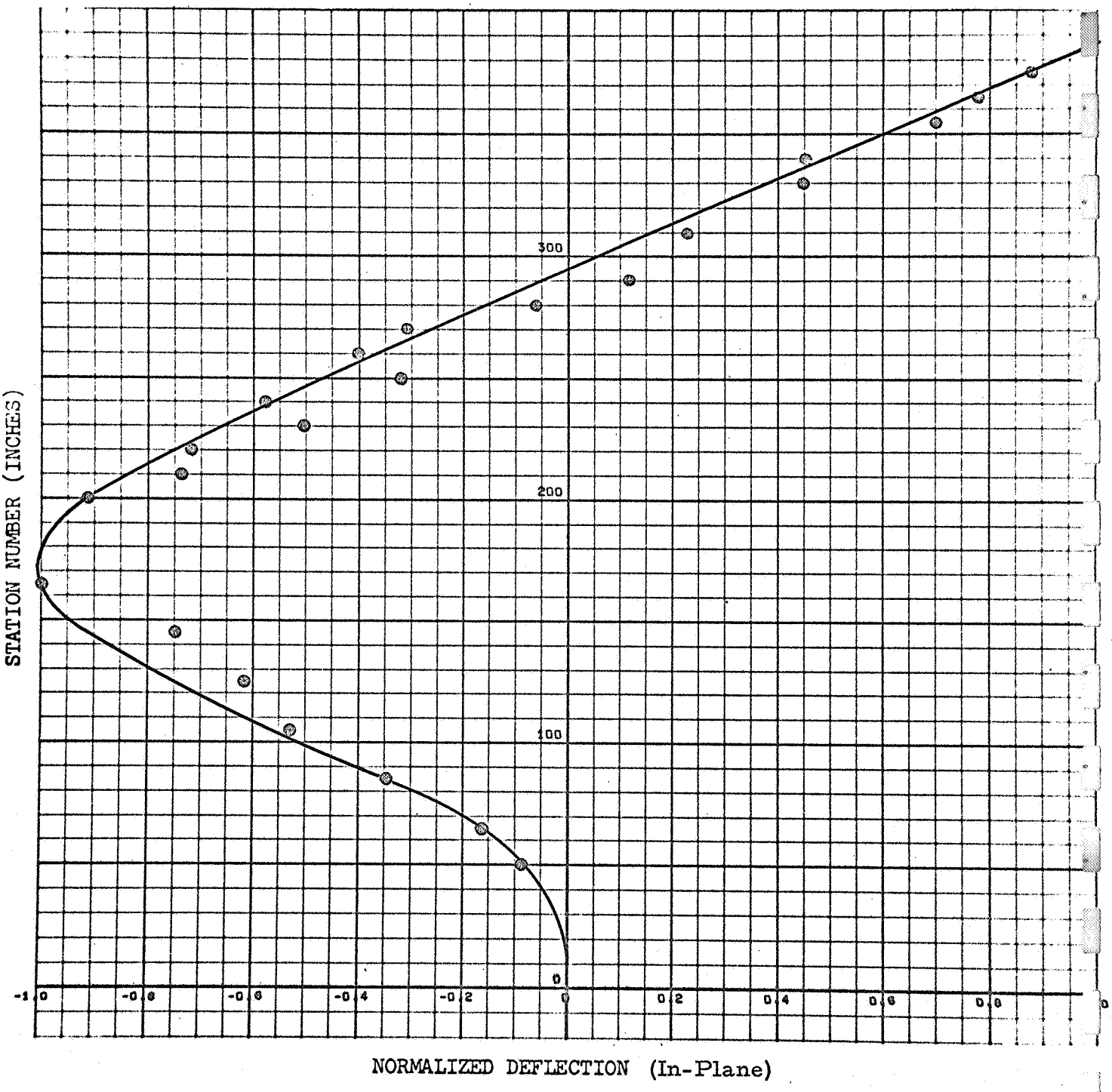

Figure C-C-22

CONFIGURATION: C

FREQUENCY: 12.54 cps

FORCE: 4.75 pounds, 0-pk

MODE NUMBER: 2

DAMPING:

TIP ACCELERATION: .066 g (Out-of-Plane)

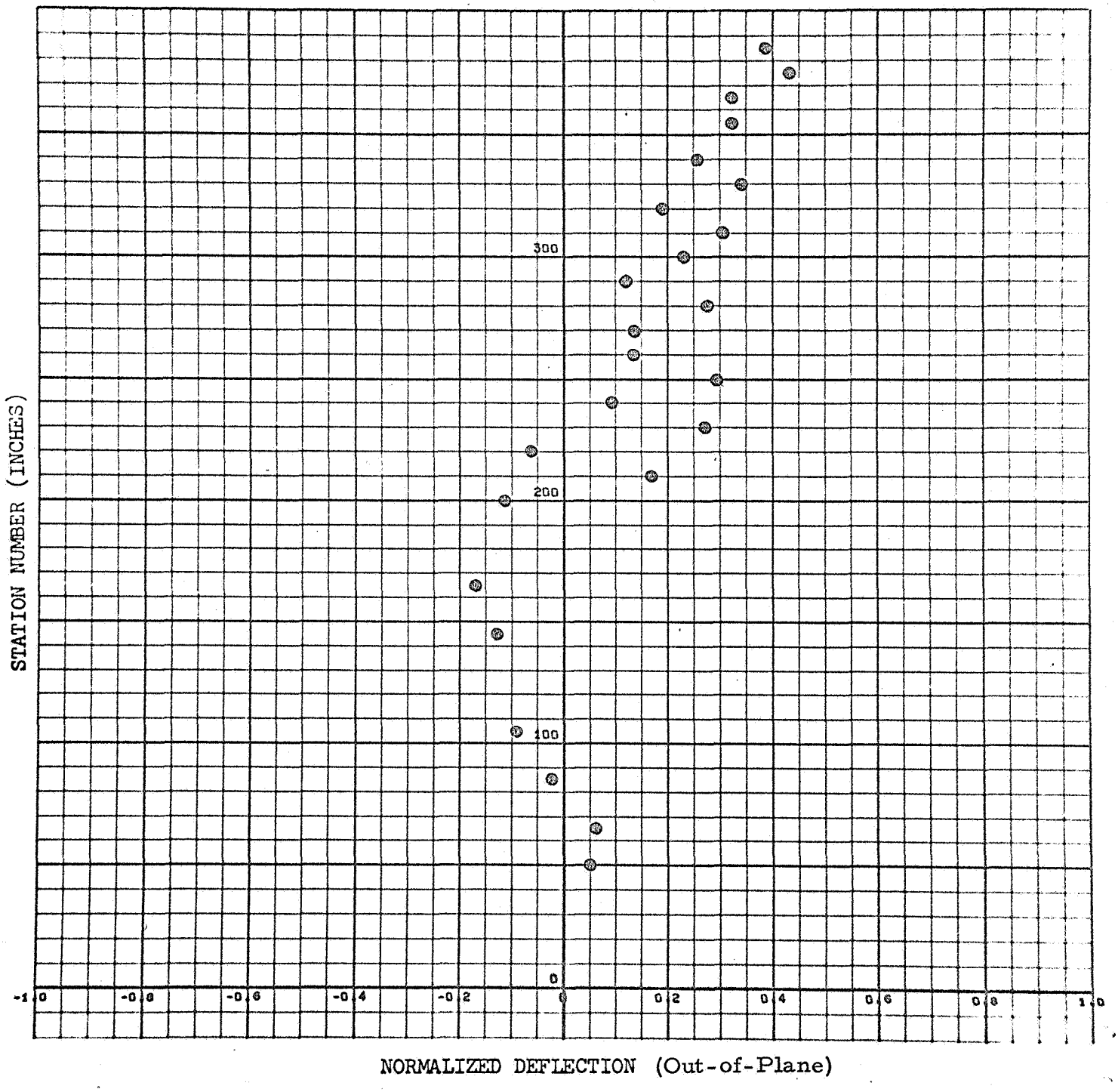

Figure C-C-23

CONFIGURATION: C

FREQUENCY: 12.82 cps

FORCE: 4.75 pounds, 0-pk

MODE NUMBER: 2

DAMPING: (See Figure C-C-38)

TIP ACCELERATION: .143 g (In-Plane)

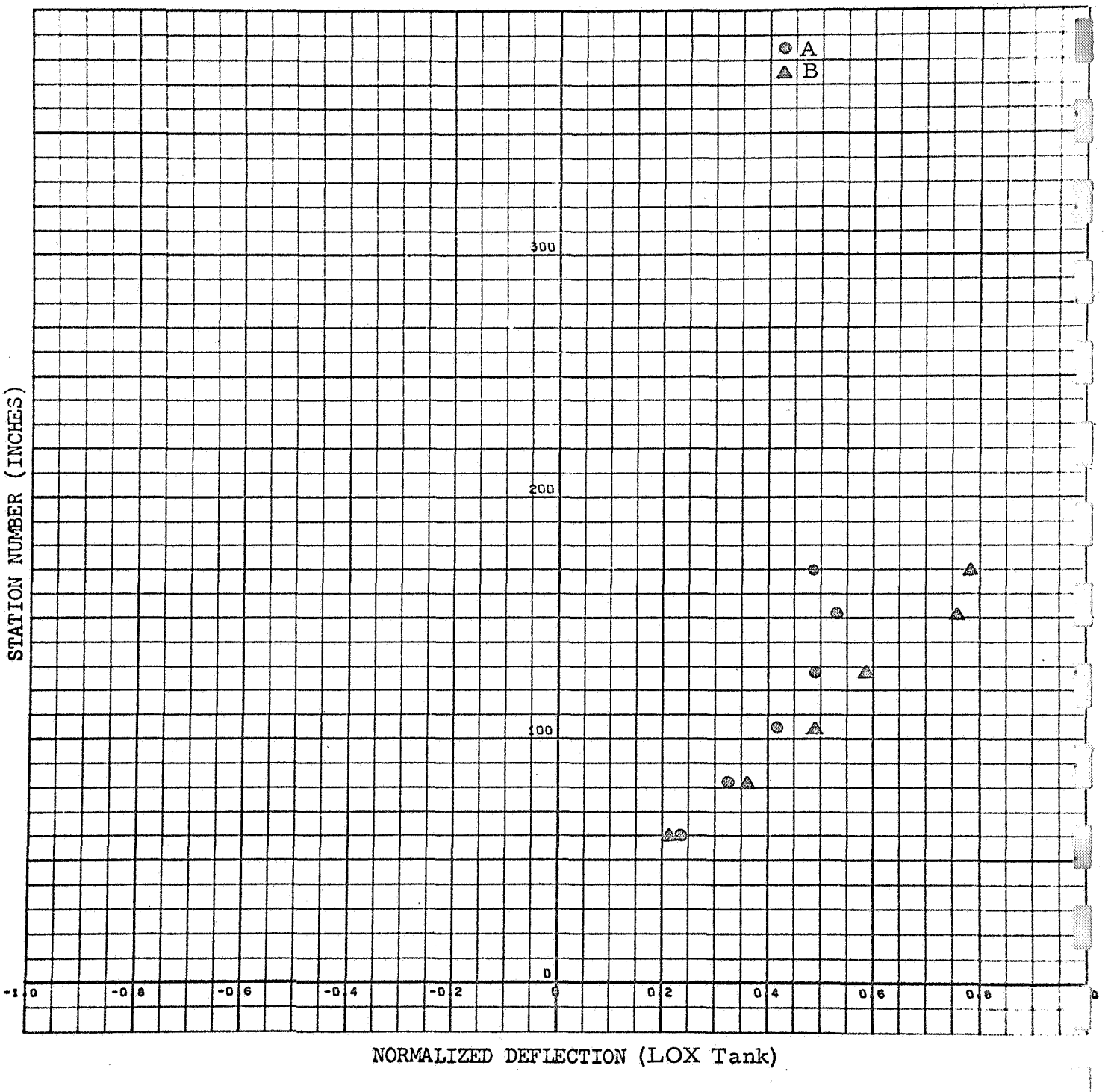

Figure C-C-24

CONFIGURATION: C

FREQUENCY: 12.82 cps

FORCE: 4.75 pounds, 0-pk

MODE NUMBER: 2

DAMPING: (See Figure C-C-39)

TIP ACCELERATION: .143 g (In-Plane)

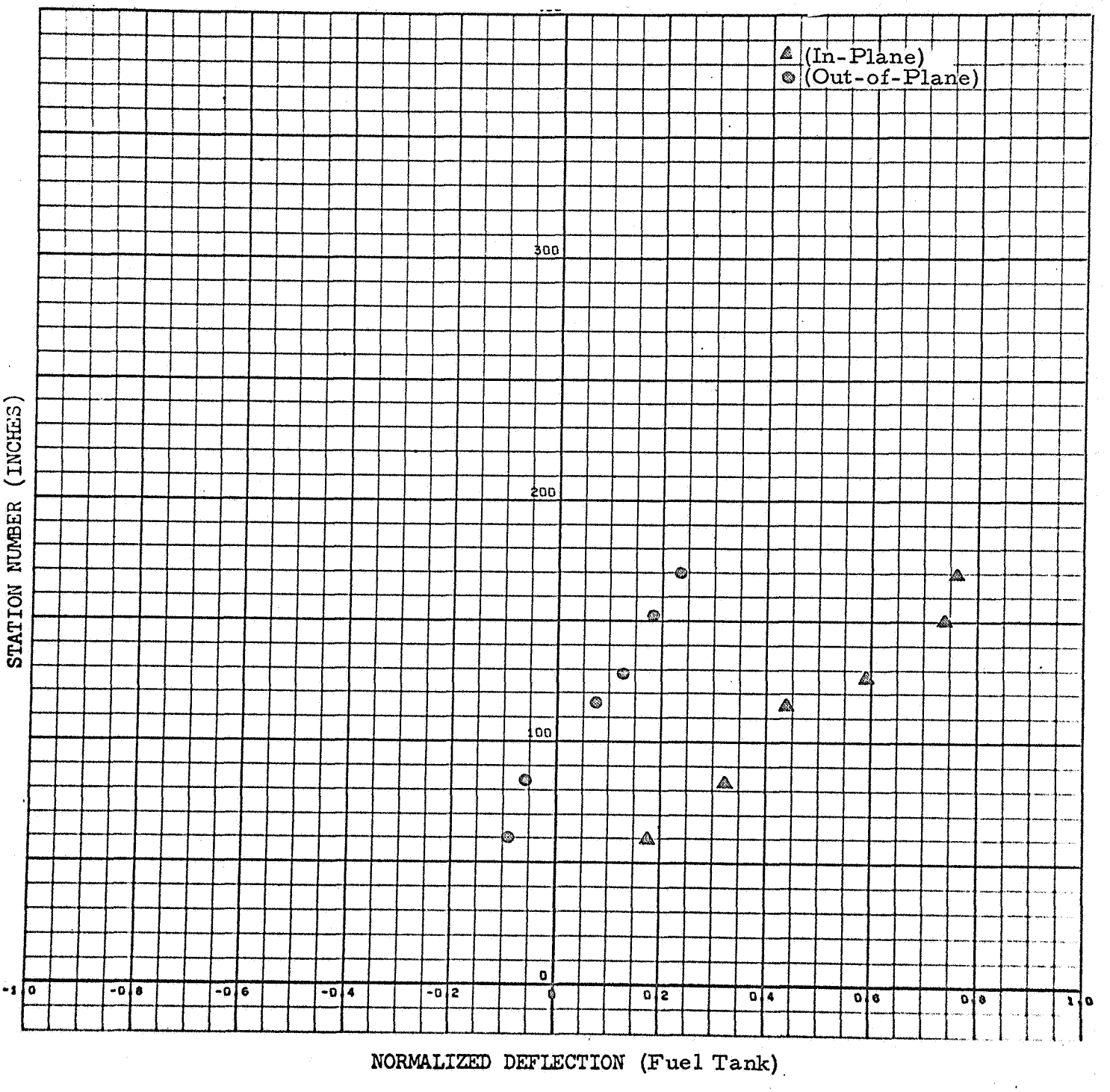

Figure C-C-25

CONFIGURATION: C

FREQUENCY: 42.3 cps

FORCE: 4.75 pounds, 0-pk

MODE NUMBER: 3

DAMPING: (See Figure C-C-37)

TIP ACCELERATION: .448 g (In-Plane)

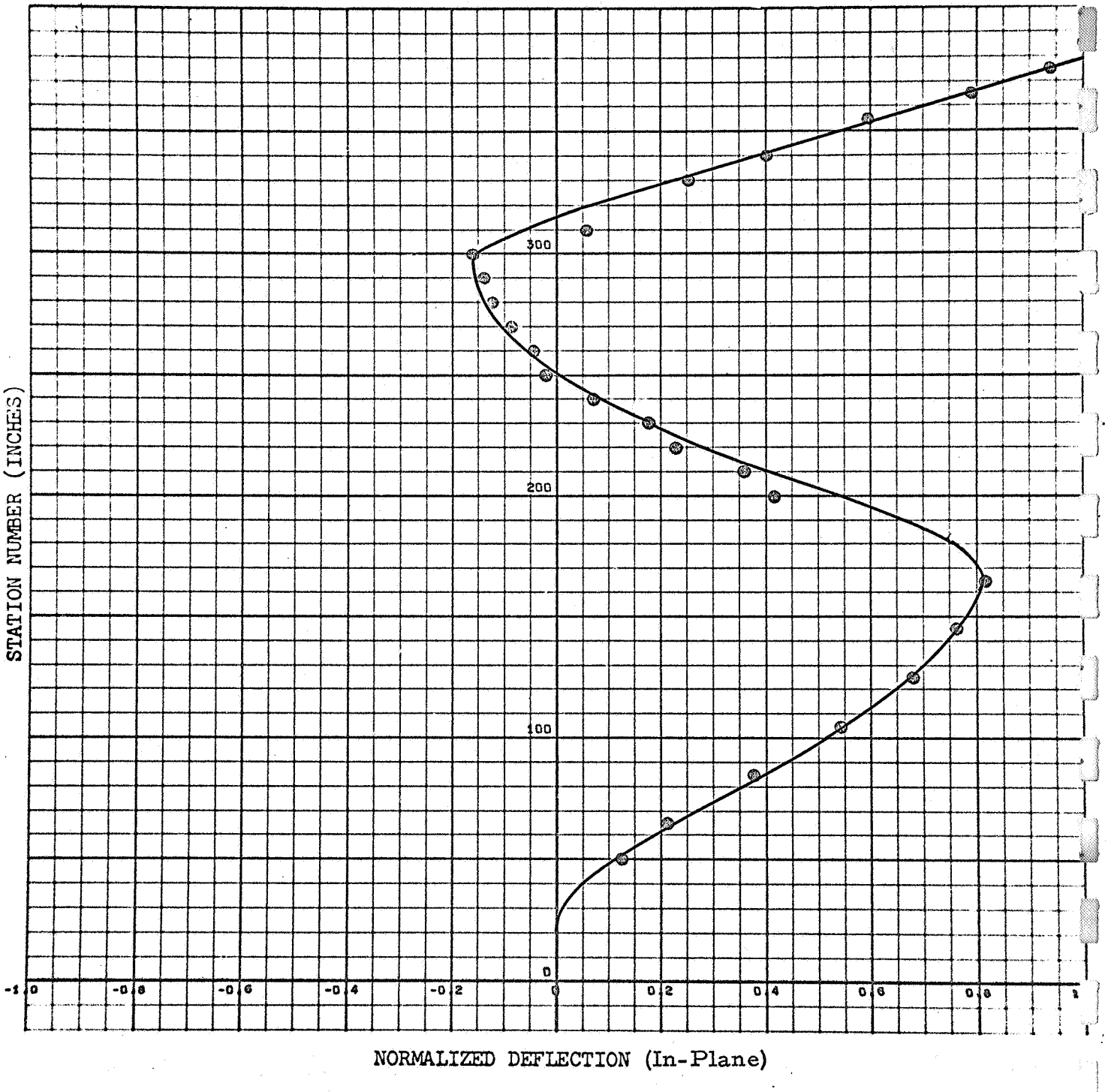

Figure C-C-26

CONFIGURATION: C

FREQUENCY: 42.3 cps

FORCE: 4.75 pounds, 0-pk

MODE NUMBER: 3

DAMPING:

TIP ACCELERATION: .058 g (Out-of-Plane)

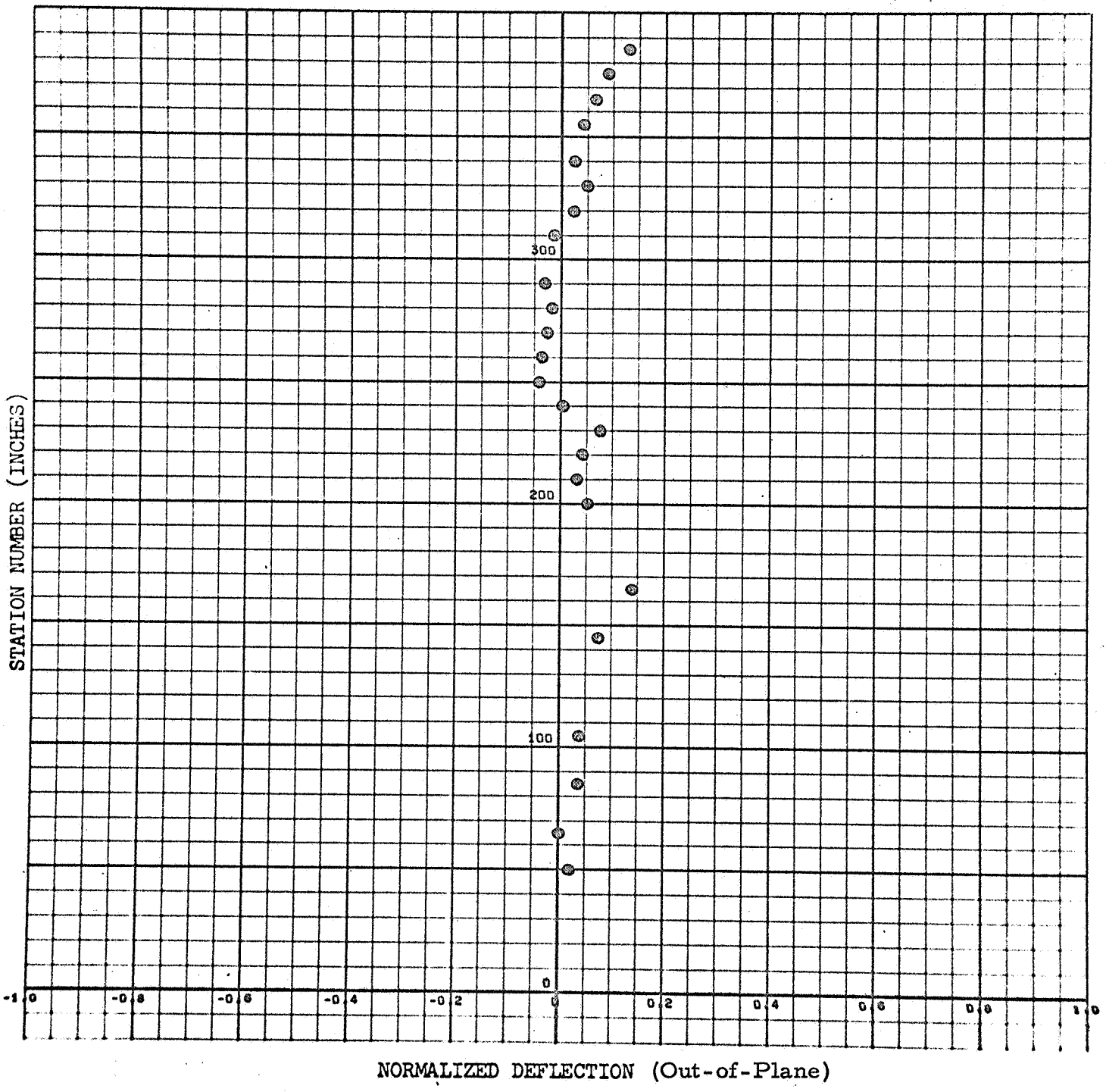

Figure C-C-27

CONFIGURATION: C

FREQUENCY: 42.4 cps

FORCE: 4.75 pounds, 0-pk

MODE NUMBER: 3

DAMPING:

TIP ACCELERATION: .448 g (In-Plane)

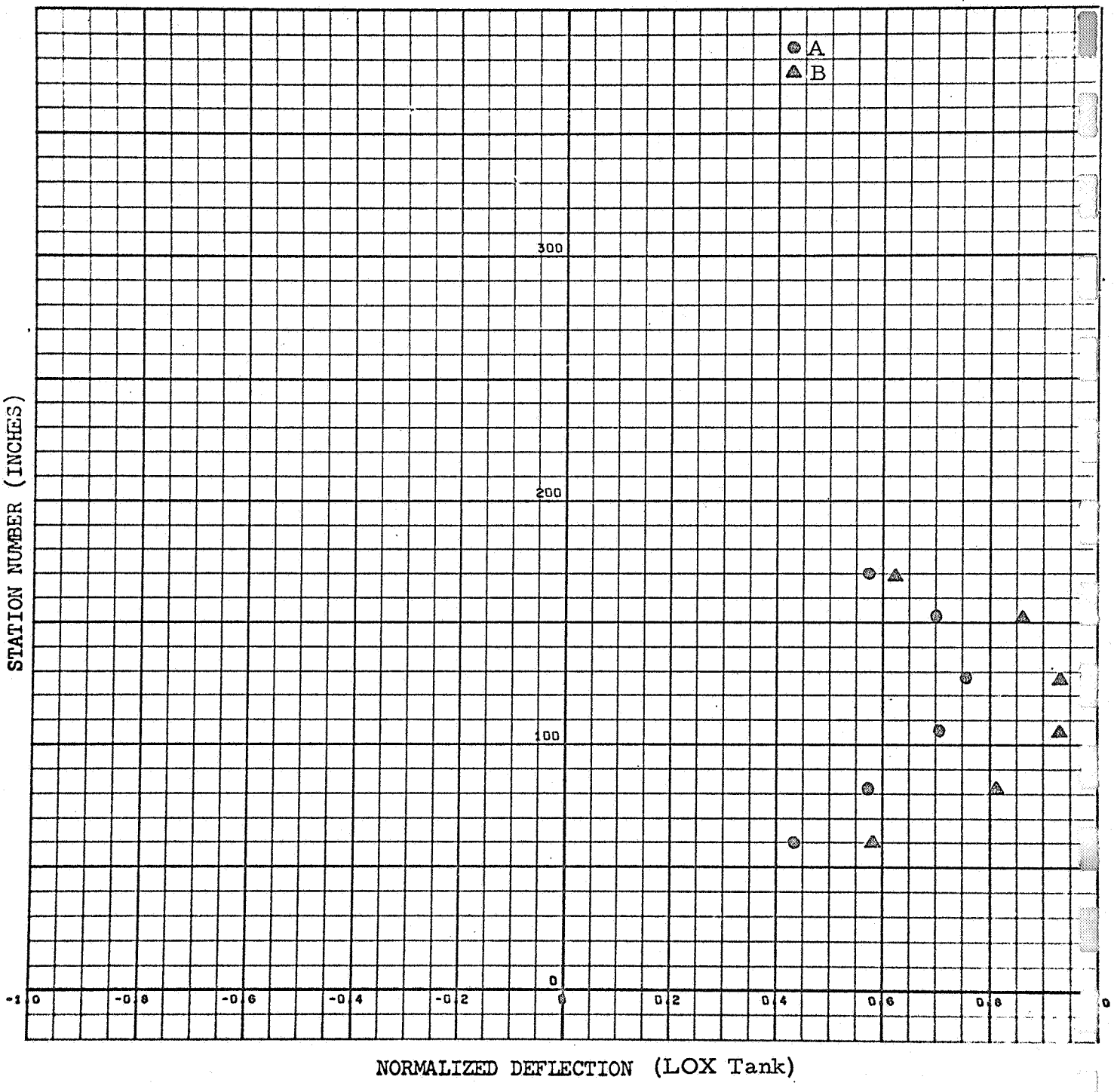

Figure C-C-28

CONFIGURATION: C

FREQUENCY: 42.4 cps

FORCE: 4.75 pounds, 0-pk

MODE NUMBER: 3

DAMPING:

TIP ACCELERATION: .448 g (In-Plane)

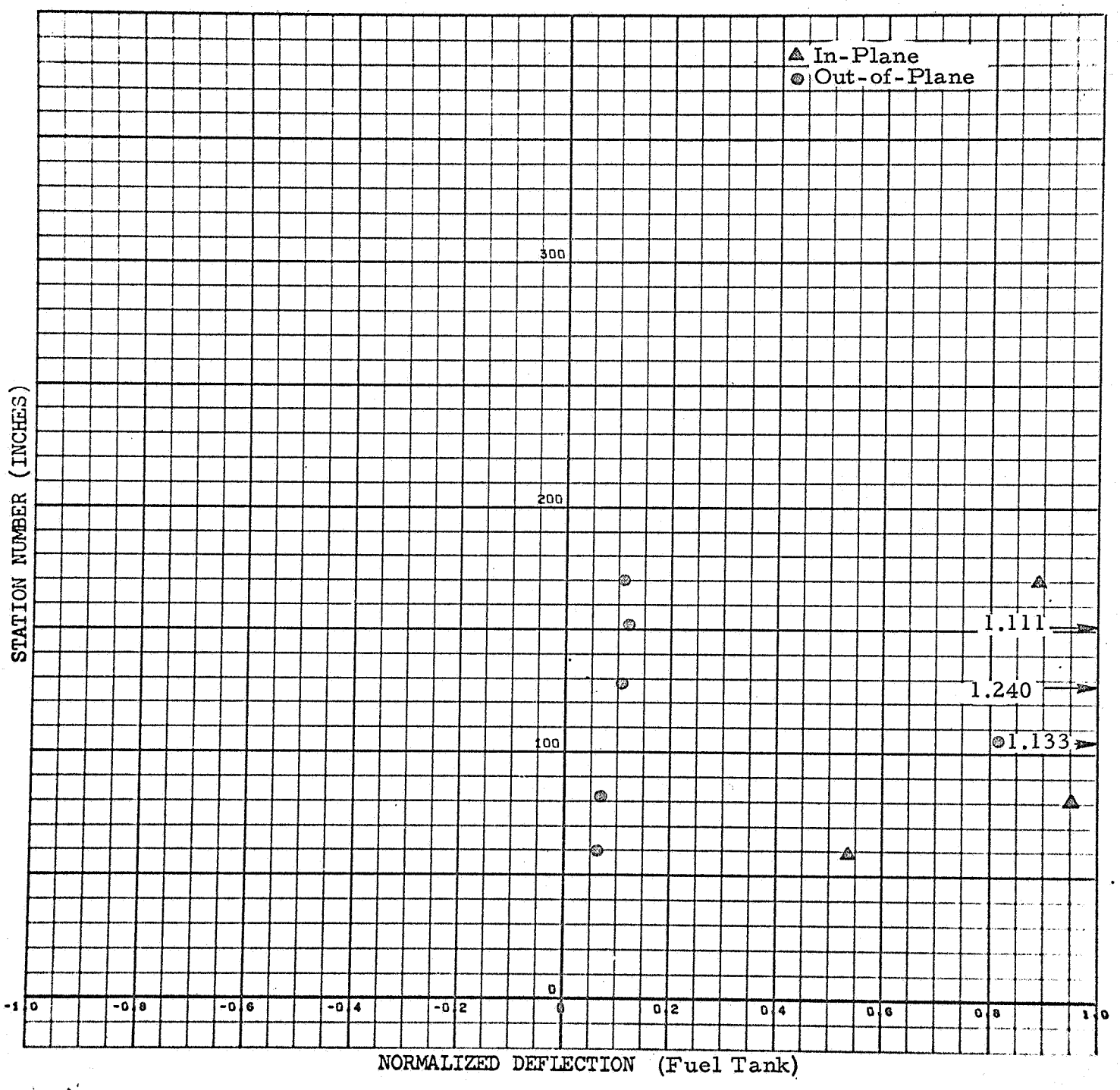

Figure C-C-29

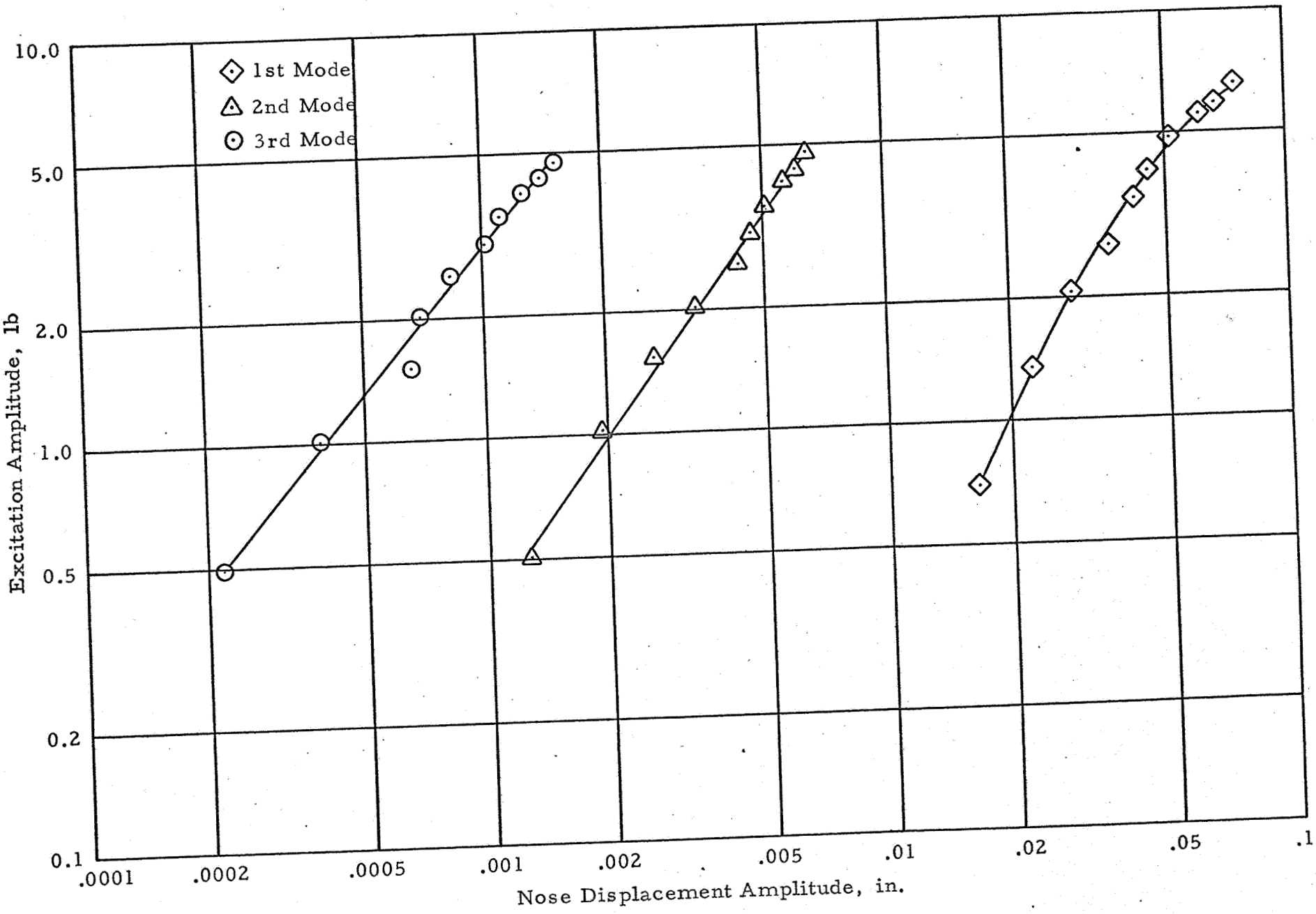

Figure C-C-30 - Resonant Responses (Configuration C)

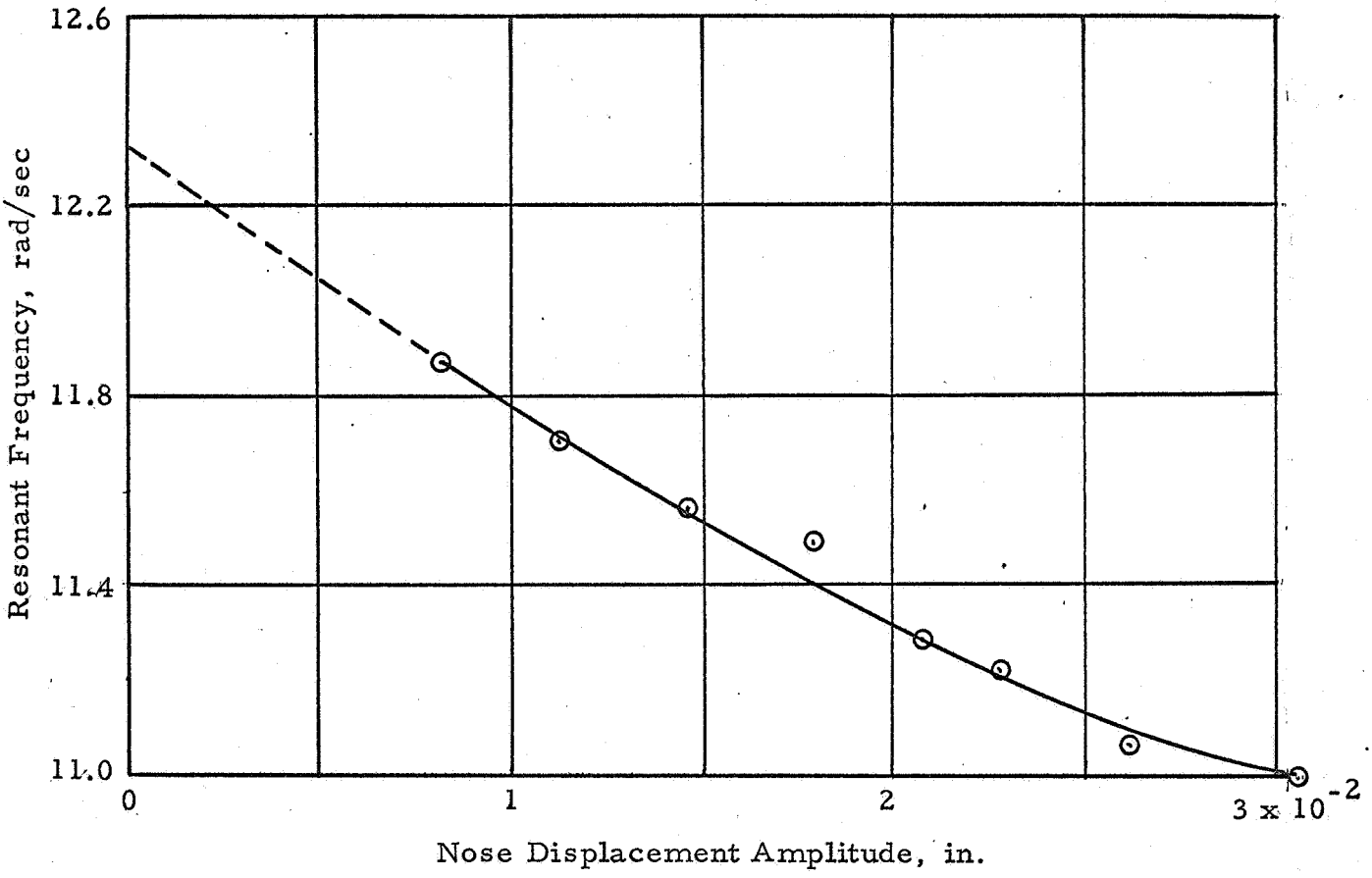

Figure C-C-31 - Variation of First Mode Frequency with Displacement Amplitude (Configuration C)

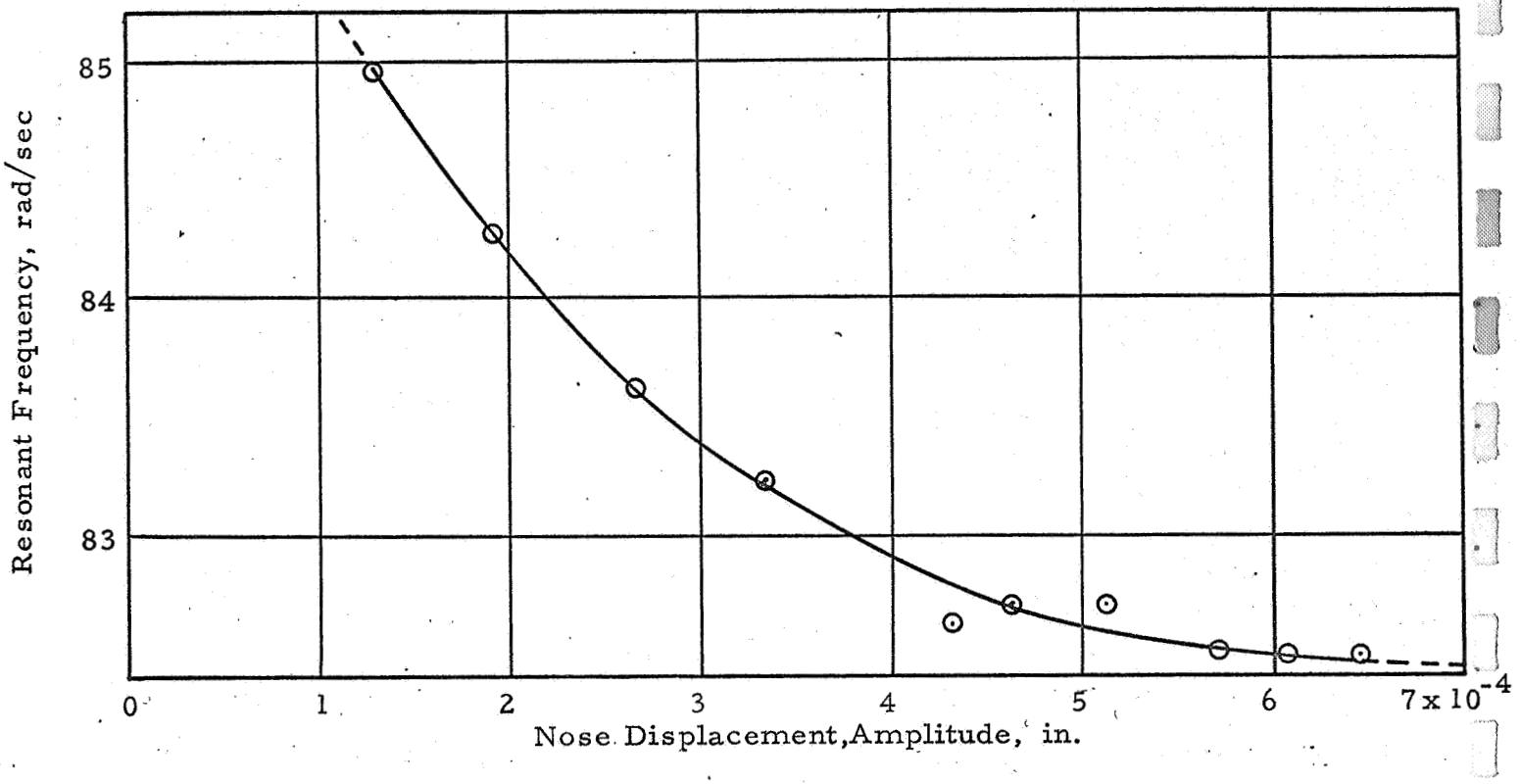

Figure C-C-32 - Variation of 2nd Mode Frequency with Displacement Amplitude (Configuration C)

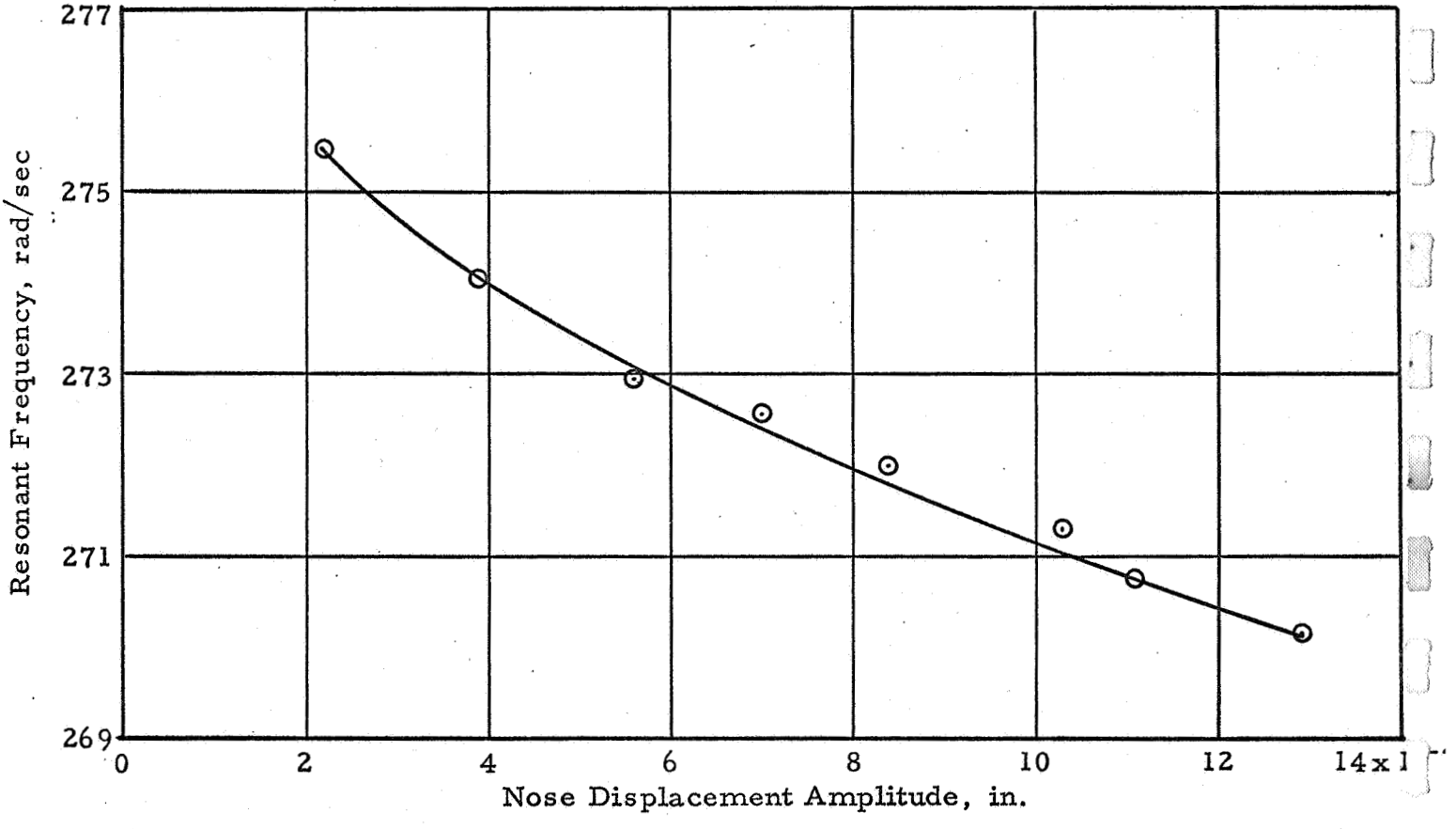

Figure C-C-33 - Variation of 3rd Mode Frequency with Amplitude, (Configuration C)

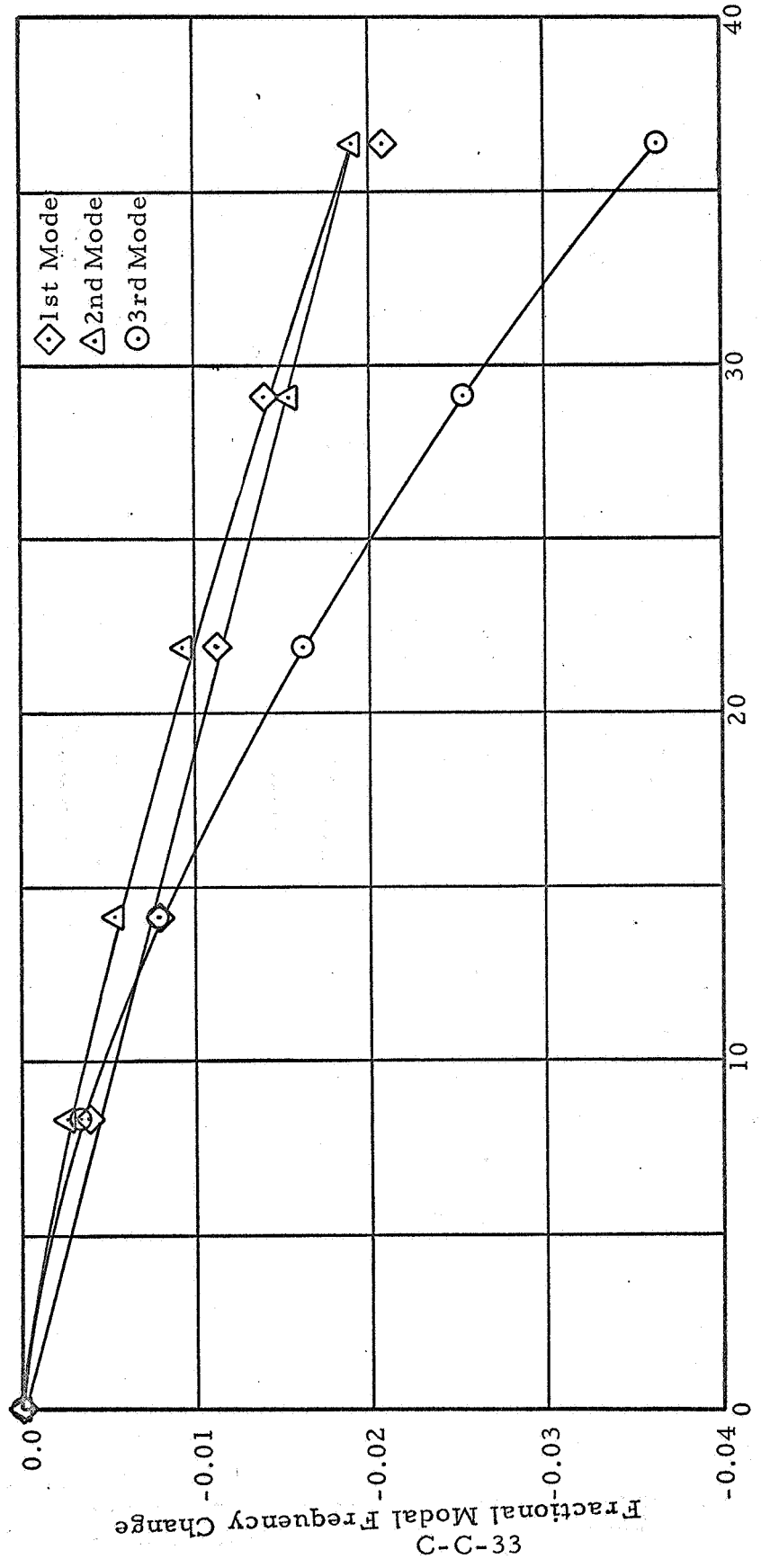

Figure C-C-34 - Generalized Mass Tests (Configuration C)

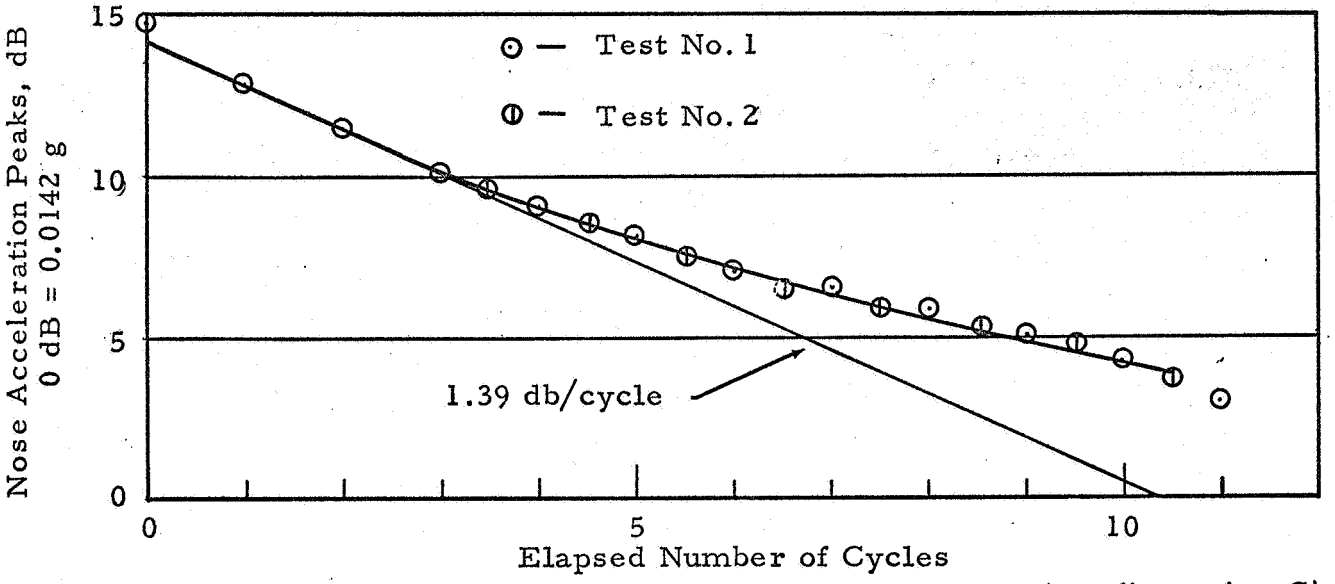

Figure C-C-35 - Decay of First Mode Free Vibration (Configuration C)

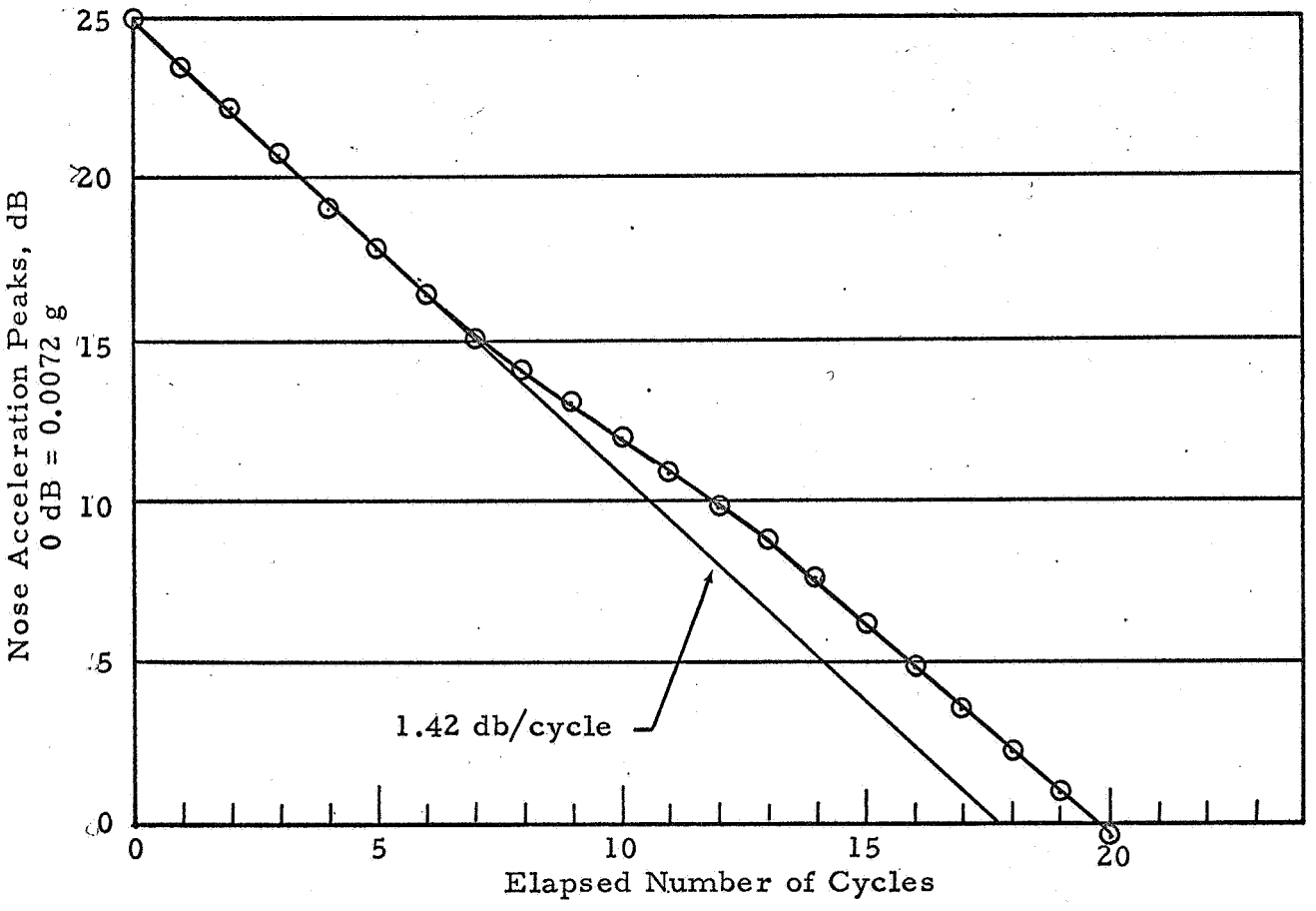

Figure C-C-36 - Decay of Second Mode Free Vibration (Configuration C)

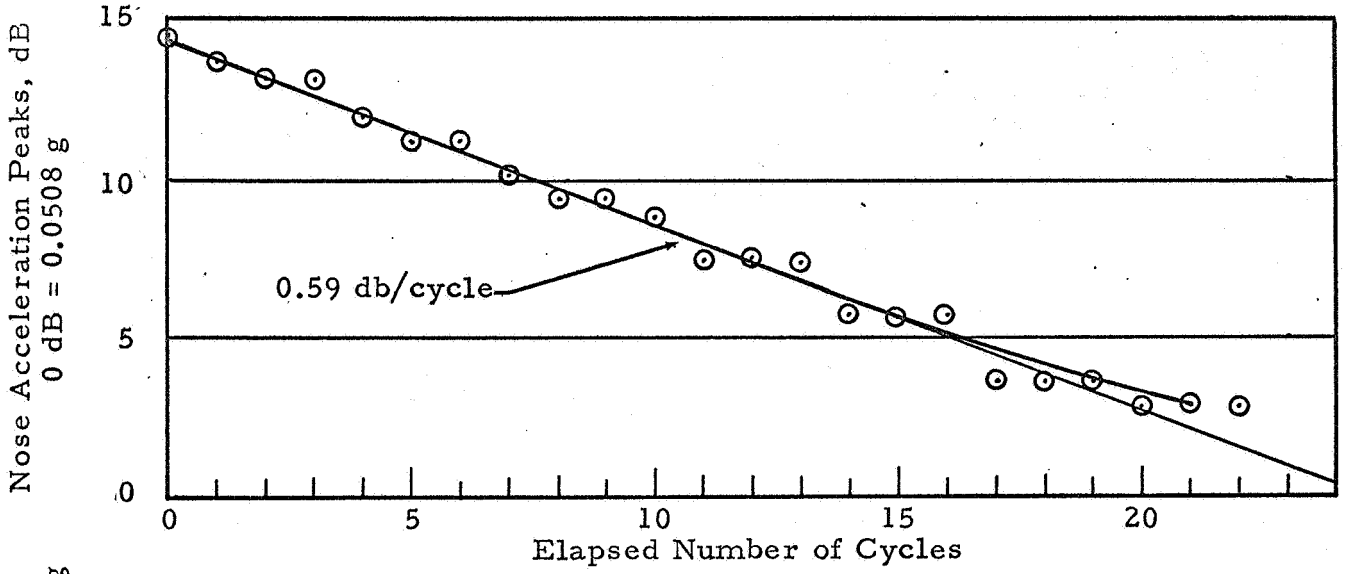

Figure C-C-37 - Decay of Third Mode Free Vibration (Configuration C)

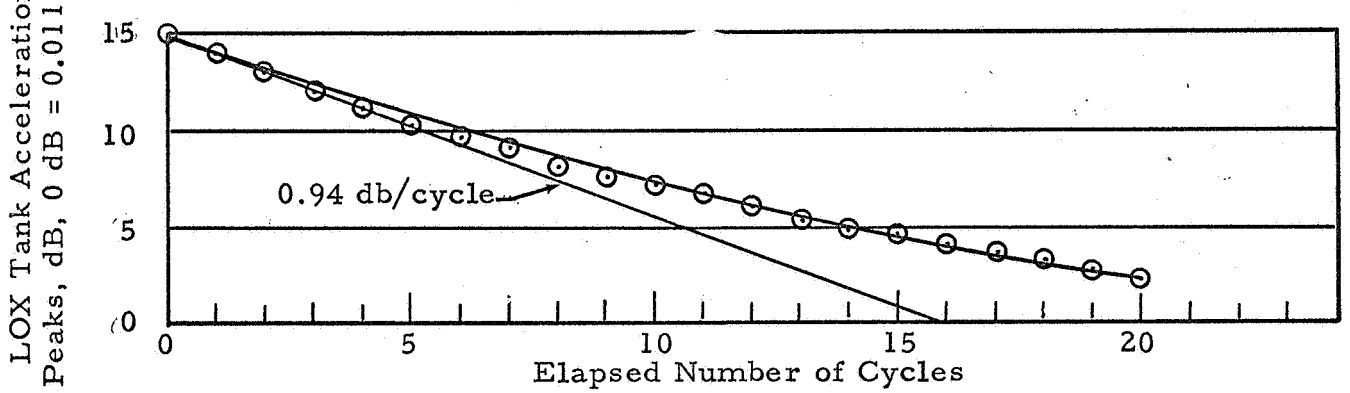

Figure C-C-38 - Decay of Second Mode Free Vibration (Configuration C)

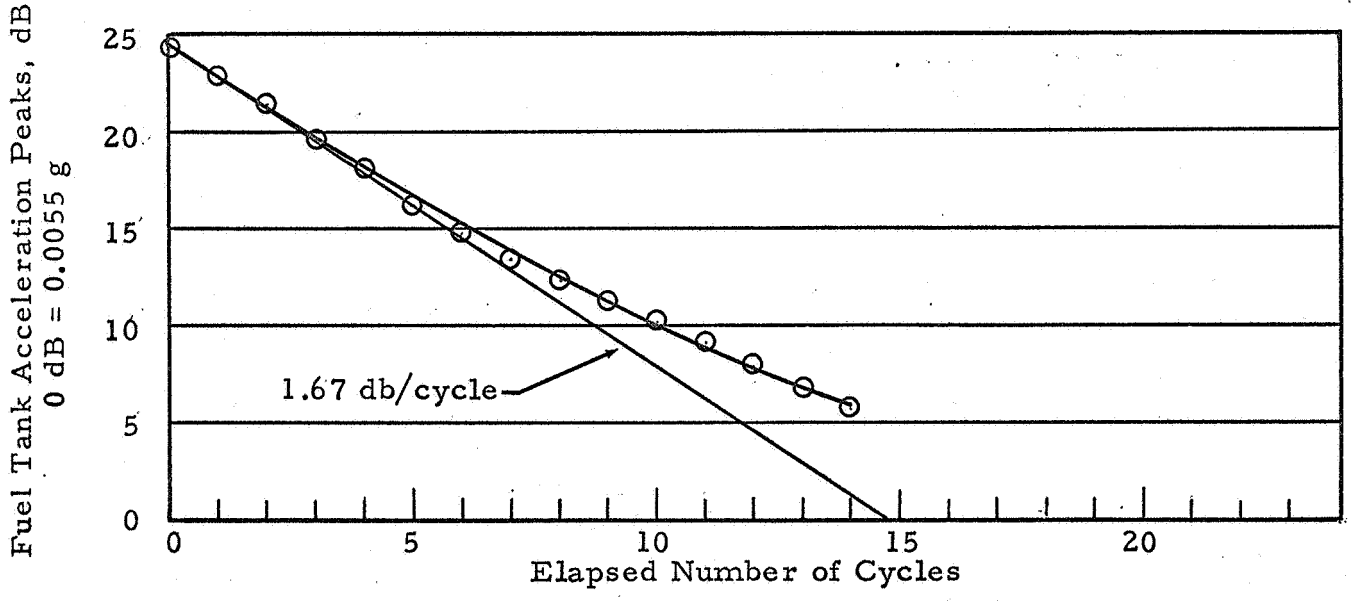

Figure C-C-39 - Decay of Second Mode Free Vibration (Configuration C)

TEST CONFIGURATION D
INDEX TO FIGURES

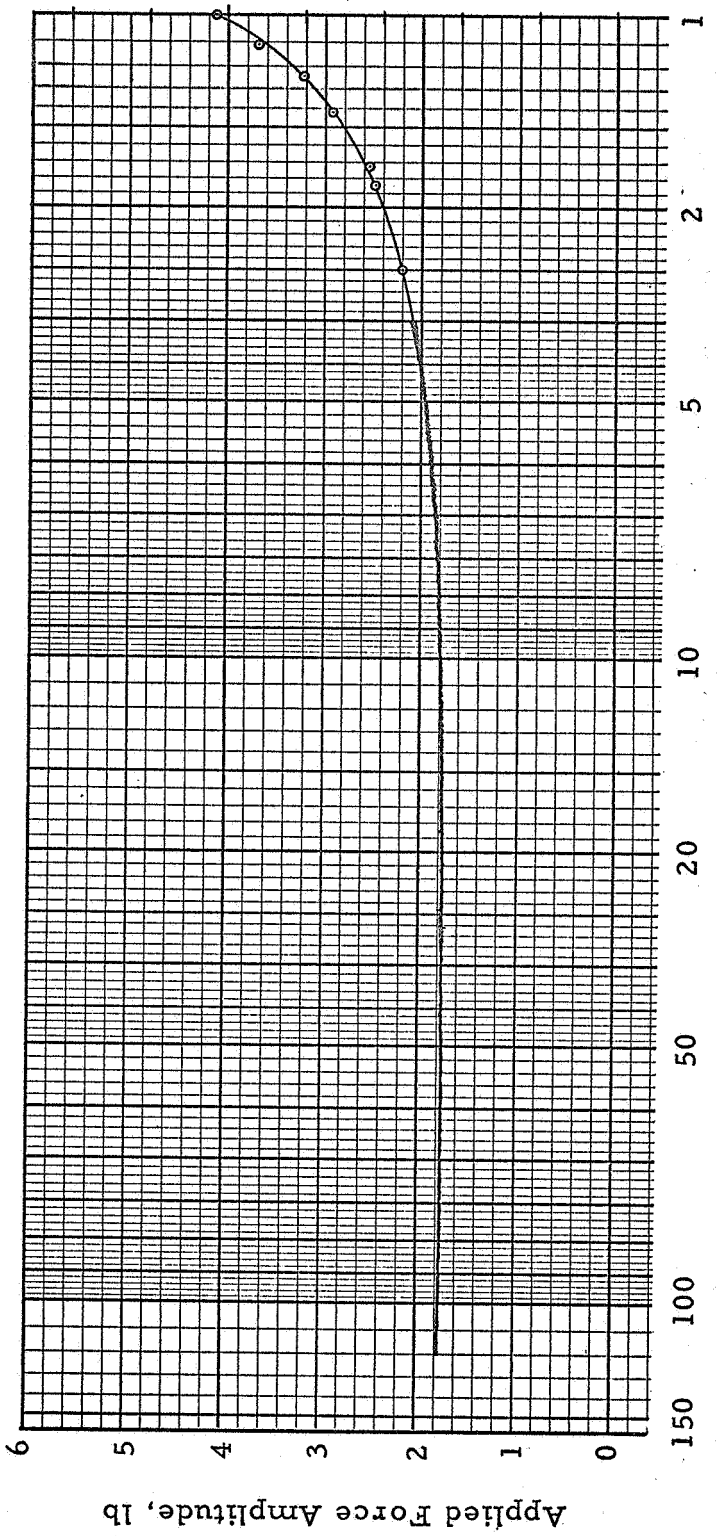

Figure C-D-1 - Variation of Applied Force Amplitude with Frequency (Configuration D)

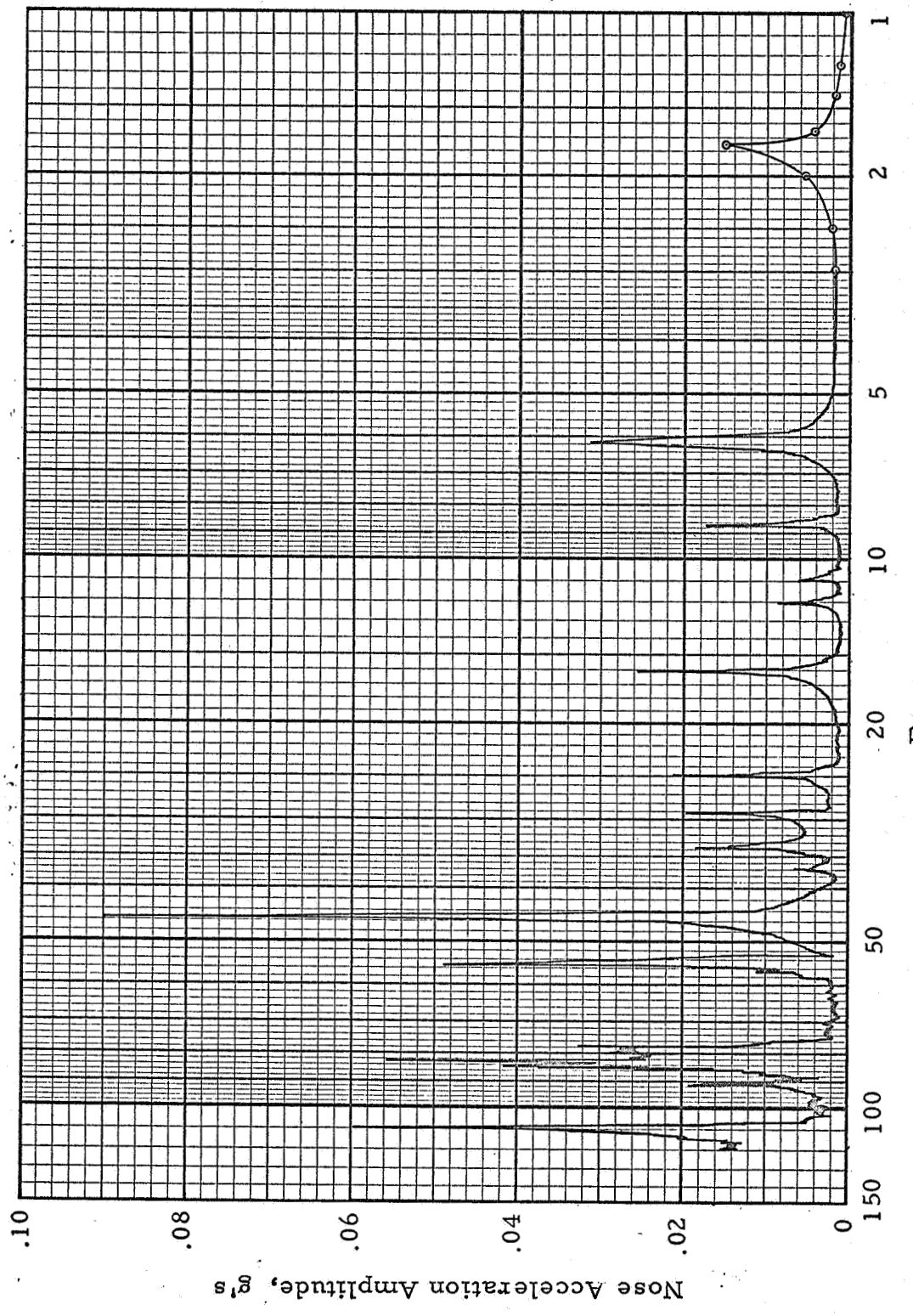

Figure C-D-2 - Frequency Response (Configuration D) Force Amplitude: 2.2 lb at 25 cps

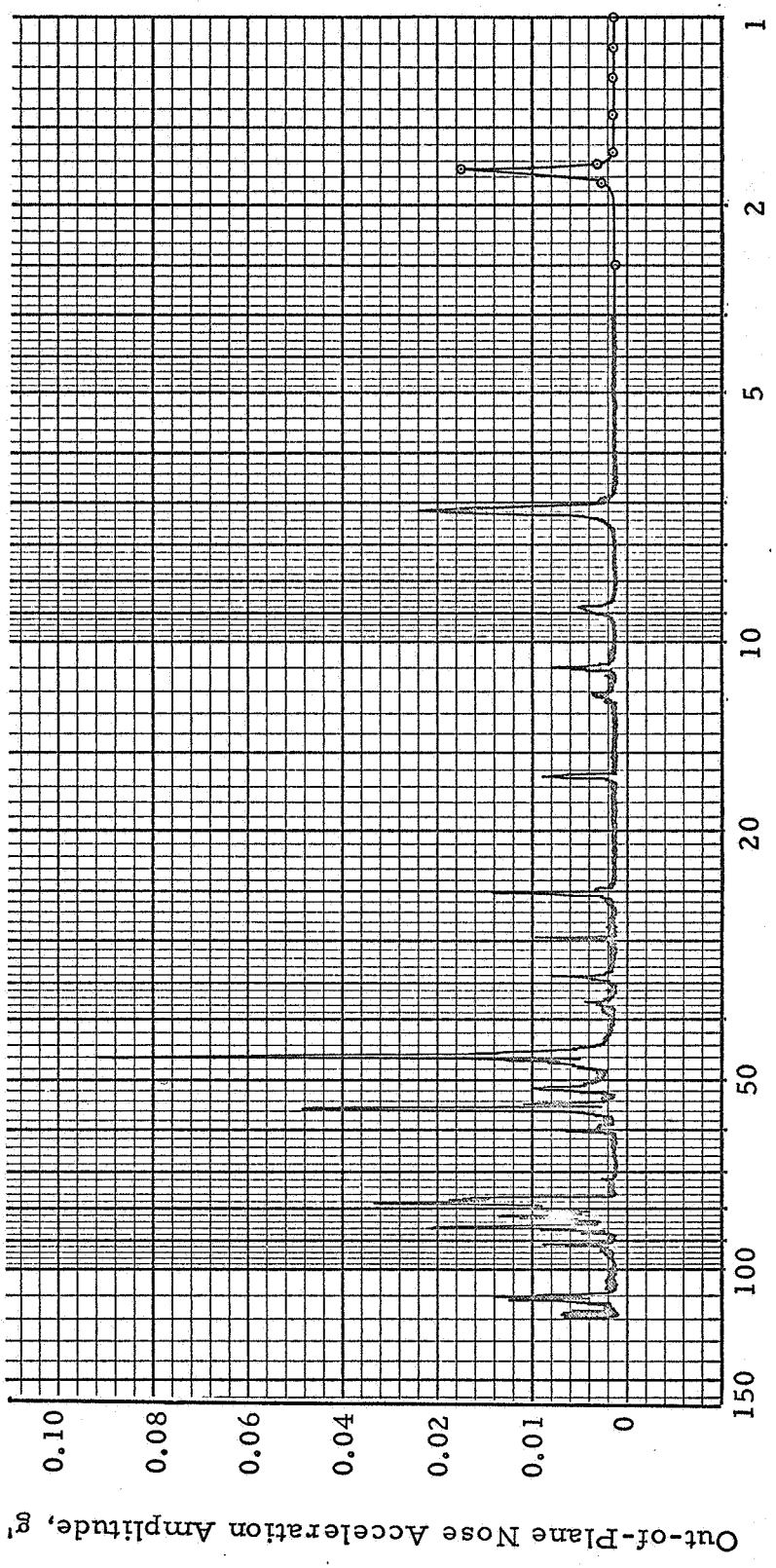

Figure C-D-3 - Frequency Response (Configuration D) Force Amplitude: 2.2 lb at 25 cps

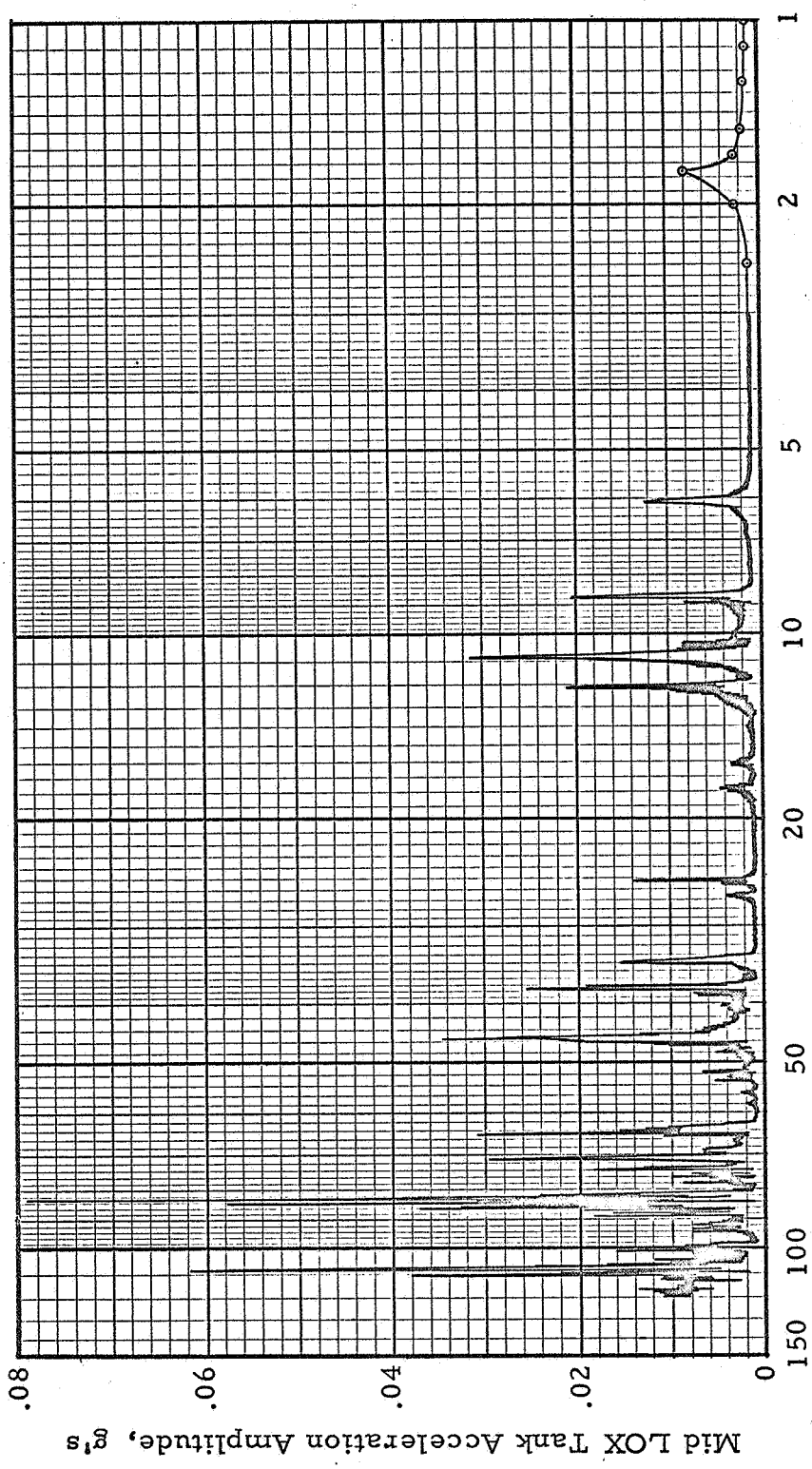

Figure C-D-4 - Frequency Response (Configuration D) Force Amplitude: 2.2 lb at 25 cps

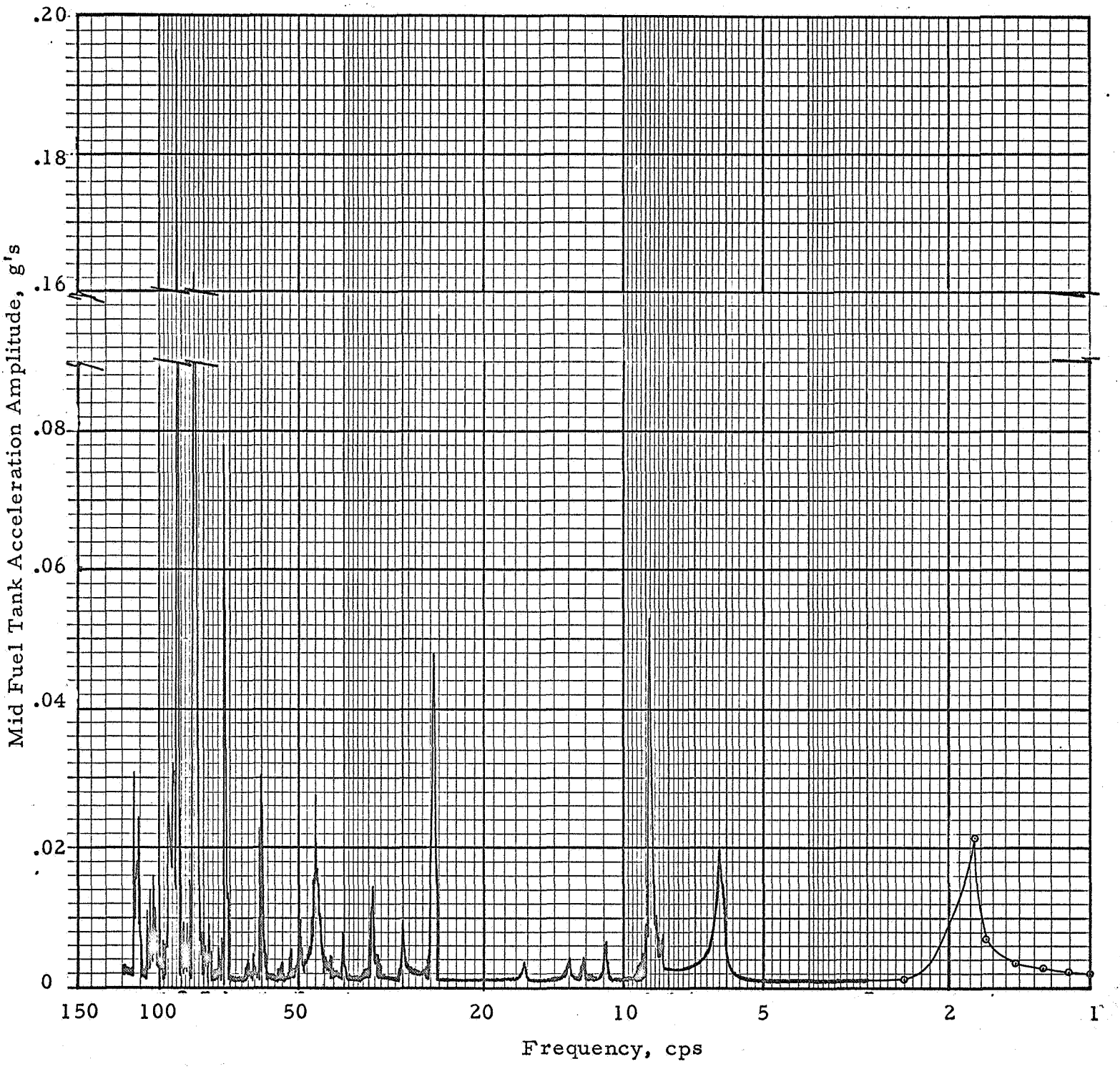

Figure C-D-5 - Frequency Response (Configuration D) Force Amplitude: 2.2 lb at 25 cps

CONFIGURATION: D

FREQUENCY: 1.76 cps

FORCE: 2.97 pounds, 0-pk

MODE NUMBER: 1

DAMPING: See Figure C-D-14

TIP ACCELERATION: .041 g (In-Plane)

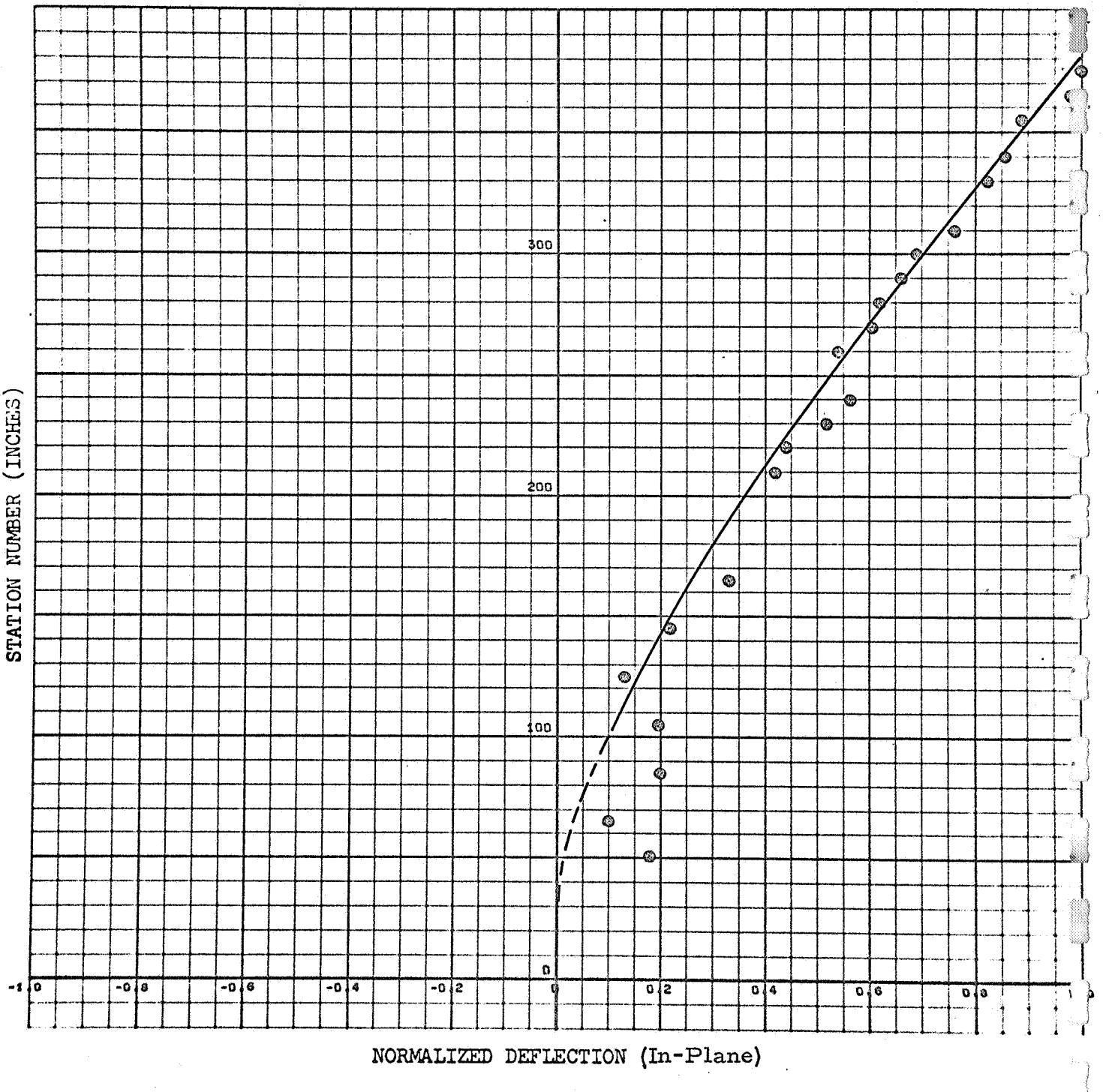

Figure C-D-6

CONFIGURATION: D

FREQUENCY: 1.76 cps

FORCE: 2.97 pounds, 0-pk

MODE NUMBER: 1

DAMPING:

TIP ACCELERATION: .017 g (Out-of-Plane)

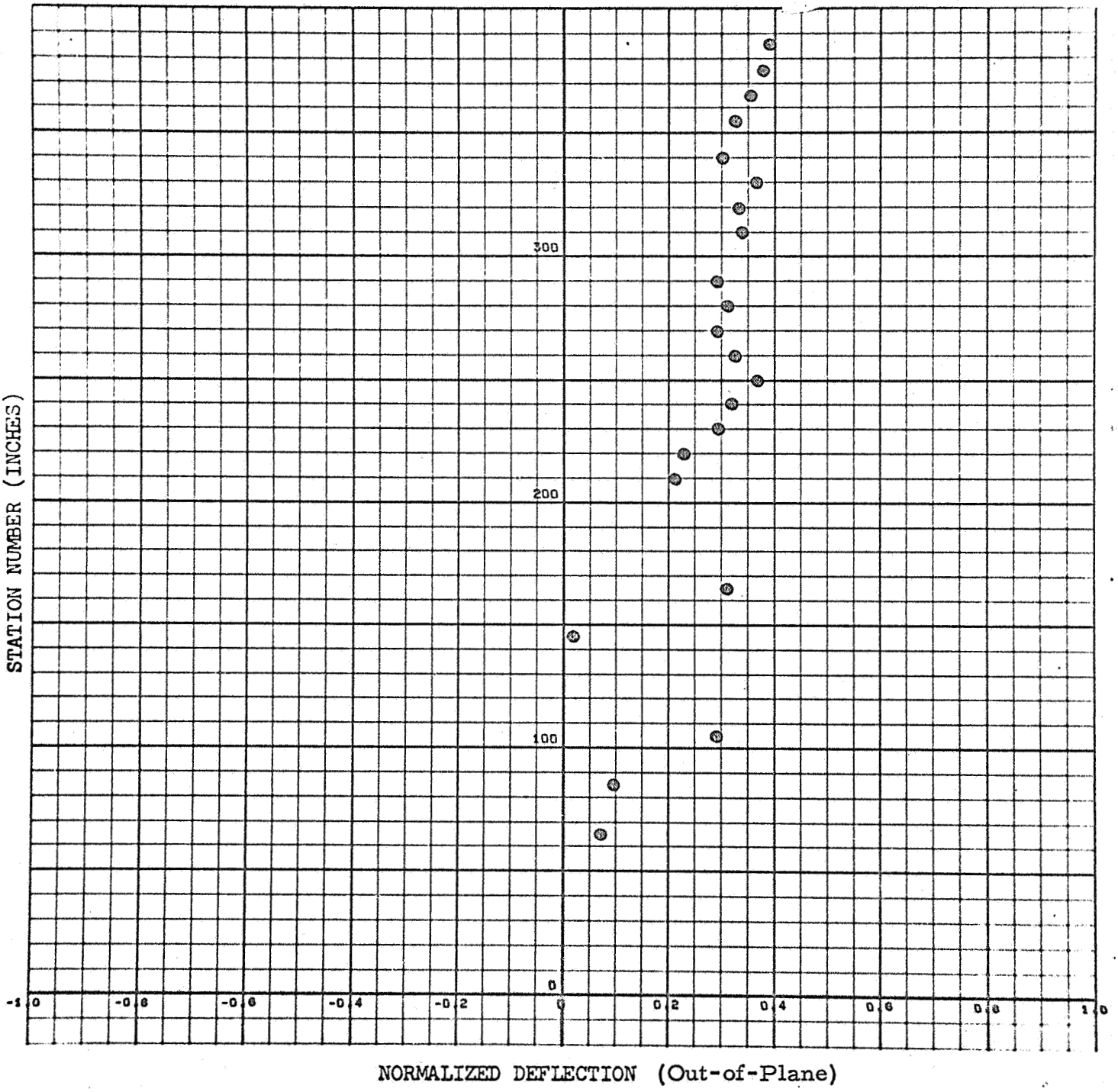

Figure C-D-7

CONFIGURATION: D

FREQUENCY: 1.76 cps

FORCE: 2.97 pounds, 0-pk

MODE NUMBER: 1

DAMPING:

TIP ACCELERATION: .041 g (In-Plane)

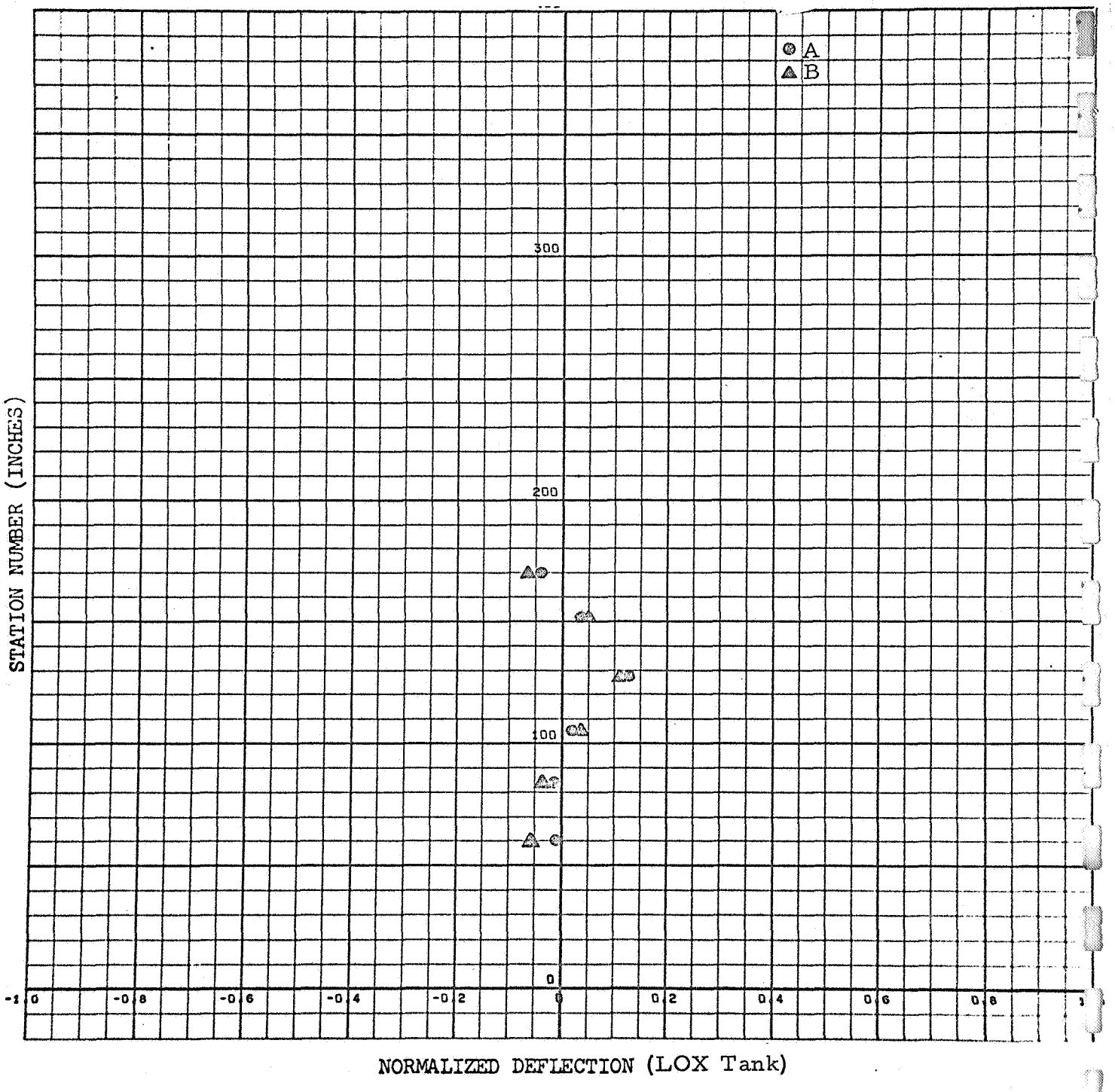

Figure C-D-8

CONFIGURATION: D

FREQUENCY: 1.76 cps

FORCE: 2.97 pounds, 0-pk

MODE NUMBER: 1

DAMPING:

TIP ACCELERATION: .041 g (In-Plane)

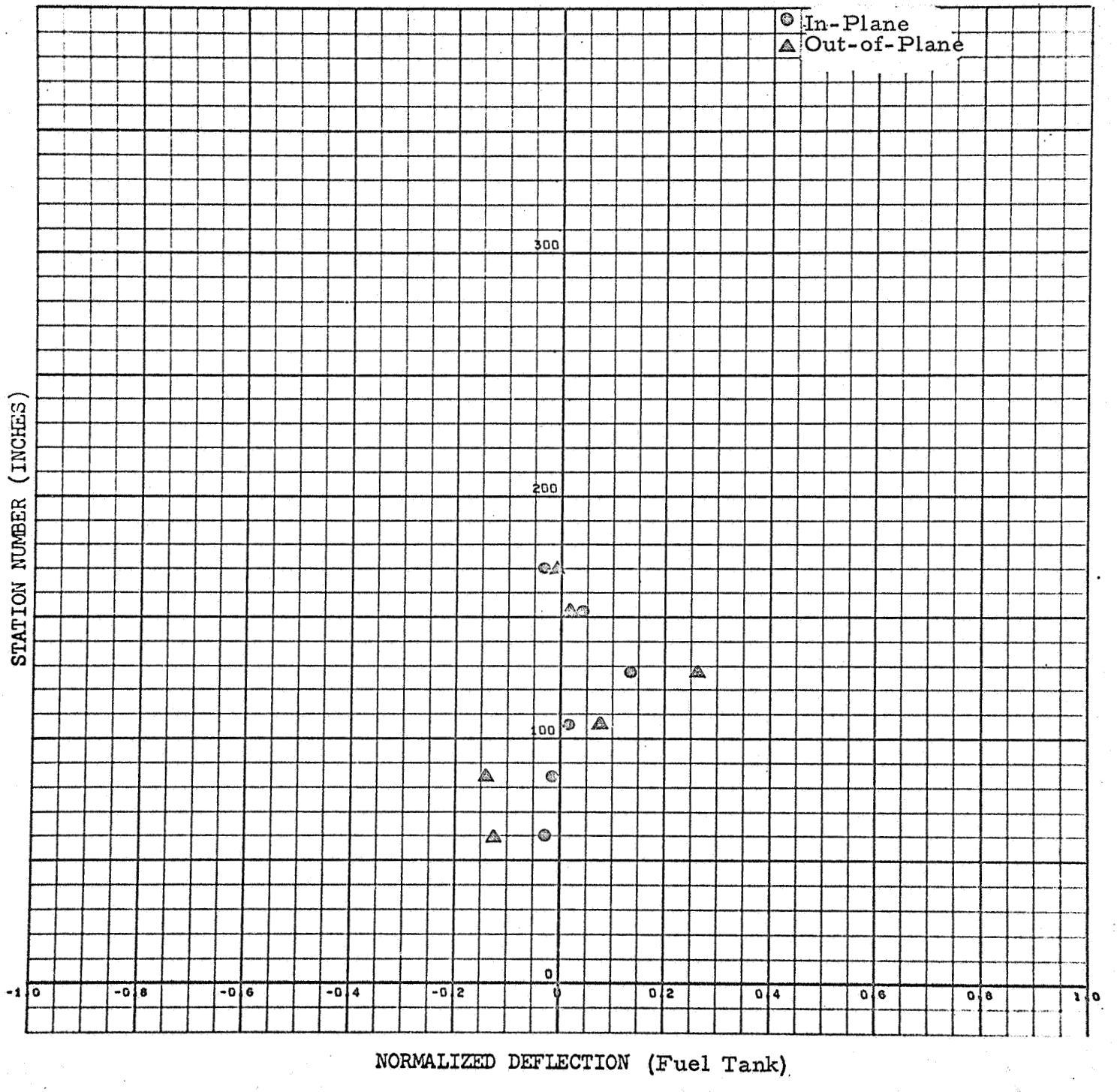

Figure C-D-9

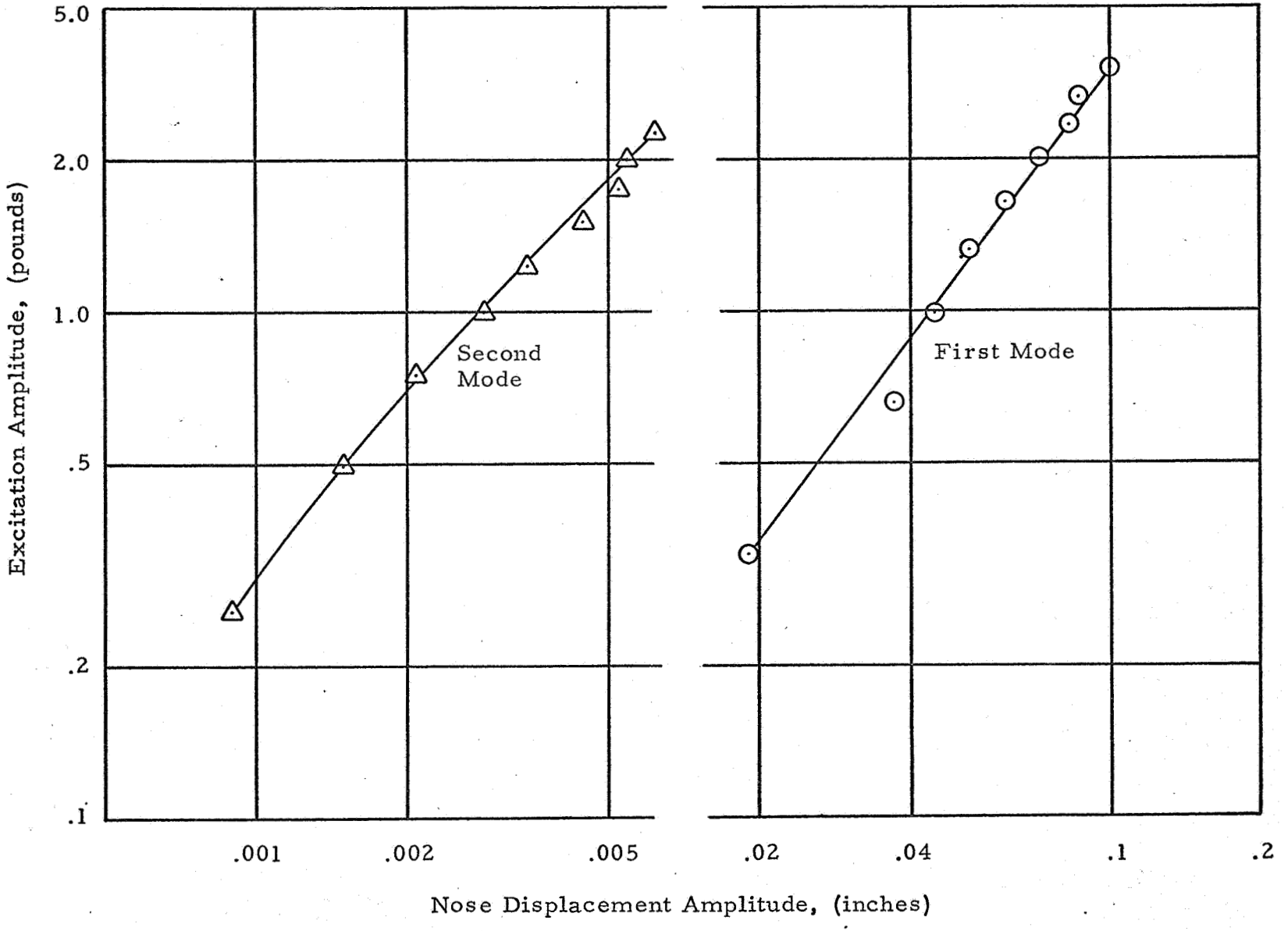

Figure C-D-10 - Resonant Responses (Configuration D)

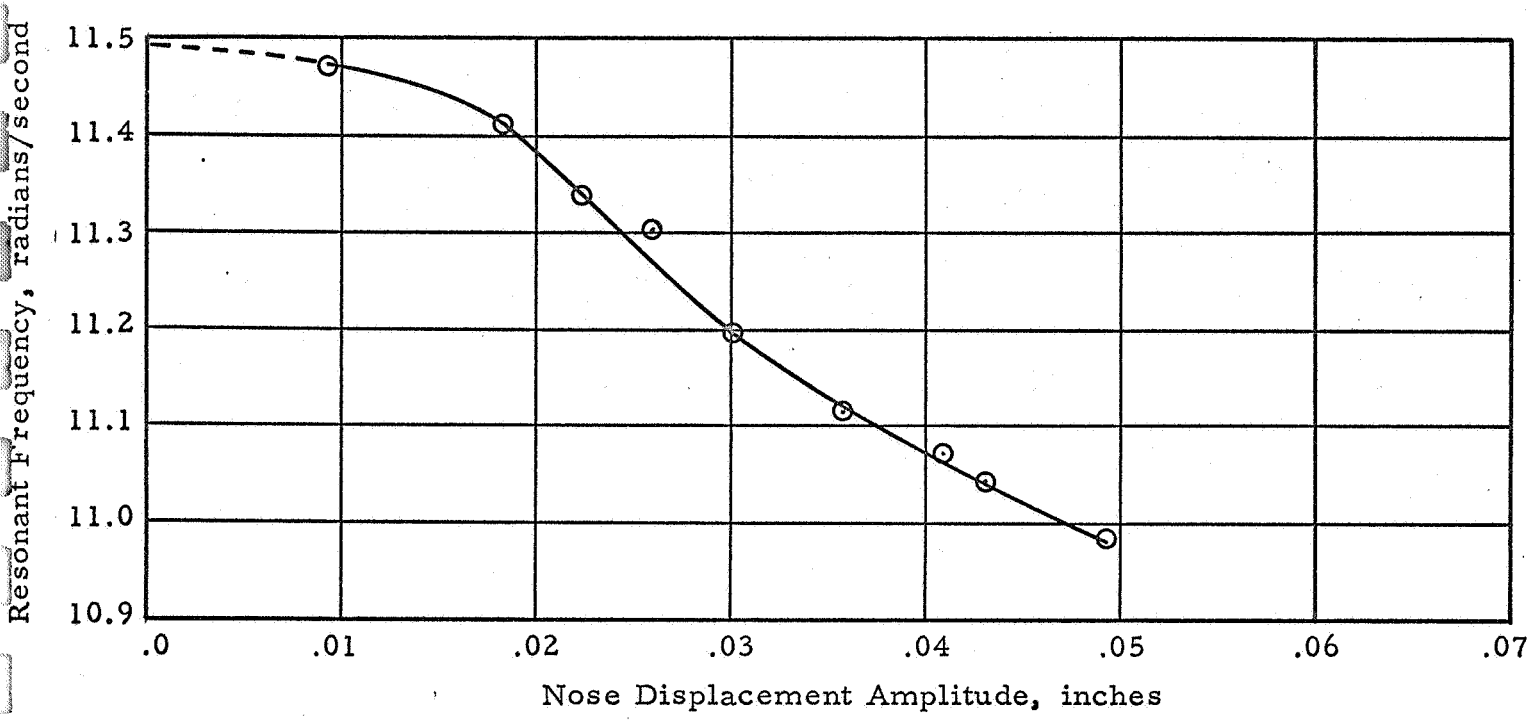

Figure C-D-11 - Variation of 1st Mode Frequency with Displacement Amplitude (Configuration D)

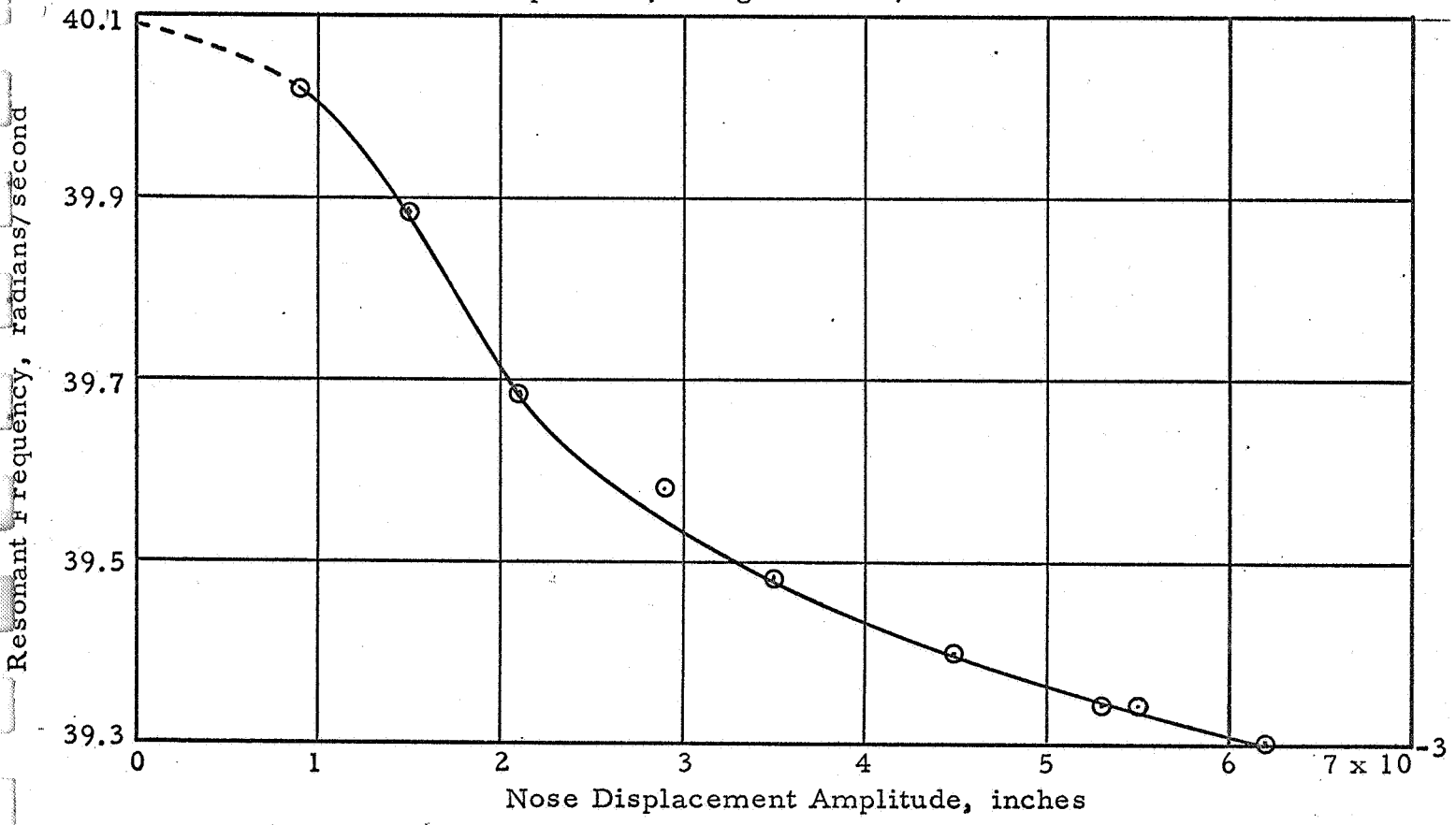

Figure C-D-12 - Variation of 2nd Mode Frequency with Displacement Amplitude (Configuration D)

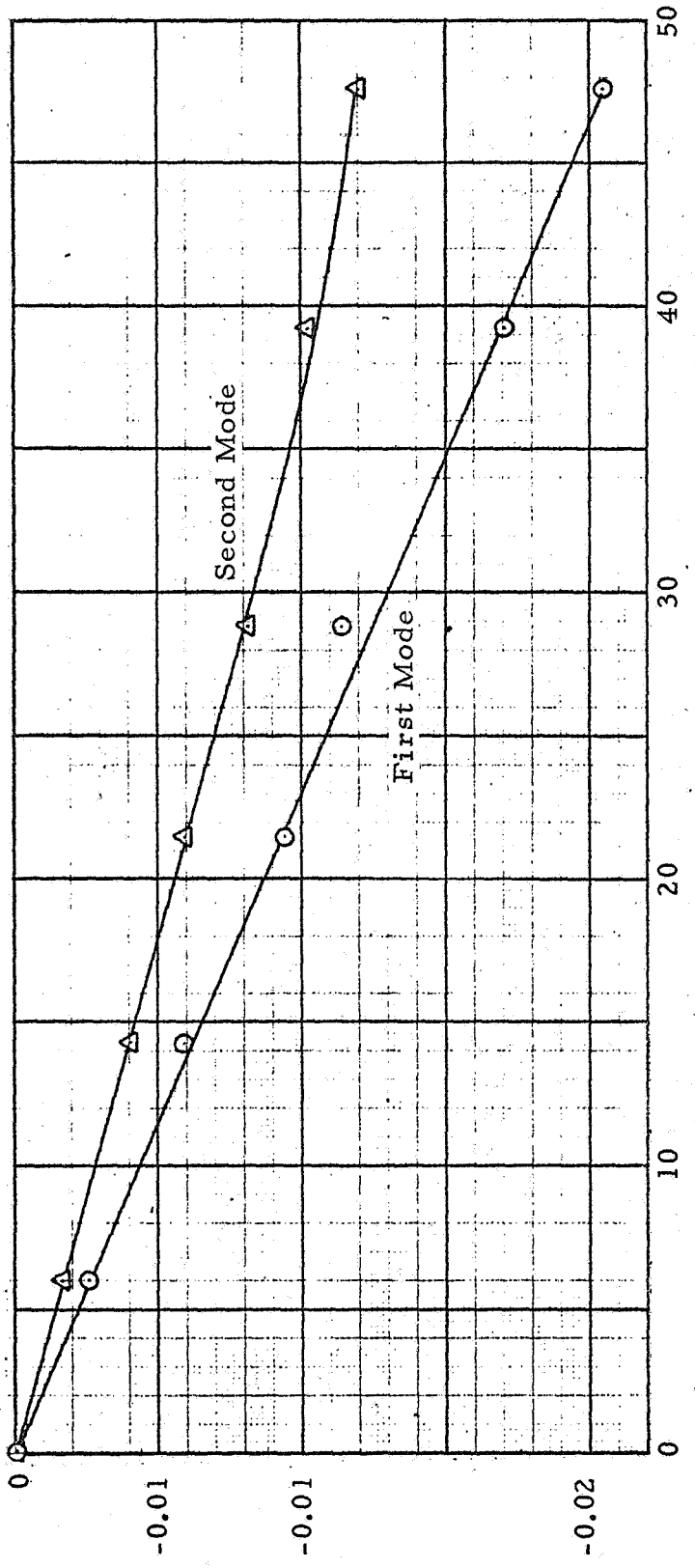

Figure C-D-13 - Generalized Mass Tests (Configuration D)

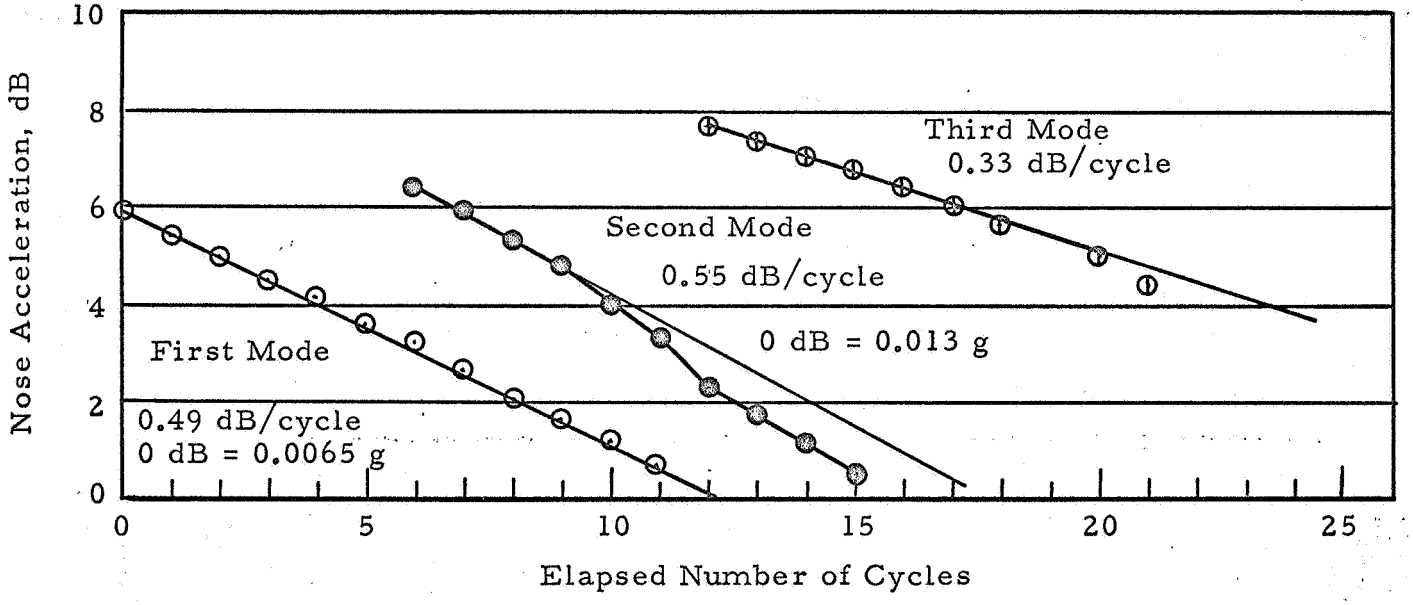

Figure C-D-14 - Decay of First Three Modal Free Vibrations (Configuration D)